



UNIVERSITY OF WYOMING

Digital Cameras and Imaging Systems for Engineers and Scientists

Digital Cameras and Imaging Systems for Engineers and Scientists

Cameron H.G. Wright

College of Engineering and Applied Science
University of Wyoming
Laramie, WY 82071

Copyright © 2022 by Cameron H. G. Wright

The author of this book makes no warranty of any kind, expressed or implied, with regard to the contents of this book. The author shall not be liable in any event for the incidental or consequential damages in connections with, or arising out of, the furnishing, performance, or use of the concepts contained herein.

10 9 8 7 6 5 4 3 2 1

All rights reserved. No part of this book may be reproduced, in any form or by any means, without permission in writing from the author.

Printed in the United States of America.

This document was typeset using LATEX, the document preparation system developed by Leslie Lamport as a special version of Donald Knuth's TeX program.

MATLAB® is a trademark of The MathWorks, Inc. and is used with permission. The MathWorks does not warrant the accuracy of the text or exercises in this book. This book's use or discussion of MATLAB® software or related products does not constitute endorsement or sponsorship by The MathWorks of a particular pedagogical approach or particular use of the MATLAB® software.

TeX is a trademark of the American Mathematical Society.



*To Dr. A. J. Welch, Professor Emeritus at the University of Texas at Austin,
who got me so interested in digital cameras and optics...
his legacy lives on in his many, many students.*

About the Author

Cameron H. G. Wright, Ph.D., P.E., is the inaugural Carrell Family Dean of the College of Engineering and Applied Science, and a Professor of Electrical and Computer Engineering at the University of Wyoming (UW), Laramie, WY. He was previously Professor and Deputy Department Head, Department of Electrical Engineering, United States Air Force Academy (USAFA), and served as an R&D engineering officer in the U.S. Air Force for over 20 years (with a total of 30 years in the U.S. military). He received the B.S.E.E. (*summa cum laude*) from Louisiana Tech University (1983), the M.S.E.E. from Purdue University (1988), and the Ph.D. from the University of Texas at Austin (1996). He is a licensed Professional Engineer in California and Wyoming. His research interests include digital cameras, signal and image processing, real-time embedded computer systems, biomedical instrumentation, and engineering education; he has served as a consulting engineer and an expert witness in several of these areas. A retired Lieutenant Colonel in the U.S. Air Force, he was awarded the Brigadier General Roland E. Thomas Award for Outstanding Contributions to Cadet Education at USAFA in 1992 and 1993. In 2005 and 2008, he was awarded the UW IEEE Student Choice Award for Outstanding Professor of the Year; the Mortar Board “Top Prof” Award at UW in 2005, 2007, and 2015; the Outstanding Teaching Award from the ASEE Rocky Mountain Section in 2007; the John A. Curtis Lecture Award from the Computers in Education Division of ASEE in 1998, 2005, and 2010; the UW Tau Beta Pi (WY-A) chapter Undergraduate Teaching Award in 2011; and the UW Ellbogen Meritorious Classroom Teaching Award in 2012. Dr. Wright is a founding member of the Technical Committee on Signal Processing Education for the IEEE Signal Processing Society, a Senior Life Member of the IEEE, and a member of ASEE, the National Society of Professional Engineers, the Biomedical Engineering Society, SPIE—The International Society of Optical Engineering, Tau Beta Pi, and Eta Kappa Nu. He is the author or co-author of over 260 papers, four book chapters, and two books.

Contents

Preface	xi
Acknowledgments	xiii
1 Introduction	1
2 Imaging, Cameras, and Eyes	3
2.1 Camera eye	4
2.2 Reduced eye model	6
2.3 Comparing cameras to eyes	7
2.4 Problems	8
3 Optical Components for Imaging	9
3.1 Lenses	9
3.2 Apertures	11
3.3 Shutters	13
3.4 Mirrors	13
3.5 Prisms	15
3.6 Beamsplitters	16
3.7 Polarizing Filters	17
3.8 Components for Low-Light Conditions	18
3.8.1 Light Amplification	18
3.8.2 Noise Reduction	19
3.9 Other Components	20
3.10 Helpful Organizations and Vendors	20
4 Basic Optics and Imaging	21
4.1 Object and image distances and sizes	21
4.2 Effects of aperture size: diffraction	24
4.2.1 Circular apertures	25
4.2.2 Rectangular apertures	26
4.2.3 Resolution criteria	29
4.2.4 Terminology related to apertures	30
4.2.5 Applying aperture-related calculations	32
4.3 Depth of field	33
4.3.1 DOF Calculations	35
4.3.2 Bokeh	37
4.4 Field of view	37
4.5 Types of Aberrations	42
4.5.1 Monochromatic aberrations	43
4.5.2 Chromatic aberration	48

4.5.3	Aberrations in general	49
4.6	Reflection and refraction	50
4.6.1	Critical angle	50
4.6.2	Snell's law	50
4.6.3	Fresnel equations	51
4.6.4	Brewster's angle	51
4.6.5	Coherence length	53
4.6.6	AR coatings	54
4.6.7	Lens flare	55
4.7	Summary	55
5	Fourier Optics for Analysis and Simulation	57
5.1	Foundation of Fourier optics	57
5.1.1	Three diffraction regions	57
5.1.2	Aperture functions	59
5.1.3	Fraunhofer diffraction and Fourier optics	60
5.1.4	Specific aperture shapes	62
5.2	PSF	63
5.3	OTF, MTF, and CTF	67
5.3.1	The OTF	67
5.3.2	The MTF	67
5.3.3	The limiting resolution	74
5.3.4	Other methods of comparison	75
5.3.5	System MTFs	77
5.3.6	The CTF	78
5.4	MTFs of special apertures	81
5.5	Apodization	85
5.6	Simulating Aberrations	89
5.6.1	Phase function of the aperture	91
5.6.2	Third-order optics	92
5.6.3	Describing aberrations	93
5.6.4	Using Zernike polynomials	94
5.6.5	Simulated Effects of Aberrations	95
5.7	Summary	102
6	Imaging Sensors	103
6.1	Non-sampling effects of the FPA	105
6.1.1	Blurring due to detector size	105
6.1.2	Other FPA blurring effects	109
6.2	Sampling effects of the FPA	110
6.2.1	Mathematical description of sampling	110
6.2.2	Sampling is not LSI	112
6.2.3	Aliasing	114
6.2.4	Anti-aliasing	116
6.3	Color Imaging: Single FPA Methods	122
6.3.1	Color Filter Arrays	122
6.3.2	Color Without a CFA	126
6.4	Color Imaging: Three FPA Method	128
6.5	Color versus Monochrome Imaging	129
6.6	1-D Linear Detector Arrays	129
6.7	Single Detector Scanning	135
6.8	Nontraditional Sensors: Biomimetic Fly Eye	136
6.9	Shutters and Temporal Effects	137

6.9.1	Global Shutter versus Rolling Shutter	137
6.9.2	Shutter Speed	137
6.9.3	Sensitivity to Light	140
6.9.4	Video Cameras	140
6.9.5	Relative Motion	141
6.9.6	Vibration	141
6.10	Summary	141
7	Video Cameras versus Still-Image Cameras	143
7.1	Video: a Time Sequence of Still Images	143
7.1.1	Frame Rate versus Shutter Speed	143
7.1.2	Motion Aliasing in Video	143
7.2	Video formats	143
7.2.1	Interlaced versus Progressive Scan	143
7.2.2	Formats Derived from Broadcast standards	143
7.2.3	Modern Digital Video Formats	143
7.3	Special Case of Cinematic Video	143
8	Camera Electronics and Interfaces	145
8.1	Image acquisition electronics	145
8.1.1	MTF Due to Hardware	145
8.1.2	MTF Due to Demosaicing Interpolation Algorithms	145
8.2	Digital versus analog interface	146
8.2.1	RS-170 and Variants	146
8.2.2	External Interfaces: CameraLink, Firewire, USB, and Variants	146
8.2.3	Internal Interfaces: MIPI Standards	146
8.3	Other factors related to cameras	146
9	Lighting and Illumination	147
9.1	Achieving Even Illumination	147
9.2	Ramifications of Illumination Wavelengths	147
9.3	Ramifications of Illumination Power Source	147
9.4	Image Noise and Flicker Due to Illumination	147
10	Image File Storage and Compression	149
10.1	Internal Image Formats	149
10.2	RAW versus Compressed	149
10.3	Compression Overview	149
10.3.1	Lossless versus Lossy	149
10.3.2	JPEG	149
10.4	Recommendations	149
11	Watermarks for Digital Images	151
11.1	Definition and Purpose of Watermarks	151
11.2	Visible versus Invisible	151
11.3	Robust versus Fragile	151
11.4	Ramifications for Research Data	151
11.5	Special Topic: Steganography	151
12	Simulating and Testing a Digital Imaging System	153
12.1	Software Tools to Support Simulation	153
12.2	MATLAB and a Fourier Optics Approach	153
12.3	Recommendations	153

Appendices	155
A Review of Fourier Transforms	157
A.1 The 1-D Continuous Fourier Transform	157
A.1.1 Properties	157
A.1.2 Fourier Transform Pairs	158
A.2 The 1-D Discrete Fourier Transform	161
A.3 The 2-D Continuous Fourier Transform	165
A.4 The 2-D Discrete Fourier Transform	166
B Review of Analog-to-Digital Conversion	169
B.1 Sampling	169
B.2 Quantizing	173
B.3 Encoding	176
B.4 Extending the Concepts to 2-D Spatial Sampling	177
C Example MATLAB programs	181
References	206

Preface

THIS book discusses the most common ways that digital still images and video frames are formed, and how the various tradeoffs such as those related to lenses, shutter speed, frame rate (for video), sensor arrays, camera settings, and storage can all affect the quality and validity of the images. Typically, a camera is used that includes a single, large-aperture lens system and a single, high-resolution focal plane sensor array. Often, a compression algorithm is used to store the image data more efficiently, and in certain cases a watermark of some sort may be applied.

The book is primarily intended for technical users of digital cameras, both still-image and video. This includes those who use cameras as stand-alone devices as part of their work, but also those who use cameras attached to devices such as microscopes, telescopes, or some other imaging apparatus (e.g., scanning laser ophthalmoscopes, fundus cameras, confocal microscopes, etc.). The underlying foundation of optics and image capture are basically the same no matter how the camera is used. Less common camera topics, such as light field cameras and quanta imaging sensors (QIS) are exciting new developments, but are beyond the scope of this book.

There are many books that address certain topics such as Fourier optics or CCD and CMOS sensor arrays in great detail, but the purpose of this book is to put it all together in a practical, system-oriented manner that is targeted more toward the *technical user* of a camera rather than a *theoretician* or a *designer*. The references section of this book will point the reader toward these more in-depth, and by necessity, more narrowly focused books, should the interest or need arise to pursue some of these topics further.

To provide such a practical introduction to the broad topic of digital camera use, a brief review of basic optical engineering is provided, including simple diffraction theory and mathematical tools such as Fourier optics, followed by a discussion of how an image is captured by photodetectors in an array. Modeling and simulations performed with tools such as Zemax OpticStudio and MATLAB® are described (along with MATLAB code to easily perform tasks such as simulating various lens aberrations and sensor array configurations), as are the tradeoffs associated with various camera types. The primary differences between choices such as still-image versus video cameras and color versus monochrome cameras are discussed, along with a practical treatment of camera/computer interfaces. Finally, some ramifications of compression methods and watermarks are discussed.

The intended readership of this text includes university students (senior or graduate-level) and working professionals in engineering or science who use cameras as part of their work in a research or industrial setting. The material may also be of interest to anyone who just wants to know more about how modern digital cameras really work, in particular serious photographers who are not intimidated by a few equations. Ideally, the reader will have a basic understanding of topics such as linear systems theory, Fourier transforms, and analog-to-digital conversion, but if not, a brief tutorial review is provided in the appendices. Previous exposure to basic optics is helpful but not necessary.

Prior to publication, the material in this text has been used in conjunction with a graduate course in electrical engineering (EE 5670, *Digital Image Formation and Acquisition*) at the University of Wyoming, and has benefited from the helpful feedback of numerous students.

MATLAB® is a trademark of The MathWorks, Inc. For product information, please contact:
The MathWorks, Inc.
3 Apple Hill Drive
Natick, MA 01760-2098 USA
Tel: 508-647-7000
Fax: 508-647-7001
Email: <mailto:info@mathworks.com>
Web: <http://www.mathworks.com>

Acknowledgments

THIS book would not have been possible without the excellent education in optics, practical optical engineering, and digital imaging I was fortunate to receive at the University of Texas at Austin in the mid-1990's. Thanks to Dr. A.J. Welch and many of the other professors there for the opportunity to learn and practice.

I would like to express my appreciation for the excellent reviewing prowess of Thad Welch and Donna Welch with draft versions of the manuscript. I would also like to thank one of my graduate students, Md. Arif Khan, who was particularly helpful with his feedback regarding the text.

The majority of the figures in this book were created by the author. Exceptions to that are certain apropos figures obtained from Wikimedia Commons,¹ for which their use in this book is allowed either under the appropriate Creative Commons license (as indicated in the citation) or are in the public domain.

I would be remiss if, in these brief acknowledgments, I omitted a “plug” related to the mechanics of writing the text: this book was typeset using L^AT_EX, a wonderfully capable document preparation system developed by Leslie Lamport as a special collection of macros for Donald Knuth’s ground-breaking T_EX program (specifically, I used the pdfL^AT_EX variant of pdft_EX created by Han The Thanh to directly produce output as a PDF file). L^AT_EX is ideally suited to technical writing, and is well supported by the worldwide members of the T_EX Users Group (TUG); investigate <http://www.tug.org/> for details. T_EX, L^AT_EX, and pdfL^AT_EX are *freely available* in the public domain (the name T_EX is a trademark of the American Mathematical Society). I used the excellent TeXstudio freeware editor (see <http://texstudio.sourceforge.net/>) as a front-end to the comprehensive TeX Live distribution of L^AT_EX freely provided by the T_EX Users Group. For maintaining the database of bibliographic references in the standard BIBT_EX syntax, I used the freely available and highly capable JabRef program (see <http://jabref.sourceforge.net/>). All these programs are not only free, but also available for a variety of operating systems. Figures in this book were created mainly with one of two programs: Canvas X and MATLAB. Canvas X is a high-end technical drawing package by Canvas GFX, Inc.; it can create and manipulate both vector and bit-mapped graphics in the same figure, providing a capability similar to both Adobe Illustrator and Adobe Photoshop combined all in one package. MATLAB, by The MathWorks, Inc., is an incredibly powerful numerical computing environment and a fourth-generation programming language, with many Toolbox extensions available for various specialized fields.

¹As of this writing, Wikimedia Commons included over 70 million freely usable media files, a database to which anyone can contribute. See <http://commons.wikimedia.org>.

Chapter 1

Introduction

ENGINEERS and scientists increasingly find themselves using digital cameras (both still-image and video) or other imaging devices to gather data, either as stand-alone devices or in conjunction with microscopes, telescopes or other equipment. This is done for a wide variety of reasons, both serious and casual. Digital cameras capable of very high quality images are continuing to become more inexpensive, much easier to use, and are rapidly becoming ubiquitous in the research lab, the development office, and in the field. The resolution of cameras built into some mobile phones today have higher resolution than top-of-the-line laboratory-grade cameras of just a few years ago! Some very inexpensive cameras, if used carefully, can be used for relatively demanding engineering and scientific purposes. An example of this is the camera module for the Raspberry Pi, a small, inexpensive single-board computer originally intended for hobbyists [1]. For unusual situations, a specialized imaging setup may be needed if an off-the-shelf camera is not appropriate, but the all the same considerations discussed in this book will apply.

The trend of lower cost and more simplified controls for digital cameras has an unintended downside, however. Many users now tend to view such digital cameras not as expensive precision instruments that should be used carefully and deliberately, but more as appliances that can be used at will, with little forethought. If the images are intended only as informal “snapshots,” then this attitude is acceptable. However, if the images are intended for more critical purposes, such as to obtain valuable data for a research project, or to officially document a project’s status, or to record forensic evidence that may have been used in a court of law, then it’s vital that the user have sufficient knowledge of how to properly use the camera, and perhaps even be able to specify the particular camera, lens, and camera/lens settings to obtain the needed images. If not, then the usefulness of the images obtained will often be greatly reduced, perhaps even to the point of making them worthless.

Suppose, for example, that you have been taking images as part of an ongoing research project for many months, and are now in the process of analyzing, evaluating, and writing up your results. How confident are you that it is valid to make certain conclusions based on the information in those images? Was the illumination sufficient and of the needed span of wavelengths? Was a color camera really needed or would monochrome have been better (the answer may surprise you)? Was the lens system and aperture setting appropriate to the light level and the resolution of the photodetector array in the camera? Did the resolution of the photodetector array provide sufficient spatial sampling to meet the sampling theorem for the level of fixed spatial detail that you need? Is the temporal sampling implied by the shutter speed, integration time, and/or video frame rate sufficient to meet the sampling theorem for any of the time-varying detail that you need? Did the camera internally modify the raw image information in some way? Did the transfer of the image data from the camera to the computer change the image information in some way? Did the image file format include a lossy compression algorithm that “threw away” important information? Should a watermark have been incorporated into the images to create a reliable time-date stamp and prevent any image manipulation from going undetected? As you

have probably guessed by now, it would be far too late to be asking these questions *after* taking your images! These questions must be answered satisfactorily *before* you begin to take data! Or, if you are presented with existing data, answers to questions such as these can provide insight as to how much to “trust” conclusions based on this data.

Choices made by the user regarding lenses, sensor resolution and sensitivity, camera type, lighting, aperture size, shutter speed (and frame rate for video), object distance, image data file format, compression method (if any), and watermark type (if any) all have serious and usually irreversible ramifications for the quality and usefulness of the images obtained. The purpose of this book is to help familiarize the reader with these issues at a practical level, such that they may make better choices *before* obtaining the needed images. Due to space limitations, we cannot treat these various subjects in great depth, with a full coverage of the underlying theory. For that, individual texts in optics, photodetectors, cameras, compression methods, and so forth would be required. The author has searched for a single text that spans these subjects at a top level that could be used as a practical introduction, but no such book was found. That was the impetus for writing this book. For more depth and theory in each of the areas spanned by this book, please see the references section at the end of this book for some recommended texts and other resources.

What this book is **NOT**: it is not a theoretical optics book, an optical engineering design book, a camera users’ manual, an artistic photography book, or a digital image processing book. However, it touches on all these areas as needed to provide the background necessary for the reader to become more proficient in choosing and using digital cameras and imaging systems.

There are many applications for which digital cameras and imaging system are used, and the requirements and constraints of the particular application must be carefully considered as the reader absorbs and applies the content of this book. Some logical grouping of applications areas includes

- general imaging (such as typical consumer still-image and video use as well as television),
- industrial imaging (primarily machine vision for various manufacturing tasks),
- scientific imaging (which, despite the name, also includes engineering users), and
- military imaging (which by necessity has its own special requirements and constraints).

This book was originally intended primarily for the scientific imaging audience, but as the writing progressed it became clear that major parts of this book apply to all four application areas.

The book begins with a brief introduction to image formation and how it relates to biological eyes. The natural comparison between eyes and cameras then follows. A brief introduction to common optical components is given. Then, a practical treatment of basic optics is provided, followed by a top-level introduction to Fourier optics that can make many optical calculations and predictions rather straightforward. This is followed by a discussion of sensor arrays (such as CCD and CMOS) used in most digital cameras, and what the ramifications are to your data as they record an image. A practical comparison of camera types is then given, followed by a short discussion of lighting and illumination considerations. The last two chapters cover image file issues, such as file format and compression, and watermarks for identification and validation of image data. Appendices provide review and tutorials for the interested reader.

Chapter 2

Imaging, Cameras, and Eyes

ESSENTIALLY all cameras developed by humans in the past and present are in some way a type of *biomimetic* (sometimes called *bioinspired*) imaging sensor. The word biomimetic pertains to human-created designs based upon known biological physiology that evolved in nature. That is, humans studied how various animals *see* the world around them, then applied known principles of optics and light detection to mimic certain aspects of how animal vision systems evolved, and thereby created cameras. Thus, knowing a little bit about eyes can help to better understand cameras. It may interest the reader to note that two optical techniques developed by humans, zoom lenses and Fresnel lenses, have not yet been found in nature. But essentially all other commonly used optical techniques are based on those that are found in nature.

There are at least ten known variants of animal eyes [2,3]. These ten types can be grouped as either non-compound eyes or compound eyes, and the non-compound eyes are what have most often been used to inspire camera design. In particular, the most frequently mimicked type of non-compound eyes on which cameras are based is called the *refractive cornea eye*, which is often informally called a *camera eye*, since it is very similar to how most modern cameras operate. This is the type of eye found in almost all mammals, birds, reptiles, and most other terrestrial vertebrates. The camera eye in animals typically uses a single large-aperture lens or lens system with a relatively large, high resolution array of photodetectors (biologists prefer to call them photoreceptors) in the retina. Of the compound eyes, the three most commonly mimicked types for cameras or vision sensors are the *apposition eye*, the *optical superposition eye*, and the *neural superposition eye*. While some interesting recent work in biomimetic vision sensors is based upon these types of compound eyes, we will not cover that topic here as it is beyond the scope of the discussion [4–6].

Mammals evolved to have eyes that permit a high degree of spatial acuity in a compact organ, along with sufficient brain power to process all the associated spatial and temporal image information. To provide even greater spatial acuity, many mammals developed foveated vision, which is where some special area of the retina has a much higher density of photodetectors, providing a higher degree of spatial acuity for images formed on that part of the retina. While foveated vision camera eyes have a relatively narrow field of view for the highest degree of spatial acuity, they evolved to have ocular muscles that allow them to be moved and scan their surroundings, thereby expanding their effective field of view [3, 7, 8]. However, this required additional complexity and brain function. Some special-purpose cameras use a foveated approach, but the vast majority of cameras use a constant density of photodetectors across the entire array, and that is the type we will concentrate on here.

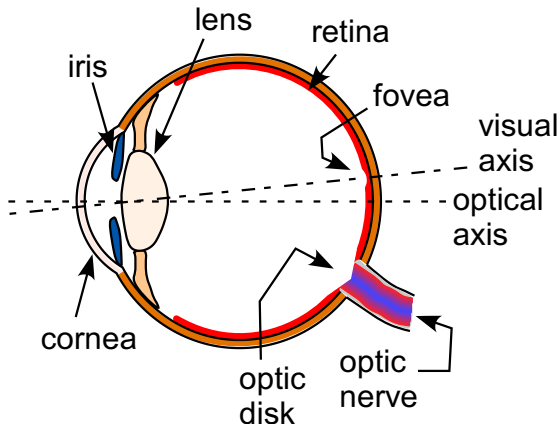


Figure 2.1: Simplified cross-sectional diagram of the human eye. The point of view is looking down on the right eye from the top of the skull.

2.1 Camera eye

Nearly all mammals, including humans, have camera eyes [9–12]. As an example, a highly simplified cross-sectional diagram of the human eye is depicted in Fig. 2.1, and the central retina (at the rear interior of the eye) is shown in Fig. 2.2. All photoreceptors in the eye (called photodetectors in a camera) exist in a given layer of the retina. Some optical terms used in the following discussion will become much more clear in the later chapter (Chapter 4) on basic optics.

The volume between the cornea and the lens (the anterior chamber) is filled with a water-like substance called the aqueous humor; the volume behind the lens (the posterior chamber) is filled with an optically clear but somewhat gelatinous substance called the vitreous humor (or vitreous body). In this type of eye, the primary refractive power is due to the air/cornea optical interface.¹ An additional refractive effect is sometimes provided by an internal lens, such as the variable-shape crystalline lens that humans use to accommodate focus for close objects. The iris (or pupil), a variable-size aperture that is located just in front of the crystalline lens, adjusts as needed to allow more or less light into the eye. The cornea, iris, and lens in a human eye is thus similar to the lens (and associated aperture) used in a camera. The collection of photoreceptors in the retina is similar to the array of photodetectors used in a digital camera.

The use of significant refractive power allows the use of a relatively large aperture in the camera eye, permitting good light gathering and keeping the blur spot acceptably small (necessary for good static acuity) in the short focal distance required of a compact vision organ.² A camera or artificial vision sensor based on a camera eye typically uses a single large-aperture lens or lens system (mimicking the cornea and lens) combined with a relatively large, high resolution focal plane array of photodetectors (mimicking the photoreceptors in the retina).

The human eye is a highly complex sensor that responds to electromagnetic (EM) stimuli at wavelengths from approximately 400–700 nm [11–13]; for obvious reasons this band is called the *visible wavelengths*. See Fig. 2.3. Ambient light enters the cornea, passes through the anterior chamber (containing the aqueous humor), through the pupil opening of the iris (that determines the effective aperture size), through the crystalline lens, and then passes through the vitreous humor before coming to focus at the retina. The retina consists of many layers of neural

¹Aquatic mammals must use a lens as the primary refractive element, since the index of refraction of water is very close the index of refraction of the corneal tissue and aqueous humor.

²Due to aberrations in the human eye, the actual point spread function (PSF) is somewhat larger than the diffraction-limited Airy disk described in the next chapter, and it has an approximately Gaussian shape. Aberrations are greater, and hence the PSF is wider, for larger pupil diameters.



Figure 2.2: Ophthalmic fundus camera image, approximately 50 deg field of view (FOV), of the central retina in the human eye. A normal right eye is shown. The bright disc seen toward the right of the image (patient's nasal side of the eye) is the optic disk (blind spot), where the optic nerve meets the eye; the darker region in the center of the image is the fovea. A normal array of blood vessels can also be seen that is providing oxygen to the inner retina.

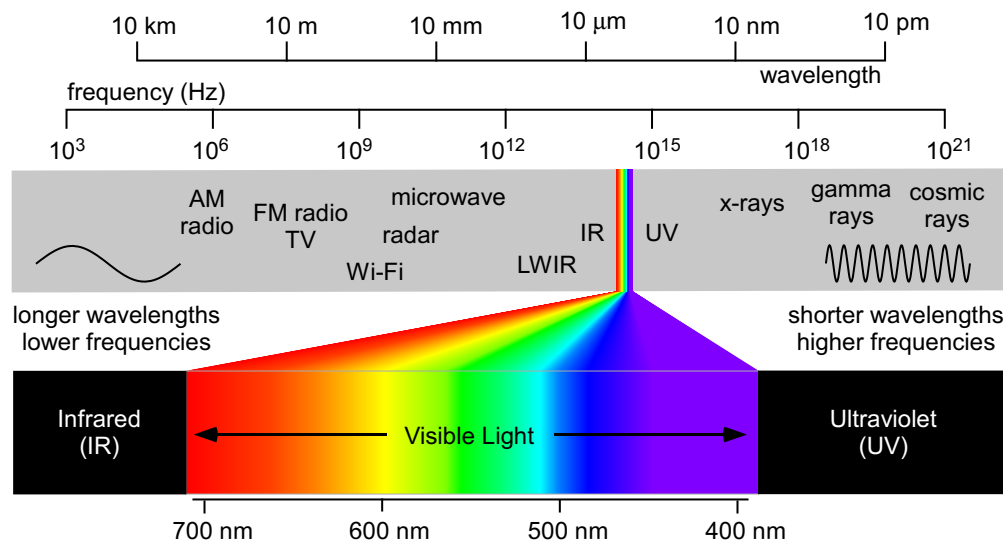


Figure 2.3: The electromagnetic (EM) spectrum, with the visible wavelengths expanded.

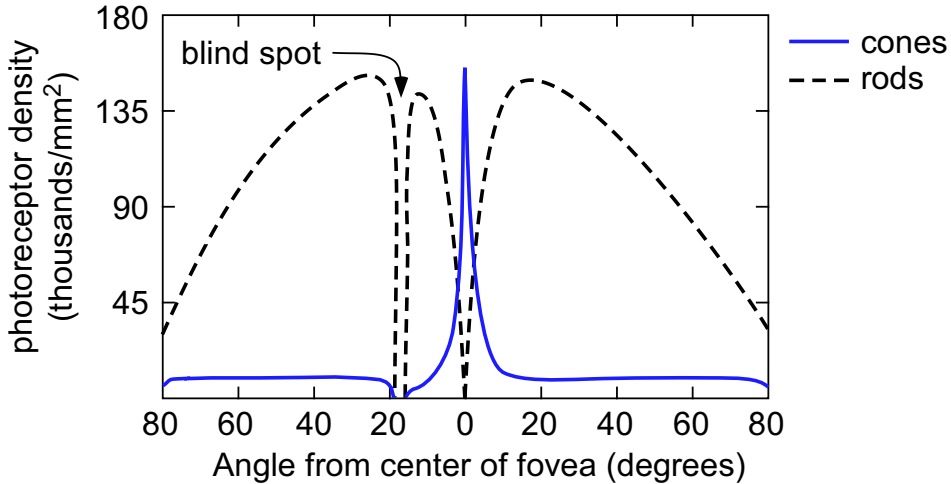


Figure 2.4: The distribution of photoreceptor density in the human retina, shown for both cones and rods. The angle is with reference to the visual axis shown in Fig. 2.1.

tissue that contains, among other things, the photoreceptors (rods, cones, and the non-imaging photosensitive ganglion cells). Note that the centered optical axis shown in Fig. 2.1 is slightly different from the physiological visual axis; while both pass through the nodal point (optical center) of the eye, the latter is referenced to the fovea, which is the area of highest acuity vision on the retina. A diagram depicting the distribution of photoreceptor density in the human retina is shown in Fig. 2.4. Note that this figure implies a maximum density of photoreceptors at the center of the fovea to be approximately 150,000 cones/mm², which translates to minimum linear separation between photoreceptors in the central fovea to be about 2.6 μm.

2.2 Reduced eye model

To help ease practical calculations related to the optics of the human eye, a simplified version of Helmholtz's schematic eye called the *reduced eye model*, shown in Fig. 2.5, is often used [9, 14]. Note the distances labeled as s_o and s_i in Fig. 2.5; these relate to the Gaussian lens equation,

$$\frac{1}{s_o} + \frac{1}{s_i} = \frac{1}{f}, \quad (2.1)$$

that will be explained in more detail in the next chapter. Compare Fig. 2.5 to Fig. 2.1. In the reduced eye model, there is a single refractive surface having a 5.5 mm radius of curvature, and a posterior nodal distance (from the nodal point to the retina) of 16.7 mm. Thus 16.7 mm would be used as the constant value for the image distance s_i in Eq. (2.1), since that is fixed by the size of the eye, and the focal length f in Eq. (2.1) would change as needed (by adjusting the accommodation of the crystalline lens) as the object distance s_o changes. This keeps the image in clear focus on the retina.

Unlike cameras, in which the photodetector array is typically a flat plane, the human retina is curved. A simple method of estimating spatial distances on the curved surface of the retina with sufficient accuracy is often helpful. The reduced eye model of Fig. 2.5 provides a straightforward technique to convert between angular span and spatial distance on the curved retina. Since a ray passing through the nodal point is by definition an undeviated ray, an angular span in degrees can be equated to a spatial distance on the retina by:

$$16.7 \text{ mm} \cdot \tan(1^\circ) = 291.5 \mu\text{m}/\text{deg}. \quad (2.2)$$

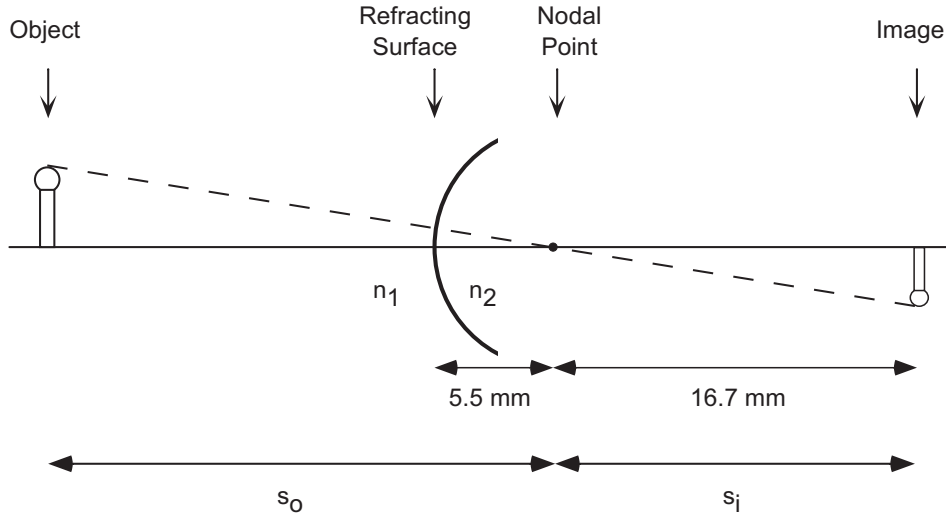


Figure 2.5: The reduced eye model for simplified calculations of human retinal distances.

As an example, the optic disk³ in a typical human eye is roughly circular and has a mean diameter of $1800 \mu\text{m}$ [15]. This value has been found to be nearly constant in all humans regardless of race, gender, or age and is often used as a “yardstick” in fundus photographs [16]. From Eq. (2.2), we see that the optic disk subtends an arc of roughly 6.2° .

Note that because the human eye is not truly spherical, these distance calculations become less accurate as one moves away from the region of the fundus near the optic disk and fovea often referred to as the posterior pole [17]. However, the peripheral regions of the retina have no critical vision anatomy, and so are not of great interest to designers of cameras or vision sensors. Therefore, the approximation of Eq. (2.2) will usually suffice.

2.3 Comparing cameras to eyes

It may be desirable to compare the spatial resolution of a digital camera to that of the human eye. Recall that the minimum spacing of photoreceptors in the fovea is about $2.6 \mu\text{m}$. An often quoted resolution limit for the human eye (based only upon the diffraction-limited point spread function of the pupil) is roughly 1 min of arc (equivalent to approximately $4.9 \mu\text{m}$ on the retina at the posterior pole of the eye); this assumes a 2 mm diameter pupil and illumination wavelength of 550 nm [18]. A *normal* (i.e., emmetropic) human eye that measures 20/20 on a standard eye chart sees with a resolution of approximately 1 minute of arc. Perhaps not coincidentally, the minimum separation of individual photoreceptors in the fovea [9], and the sampling theorem requirement of at least two samples per cycle of spatial frequency [19], together yield a physiological resolution limit for the eye of $(2)(2.6 \mu\text{m}) = 5.2 \mu\text{m}$, or just over 1 minute of arc [20], closely matching the theoretical optical resolution limit due to the diffraction-limited cutoff frequency of a 2 mm pupil in daylight, as well as the empirical resolution found in humans.⁴ This implies that evolution “tuned” the optics and the photodetector spacing in the human eye for the greatest efficiency. As a side note, certain types of acuity in human vision, such as vernier acuity, have been shown to exceed a resolution of 1 minute of arc, most likely due to higher level processing in the brain’s visual cortex [9].

A comparison of the spectral sensitivity of a typical silicon-based charge-coupled device

³The optic disk, shown in Fig. 2.2, is the nearly circular “blind spot” where the optic nerve exits the orb of the eye; no photodetectors exist inside the area of the optic disk.

⁴All these optical terms will be discussed in later chapters.

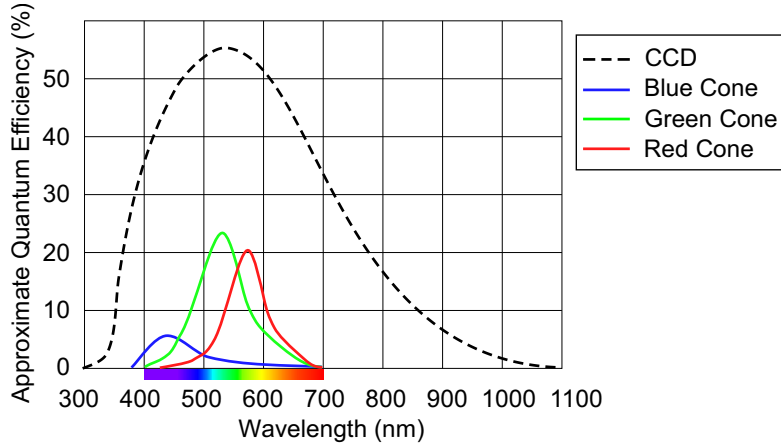


Figure 2.6: Comparison of the spectral sensitivity of a typical CCD array to the three types of cones in the human eye.

(CCD) imaging array in a digital camera to that of the human eye is also interesting; see Fig. 2.6. Note the CCD array can detect EM radiation well into the infrared region (although these wavelengths are significantly attenuated by most standard lens glass). CMOS (complementary metal oxide semiconductor) arrays are also typically silicon-based, and have very similar spectral sensitivity. These points will be discussed further in later chapters.

As mentioned earlier, the camera eye, of which the human eye is a particularly good example, is the basis from which nearly all standard cameras and vision sensors designs are derived. An optical system is used to bring an image to focus on a focal plane array (FPA), which then spatially samples the image. The FPA typically is rigidly attached to the sensor or camera frame, and cannot move. The focal length of the lens system is also typically fixed (except for zoom lenses).⁵ If some particular object distance s_o is desired using a camera, the optical center (i.e., nodal point) of the lens or lens system must be moved axially to ensure that the image distance s_i determined by Eq. (2.1) is equal to the distance between the nodal point and the fixed FPA, thus keeping the image in focus on the FPA. This mechanical movement of the lens nodal point is performed automatically inside the lens casing of a typical photographic lens system as the focus distance is changed on the lens; no operator adjustment is required. The very simple camera eye model just described can be used to analyze or design a wide variety of cameras and vision sensors, at least for a first level of approximation.

Many optical terms have been used in this discussion of the eye without specifically defining them, in the interest of brevity. The next chapters include a more complete discussion of practical optics and sensors as related to cameras, in which these terms are more formally defined.

2.4 Problems

1. blah blah
2. blah blah
3. blah blah

⁵In photography, a fixed focal length lens is often called a *prime* lens. A prime lens is designed to be optimum at its fixed focal length, whereas a zoom lens must be designed with unavoidable compromises to operate acceptably over some range of focal lengths. Thus the highest quality lenses are typically prime lenses.

Chapter 3

Optical Components for Imaging

BEFORE exploring various calculations that are useful for the optics used in digital cameras and imaging, a brief introduction of optical components is helpful. This chapter constitutes a “quick tour” of some common optical components that apply to imaging and sensors in the context of typical engineering and scientific use. This is *not* an exhaustive treatment of all the types of optical elements and devices—that would require an entire book all by itself. More detail can be found in [10, 18, 20–30]

Which optical components are most applicable to cameras, image sensors, and typical optical setups used by engineers and scientists? A partial list would include:

- lenses,
- apertures,
- shutters,
- mirrors,
- certain types of prisms,
- certain types of beamsplitters,
- polarizing filters, and
- components for low-light conditions

3.1 Lenses

One of the most important categories of optical components for digital cameras is that of lenses. There are many, many types and variations of lenses. For example,

- some are positive (converging) lenses;
- some are negative (diverging lenses);
- some have curvature on both sides;
- some have curvature on just one side, and a planar (flat) surface on the other side;
- some are spherical in curvature;
- some are aspherical in curvature; and
- some (most) have antireflective coatings.

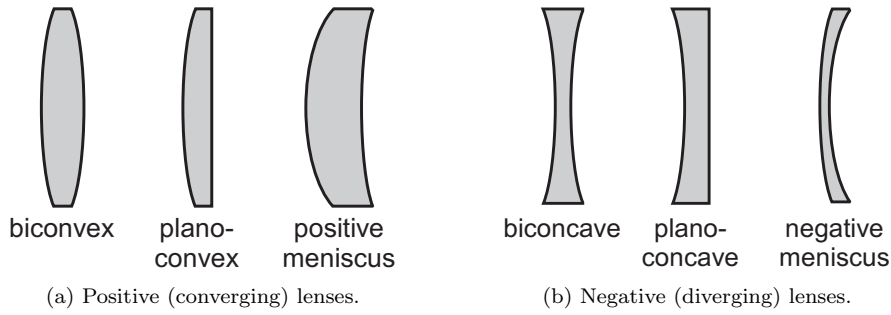


Figure 3.1: Common types of lenses.

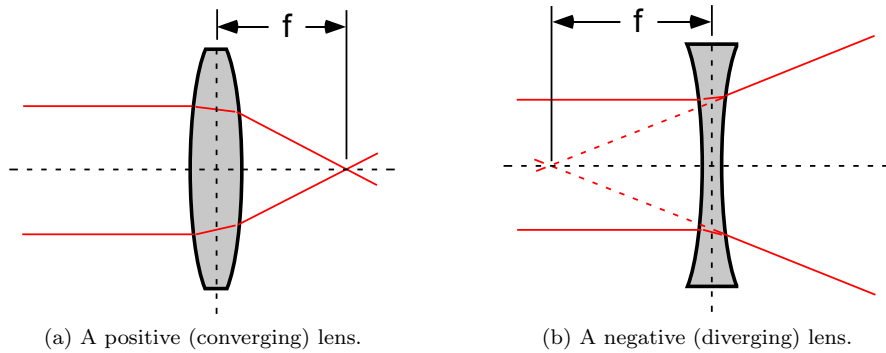


Figure 3.2: Interaction of light rays with positive and negative lenses.

Multiple lenses can be combined into one lens system; this is the most common configuration for camera lenses. As mentioned previously, a lens system with a fixed focal length is called a *prime* lens. A lens system with a variable focal length is called a *zoom* lens. Some lenses have additional capabilities, such as autofocus and/or image stabilization, which require communication between the lens system and the camera body. There is no such thing as a perfect lens; all have *aberrations* that degrade the quality of an image formed with the lens.

Some common shapes for individual positive and negative lenses, and their associated names, are shown in Fig. 3.1. A positive lens is also called a converging lens because light rays from a distant source (at the *object plane*) will converge to a focal point (at the *image plane*) on the other side of the lens. This can be seen in Fig. 3.2(a). A negative lens is also called a diverging lens because light rays from a distant source will appear to diverge on the other side of the lens; this results in a virtual focal point on the same side of the lens as the light source. This can be seen in Fig. 3.2(b).

The distance between the optical center of the lens (also called the nodal point) and the focal point, along the optical axis, is called the focal length f of the lens. Note that many commercial lens systems show what is called focal distance marked on the outer body of the lens, but that value is not quite equal to the value f defined here. The focal distance marked on a commercial lens body is the distance from the plane of focus (the object plane) to the image plane (where the sensor or film is located). An asymmetrical lens may have two different focal lengths for the two possible orientations of the lens. The focal length is given in units of linear distance, most commonly millimeters. The reciprocal of the focal length is called the power of the lens; if the focal length is expressed in meters, then this reciprocal value is the power of the lens in units called diopters. In addition to the focal length, another important lens parameter is the diameter, which is also usually expressed in millimeters.

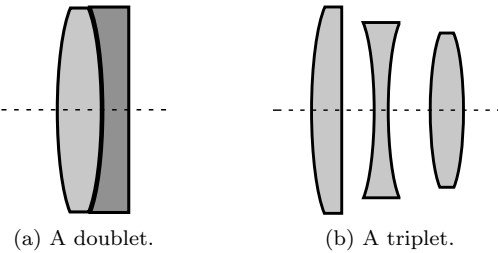


Figure 3.3: Multiple simple lenses used in combination to reduce overall aberrations.

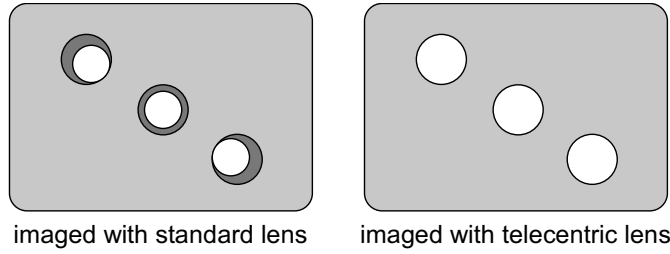


Figure 3.4: Simulated images taken with a standard lens versus a telecentric lens.

One reason multiple simple lenses are combined into a lens system is to reduce the overall aberrations of the system compared to the aberrations of any single lens. Lenses of different materials, such as crown glass and flint glass, have different properties such as the indices of refraction, dispersion of various wavelengths, etc. These differences are used to design an overall lens system that can produce a higher quality image than any single lens by itself. Two very common lens combinations are the doublet and the triplet shown in Fig. 3.3. This will be explained further when aberrations are more fully discussed.

Multiple lenses and an aperture can be designed in a special way to achieve what is called a *telecentric* lens. In this type of design, only parallel principle rays of light from the object are allowed through the aperture opening to form an image at the image plane. While this design cuts down the amount of light gathered by a lens, it greatly reduces changes in image size when the object distance changes (i.e., the lens exhibits constant magnification), but only over a limited distance called the *telecentric range* of the lens. This characteristic also reduces perspective distortions of the object. It is important to note that standard object-image calculations discussed in Chapter 4 do **not** apply to telecentric lenses. A simulated comparison of two images, one taken with a standard lens and one taken with a telecentric lens, is shown in Fig. 3.4. The object is a thick metal plate with three holes drilled in it. Telecentric lenses are used in applications such as machine vision to measure object sizes (i.e., metrology) and microlithography (e.g., for IC manufacturing). As a result of the extra constraints on a telecentric lens, they are larger, heavier, and more expensive than standard lenses of similar focal length. Variations such as object-space telecentric, image-space telecentric, and double telecentric are available. This is a specialized topic; for more information consult catalogs or web sites of lens manufacturers.

3.2 Apertures

Another very important category of optical component is that of apertures. An aperture is the “hole” through which light passes on its way to the image plane. The size (i.e., area) of the aperture opening is a very important parameter in forming an image. Most camera lens systems include a variable aperture incorporated inside the lens housing.

The aperture opening determines how much light is allowed to pass through the lens; this

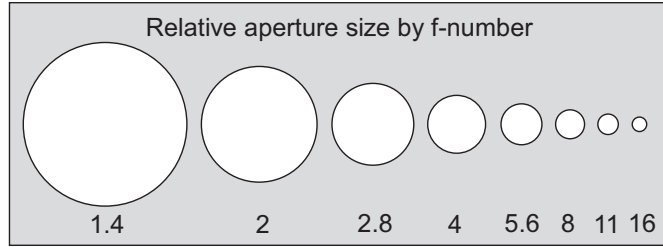


Figure 3.5: Comparison of the relative aperture size for a given focal length according to the f-number. Larger f-numbers mean smaller apertures.



Figure 3.6: Comparison of the largest (f/1.4) and smallest (f/16) aperture available for a Minolta 50 mm f/1.4 prime lens. [31]

amount of light is proportional to the area ($A \approx \pi r^2 = \pi d^2/4$) of the opening.¹ This, combined with shutter speed and the sensitivity of the sensor array, determine what is called the *exposure* of the image. The aperture also limits the angle of the light rays that are allowed through the lens, which has an effect on what is called the *depth of field* of an image. Both of these concepts are explored in more detail in later chapters.

For cameras, most apertures are part of a lens system that has a specific focal length. The ratio of the focal length to the aperture diameter is called the *f-number*. Common f-numbers for commercial lenses are 1.4, 2, 2.8, 4, 5.6, 8, etc. The larger the f-number for a given focal length, the smaller the aperture size. This can be seen in Fig. 3.5. The f-number is often written compactly as f/#, such as f/1.4. This notation does **not** imply an extra division operation; the division of focal length by aperture diameter has already been performed to arrive at the f-number. Another notation is as a ratio, such as 1:1.4. The f-number is also sometimes abbreviated as *N* in some equations.

Note the progression of f-numbers listed is related by a factor of $\sqrt{2} \approx 1.414$, because to double (or halve) the area of the aperture opening, the diameter must change by a factor of $\sqrt{2}$. A doubling or halving of the aperture areas is called a change of one “f-stop.” For example, a change from f/1.4 to f/2 is a change of one f-stop, and when set to f/2 only half the light is admitted to the sensor compared to when it was set to f/1.4.

An example of the same lens with large and small aperture settings can be seen in Fig. 3.6, which shows a Minolta 50 mm f/1.4 lens, with the aperture “wide open” to f/1.4 and “closed down” to f/16. Note that a commercial lens such as this is typically specified by its focal length and its largest aperture.

In later chapters, we will use the aperture size to calculate and predict various important aspects about image formation. To enhance the clarity of the calculations, we will often use

¹The equation is written as $A \approx \pi r^2$ instead of $A = \pi r^2$ because the aperture is only approximately circular.

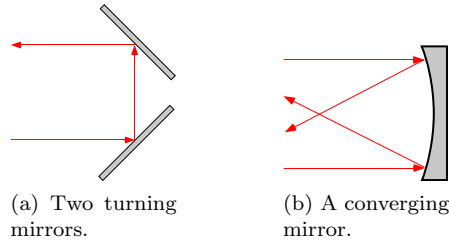


Figure 3.7: Examples of mirrors as used in many optical designs.

the aperture diameter and the focal length of the lens separately rather than combined into f-number. But most experienced camera users will refer to the f-number.

3.3 Shutters

A shutter is a device or method by which you can “turn on” and “turn off” light gathering by the camera’s sensor array. Some shutters are mechanical, as in a very fast, high precision “curtain” which opens only for a desired period of time, then closes again. Some shutters are electronic, in that resetting the sensor array and reading out the accumulated charge due to the incident photons after a given period of time accomplishes the same effect as a mechanical shutter. In mathematical terms, the shutter speed determines the *integration time* of light on the sensor. As mentioned above, shutter speed, aperture size, and sensor sensitivity taken together determine exposure of an image. The shutter speed also determines the amount of “blur” moving objects have in an image. These concepts are explored more fully in later chapters.

3.4 Mirrors

Mirrors are used in many optical systems designs. The primary use of a mirror is to change the direction of light propagation. For example, a 45-degree planar (flat) mirror can be used to change the direction of light by 90 degrees (albeit with an accompanying image reversal). Two 45-degree mirrors can change the light propagation direction by 180 degrees, as shown in Fig. 3.7(a). Such flat mirrors are sometimes called *turning mirrors*. A concave-curved mirror (often with a parabolic curvature) is called a converging mirror or a focusing mirror, since it brings light to convergence (focus) at its focal distance. This is shown in Fig. 3.7(b).

Mirrors can be used to “fold up” an optical design into a more compact space, such as the Schmidt-Cassegrain telescope. The light path of the Schmidt-Cassegrain design is shown in Fig. 3.8(a); lenses for the telescope eyepiece would be mounted at the right of the telescope housing. When both reflection (mirrors) and refraction (lenses) are used in an optical design, it is called a *catadioptric* optical system. A Minolta 500 mm f/8 catadioptric lens mounted on a Sony Alpha 55 camera is shown in Fig. 3.8(b).

Mirrors and partially-mirrored surfaces are also used to create an optical “cavity” that resonates at a specific wavelength to create a laser beam. Another use of mirrors is to steer a light source (such as a laser) to a specific point on a target plane, as depicted in Fig. 3.9. The small electric motors used to rotate the steering mirrors are called *galvanometers*. The timing and angles of the mirror deflections can be easily set to produce a full *raster scan* of the target plane, and the captured reflectance of such illumination produces a 2-D image of whatever objects exist at the target plane.

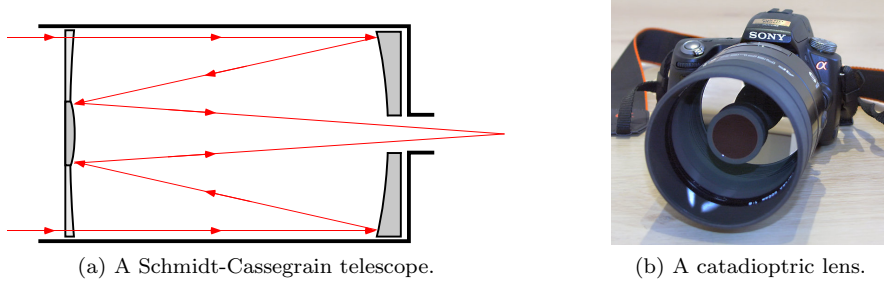


Figure 3.8: Examples of how mirrors can be used to “fold up” a long focal length optical design into a compact space. Credit for (b): [32]

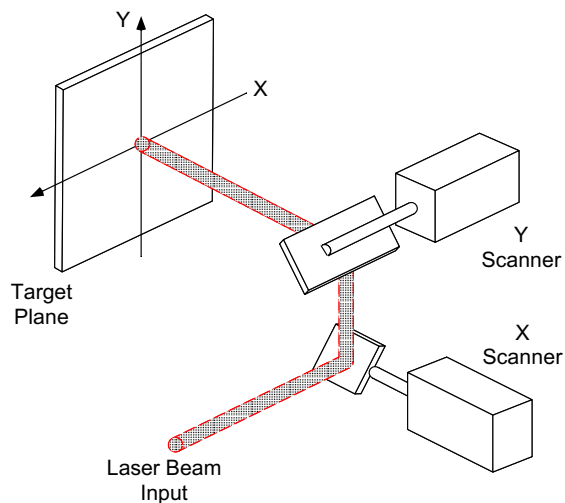


Figure 3.9: Diagram of two partially rotating mirrors, mounted in quadrature, that can steer a light source such as a laser beam to any location on the target plane.

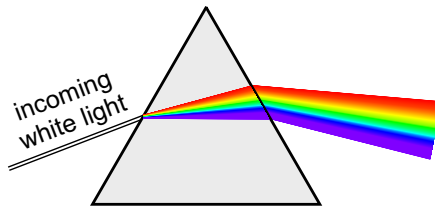


Figure 3.10: Illustration of how a prism can separate white light into the various constituent wavelengths.

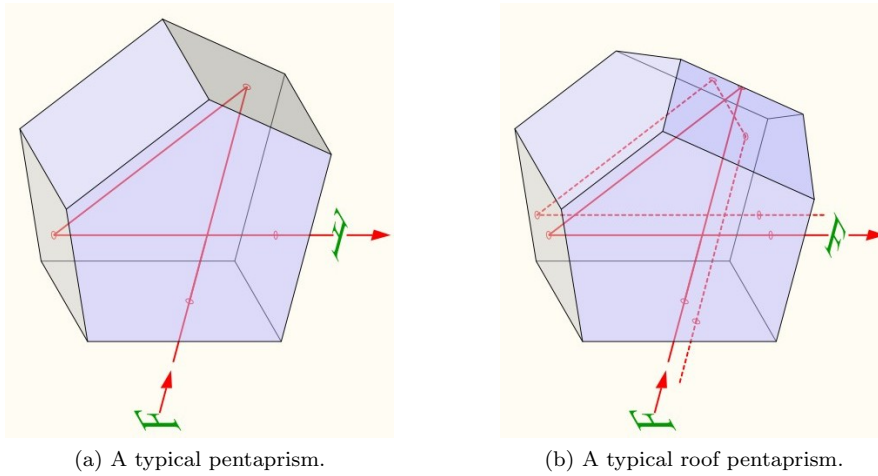


Figure 3.11: Examples of how pentaprisms can be used to redirect light in a compact form factor.
Credit for (a): [33] Credit for (b): [34]

3.5 Prisms

Prisms are used in a wide variety of optical designs. Most people are familiar with how prisms can be used to separate white light into the various constituent wavelengths,² as shown in Fig. 3.10. However, in the context of cameras, a common type of prism is the *pentaprism*, a five-sided glass or plastic component which includes two internally reflective surfaces. A pentaprism redirects light by a constant 90 degrees without the image reversal that would occur if a single 45 degree mirror was used. A six-sided variant (with three internally reflective surfaces), called a *roof pentaprism*, is more common in cameras.

A standard pentaprism is shown in Fig. 3.11(a). The figure shows how it redirects light by 90 degrees, yet maintains the “up-down” and “left-right” orientation of the source image. The roof pentaprism, shown in Fig. 3.11(b), preserves the “up-down” orientation of the original source, but intentionally “flips” the “left-right” orientation. This latter type of prism is used in single lens reflex (SLR) camera designs to redirect light from the SLR focusing screen to the viewfinder eyepiece. The “left-right” flip is needed to produce the correct image orientation to the camera user looking into the viewfinder at the eyepiece. As will be explained in Chapter 4, the camera lens inverts the image, both “up-down” and “left-right.” The internal reflex mirror in the SLR, due to its orientation, corrects the “up-down” but not the “left-right” image reversal. Thus the roof pentaprism performs the remaining needed “left-right” reversal. The interior design of the SLR will be discussed in a later chapter. The shape of the roof pentaprism is the reason many SLRs are somewhat triangular on top.

²Other methods, such as diffraction gratings, can also separate white light into its various wavelengths.

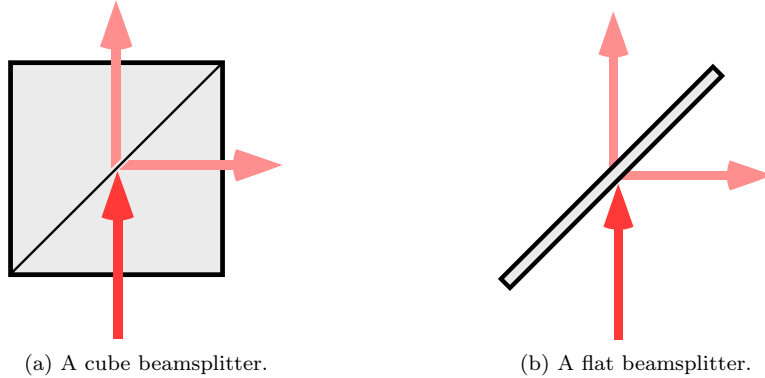


Figure 3.12: Two common types of beamsplitters. A single incoming light path is split into two outgoing paths, typically 90 degrees from each other.

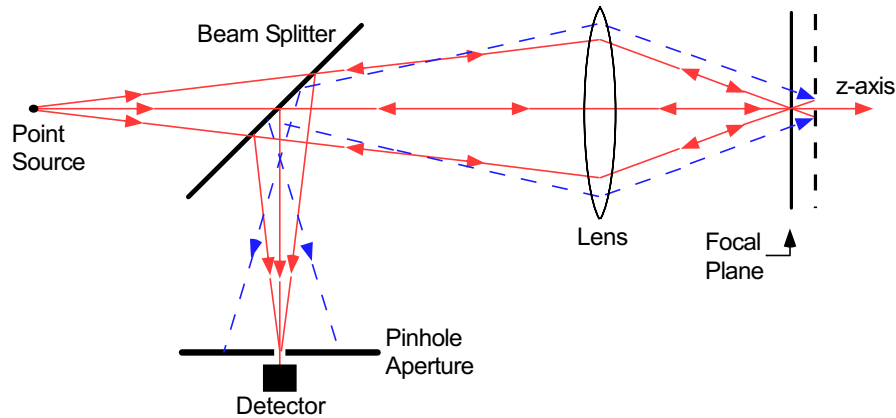


Figure 3.13: Simplified diagram of a confocal imaging system. Only light reflected from a specific depth along the z -axis is allowed through the pinhole aperture to the photodetector.

3.6 Beamsplitters

A beamsplitter is a device which takes one incoming light path, and splits it, typically into two outgoing paths. Most commonly, one of the two outgoing paths is a continuation of the incoming direction and the other direction is rotated 90 degrees. The two most common types of beamsplitters, shown in Fig. 3.12, are cube and flat. Cube beamsplitters are generally inexpensive, and are available in many sizes. Flat beamsplitters tend to be more expensive but more compact, and exhibit fewer undesirable internal reflections that are common to cube beamsplitters.

Beamsplitters are usually quite sensitive to the wavelength and polarization of the incoming light. While a 50/50 beamsplitter is common, other ratios of the two outgoing beams are also available. Some beamsplitters are used as simple “pass through” glass in one direction, but their reflective properties in the opposite direction are critical to the overall optical design.

Beamsplitters, as used in many optical setups, are typically located external to a camera. As part of a larger optical design, beamsplitters can help create an imaging system that may or may not even use a traditional camera. For example, a simplified diagram of a confocal imaging system that uses a photodetector rather than a camera is shown in Fig. 3.13. The beamsplitter and the pinhole aperture are both vital to the correct operation of the system, which only allows light to be imaged that is reflected from a specific depth along the z -axis. Light from other depths is rejected. Note the beamsplitter is used as just “pass through” glass to get light from



(a) Photo taken without (left) and with (right) a polarizing filter.



(b) Without a polarizing filter.

(c) With a polarizing filter.

Figure 3.14: Examples of images taken with and without a polarizing filter. The bottom two images are of a cranchiid squid (also called a glass squid), observed during NOAA’s Operation Deep Scope Expedition of 2004.

the point source to the sample. The return light path is reflected down to the aperture.

3.7 Polarizing Filters

Polarization of light will be discussed more fully in Chapter 4 as part of the discussion on refraction and reflection. For the context of this chapter, recall that the polarization state of light can be linear (at any angle perpendicular to the path of light propagation), circular (rotating clockwise or counterclockwise), or some combination. Randomly polarized light is often called unpolarized, but since any light reflected from a non-metallic surface becomes polarized to some degree, most ambient light in an uncontrolled environment has a significant level of polarization.

Polarizing filters allow the user to modify the polarization of light that is recorded for an image. There are artistic reasons for doing so, such as making the sky appear to be a deeper blue or to make vegetation appear to have a more lush green appearance, but for technical users the reasons usually are either to control undesirable reflections (since reflected light tends to be highly polarized) or to select the polarity of the light being recorded. Examples of images taken with and without a polarizing filter are shown in Fig. 3.14.

A polarizing filter is designed to pass through only light with a certain angle of linear polarization. The filter can be manually rotated to allow the user to select the desired polarization angle. **Important note:** Users of modern cameras should be aware that features such as automatic exposure control and autofocus will not work correctly with linearly polarized light. In response to this, newer polarization filters have two stages of polarization: in the first stage, only linear polarized light of the desired angle is allowed to pass; then in the second stage the linearly polarized light is converted to circularly polarized light that allows modern cameras to work properly. This two-stage process can be seen in Fig. 3.15. These newer filters are sometimes called *circular polarization filters*. Older linear polarizing filters, intended for film cameras, should not be used with modern digital cameras.

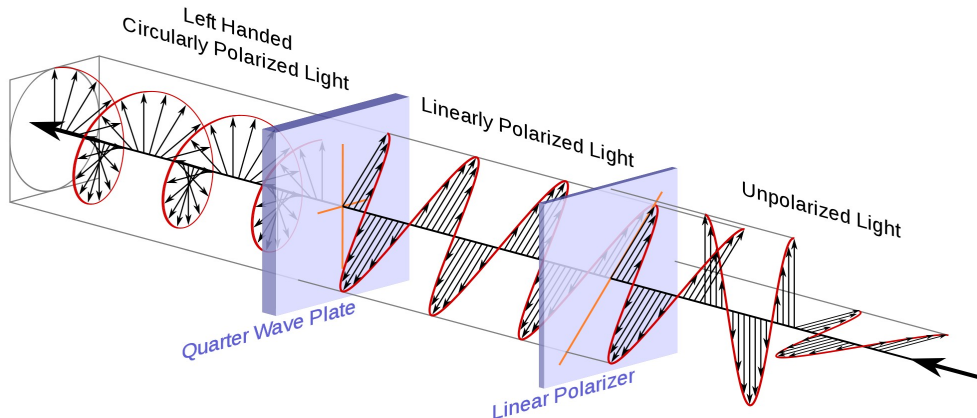


Figure 3.15: Conceptual diagram of how a modern circular polarization filter works.

3.8 Components for Low-Light Conditions

Many times, engineers and scientists who are using imaging in their work find the need to operate in low light situations. This challenges even the best cameras and imaging detectors. For low light situations, the two primary concerns are light amplification and noise reduction.

3.8.1 Light Amplification

Light amplification is just what the term implies: we find a way to take very few photons, and somehow turn that into a strong, usable signal. We need to differentiate between devices that to a large degree preserve the (x, y) spatial relationship of the incoming photons, and those that do not. The former devices are called intensified imaging devices, because they naturally preserve the 2-D image. The latter devices, often called point detectors, simply magnify the signal due to the incoming photons regardless of from where in the (x, y) plane they arrive, and these devices do not by themselves form a 2-D image. However, with the addition of scanning or light-steering optics (such as shown in Fig. 3.9), the signal may be associated with a point on the (x, y) plane and a rudimentary image can then be formed.

As implied above, an intensified imaging device amplifies the intensity of available light in an optical system, while largely preserving the 2-D spatial relationship of the image. It allows usable images to be produced in low-light conditions, but typically comes at the expense of reduced image resolution and increased noise. Often, an *image intensifier* stage is coupled to a focal plane array detector such as a charge-coupled device (CCD) array or a complimentary metal-oxide semiconductor (CMOS) array. Typical image intensifiers have three main components: a photocathode, an electron multiplier such as a microchannel plate (MCP), and a phosphor screen; see Fig. 3.16. This is the same technology used in night vision goggles. Note that due to the characteristics of the phosphor screen, the low-light image is nearly monochromatic. An image intensifier can also be used to covert light from one band of wavelengths to another. Devices in this category include intensified CCD (ICCD) and intensified CMOS (ICMOS). Another type of image-preserving low light sensor array is the electron-multiplying CCD (EMCCD); the EMCCD employs a different method to produce a usable image in very low light. Each of these devices is rather specialized and have various trade-offs and limitations; for more information, consult reference [35] as well as catalogs or web sites of the appropriate manufacturers.

The most well-known low light point detector is the photomultiplier tube (PMT). PMTs, a type of vacuum tube, have very high sensitivity, low noise, and fast response times. They can be used to directly magnify light in the UW, visible, and IR wavelengths, depending upon the type of photocathode used. If coupled with a scintillator, other forms of radiation such as x-rays, gamma

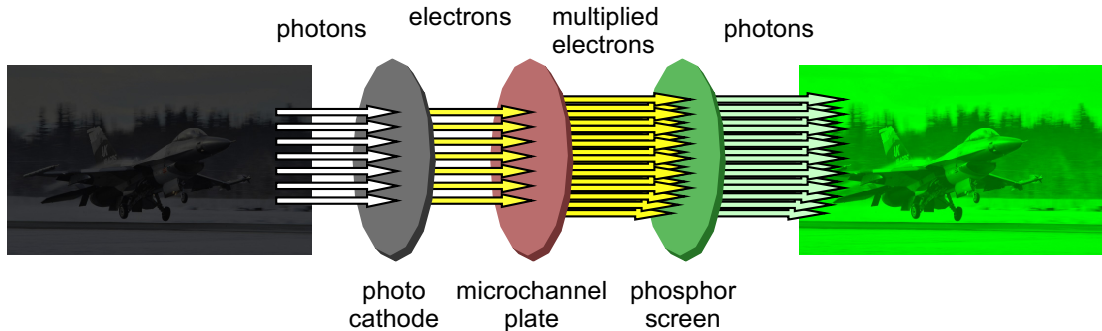


Figure 3.16: Conceptual diagram of how a generic image intensifier works.

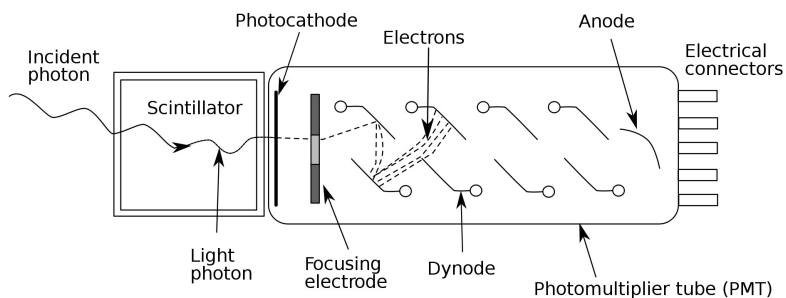


Figure 3.17: Schematic diagram of a photomultiplier tube, coupled to a scintillator.

rays, or neutrons can be detected by a PMT. Such an arrangement is shown in Fig. 3.17. In a PMT, photons strike the photocathode, which emits electrons due to the photoelectric effect. The electrons are directed, via a focusing electrode, to an electron multiplier. The electron multiplier is most often a discrete series of increasingly positive voltage dynodes that exhibit secondary emission of many more electrons than the number that struck the dynode.³ Following the series of dynodes, the greatly amplified number of electrons are captured by the anode, and produce an electrical output signal. Note that, unlike the image intensifier, the multiplied electrons are never converted back to photons. As an alternative to PMTs, semiconductor devices such as avalanche photodiodes can also be used as low light point detectors, but they lack the massive amplification gain of the PMT.

3.8.2 Noise Reduction

While PMTs exhibit low noise, devices such as ICCDs and ICMOS typically require extra effort to reduce the noise level, particularly noise due to *dark current*. Dark current occurs when a pixel location in a detector array emits an electron due to thermal fluctuations rather than due to a photon arrival. Reducing the temperature of the detector array reduces the dark current, so some sort of cooling mechanism is often used. One of the most common cooling mechanisms used for devices such as ICCDs or ICMOS is based on the thermoelectric effect (i.e., the Peltier effect). A thermoelectric cooler (TEC) is a two-sided device, which “moves” heat from one side (the detector array side) to the other side (where a heat sink dissipates heat) when DC current is applied. Other cooling approaches use either air or liquid heat exchangers.

Another technique for reducing the effects of dark current is to incorporate on the sensor array

³While discrete dynodes are the most well known type of electron multiplier for a PMT, other types such as microchannel plates are used in some designs.

some number of non-imaging photodetector sites, typically around the periphery of the array. These photodetector sites are identical to imaging photodetector sites, but they are covered with an opaque mask by the array manufacturer. The idea is that any electron generation from the non-imaging photodetector sites must be due to dark current. An average value of the “signal” due to this non-imaging dark current can then be subtracted from the imaging signals to help cancel out effects of dark current. For highly critical scientific imaging applications, the fact that dark current varies a small amount from one pixel site to another makes this method insufficient. For such critical applications, the imaging part of the sensor is temporarily covered and the resulting “signal” due to dark current is recorded for every pixel location. This pattern of dark current “signal” can then be subtracted on a pixel-by-pixel basis.⁴ By combining a “dark” image signal with a “very bright, near saturation” signal, adjustments can be made that both mitigate dark current and also correct for non-linear photodetector response. More detail on such techniques are beyond the scope of this book, and are highly dependent on the specific application.

3.9 Other Components

Only a small subset of optical components, those common to most imaging setups, were discussed in this chapter. More specialized situations may require other types of optical components. An incomplete list of other components would include: collimators, beam expanders, lasers (diode, gas, or solid state), acousto-optic modulators (also called Bragg cells), electro-optic modulators, optical fibers, optical waveguides, fiber Bragg gratings, diffraction gratings (transmission or reflective), Fresnel prisms, neutral density filters, wavelength-dependent filters, and waveplates.

Any optical setup also needs to hold the components in the proper position, and given the very small optical wavelengths involved, even tiny misalignments can ruin a setup. Therefore, it is prudent not to skimp on ancillary components such as mounts, holders, brackets, clamps, rails, positioners, optics tables, and so forth.

3.10 Helpful Organizations and Vendors

If one is new to the world of optics and imaging, the field can seem overwhelming. For help with general photography topics, there are many websites, but a good starting place is Cambridge in Colour (<http://www.cambridgeincolour.com/>). On a more technical level, two related professional societies for engineers and scientists are SPIE, the international society for optics and photonics (<http://spie.org/>); and OSA, the Optical Society of America (<http://www.osa.org/>). The Optics.org web portal (<http://optics.org/>) has many informative documents and product reviews. Two of the better known vendors of optical components are Newport Optics, which offers very high quality but typically very expensive products (<http://www.newport.com/>), and Edmund Optics Worldwide, which also offers many types of components, but at a broader range of prices (<http://www.edmundoptics.com/>).

⁴This pixel-by-pixel variation is a component of what is often referred to as “fixed pattern noise.”

Chapter 4

Basic Optics and Imaging

THE author has found that one of the most common problems encountered by engineers and scientists using digital cameras or other imaging sensors for serious use is a misunderstanding of fundamental optics and image sampling concepts. Therefore, an introduction to optics is provided here (and sampling is mainly covered in Chapter 6 and Appendix B). This book is by no means meant to be an exhaustive reference for optics or optical engineering. In just a modest number of pages, information is covered that spans many books. Only enough detail is included here that experience has shown is most important to the majority of digital camera and imaging device users. For more detail, see Refs. [10, 18, 21, 22, 24, 26, 36–43]. For the purpose of this discussion, incoherent light sources are assumed; coherent light sources such as lasers require a slightly different treatment. Non-traditional imaging modalities, such as light-field cameras, and special cases, such as telecentric lenses, are also not discussed here. The reader should already be familiar with the basic optical components that are often used for imaging, as discussed in Chapter 3.

4.1 Object and image distances and sizes

A clear image can be formed when light, reflected from an object or scene (at the object plane), is brought to focus on a surface (at the image plane). In a camera, the film or sensor array is located at the image plane to obtain the sharpest image. One way to create such an image is with a converging lens or system of lenses. A simplified diagram of this is shown in Fig. 4.1, which identifies parameters that are helpful for making some basic calculations. One such basic

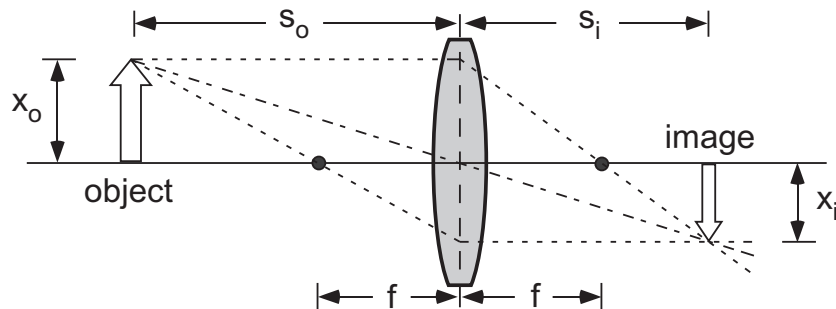


Figure 4.1: Distances for object (s_o) and image (s_i) with a single lens of focal length f .

calculation utilizes the *Gaussian lens formula*, also called the thin lens formula, given as

$$\frac{1}{s_o} + \frac{1}{s_i} = \frac{1}{f}, \quad (4.1)$$

which assumes the object is in focus at the image plane, and that the small angle approximation¹ (where $\sin(\theta) \approx \theta$, $\tan(\theta) \approx \theta$, and $\cos(\theta) \approx 1$) is appropriate for the light rays. Eq. (4.1) is based upon the simple optical arrangement depicted in Fig. 4.1 containing a single thin lens of focal length f , but can be used within reason for a compound lens system (constructed from a combination of multiple simple lenses, where the overall focal length of the system is f) such that the optical center (i.e., the *nodal point*) of the lens system takes the place of the center of the single thin lens [18]. Note that focal length and most other optical parameters are dependent on the wavelength λ of the light. As mentioned in the previous chapter, the focal distance marked on the body of many commercial lens systems is not f , but instead is equal to $s_o + s_i$. Most high-end commercial cameras have a small mark on the camera body to show the position of the s_i plane inside the camera.

The focal length is usually known, and when given one of the two axial distances (s_o or s_i) in Fig. 4.1, the other axial distance is easily calculated. When the distance to the object plane s_o is at infinity, the distance to the image plane s_i is equal to the focal length f . The term *optical infinity* is used to describe an object distance which results in an image plane distance s_i that is very close to the focal length f . For example, some designers use $s_o \geq 100f$ as optical infinity, since in this case s_i is within 1% of f . On the other hand, for visual acuity exams of the human eye, optometrists and ophthalmologists generally use the equivalent of $s_o \approx 338f$ as optical infinity [11].

Results of Eq. (4.1) are also useful for calculating distances perpendicular to the optical axis (i.e., transverse distances). The relationship of similar triangles provides the equality

$$\frac{x_o}{s_o} = -\frac{x_i}{s_i}, \quad (4.2)$$

which allows calculation of x_o or x_i when the other three values are known. The minus sign accounts for the optical image inversion that is shown in Fig. 4.1. Calculating transverse distances in an optical setup is often required, such as when the need arises to calculate the size of objects at the image plane or to know about spatial sampling distances at the image plane.

Example 4.1 Simple optical calulations

Given: Your camera has a lens with a 28 mm focal length. You are imaging an object that is $y = 45$ mm wide, and $x = 20$ mm tall, from a distance (s_o) of 3 m. Determine: distance of the image plane from the nodal point of the lens (i.e., s_i), along with the width and height of the object's image (at the image plane, ignoring image inversion).

Solution: First, solve for $s_o = 3$ m using Eq. (4.1).

$$\begin{aligned} \frac{1}{s_i} &= \frac{1}{f} - \frac{1}{s_o} = \frac{1}{28 \times 10^{-3}} - \frac{1}{3} = 35.38 \\ s_i &= \frac{1}{35.38} = 28.26 \times 10^{-3} \text{ or } \boxed{28.26 \text{ mm}} \end{aligned}$$

Then solve for x_i and y_i using Eq. (4.2).

$$\begin{aligned} x_i &= s_i \frac{x_o}{s_o} = 28.26 \times 10^{-3} \left(\frac{20 \times 10^{-3}}{3} \right) = 188.4 \times 10^{-6} \text{ or } \boxed{188.4 \mu\text{m}} \\ y_i &= s_i \frac{y_o}{s_o} = 28.26 \times 10^{-3} \left(\frac{45 \times 10^{-3}}{3} \right) = 423.9 \times 10^{-6} \text{ or } \boxed{423.9 \mu\text{m}} \end{aligned}$$

¹This is sometimes called the *paraxial approximation* and is part of the *Gaussian approximation*.

Regarding this example, the object distance s_o is 107 times the lens focal length, which is why the image distance s_i is not much different from the focal length. One definition of magnification is the ratio of image size to object size. The example just shown yields a magnification of 9.42×10^{-3} (calculated along either axis).

Modern cameras and vision sensors based on the mammalian camera eye typically place a focal plane array (FPA) of photodetectors (such as a CCD or CMOS sensor array) at the image plane. This array introduces spatial sampling of the image, where the center-to-center distance between individual photodetector locations (i.e., the spatial sampling interval) equals the reciprocal of the spatial sampling frequency. Spatial sampling, just like temporal sampling, is limited by the well-known sampling theorem: only spatial frequencies in the image up to one-half the spatial sampling frequency can be sampled and reconstructed without aliasing [44]. Sampling and aliasing are discussed more fully in Appendix B.

Aliasing is evident when the reconstructed image shows incorrect spatial frequencies that are lower than the true image. Aliasing in an image is most noticeable to humans with regard to periodic patterns, such as the stripes of a person's tie or shirt which, when aliased, tend to look broader and distorted [44]. Note that most real-world images are not strictly bandlimited, so some amount of aliasing is usually inevitable in digitized images.

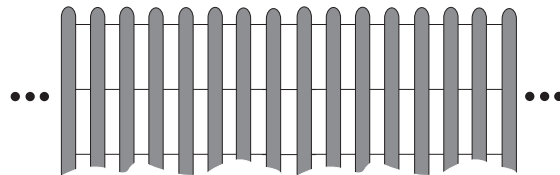
Fourier theory tells us that even a complex image can be modeled as an infinite weighted sum of spatially sinusoidal frequencies [44, 45]. Knowing how these spatial frequencies are sampled can predict how well a camera may perform. Eq. (4.2) allows us to map transverse distances between the object plane and the image plane and understand how the spatial sampling interval compares to the various transverse distances in the image.

Example 4.2 Optical distances, spatial sampling, and aliasing

Given: As a real-world example that highlights the use of these relationships, suppose you need to remotely monitor the condition of a small experimental snow fence at a certain point along a northern route interstate highway, using a digital camera. The individual slats of the snow fence are made of a new *environmentally green* recycled material which may or may not hold up under the wind pressures expected during the winter; that's the purpose of the monitoring. The imaging only needs to detect if a slat breaks and thus appears to be missing. The camera will be an inexpensive webcam that will periodically capture images of the snow fence and transmit the images back to a monitoring station. The webcam uses a 1.3-megapixel CCD rectangular sensor array ($1280 \text{ H} \times 720 \text{ V}$ pixels), and the physical size of the CCD array inside the camera is 19.2 mm horizontally by 10.8 mm vertically.² The aspect ratio of each image frame taken with this camera is 16:9, and the aspect ratio of each individual photodetector (pixel) in the CCD array is 1:1 (i.e., square), such that the center-to-center pixel spacing is the same in the x -direction and the y -direction. The webcam uses a built-in 22.5 mm focal length lens which is permanently fixed at a distance from the CCD array such that it will always focus on objects that are relatively far away (i.e., optical infinity). The snow fence is made up of very dark colored slats that are 2.44 m (about 8 feet) high and 200 mm wide, with 200 mm of open space between adjacent slats. In the expected snowy conditions, the contrast of the dark slats against the light colored background should allow a good high-contrast daytime image of the snow fence, within the limits of spatial sampling requirements. No nighttime images are needed. See the figure below for a simple illustration of what the snow fence might look like, not necessarily drawn to scale nor at the actual viewing distance, with snow at the base obscuring some unknown part of the slat height. Assume the fence extends to the right and left of the figure a considerable

²It's traditional for manufacturers of cameras, monitors, televisions, etc., to provide size specifications as (horizontal, vertical), and aspect ratios as H:V, so this is how the information is provided. However, this is the *opposite* of most image processing and linear algebra books where dimensions are usually specified as (row, column).

distance beyond what the simple figure shows.



You would like to view as wide a section of the experimental snow fence as possible, so you want to place the camera as far away from the fence as possible. Thus you need to calculate the maximum distance you can place the webcam from the fence and yet still be able to easily make out individual slats in the image, assuming the primary limiting factor is the spatial sampling frequency of the image. Assume the optical axis of the camera is perpendicular to the fence, so you can neglect any possible angular distortions.

Solution: While the periodic nature of the slats is not a sinusoidal pattern (it is actually closer to a square wave), the spatial period of the slats is equal to the fundamental frequency of a Fourier sum that would model the image of the fence, and the individual slats will be visible with acceptable fidelity (for this specific application) if this fundamental frequency is sampled properly [44]. The sampling theorem requires a minimum of two samples per cycle; one complete cycle at the fundamental frequency is a single slat/opening pair. Thus the 200 mm slat plus a 200 mm opening at the object plane must span two (or more) pixels at the image plane for adequate sampling to occur. Another way to say this is that the pixel spacing, mapped to the object plane, must be 200 mm or less in the horizontal direction (the vertical direction is not as important for this image; why?). At the image plane, the center-to-center pixel spacing is $19.2 \text{ mm}/1280 = 15 \mu\text{m}$. Referring back to Fig. 4.1, we know that $s_i = 22.5 \text{ mm}$ since the object plane is at optical infinity. Using similar triangles, we get $(22.5 \text{ mm}/15 \mu\text{m}) = (s_o/200 \text{ mm})$, thus $s_o = 300 \text{ m}$, which is the maximum distance allowed from the camera to the snow fence. If the camera is placed farther away than 300 m, the fundamental spatial frequency of the snow fence will alias, and the image would likely be unacceptable.

It's important to reiterate that the previous examples assumed the use of a standard lens, *not* a telecentric lens. Unless otherwise noted, the remainder of the text also assumes the use of standard lenses.

Distance and size calculations for simple optical setups are straightforward. The assumptions inherent in the simple equations provided often won't get you the exact answer, but will get you close. One of the more useful applications of these calculations is related to spatial sampling. Technical users often need to know roughly how many pixels of the FPA are detecting an object or pattern of interest.

4.2 Effects of aperture size: diffraction

Ray tracing and simple calculations associated with geometric optics can provide some quick and helpful approximations, but you can't avoid the effects of diffraction and the ramifications of imperfect lenses (i.e., aberrations). We first turn to diffraction.

Diffraction is a basic concept of optics that is very important to properly understanding image formation, yet is it often misunderstood or ignored. Due to the unavoidable effects of diffraction, no real-world lens can focus light to an infinitesimally tiny point; there will be some minimum *blur spot*. The primary factor that determines the size of the minimum blur spot due to diffraction is the size of the aperture through which light is allowed to pass.

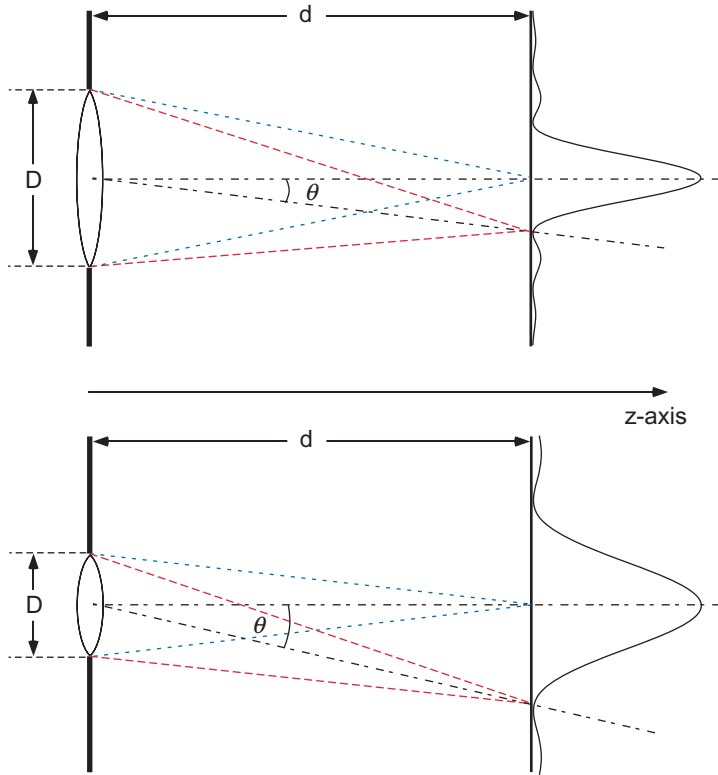


Figure 4.2: Minimum blur spot due to diffraction of light for some specific wavelength. Notice how a larger aperture (D) for the top figure results in a smaller blur spot.

4.2.1 Circular apertures

Two simple optical setups with circular apertures are depicted in Fig. 4.2, where the top setup has a larger aperture than the bottom one. Note the different size of the resulting the blur spots due to diffraction. In the figure, if the object plane is at optical infinity, then $d = f$, the focal length of the lens. The diameter of the aperture is shown as D ; this aperture size could be due to the physical diameter of the lens in a very simple optical setup, or by the (often variable) aperture diaphragm of a more complex lens system. When there is more than one aperture in a lens system, the controlling aperture is called the *aperture stop*.

Interestingly, no lens is needed to observe this same phenomenon of diffraction, only an aperture. If the distance d is great enough (as discussed in Chapter 5), then the same distribution of light in the blur spot will result. Using a lens simply makes the value of d something reasonable (e.g., the focal length of the lens for a distant light source).

Let's discuss Fig. 4.2 in more detail. As light travels from the lens to the image plane, differences in path length are inevitable. Where the difference in path length equals some odd integer multiple of $\lambda/2$, a region of lower intensity (dark) appears due to destructive interference; where the difference in path length equals some even integer multiple of $\lambda/2$, a higher intensity (bright) region appears due to constructive interference.

With a circular aperture, the blur spot (sometimes called the “diffraction pattern”) will take the circularly symmetric shape of what is often called an *Airy disk*, defined by Eq. (4.3) below.³ Note the squaring operation in the equation to yield intensity of the light, as appropriate for

³Function J_1 shown in Eq. (4.3) is known as a first-order Bessel function of the first kind. One way to define this function is by the infinite series $J_1(x) = \frac{x}{2} - \frac{(x/2)^3}{1^2 \cdot 2} + \frac{(x/2)^5}{1^2 \cdot 2^2 \cdot 3} - \dots$. See the MATLAB function `besselj`.

incoherent light sources.

$$I(x, y) = I_0 \left[\frac{2J_1\left(\frac{\pi D \rho}{\lambda d}\right)}{\frac{\pi D \rho}{\lambda d}} \right]^2, \quad \rho = \sqrt{x^2 + y^2} \quad (4.3)$$

Here, x and y are rectangular coordinates (expressed in linear units) at the image plane, which is located at a distance d from the lens. The *angular* separation between the center peak and the first minimum of an Airy disk, as shown in Fig. 4.3(a), is $\theta = 1.22\lambda/D$, which confirms the inversely proportional relationship between the blur spot diameter and the aperture diameter that was shown in Fig. 4.2. This value of θ is often referred to as the angular resolution, assuming the use of what is known as the Rayleigh criterion [18]. More about resolution criteria such as Rayleigh will be discussed soon. In linear units at the image plane, the first minima of the Airy disk would occur at $\rho = \pm 1.22\lambda d/D$, with ρ as defined in Eq. (4.3), and with d and D as shown in Fig. 4.2.

While the angular measure from the peak to the first minimum of the blur spot is $1.22\lambda/D$, the *diameter* of the blur spot at the *half-power point* is shown in Fig. 4.3(a) to be approximately λ/D ; this diameter, sometimes referred to as the size of the blur spot, is often of interest. The size of the blur spot is what determines what is often called the *diffraction limit* of an optical system; however, keep in mind that the blur spot size may be dominated by lens aberrations, not diffraction, as discussed later. Note that certain highly specialized techniques can result in spatial resolution somewhat better than the theoretical diffraction limit, but that is beyond the scope of this discussion [46].

Why is both amplitude (b) and intensity (c) of an Airy disk shown in Fig. 4.3? While both eyes and cameras perceive light as intensity, not amplitude, the amplitude version of the Airy disk image is found in many optics books, probably because it shows the structure of the sidelobe “rings” much better than the intensity version. But keep in mind that what you would see or record with your camera would be intensity, not amplitude.

4.2.2 Rectangular apertures

While nearly all telescope, microscope, and camera lenses are circular, and have approximately circular apertures, there are instances (such as with certain spectrometers, for example) when the aperture is rectangular. It should come as no surprise to the reader that the blur spot, or diffraction pattern, would not be proportional to a squared Bessel function in that case, but instead it would be proportional to a squared sinc function, where sinc is defined as $\sin(\pi x)/(\pi x)$. Eq. (4.4) applies to a rectangular aperture; the sinc is squared in the equation to yield intensity.

$$I(x, y) = I_0 \operatorname{sinc}^2\left(\frac{D_x x}{\lambda d}\right) \operatorname{sinc}^2\left(\frac{D_y y}{\lambda d}\right) \quad (4.4)$$

What does the blur spot from a rectangular aperture “look like” as an image? A 2-D image view of such a blur spot is shown in Fig. 4.4, both as amplitude (a) and as intensity (b). Once again, the amplitude version shows the structure of the sidelobes better than the intensity version. But keep in mind that what you would see or record with your camera would be intensity, not amplitude. In the example shown in Fig. 4.4, the horizontal dimension of the rectangular aperture was half the size of the vertical dimension, opposite of the relative dimensions of the resulting diffraction pattern shown in the figure. Consistent with most common optics texts, the x -axis is horizontal, the y -axis is vertical, and the origin is at the center of the image.⁴

The *angular* separation between the center peak and the first minimum of the sinc squared function in each dimension would be $\theta_x = \lambda/D_x$, and $\theta_y = \lambda/D_y$. In linear units, the first minima would occur at $x = \pm \lambda d/D_x$, and $y = \pm \lambda d/D_y$.

⁴Many image processing texts use a different convention for the x and y axes, and for the origin.

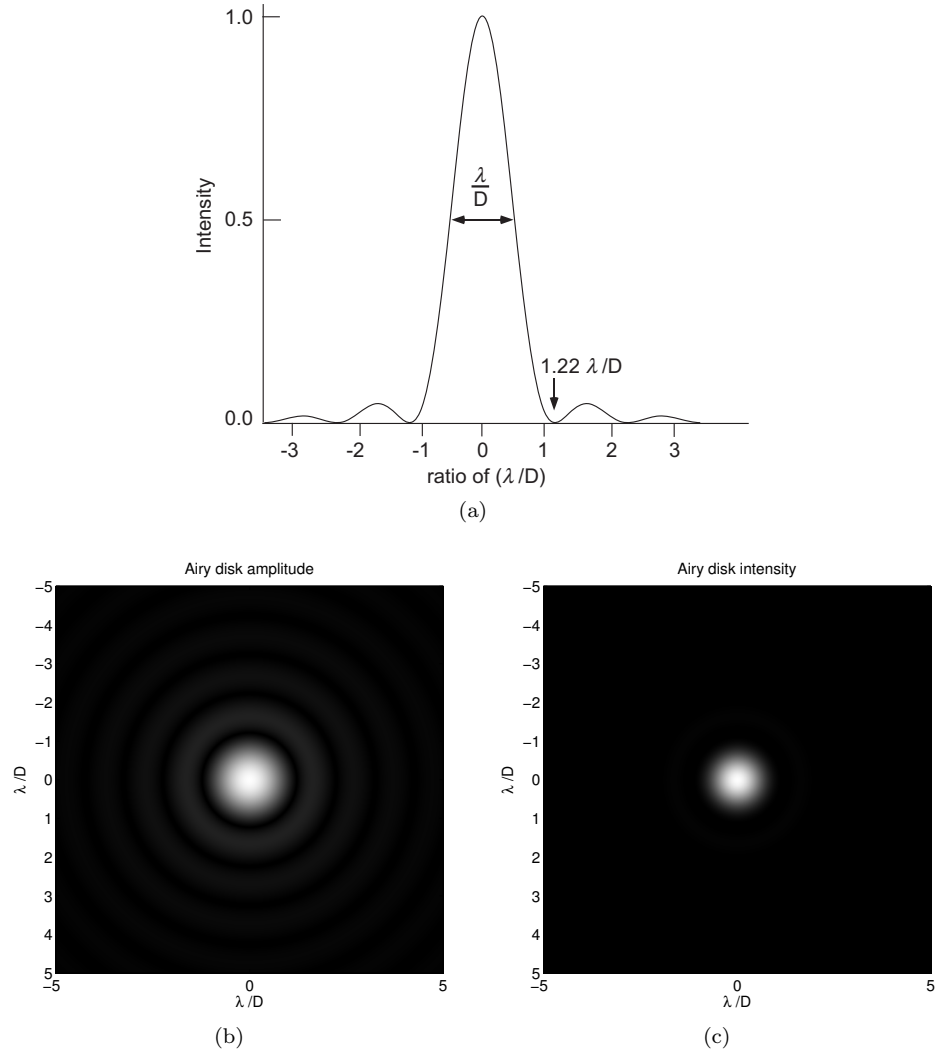


Figure 4.3: In (a), a 1-D cross section is shown of a normalized Airy disk blur spot due to diffraction of light when the aperture is circular. A 2-D image view of an Airy disk is shown in (b) as amplitude and in (c) as intensity. Note that eyes and cameras perceive light as intensity, not amplitude.

How does the square of two times the Bessel function expressed in Eq. (4.3) compare to the squared sinc function in Eq. (4.4)? In one dimension, they are very similar, as can be seen in Fig. 4.5. The location of the minima are slightly different, and the height of the sidelobes is lower overall for the Airy disk. But in two dimensions, the difference is much more obvious, as can be seen by comparing Fig. 4.3 versus Fig. 4.4, due to the expected circular versus rectangular symmetry.

It should be reiterated here that in nearly all cases when using standard cameras, the blur spot will be circularly symmetric because the defining aperture will be circular. For the diffraction-limited case, it will be defined by Eq. (4.3). When aberrations (discussed in Section 4.5) dominate, the blur spot will be larger and most likely have some shape other than an Airy disk, such as a Gaussian, but it will still exhibit circular symmetry to a large extent.

Example 4.3 Minimum blur spot

Given: Suppose you're using an off-the-shelf prime lens with a focal length of 55 mm. The lens aperture can be adjusted from f/1.4 to f/22. Neglect aberrations, so diffraction is the only determinant of blur spot size. Assume a wavelength of $\lambda = 550$ nm for light, unless otherwise noted. Determine the following values.

- Minimum and maximum **angular** blur spot diameter (half power point of the Airy disk).
- Minimum **linear** blur spot diameter (half power point, at the image plane) if the object is at optical infinity.
- Minimum **linear** blur spot diameter (half power point, at the image plane) if the object is at a distance of 1 m.
- Minimum **linear** blur spot diameter (half power point, at the image plane) if the object is at ∞ and you're using **infrared** light with $\lambda = 5 \mu\text{m}$.

Solution: Recall that f-number is focal length divided by aperture diameter. Then the maximum aperture diameter, at f/1.4, is $D = 55/1.4 = 39.29$ mm. The minimum aperture diameter, at f/22, is $D = 55/22 = 2.5$ mm.

- The angular blur spot diameter (BSD) at the half power point is equal to λ/D . The minimum angular blur spot diameter is when using f/1.4, so $\text{BSD} = 550 \text{ nm}/39.29 \text{ mm} = 14 \mu\text{rad}$. The maximum angular blur spot diameter is when using f/22, so $\text{BSD} = 550 \text{ nm}/2.5 \text{ mm} = 220 \mu\text{rad}$.
- To convert from angular units to linear units, just multiply by the distance s_i to the image plane. At optical infinity, $s_i = f = 55$ mm. The minimum linear blur spot diameter at the image plane is thus $(14 \mu\text{rad})(55 \text{ mm}) = 770 \text{ nm}$.
- At $s_o = 1 \text{ m}$, $s_i = 58.2 \text{ mm}$ (confirm this for yourself), so the minimum linear blur spot diameter at the image plane is $(14 \mu\text{rad})(58.2 \text{ mm}) = 815 \text{ nm}$.

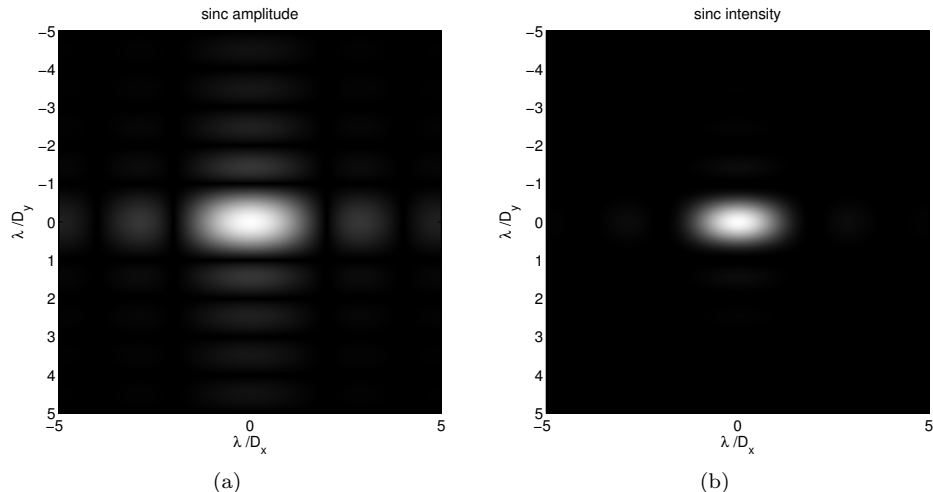


Figure 4.4: A 2-D image view of the blur spot from a rectangular aperture, shown in (a) as amplitude and in (b) as intensity, due to diffraction of light. The horizontal dimension of the rectangular aperture was half the size of the vertical dimension. Note that eyes and cameras perceive light as intensity, not amplitude.

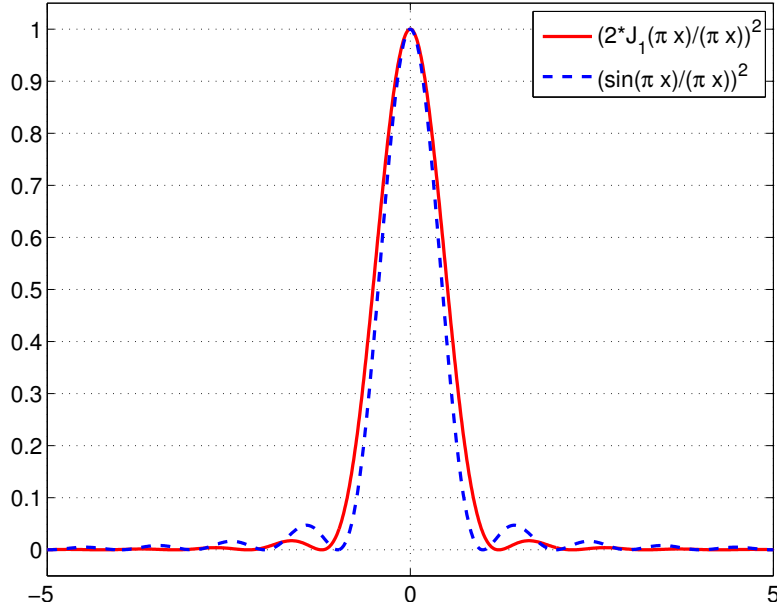


Figure 4.5: Comparison of the square of two times a Bessel function and a squared sinc function, where sinc is defined as $\sin(\pi x)/(\pi x)$.

- Change to infrared light at $\lambda = 5 \mu\text{m}$, and the minimum angular blur spot diameter is $\text{BSD} = 5 \mu\text{m}/39.29 \text{ mm} = 127.3 \mu\text{rad}$ (much larger than $14 \mu\text{m}$). The minimum linear blur spot diameter at the image plane, using this wavelength of light, is $(127.3 \mu\text{rad})(55 \text{ mm}) = 7 \mu\text{m}$.

This example illustrates the dependence of the blur spot size on both aperture diameter and wavelength.

4.2.3 Resolution criteria

As mentioned previously, the term *diffraction limit* of an optical system has meaning only in the context of some specified resolution criterion. Commonly used resolution criteria include Rayleigh, Abbe, and Sparrow; others (such as the Dawes limit or the Houston criterion) are also mentioned in the literature [18, 21]. Knowing the diffraction limit of an optical system can be a valuable piece of information.

The basic idea of a resolution criterion comes from the desire to quantify the minimum distance between two spots (usually assumed to be Airy disks of equal intensity and size, due to a circular aperture of diameter D) such that they can be recognized as two distinct spots. This distance can be specified as an angular measure (where the small angle approximation of $\sin \theta \approx \theta$ is usually assumed) or as a linear measure. As the two spots are moved closer together, there will be some minimum distance at which they blend into each other and cannot be perceived as separate objects. Since perception by a human was part of the original definition, there has been disagreement about the value of that minimum distance. This helps explain the existence of multiple resolution criteria. Three of the most commonly used criteria are defined in Table 4.1.

The Rayleigh criterion defines the minimum distance as the point where the maximum of one Airy disk aligns with first minimum of the other Airy disk. This means the minimum angular separation between the center of the two spots is $\theta_R = 1.22\lambda/D$, and the dip in intensity between the two peaks is about 26.3%. Some early researchers felt this was too conservative. The Abbe criterion (sometimes called the Houston criterion) specifies the minimum angular separation

between the center of the two spots to be $\theta_A = \lambda/D$, and the dip in intensity between the two peaks is about 5%. Note that the Abbe criterion also matches the diameter of the Airy disk at full width half maximum (FWHM), as can be seen in Fig. 4.3(a). The Sparrow criterion specifies the minimum angular separation between the center of the two spots to be the distance at which the dip in intensity between the two peaks just barely goes away, and this has been found to be $\theta_S = 0.94\lambda/D$. These three cases are shown in Fig. 4.6.

The Rayleigh and Abbe criteria are the ones most often used in microscopy, and the Sparrow criterion is more often used in astronomy. For digital photography and imaging, there is no clear agreement, although a quick scan of the literature seems to show that the Abbe criterion or its equivalent (under other names) shows up most often.

Which is best for your application? As always, it depends on the application! The Abbe criterion is the simplest, and is between the Rayleigh and the Sparrow, so perhaps it is a good choice for many cases. When an optical system is dominated by aberrations, such resolution criteria and the implied diffraction limit are no longer useful measures, as the blur spot will be larger (sometimes much larger) than a diffraction limited blur spot. The shape of the blur spot in an aberration-dominated system will usually not be the shape of an Airy disk; a Gaussian shape is fairly common. This will be discussed in more detail later.

4.2.4 Terminology related to apertures

Any discussion of aperture should mention that the various subfields of optics (astronomy, microscopy, fiber optics, photography, etc.) use different terms to describe the aspects related to the effective aperture of the system [23].

In astronomy, the actual aperture size as discussed above is typically used. This aperture size is usually equal to the effective diameter of the telescope's objective lens or main mirror.

In microscopy, it is common to use *numerical aperture*, defined as $NA = n \sin \phi$, where n is the index of refraction of the medium through which the light travels, and ϕ is the half-angle of the maximum cone of light that can enter the lens. The dependence on n is why some microscope techniques use oil-immersed objective lenses, since the oil has a higher index of refraction than air. The angular resolution of a standard microscope is often specified as $\lambda/2NA$. A simplified diagram showing the angle ϕ related to the numerical aperture of a lens is shown in Fig. 4.7. From this figure the relationship between the f-number of a lens and the numerical aperture of a lens can be determined. A useful approximation that holds in most cases is $f/\# \approx 1/2NA$.

For multi-mode fiber optics, numerical aperture is typically defined as $NA = n \sin \phi \approx \sqrt{n_1^2 - n_2^2}$, where n is the index of refraction of the medium through which the light travels prior to entering the fiber, n_1 is the index of refraction of the fiber core and n_2 is the index of refraction of the fiber cladding. See Fig. 4.8. This can provide an approximation for the largest acceptance angle ϕ for the cone of light that can enter the fiber such that it will propagate along the core of the fiber. Light arriving at the fiber from an angle greater than ϕ would not continue very far down the fiber. Note: It's becoming common to use this same definition for *all* optical fibers, including single-mode fibers, but in reality the true (and more narrow) acceptance angle

Table 4.1: Comparison of three common resolution criteria used to predict the diffraction limit of an optical system, with θ , d and D defined as shown in Fig. 4.2, and ρ defined as in Eq. (4.3).

Criterion	Angular separation (in radians)	Linear separation at the image plane	Dip in intensity between peaks
Rayleigh	$\theta_R = 1.22\lambda/D$	$\rho_R = 1.22\lambda d/D$	26.3%
Abbe	$\theta_A = \lambda/D$	$\rho_A = \lambda d/D$	5%
Sparrow	$\theta_S = 0.94\lambda/D$	$\rho_S = 0.94\lambda d/D$	none

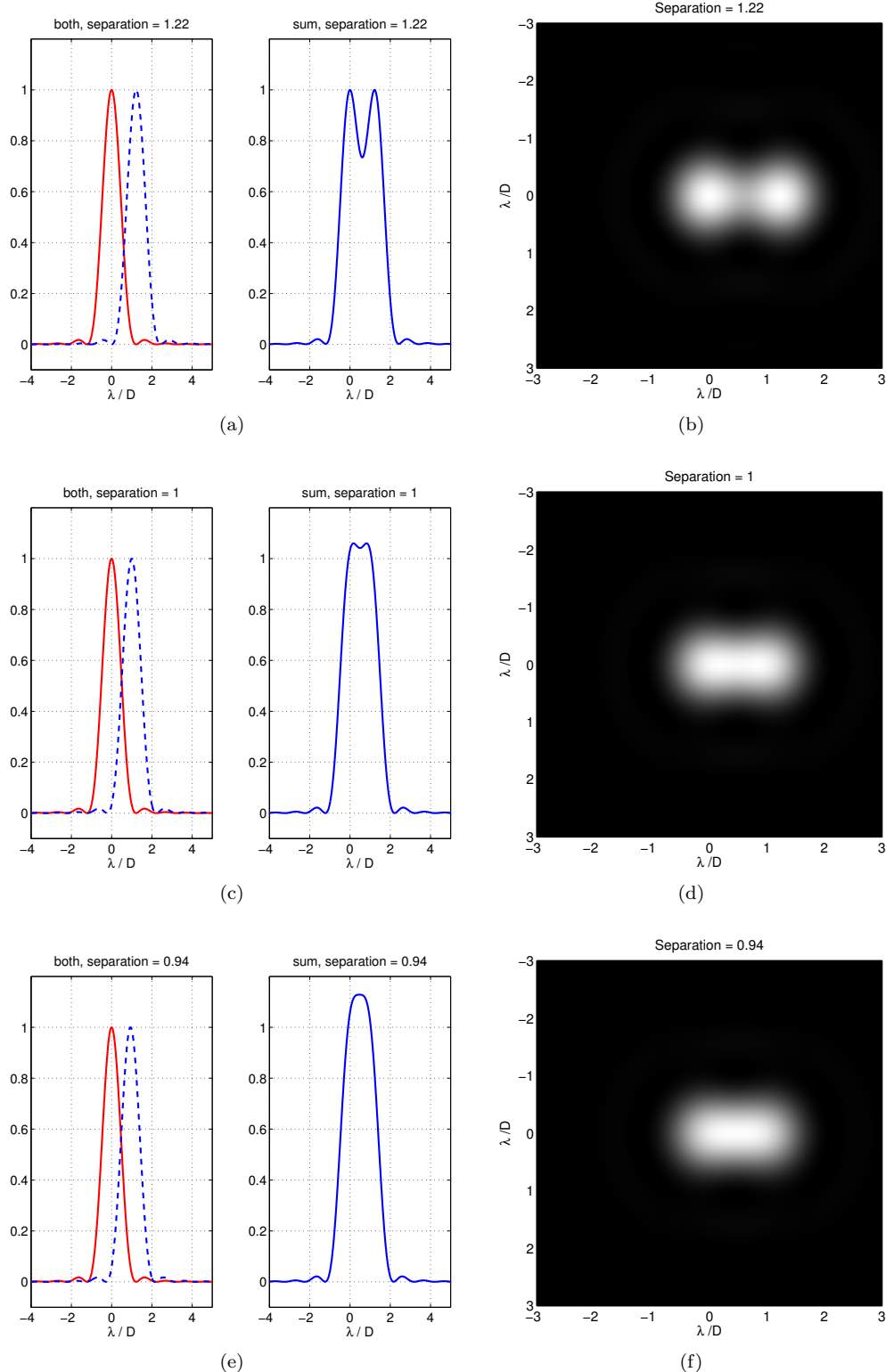


Figure 4.6: A comparison of three resolution criteria used to predict the diffraction limit of an optical system. Top: Rayleigh criterion. Middle: Abbe criterion. Bottom: Sparrow criterion.

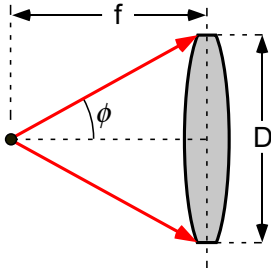


Figure 4.7: A simplified diagram showing the angle ϕ related to the numerical aperture of a lens.

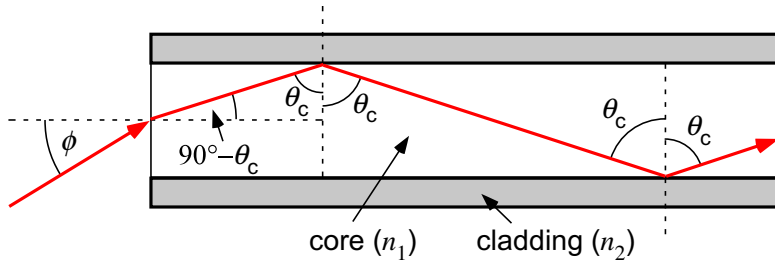


Figure 4.8: A multi-mode optical fiber, showing the angle ϕ related to the numerical aperture of the fiber tip. Angle $\theta_c = \arcsin(n_2/n_1)$ is the critical angle for total internal reflectance.

for a single-mode fiber depends on more than just the indices of refraction... so beware!

In photography, the far more common measure related to aperture size is the *f-number* that was first discussed in Chapter 3. Note that to obtain the same image exposure for a camera, an increase of one *f-stop* must be matched by twice the integration time (called the *shutter speed* in photography) of the photosensor. Using the f-number to infer the light-gathering capacity of a lens is really only true for objects at optical infinity, but this subtle point is almost always ignored in photography. The exception to this is for *macro photography*, where the object of interest is very close to the camera. In that case, a variant called the *working f-number*, or N_w is sometimes used. The definition of the working f-number is $N_w \equiv 1/(2NA_i) \approx (1 + |m|)N$, where NA_i is the numerical aperture measured from the image plane to the lens, m is the lens's magnification,⁵⁾ and N is the uncorrected f-number.

Whether the aperture is is discussed with reference to D , NA , $f/\#$, or some other measure is dependent upon the application. Regardless of how it is discussed, the effect of aperture size on imaging, due to unavoidable diffraction, should not be ignored.

4.2.5 Applying aperture-related calculations

How is this topic of aperture size pertinent to someone who needs to intelligently use a digital camera? First, you will never be able to image any detail smaller than the blur spot. Second, there is sometimes the desire in certain applications to “match” the optics to the photosensors. For example, if the optics design results in a blur spot that is significantly smaller than the photosensitive area of an individual photodetector (e.g., the size of a single pixel in a CCD array), then one could say that the optics have been *overdesigned*. A blur spot nearly the same size as the photosensitive area of an individual photodetector results when the optics have been tuned to match the sensors (ignoring for the moment the unavoidable spatial sampling limits that a photodetector array will impose on the image). There are many instances, sometimes due to considerations such as cost/weight/size of the optical system and sometimes due to other

⁵For example, $m_x = x_i/x_o$ is the linear magnification in the x direction. Circular lenses yield $m_x = m_y = m$.

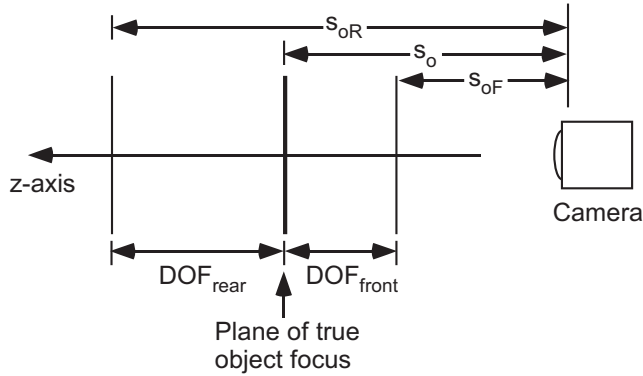


Figure 4.9: Front and rear depth of field (DOF), compared to point of focus s_o .

reasons, that the optical system is purposely designed to result in a blur spot much larger than the photosensitive area of an individual photodetector. This trade-off will be mentioned again later.

Example 4.4 Matching aperture size to sensor size

Given: For the webcam problem described earlier, what aperture size would be needed to approximately match a diffraction-limited blur spot to the pixel size?

Solution: The angular blur spot size is approximately λ/D , so the linear blur spot size at the image plane is $(\lambda/D)s_i$. The pixel size was previously found to be $15 \mu\text{m}$. If we assume a wavelength near the midband of visible light, 550 nm , then the requirement is for

$$D = \frac{\lambda}{x_d} s_i = \frac{550 \times 10^{-9}}{15 \times 10^{-6}} 22.5 \times 10^{-3} = 825 \times 10^{-6} \text{ m or } 825 \mu\text{m}.$$

Since the focal length of the lens was given as 22.5 mm , this would require a lens with an f-number of $f/D = 27.27$, which is an achievable aperture for the lens system. However, the likelihood of a low quality lens in the webcam would mean that aberrations (discussed later) would probably dominate the size of the blur spot, not diffraction. Aberrations always make the blur spot larger, so if aberrations are significant then a larger aperture would be needed in an attempt to get the blur spot back down to the desired size.

4.3 Depth of field

The size of the effective aperture of the optics not only helps determine the size of the diffraction limited blur spot (and the amount of light admitted for the exposure), but also helps determine the depth of field (DOF) of the image. While Fig. 4.1 implies there is only a single distance s_o for which an object can be brought to focus at distance image distance s_i , DOF describes the practical reality that there is an axial range of distances over which objects are imaged with *acceptable* sharpness. Thus an object within the range of $(s_{oF} = s_o - \text{DOF}_{\text{front}})$ to $(s_{oR} = s_o + \text{DOF}_{\text{rear}})$, as depicted in Fig. 4.9, would be imaged with acceptable sharpness. Depth of field is a concept many are familiar with, but one that few really understand; there are certain myths and misconceptions that are repeated even in well-respected books.

For a given focal length, a larger aperture results in a larger angle of convergence of light onto the image plane. This larger angle means that any change in axial distance closer or farther than s_o will have a greater blurring effect with a larger aperture than would the same change in distance using a smaller aperture. The amount of blurring is quantified by a value called the

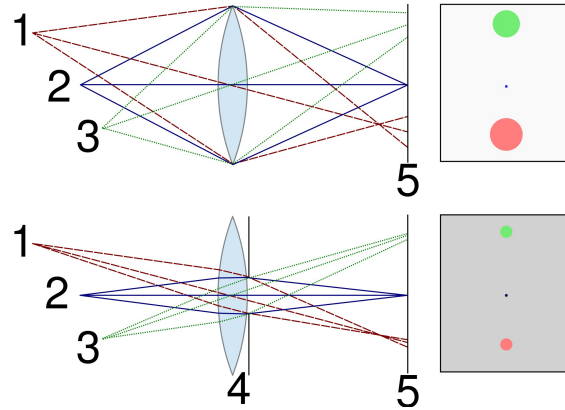


Figure 4.10: Illustration of how aperture size affects the circle of confusion for light coming from a distance other than s_o (point 2). A larger aperture (top) results in a larger circle of confusion for a given distance, and thus more blurring in the image. [47]

circle of confusion (CoC). A larger CoC means more blurring. The relationship between the CoC, object distance, and aperture size can be seen in Fig. 4.10, where distance s_o is labeled as point 2. The limits of DOF are determined by the largest acceptable CoC. Because the CoC is larger for the larger aperture, then if all other things are equal, the acceptable DOF is smaller for larger apertures.

Don't be misled by Fig. 4.9; the limits to DOF don't change abruptly; the sharpness of focus changes gradually. The point of focus at distance s_o is the sharpest region of the image; in the absence of aberrations this is where the diffraction limit determines sharpness. As you move closer or farther from s_o , the sharpness gradually decreases. At distances other than s_o , the CoC will be larger than the diffraction limited blur spot. Beyond the limits of the DOF, the sharpness has fallen below an acceptable level, which means the CoC has grown too large to be acceptable for object distances outside the range of the DOF.

An "acceptable" size for a CoC is quite subjective and application dependent, and there are many issues related to CoC that are beyond the scope of this text. However, there are some rules of thumb that are widely used to obtain a reference value for CoC, one of the most common of which is called the " $d/1500$ " rule. In simple terms, the " $d/1500$ " rule states that the reference value for CoC is equal to the diagonal measure of the sensor array (or film) divided by 1500. For a standard 35 mm film camera or an equivalent "full frame" digital camera, the sensor dimensions are 36 mm wide by 24 mm high, so the diagonal measure is $d = \sqrt{36^2 + 24^2} = 43.27$ mm, and $d/1500 = 0.02884 \approx 0.029$ mm. The reference value for CoC is used in DOF calculations, and the dimensions and CoC of a variety of commonly available sensors used in digital cameras are given in Table 4.2. The values given in the column for crop factor in Table 4.2 are useful for the next section discussing field of view, where the effect of crop factor on DOF is also discussed.

While photographers often manipulate DOF for artistic purposes, sensor system designers and technical camera users are often more interested in either maximizing the DOF or being able to predict the DOF with reasonable accuracy. In general, the $\text{DOF}_{\text{front}}$ is always less than DOF_{rear} . At relatively small values of s_o (when focusing on objects near the camera), the ratio of $\text{DOF}_{\text{front}}/\text{DOF}_{\text{rear}}$ is close to unity. As s_o is increased, the ratio of $\text{DOF}_{\text{front}}/\text{DOF}_{\text{rear}}$ decreases, and there is a certain point at which DOF_{rear} extends to optical infinity; this value of s_o is called the *hyperfocal distance*, symbolized as H . When $s_o = H$, $\text{DOF}_{\text{front}} = H/2$ and $\text{DOF}_{\text{rear}} = \infty$, thus all objects from $H/2$ to ∞ would be imaged with acceptable sharpness. When the sensor system or camera is set to the hyperfocal distance, the DOF is the largest possible distance for a given focal length and aperture size. Therefore, the hyperfocal distance H is often of interest to

Table 4.2: Representative sensor sizes for popular consumer cameras, a reference value for circle of confusion (CoC) based on the $d/1500$ rule, and the associated crop factor compared to a 35 mm film camera. Sensor sizes may vary slightly by manufacturer or model year.

Format	Sensor size (w × h)	CoC	Crop factor
35 mm (full frame)	36 mm × 24 mm	0.029 mm	1.0
APS-H (Canon)	27.9 mm × 18.6 mm	0.022 mm	1.3
APS-C (Nikon DX, others)	23.6 mm × 15.7 mm	0.019 mm	1.5
APS-C (Canon)	22.2 mm × 14.8 mm	0.018 mm	1.6
Foveon (Sigma)	20.7 mm × 13.8 mm	0.017 mm	1.7
Four Thirds (Olympus)	17.3 mm × 13 mm	0.014 mm	2.0
Nikon CX (Nikon 1 series)	13.2 mm × 8.8 mm	0.011 mm	2.7
1/1.8" (Canon Powershot)	7.18 mm × 5.32 mm	0.006 mm	4.8
1/2.3" (various)	6.17 mm × 4.55 mm	0.005 mm	5.6
1/3" (iPhone 6)	4.80 mm × 3.60 mm	0.004 mm	7.2

the sensor system designer or technical camera user. The value of H can be found by calculating

$$H = \frac{fD}{c} + f = \frac{f^2}{Nc} + f \approx \frac{f^2}{Nc}, \quad (4.5)$$

where f is focal length of the lens, D is aperture diameter, c is the reference value for circle of confusion from Table 4.2, and $N = f/D$ is the f-number. Since in most cases, $H \gg f$ and the f-number is more readily available than the aperture diameter, the approximation of f^2/Nc is often used.

4.3.1 DOF Calculations

The front and rear boundaries of depth of field can be found in terms of hyperfocal distance H .

$$s_{oF} = \begin{cases} \frac{Hs_o}{H + (s_o - f)} \approx \frac{Hs_o}{H + s_o} & \text{for } s_o < H \\ \frac{s_o}{2} & \text{for } s_o \geq H \end{cases} \quad (4.6)$$

$$s_{oR} = \begin{cases} \frac{Hs_o}{H - (s_o - f)} \approx \frac{Hs_o}{H - s_o} & \text{for } s_o < H \\ \infty & \text{for } s_o \geq H \end{cases} \quad (4.7)$$

The total depth of field distance, DOF, is then easily defined as

$$\text{DOF} = \text{DOF}_{\text{rear}} + \text{DOF}_{\text{front}} = s_{oR} - s_{oF}. \quad (4.8)$$

If the point of focus s_o is set to H or greater, then DOF is obviously ∞ . If $s_o < H$ but greater than a few focal lengths, a useful approximation is

$$\text{DOF} \approx \frac{2Hs_o^2}{H^2 - s_o^2} \approx \frac{2Ncf^2s_o^2}{f^4 - N^2c^2s_o^2}. \quad (4.9)$$

For macro photography, where $s_o \ll H$, it's more appropriate to use a form that takes into account the magnification, such as

$$\text{DOF} = \frac{2Nc(m+1)}{m^2 - \left(\frac{Nc}{f}\right)^2} \approx \frac{2Nc(m+1)}{m^2}. \quad (4.10)$$

Note that in macro photography, DOF is typically very small, so focusing s_o to exactly the desired point is critical.

Example 4.5 DOF calculations

Given: A Canon EOS 450D digital single lens reflex (DSLR) camera, using the Canon variant of the APS-C sensor, is to be used.

- What is the hyperfocal distance and the total depth of field for this camera when using a 50 mm lens set at f/2.8 and focused to a point 10 m from the nodal point of the lens?
- Compare to when using a 100 mm lens also set at f/2.8 and focused to a point 10 m from the nodal point of the lens.

Solution: From Table 4.2, the CoC for this camera is 0.018 mm.

- 50 mm lens: Using Eq. (4.5), $H = 49.65$ m. Using Eq. (4.9), $\text{DOF} = 4.2$ m.
- 100 mm lens: $H = 198.5$ m and $\text{DOF} = 1.01$ m.

The relationship of focal length to DOF can be easily seen in this example.

The fact that DOF is dependent on focal length, f-number (which itself is a function of focal length and aperture diameter), CoC, and the distance s_o to the point of focus makes it difficult for many people to fully understand the ramifications of changing one or more of these variables. The easiest method is to hold everything constant except one variable and examine the changes in DOF. For example, if the only variable that changes is the focal length of the lens, then as f goes up, DOF goes down, as shown in the previous example. In this case, you have to decide if you want to hold f-number constant or aperture diameter constant (since N depends in part on f), but in either case, the DOF goes down as f goes up. DOF also goes down as s_o goes down, when all other variables are held constant. DOF goes up as f-number goes up, which is the same as saying DOF goes up as aperture diameter goes down. The only other variable, CoC, depends upon the sensor size in the camera. When two or more variables change, it becomes harder to predict the outcome; the equations above will help. One point of confusion is the tendency to mix up the CoC with the diffraction limited blur spot. The former is only of interest at distances other than s_o , whereas the latter is only defined at s_o . To further complicate matters, a larger aperture results in a smaller diffraction limited blur spot at s_o , but also results in a larger circle of confusion at distances other than s_o . It's easy to see where all the misunderstandings about DOF come from.

If you're using a camera of the SLR type, beware of being misled about the DOF. The image you see through the viewfinder is at the maximum aperture opening, to provide the brightest image possible, so the DOF you see in the viewfinder will usually not be DOF recorded in the image, since the image exposure will likely be at some smaller aperture opening. When you press the shutter button to record the image, the aperture is stopped down (as the mirror is going up to clear the path to the sensor) to whatever exposure setting is being used. If you want to preview the actual DOF, most cameras have a button or switch for this, but keep in mind the viewfinder image then will be somewhat darker, making manual focus more difficult.



Figure 4.11: A photograph of Christmas lights with significant defocus aberration, using a Canon 85 mm f/1.8 lens. The bokeh shows up as polygonal shapes due to the 8-bladed aperture diaphragm being slightly closed. If the lens had been set to full aperture (f/1.8), these shapes would be much smoother and not noticeably polygonal. [48]

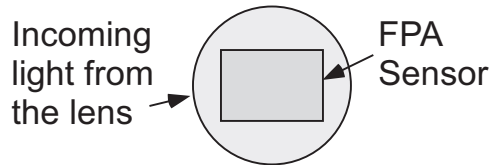


Figure 4.12: Incoming light more than covers the sensor in most situations.

4.3.2 Bokeh

Any treatment of DOF implies that some parts of an image will be out of focus. How various out of focus objects appear in an image is often discussed using the term *bokeh*. The term is believed to have come from the Japanese word “boke,” which means “blur” or “haze.” Bokeh is used to describe the aesthetic quality of the blur in the out-of-focus areas of an image, and has been defined as the way in which a lens renders out-of-focus points of light. Differences in lens aberrations and aperture shape cause some lens designs to blur the image in a way that seems to be pleasing to humans, while others produce blurring that is often deemed to be unpleasant or distracting. This is the rather subjective essence of “good” versus “bad” bokeh. Note that bokeh occurs only for parts of an image that lie outside the depth of field. A vivid example of bokeh is shown in Fig. 4.11.

4.4 Field of view

The field of view (FOV) for a camera or sensor system is the span over which a given scene is imaged. While it may seem at first that the aperture size and shape might determine FOV, in typical imaging situations it does not. If too small of an aperture is used at the wrong point in an optical system, it can restrict the FOV to less than the full sensor dimensions. This is called “vignetting” and is almost always unintentional, with the exception of when using certain super-wide-angle lenses. A typical imaging situation is depicted in Fig. 4.12, where it can be seen that the size and shape of the focal plane array (FPA) sensor will have a controlling effect on the FOV. For this reason, the sensor is sometimes called the *field stop*. The approximate FOV is determined only by the geometry of Fig. 4.1, where x_i would be one-half the size (in that dimension) of the imaging sensor array or of the film, and x_o would be one-half the linear FOV at distance s_o . A variation on Fig. 4.1 that shows how only s_i and sensor size determine FOV is provided in Fig. 4.13(a).

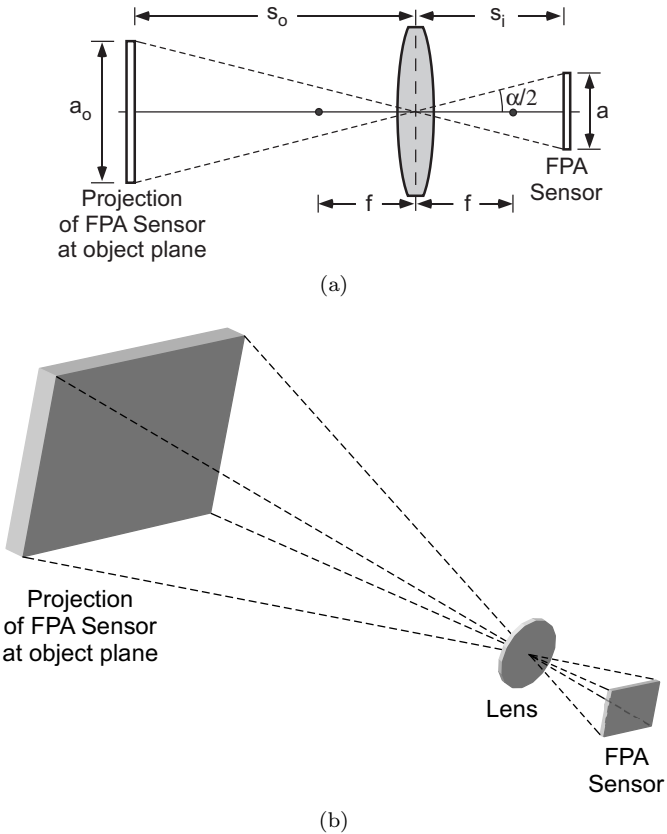


Figure 4.13: Geometry that determines the FOV for a given sensor size and focal length lens.

Since *angular* FOV is independent of object distance, it is the more frequently used form of FOV. For an imaging sensor (or film) of size a in a given direction, the angular FOV (in radians) in that direction is

$$\alpha = 2 \arctan \left(\frac{a}{2s_i} \right). \quad (4.11)$$

To convert angular FOV to linear FOV at some distance s_o , simply calculate $a_o = \alpha s_o$, assuming α is expressed in radians. Only when the system is set to focus at optical infinity does Eq. (4.11) take on the commonly seen form of $\alpha = 2 \arctan(a/2f)$. This often cited form of the equation is not useful at close focusing distances, such as for macro photography, whereas Eq. (4.11) is appropriate for any focusing distance. One of the implications of Eq. (4.11) that is often overlooked is that the FOV is at its widest only when the camera system is set to focus at optical infinity, since at that setting s_i is at its smallest value of f . As the point of focus s_o decreases, s_i increases, which reduces the FOV. **Side note:** for practical design reasons, some lenses exhibit what is called *focus breathing*, which is when the effective focal length f of a supposedly fixed focal length lens goes down as the focus distance s_o goes down. For example, a highly-regarded lens such as the Canon EF 100 mm f/2.8 Macro Lens has a nominal focal length of 100 mm. But at its minimum focus distance, it's been reported that the effective focal length is closer to 70 mm. This obviously would have an impact on many optical calculations, including FOV. Moral of the story: test and measure, don't assume!

The shape of the FOV matches the shape of the sensor array or film that is used to capture the image, not the shape of the aperture; this can be easily seen in Fig. 4.13(b). While optics are typically transversely circular, sensor arrays and film are more often rectangular, so the FOV would then also be rectangular, with the same aspect ratio (i.e., width:height or hor-

izontal:vertical) as the sensor. As can be seen in Table 4.2, the most common aspect ratio for digital camera sensors is 3:2, so the resulting FOV aspect ratio would also be 3:2 when using these cameras.

Example 4.6 Simple FOV calulations

Given: For the webcam problem described earlier, the lens focal length was 22.5 mm and the distance to the snow fence could be a maximum of 300 m. Determine the following.

- Assuming the point of focus is at the maximum distance for the snow fence, what is the angular FOV of the camera?
- How much of the snow fence will be imaged at the maximum distance of the camera from the fence?

Solution:

- The FOV is determined using Eq. (4.11), given the sensor array dimensions and s_i . Since the snow fence can be considered to be located at optical infinity, the value of s_i can be assumed to be the focal length of the lens. The sensor size was given as 19.2 mm horizontally by 10.8 mm vertically, and the lens focal length was given as $f = 22.5$ mm. The horizontal angular FOV is found to be $2 \arctan(19.2 \text{ mm}/2(22.5 \text{ mm})) = 0.807 \text{ rad} = 46.2^\circ$. The vertical angular FOV is found by calculating $2 \arctan(10.8 \text{ mm}/2(22.5 \text{ mm})) = 0.471 \text{ rad} = 27.0^\circ$.
- The maximum distance for s_o was found previously to be 300 m. From the figure of the snow fence shown on page 24, it is obvious that the horizontal FOV is what determines how much of the fence will be imaged. At a range of $s_o = 300$ m and a horizontal angular FOV of 0.807 rad, the horizontal linear distance of the fence that will be imaged is $(300)(0.807) \approx 242$ m.

The answer to the question about how much of the snow fence would be imaged could also have been calculated using Eq. (4.2), where $s_o = 300$, $x_i = 19.2 \times 10^{-3}$, and $s_i = 22.5 \times 10^{-3}$, and ignoring image inversion. However, you would then find the answer would be 256 m, not the value of 242 m that was found above! What's going on? Recall that Eq. (4.1) and Eq. (4.2) together assume that the small angle (paraxial) approximation is appropriate, and for the FOV angle in this problem that approximation does not hold. To avoid ambiguities and be consistent with the literature, use Eq. (4.11) to calculate FOV.

The previous example used a fairly low-quality webcam. An example using a higher-quality DSLR camera may be instructive.

Example 4.7 More FOV calulations

Given: A Canon EOS 450D DSLR camera, using the Canon variant of the APS-C sensor, is to be used.

- Using a 50 mm lens focused to a point 10 m from the nodal point of the lens, what is the horizontal angular and linear (at 10 m) FOV?
- Using a 100 mm lens focused to a point 10 m from the nodal point of the lens, what is the horizontal angular and linear (at 10 m) FOV?
- Using a 100 mm lens focused to a point 100 m from the nodal point of the lens, what is the horizontal angular and linear (at 100 m) FOV?

Solution: From Table 4.2, the sensor dimensions of this camera are 22.2 mm \times 14.8 mm, so the horizontal measure of 22.2 mm will be used as a . Use Eq. (4.1) to find s_i , and Eq. (4.11) to find α .

- $s_i = 50.25 \text{ mm}$, $\alpha = 0.435 \text{ rad} = 24.9^\circ$. Linear FOV at 10 m is 4.35 m.
- $s_i = 101 \text{ mm}$, $\alpha = 0.219 \text{ rad} = 12.5^\circ$. Linear FOV at 10 m is 2.19 m.
- $s_i = 100.1 \text{ mm}$, $\alpha = 0.221 \text{ rad} = 12.7^\circ$. Linear FOV at 100 m is 22.1 m.

If instead you used Eq. (4.2) to calculate the linear FOV, you would get 4.42 m, 2.20 m, and 22.2 m, respectively. Longer focal length lenses have a more narrow FOV, and thus are closer to meeting the constraints of the small angle approximation, so the values tend to agree more with Eq. (4.11). This is only for illustration; use Eq. (4.11) to calculate FOV.

Since the size and shape of the sensor affects the FOV so much, a closer look at some typical sensor sizes is warranted. See Fig. 4.14. Note that the value of crop factor, first mentioned in Table 4.2, is also given in Fig. 4.14. The crop factor is an attempt by camera manufacturers to provide an easy to use guide for how much of an image to expect to be recorded compared to a 35 mm film camera, since most photographers were so used to that as a standard. Since the comparison is to 35 mm film, that size has a crop factor of 1.0. Formally, the crop factor is the ratio of the diagonal length of 35 mm film to the diagonal length of the sensor. It gets its name from the fact that the effect of using a smaller sensor size is similar to cropping a photo taken with a 35 mm camera, where the same focal length lens is used for both images. This effect can be readily seen in Fig. 4.15.

Warning: even expensive DSLRs tend to have viewfinder images that crop the true image a bit compared to what will be recorded in the image. Therefore, don't expect the recorded image to have exactly the same FOV that you see in the viewfinder. The true FOV of the image can be predicted by the equations presented here.

Some authors call crop factor the *lens multiplication factor*, or LMF, since it also provides a way to predict how a given focal length lens will perform on a digital camera compared to how it would have performed on a 35 mm camera. For example, an 85 mm lens used on a camera with a crop factor (or LMF) of 1.6 would produce images very similar to a 35 mm camera using a $(85)(1.6) = 136 \text{ mm}$ lens! To reverse the example, many photographers preferred to use an 85 mm lens with their 35 mm film cameras for taking human portraits. If they were using a digital camera with a crop factor of 1.6, then they would need to use a lens with a focal length of 53 mm to get nearly the same FOV for the image. But that's not the whole story.

Not just the FOV is affected by crop factor, **but also the DOF**. Since the reference circle of confusion, as listed in Table 4.2, also changes for different sensor sizes according to changes in the diagonal length of the sensor, the DOF changes. Specifically, the DOF expected for a reference 35 mm camera must be divided by the crop factor, if all other things are equal. However, that statement can be misleading. An example will help.

Example 4.8 FOV and DOF calulations

Given: A researcher has previously recorded test data using a 35 mm camera with an 85 mm lens at f/2.8 and a focal distance of $s_o = 3 \text{ m}$. After purchasing a Canon EOS 450D DSLR camera (using the Canon APS-C sensor), the researcher wishes to take a images with essentially the same FOV and DOF. The test setup dictates that the focal distance of s_o remains at the previous value of 3 m. What focal length lens and aperture should be used?

Solution: From Table 4.2, the crop factor for the DSLR camera is 1.6, so to achieve the same approximate FOV a lens of $85/1.6 = 53 \text{ mm}$ should be used. While 53 mm is not a common focal length for a fixed lens, it could probably be achieved with a zoom lens. A quick check using Eq. (4.1) and Eq. (4.11) will show that in that case the FOV for both cameras is 23.3° horizontally, and 15.6° vertical. Using Eq. 4.9, the DOF for a 35 mm camera with an 85 mm lens set at f/2.8 and a focal distance of $s_o = 3 \text{ m}$ is found to be 202.3 mm. However, if the same aperture of f/2.8 is used with the DSLR and a 53 mm lens set to a focal distance of $s_o = 3 \text{ m}$, the DOF is found to be 323.6 mm. The DOF is larger because the focal length of the lens is so much shorter. To achieve approximately the same DOF as before (when using the 35 mm

camera), the 53 mm lens would need to be set to f/1.753. Even if the lens allowed that large an aperture (unlikely for a zoom lens), the aperture adjustment ring would not have a detent for such a setting. This example shows that while the equations can tell you how to theoretically convert from one camera sensor size to another, the practical reality is that the availability of lenses makes it difficult to exactly duplicate the FOV and DOF for both cameras. A general rule of thumb is that if you select the lens focal length based on the desired FOV, a camera with a smaller sensor size will have a deeper DOF.

Because of the relationship between focal length and FOV, lenses are often classified by a name that implies the approximate FOV. For historical reasons, these lens classifications tend

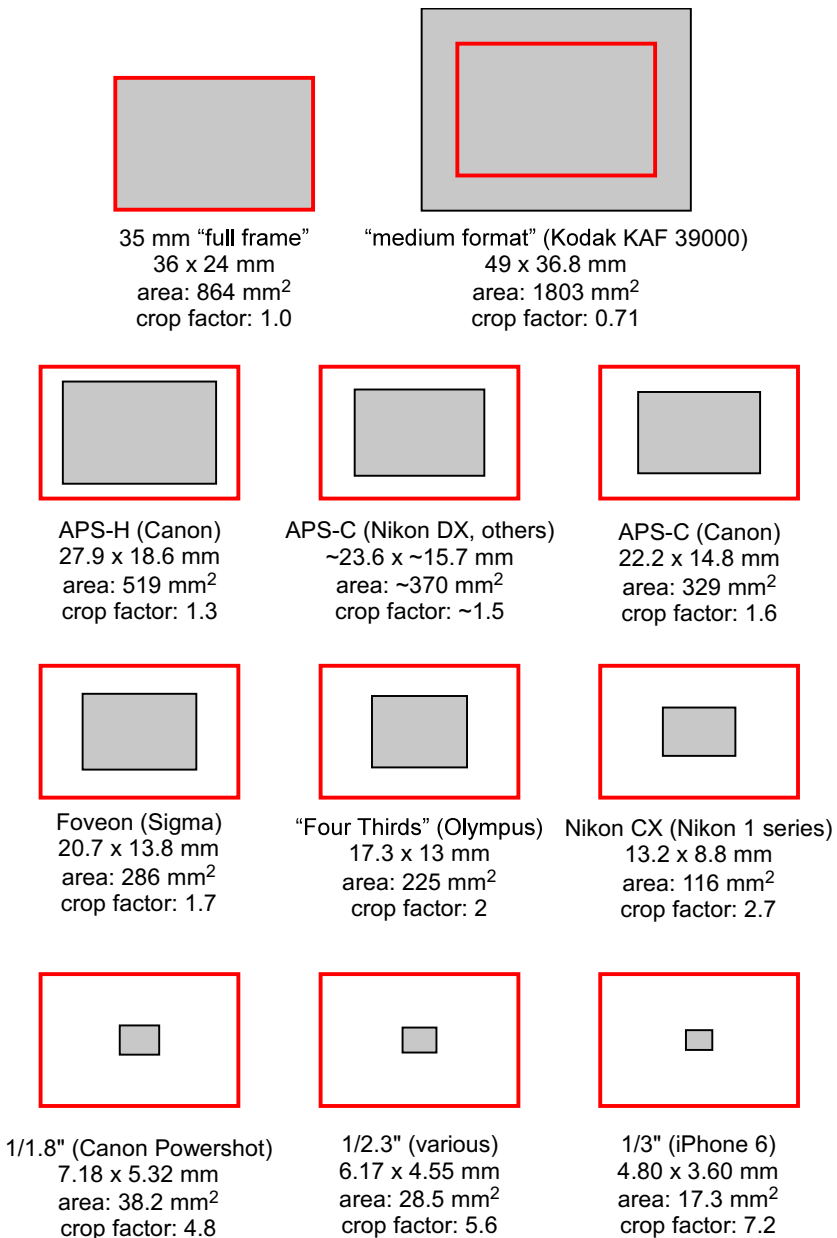


Figure 4.14: A comparison of sensor sizes (gray rectangle) used in many popular digital cameras, compared to the “full frame” size of 35 mm film (red rectangle).

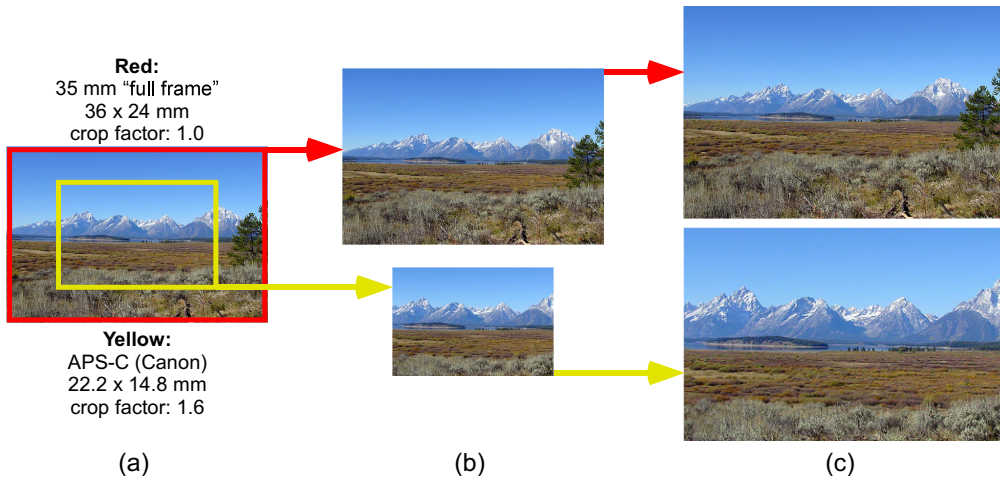


Figure 4.15: A simulated comparison of an image taken with two cameras each using the same focal length lens. One was a “full frame” digital camera (red rectangle in (a)) and the other was a digital camera using a Canon APS-C sensor (yellow rectangle in (a)), which has a crop factor of 1.6. Subfigure (b) shows a comparison of the two imaged areas, and subfigure (c) shows the actual full image that would be obtained with each camera.

to be thought of relative to a 35 mm camera, in which case these names are:

Fisheye: f of 8 to 10 mm for circular (vignetted) images, f of 15 to 18 mm for full-frame images. Diagonal FOV up to 180° .

Ultra-wide-angle: f of 18 to 24 mm. Diagonal FOV at 24 mm is about 84° .

Wide-angle: f of 24 to 35 mm. Diagonal FOV of 84° to 64° .

Normal: f of 36 to 60 mm. Diagonal FOV of 62° to 40° .

Short to medium telephoto: f of 85 to 135 mm. Diagonal FOV of 30° to 10° .

Long telephoto: f of 135 to 300 mm. Diagonal FOV of 10° to 8° .

Super telephoto: f of over 300 mm. Diagonal FOV from 8° to less than 1° .

When using a camera with some other sensor size, use the crop factor to convert. For example, a 35 mm lens would be considered a “wide-angle” lens for a 35 mm camera, but if used with a DSLR having a Canon APS-C sensor it would provide a FOV that would make it a “normal” lens. Specifically, since $(35)(1.6) = 56$, the 35 mm lens on the DSLR would have the same FOV as would a 56 mm lens on a 35 mm camera. Keep in mind that both FOV and DOF need to be considered when the sensor size changes.

A final point regarding FOV is that even expensive DSLRs tend to present an image in the viewfinder that crops the image slightly compared to what will be recorded by the camera sensor. Don’t expect the recorded image to depict exactly the same FOV as what you see in the viewfinder; it will be slightly larger.

4.5 Types of Aberrations

Up to this point in the text, the paraxial approximation and Gaussian optics have been used to greatly simplify the optical calculations. The paraxial approximation assumes that light rays follow paths near the optical axis of the lens or lens system, with only small angular

deviations from the axis. In this regime, the small angle approximation holds. It was pointed out that certain FOV calculations in the previous section violated the paraxial approximation, and recommendations were provided for how to handle that situation.

The paraxial approximation is also used for what is called *Gaussian optics*. But Gaussian optics is even more restrictive, due to its assumption that all the optical surfaces are either flat or are portions of a sphere, which linearizes many otherwise complicated solutions to optical problems. While real-world optical systems differ from the assumptions of Gaussian optics, the method greatly simplifies calculations and can provide surprisingly close answers even when light rays that are not near the optical axis are included. However, Gaussian optics completely ignores any aberrations in the system. An optical aberration can be thought of as a departure from the predictions of Gaussian optics.

No optical system is perfect, and the imperfections result in what are called aberrations [18]. Most aberrations are due to imperfections in lenses, and are categorized as either *monochromatic* or *chromatic*. Up to this point, the discussion has centered on aspects of an optical system that must be considered one wavelength at a time.⁶ This is how monochromatic aberrations are treated. Chromatic aberration, on the other hand, is by definition a function of multiple wavelengths. This chapter provides an introduction to aberrations; a more mathematical treatment is provided in Chapter 5. For much more detail about optical aberrations, see the references (in particular Smith [21]).

In general, aberrations will cause the blur spot to be larger than the minimum-size blur spot as determined by diffraction. In addition to an increase in size, the shape of an aberrated blur spot will also tend to diverge from the shape dictated by diffraction (such as the common Airy disk due to a circular aperture), often taking on a more Gaussian shape (without the sidelobe “rings” of the Airy disk). For most applications using cameras and imaging sensors, a simplified multi-step approach to optical analysis is recommended. Begin by using the paraxial approximation and Gaussian optics to obtain a simple first-order solution, then account for diffraction, then account for aberrations.

4.5.1 Monochromatic aberrations

Common forms of monochromatic aberrations include

- spherical,
- coma,
- astigmatism,
- field curvature,
- defocus, and
- distortion (barrel, pincushion, mustache).

Piston and tilt are sometimes mentioned as monochromatic aberrations, but they are not true optical aberrations, in that they do not represent a curvature in the wavefront of light; they will not be discussed further. Defocus, which is when the object of interest is outside the DOF, will also not be discussed in detail here. However, optometrists and ophthalmologists are interested in defocus, since it provides a method to describe conditions such as myopia and hyperopia.

Monochromatic aberrations are primarily due to either an unintended imperfection (which is usually caught and eliminated in the lens manufacturing stage) or an intentional mismatch between the actual geometry of a lens and the geometry of the lens that would be required to

⁶Depending upon the needs of the application, the sensor designer or camera user can make individual calculations at many wavelengths, two calculations at the longest and shortest wavelengths, or one calculation at the approximate midpoint of the range of wavelengths.

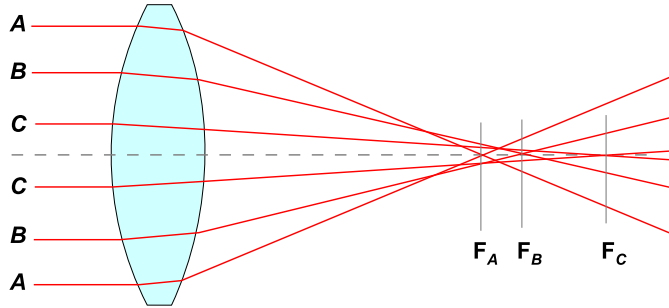


Figure 4.16: An example of spherical aberration, in which three different points of focus exist for light entering the lens at three different radii. [49]

take into account the exact nature of the propagation of light. This intentional mismatch is due to the much higher cost of producing a geometrically perfect lens. For example, a common form of monochromatic aberration is spherical aberration, which occurs when the lens is manufactured with a curvature that matches a section of a sphere; it is much cheaper to fabricate this type of lens than what is called an *aspheric* lens which more closely matches the physics related to the propagation of light.

Spherical aberration

A spherical curvature for a lens deviates from the true geometry of the propagation of light. This causes incorrect focus, but the effect is negligible near the center of the lens. An example of spherical aberration is shown in Fig. 4.16, where light entering the lens at three different radii are shown to come to focus at three different points. If objectionable misfocus due to spherical aberration is to be avoided, a smaller aperture setting must be used to restrict light to the center region of the lens. A typical spherical lens made from crown glass ($n = 1.5$) exhibits spherical aberration such that only 43% of the center lens area (i.e., 67% of the lens diameter) can be used, if objectionable misfocus due to spherical aberration is to be avoided.

Spherical aberration is one of the main reasons why a large aperture setting (i.e., low $f/\#$) usually results in a poorer image than a smaller aperture (i.e., larger $f/\#$) setting, although reducing the aperture size too much will also begin to degrade the image due to diffraction effects on the blur spot. This is why most lenses have a “sweet spot” aperture setting, typically around the middle range of the allowable aperture settings, at which the image quality is highest due to the tradeoff between spherical aberration and diffraction.

An example of a plano-convex lens with and without spherical aberration is shown in Fig. 4.17. The top subfigure is a depiction of a perfect ideal lens without spherical aberration: all incoming rays are focused at the focal point predicted by Gaussian optics. The bottom subfigure depicts a real lens with a spherical surface, which produces spherical aberration: the different rays do not come together at one focal point. The farther the rays are from the optical axis, the closer to the lens they intersect the optical axis (i.e., positive spherical aberration). Note that this subfigure is intentionally exaggerated for clarity. This figure also brings up another important point: lenses with two different radii of curvature, such as the plano-convex shown here, have a preferred orientation to minimize spherical aberration. The orientation of the plano-convex lens shown in this figure is the opposite of how you should be using the lens for the way in which the light rays are incident on the lens. If you flip this lens around, the effects of spherical aberration will be much less. The reasons for this are beyond the scope of this discussion.

In addition to the user adjusting the aperture to control spherical aberration, there are ways that lens designers can reduce the spherical aberration of a lens. For example, multiple spherical lens elements can reduce the overall spherical aberration of the multi-element lens system through a combination of convex and concave lenses. If that approach is insufficient, an

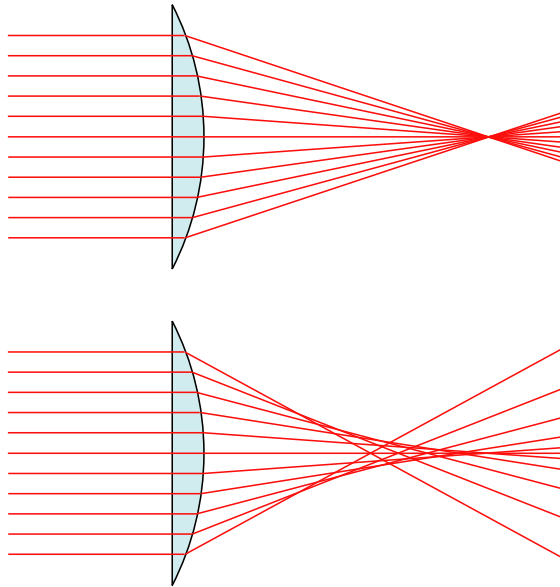


Figure 4.17: A plano-convex lens without (top) and with (bottom) spherical aberration.

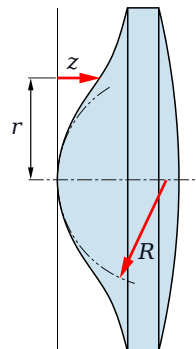


Figure 4.18: An example shape of a common molded aspheric biconvex lens. [50]

aspheric lens element can be fabricated with almost zero spherical aberration, and also reduce other aberrations at the same time. Full-size aspheric lenses are usually made by grinding and polishing glass to the desired shape; this tends to be very costly. Small aspheric lenses can now be molded from plastic (and sometimes glass); this can be done inexpensively. Such small aspheric elements are used in some small consumer cameras (including some mobile phone cameras), laser diode collimators, fiber optic couplers, etc. An example shape of a common molded aspheric biconvex lens is shown in Fig. 4.18. The deviation of the left-side curvature from spherical radius R is determined from an aspheric design equation for $z(r)$; more details about this can be found in the literature.

Coma

Coma tends to be more of a problem with reflective telescopes that use parabolic mirrors, but is also found in lens systems. This type of aberration results in off-axis point sources appearing distorted at the image plane, so they appear to have a tail (coma) like a comet. See Fig. 4.19. Coma is formally defined as a variation in magnification over the entrance pupil. Combinations of lenses designed to minimize both spherical aberration and coma are called *bestform* lenses.

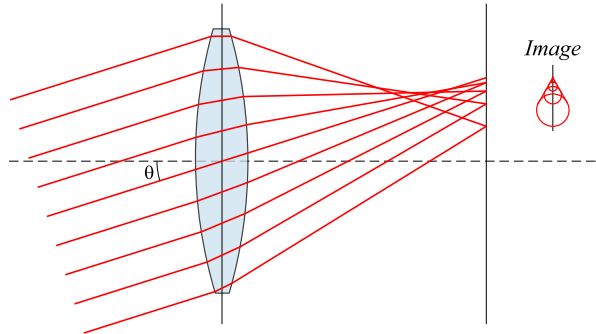


Figure 4.19: An example of coma. [51]

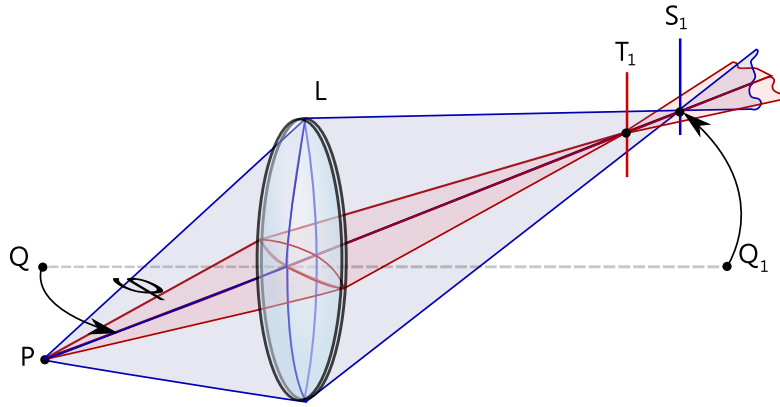


Figure 4.20: An example of astigmatism. Different focal points exist for rays propagating in perpendicular planes. See how the perspective from off-axis point P results in a different apparent shape of the lens compared to how it would appear from on-axis point Q. [52]

Astigmatism

Astigmatism is present when light rays that propagate in two perpendicular planes come to a focus at different distances. Astigmatism can be due to errors in axial symmetry of the lens, which is a problem for all areas in the FOV. This is the type of astigmatism found in both manufactured lenses and biological eyes. Astigmatism also occurs in lenses that have no axial symmetry problems; in that instance it is due to a perspective shift of how the lens surface presents to the point of the light source. An example of this second form of astigmatism is shown in Fig. 4.20; it is a problem only for off-axis regions of the image, not axial regions. Compound lens systems that are corrected for spherical aberration, coma, and astigmatism called *anastigmats*. Essentially all modern high-end photographic lenses are “close” to being anastigmatic.

Field curvature

Field curvature is sometimes called “Petzval field curvature.” It manifests itself as a warping in the image of a planar object due to using a planar focal surface, when the ideal focal surface really should be curved. This effect can be seen in Fig. 4.21. The human retina is curved, so field curvature is far less of a problem for our eyes than it is for cameras, where the focal plane sensor array is flat. Most modern photographic lenses are designed to minimize field curvature. They

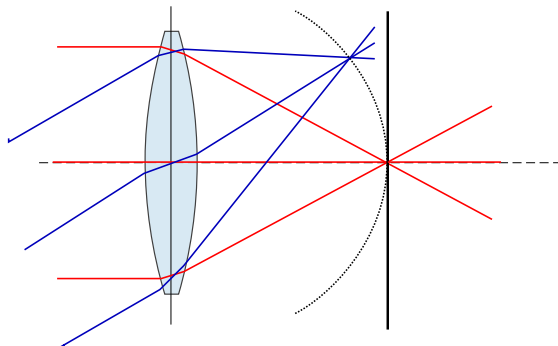


Figure 4.21: An example of field curvature. [53]

effectively have a focal length that increases slightly with ray angle, counteracting the distorting effects of a planar focal image surface. Field curvature, when present, results in a slight blurring of off-axis points. Don't confuse field curvature with distortion, the latter of which is discussed next.

Distortion

There are two main types of distortion: barrel and pincushion. A combination of both types is often called mustache distortion. Distortion is found more often in zoom lenses than in prime lenses, particularly wide-range zoom lenses, due to the unavoidable tradeoffs inherent in such a lens. Some non-macro prime lenses will show such distortions when used to focus at very close distances.

Barrel distortion exists when image magnification *decreases* with distance from the optical axis. The apparent effect is that of a planar image which has been mapped around a sphere (or a barrel). Fisheye (ultra-wide-angle) lenses, which can have nearly hemispherical FOVs, accept this type of distortion as a way of mapping an infinitely wide object plane into a finite image area.

Pincushion distortion exists when image magnification *increases* with the distance from the optical axis. The visible effect is that lines in a planar image that do not go through the center of the image are bowed inwards, towards the center of the image, similar to a pincushion.

Mustache distortion is a mixture of both barrel and pincushion distortion; it is sometimes referred to as complex distortion. It is less common than barrel or pincushion distortion, but not particularly rare. Typically, mustache distortion appears as barrel distortion close to the image center and gradually turns into pincushion distortion towards the image periphery. This makes horizontal lines in the top half of the frame look like a handlebar mustache, which is probably where it got the name.

The three forms of distortion are depicted in Fig. 4.22. Most modern high-end prime photographic lenses do not exhibit these distortions to a noticeable level if used over reasonable focus ranges. Even very expensive zoom lenses, especially wide-range ones (e.g., there is a 18–200 mm zoom lens available from a top manufacturer), will often show noticeable distortion. Super-wide-angle lenses inevitably show barrel distortion, but that is a necessary tradeoff for this type of lens, as mentioned earlier.

If you find objectionable levels of distortion present in your images, there is no easy optical method to reduce this type of aberration if it is caused by the lens you are constrained to use. However, as an alternative you can obtain the image, transfer it to your computer, then use image processing software to warp the image with the opposite type of distortion and “correct” the image that way. Some off-the-shelf programs, such as Adobe Photoshop and GIMP (the latter of which is public domain), have built-in manual lens distortion correction; other, typically more expensive, programs have automatically calibrated distortion correction.

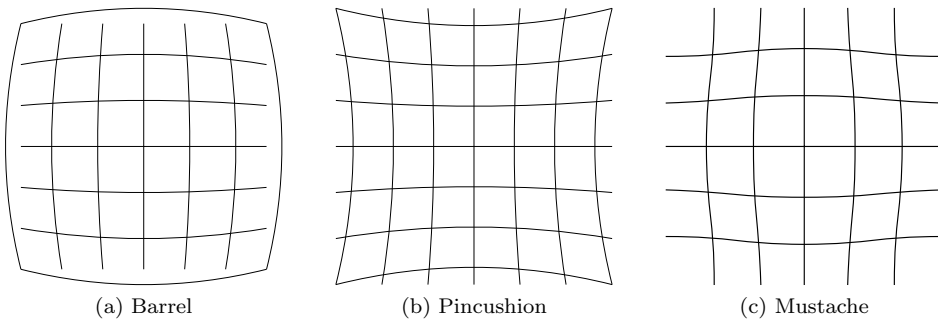


Figure 4.22: Three forms of the monochromatic aberration called distortion.

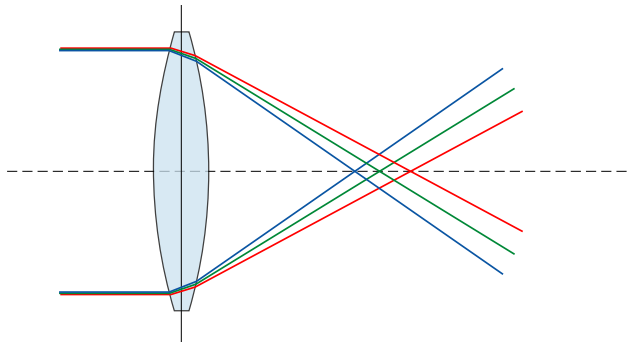


Figure 4.23: An example of chromatic aberration. [54]

4.5.2 Chromatic aberration

Chromatic aberration is primarily due to the unavoidable fact that the refractive index of any material, including lens glass, is wavelength dependent. Therefore, a single lens will exhibit slightly different focal lengths for different wavelengths of light as shown in Fig. 4.23.

The fact that monochromatic aberrations are also wavelength dependent means that even differences in monochromatic aberrations due to differences in wavelength can be considered contributors to chromatic aberration. Chromatic aberration appears in a color image as fringes of inappropriate color along edges that separate bright and dark regions of the image. Even monochrome images can suffer from degradation due to chromatic aberration, since a typical monochrome image using incoherent light is formed from light intensity that spans many wavelengths.

There are two kinds of chromatic aberration: axial and transverse. Axial (also called longitudinal) chromatic aberration occurs when different wavelengths of light are focused at different *distances* from the lens. This effect is found throughout the image, and can be reduced by using a smaller aperture (i.e., larger $f/\#$), since this increases the DOF such that the less-than-perfect focus of various colors is not as noticeable. Transverse (also called lateral) chromatic aberration occurs when different wavelengths of light are focused at different *positions* in the focal plane (because the magnification and/or distortion of the lens varies with wavelength). This effect is typically not found near the center of the image, but increases toward the edge of the image. Transverse chromatic aberration cannot be reduced by adjusting the aperture.

A common way lens designers reduce chromatic aberration is to combine multiple lens elements of different materials. The most common type is called an *achromatic doublet*, with two

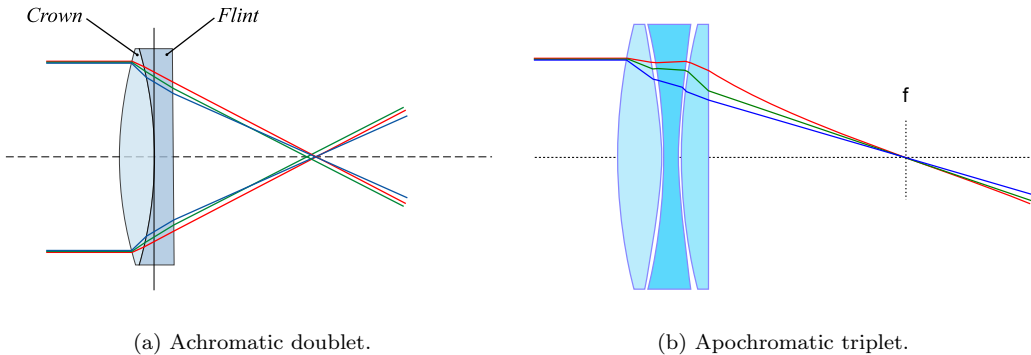


Figure 4.24: Compound lenses using multiple types of glass for reducing chromatic aberration. Credit: (a) [55] and (b) [56]

lens elements made of crown glass and flint glass, as shown in Fig. 4.24(a). It corrects for two wavelengths. Using more than two lens elements is also common; this is more expensive but can provide better correction. An *apo*chromatic triplet (or APO) shown in Fig. 4.24(b), for example, corrects for three wavelengths. Even better correction can be achieved with low-dispersion glass (typically containing fluorite), but these lenses are quite expensive. A *superachromatic* lens made from fluorite glass can correct for four wavelengths, along with correction for spherical and other aberrations.

4.5.3 Aberrations in general

In multiple-lens optical systems, aberrations of all types can be mitigated using special combinations of convex and concave lenses and specific types of glass; this is usually described as *corrected optics*. High quality corrected optics, although expensive, can achieve images very close to the theoretical ideal. Spherical aberration, by itself, can be minimized even in a single lens system by using (a relatively expensive) aspheric lens.

Most readers of this book aren't lens designers, but rather lens users. So how does the lens user deal with aberrations? First, use the best corrected optics you can afford or borrow. This will make everything much, much easier. Run some tests with your particular lens/camera combination and find the "sweet spot" aperture for your lens and focus distance to suit your particular application. If there are still residual problems with specific types of aberrations, try to address them individually. For example, if chromatic aberration is a problem, you could try to restrict the wavelengths used for your illumination. If barrel or pincushion distortion is a problem, you could use a warping algorithm via image processing. **Note:** It is critical that if your images are to be used as data for research and publications, you must be sure to explicitly report any and all image processing manipulations performed on the images.

There will always be some degree of aberrations present in any real-world optical system. Aberrations always tend to enlarge (and reshape) the diffraction limited blur spot. High quality lenses that are readily available in the visible range, when used as intended by the designer, do a very good job of minimizing the various aberrations. Lenses in other wavelength ranges, such as IR, may have a much higher level of aberrations. Your specific application will determine if you need to take additional steps to mitigate aberrations. Aberrations, and simulating their effects, are revisited again in Section 5.6, in the context of Fourier optics.

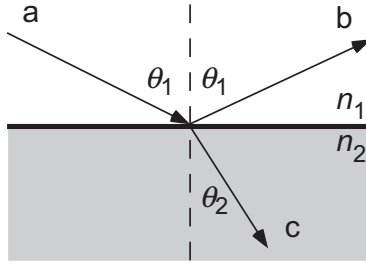


Figure 4.25: Reflection (ray b) and refraction (ray c) of incident light (ray a) encountering a boundary.

4.6 Reflection and refraction

When light enters an optical system, it encounters a boundary between two different indices of refraction (n). For example, when light propagates through air ($n_1 = 1.0$) and encounters a lens made of crown glass ($n_2 = 1.5$), part of the light energy is refracted and part of it is reflected at this boundary (see Fig. 4.25). The refracted part would pass into the lens, albeit with a changed path direction (unless the light ray was normal to the boundary). The reflected part does not enter the lens; it “bounces off” the boundary with an exit angle equal to the arrival angle (θ_1 in Fig. 4.25). Only *specular reflection* is considered here, where any irregularities in the boundary surface are small compared to the wavelength (i.e., an optically smooth surface). If this is not true, *diffuse reflection* (i.e., scattering) occurs. Diffuse reflection results in multiple angles of reflection and is often treated in a probabilistic manner. Such an optically rough surface is called a *Lambertian surface*.

4.6.1 Critical angle

In the air-to-lens example above, $n_2 > n_1$. If the converse is true (where $n_2 < n_1$), then there exists a critical angle θ_c for the angle of incidence θ_1 shown in Fig. 4.25 such that

$$\theta_c = \arcsin\left(\frac{n_2}{n_1}\right); \quad (4.12)$$

note that the arcsin is not defined for $n_2 > n_1$. If $n_2 < n_1$, then for any angle of incidence where $\theta_1 \geq \theta_c$, *total internal reflection* will occur and no light will cross the boundary to be refracted. Total internal reflection is the main phenomenon that allows optical fibers to work, for example, as shown in Fig. 4.8. For a multiple lens system using different types of glass, there may be many such boundaries at which the index of refraction changes, including those for which $n_2 < n_1$. However, multiple lens systems are designed such that $\theta_1 < \theta_c$ and total internal reflection is not an issue.

4.6.2 Snell's law

The familiar Snell's law

$$\frac{\sin \theta_1}{\sin \theta_2} = \frac{n_2}{n_1} \quad (4.13)$$

predicts the angle of refraction;⁷ the angle of specular reflection is always equal to the angle of incidence as shown in Fig. 4.25. The reflectance R is the fraction of incident light intensity (i.e.,

⁷Snell's law is named after Willebrord Snellius (born Willebrord Snel van Royen) (1580–1626). The spelling of Snell's name has been Anglicized; the more correct Dutch spelling is Snel (or Snellius), but Snell is overwhelmingly found in the literature. Note that Snell's law and other significant discoveries in optics were made by Middle Eastern scientists such as Ibn Sahl (c. 940–1000) and Ibn al-Haytham (c. 965–1039) many hundreds of years

power) that is reflected, and the transmittance T is the fraction of incident light intensity that is refracted. Obviously, conservation of energy requires that $R+T=1$. In order to determine how much of the incident light will be reflected, we need to take into account the polarization state of the incident light. The direction of polarization is referenced to the direction of the electric field lines of the electromagnetic wave.

4.6.3 Fresnel equations

Assume the page on which the plot of Fig. 4.25 appears is the plane of incidence for the incoming light. If the incident light is polarized such that the electric field is perpendicular to the plane of incidence, then we call it *s-polarized* and the reflectance is denoted R_s . If light is polarized such that the electric field is parallel to the plane of incidence, we call it *p-polarized* and the reflectance is denoted R_p .

A common form of the Fresnel equations,⁸ which predict the values of R_s and R_p is:

$$R_s = \left| \frac{n_1 \cos \theta_1 - n_2 \cos \theta_2}{n_1 \cos \theta_1 + n_2 \cos \theta_2} \right|^2, \quad T_s = 1 - R_s; \quad (4.14)$$

and

$$R_p = \left| \frac{n_1 \cos \theta_2 - n_2 \cos \theta_1}{n_1 \cos \theta_2 + n_2 \cos \theta_1} \right|^2, \quad T_p = 1 - R_p. \quad (4.15)$$

If the light is unpolarized (i.e., randomly polarized), then a common estimate is $R = (R_s + R_p)/2$.

The assumption is that materials on each side of the boundary have a permeability μ approximately equal to the permeability of a vacuum (μ_0). This tends to be true for most common optical materials. The completely general Fresnel equations are more complicated than this.

To obtain the form of the Fresnel equations only in terms of the angle of incidence θ_1 , use Snell's law and basic trigonometry to replace θ_2 :

$$R_s = \left| \frac{n_1 \cos \theta_1 - n_2 \sqrt{1 - \left(\frac{n_1}{n_2} \sin \theta_1 \right)^2}}{n_1 \cos \theta_1 + n_2 \sqrt{1 - \left(\frac{n_1}{n_2} \sin \theta_1 \right)^2}} \right|^2, \quad T_s = 1 - R_s; \quad (4.16)$$

and

$$R_p = \left| \frac{n_1 \sqrt{1 - \left(\frac{n_1}{n_2} \sin \theta_1 \right)^2} - n_2 \cos \theta_1}{n_1 \sqrt{1 - \left(\frac{n_1}{n_2} \sin \theta_1 \right)^2} + n_2 \cos \theta_1} \right|^2, \quad T_p = 1 - R_p. \quad (4.17)$$

Note that if you plot the Fresnel equations in terms of θ_1 , you will find an angle at which no p-polarized light will be reflected (i.e., $R_p = 0$), which can be seen in Fig. 4.26.

4.6.4 Brewster's angle

The angle of incidence for p-polarized light, for which it is completely transmitted through an optical boundary, with no reflection, is called Brewster's angle⁹ θ_B . The value of θ_B is given by

$$\theta_B = \arctan \left(\frac{n_2}{n_1} \right). \quad (4.18)$$

before Snel, Descartes, Newton, Abbe, Rayleigh, and so on were born [57]. Many texts fail to mention this. It's also interesting to note that Snell's law follows directly from Fermat's principle of least time, which in turn follows from the propagation of light as waves, and is consistent with quantum electrodynamics.

⁸Named after Augustin-Jean Fresnel (1788–1827), a French engineer and physicist who contributed significantly to the establishment of the theory of wave optics.

⁹This special angle of incidence is named after the Scottish physicist Sir David Brewster (1781–1868).

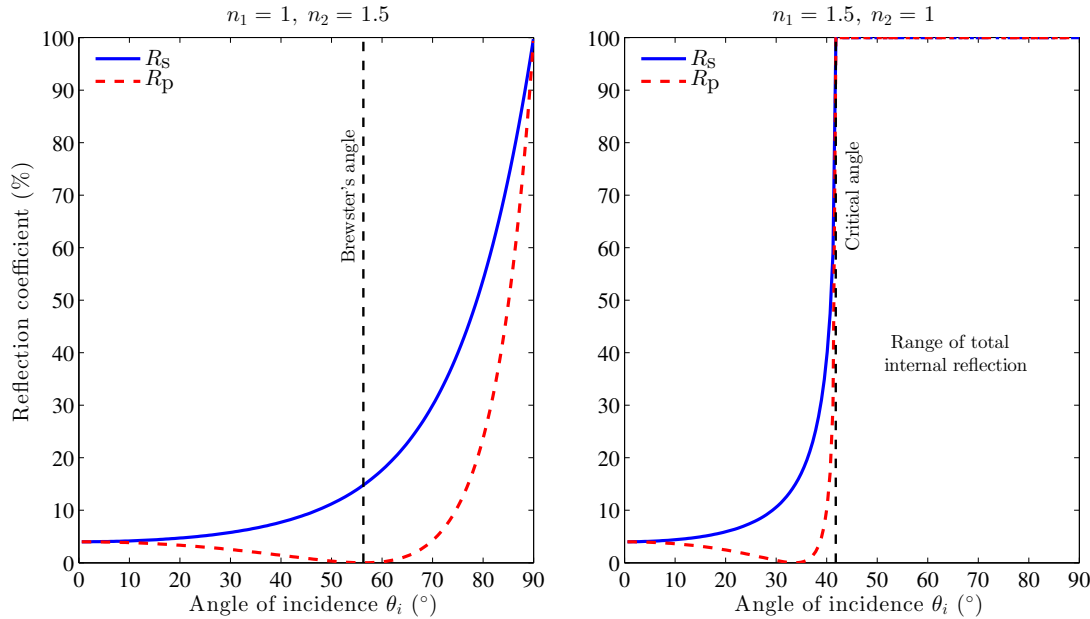


Figure 4.26: Reflected light (R_s and R_p) versus angle of incidence for two different boundaries.

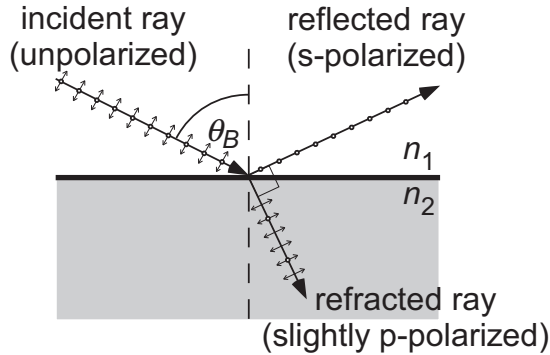


Figure 4.27: Light incident at Brewster's angle θ_B reflects only as s-polarized light.

Applying Eq. (4.18) to the two scenarios in Fig. 4.26, you will find Brewster's angle is 56.31° for the left subfigure, and 33.69° for the right subfigure. Don't confuse Brewster's angle with the critical angle for total internal reflection that was defined by Eq. (4.12); they relate to two very different phenomena. In Fig. 4.26, there is no critical angle for the left subfigure (since $n_2 > n_1$), but for the right subfigure, the critical angle is 41.81° .

When unpolarized light is incident to a boundary at angle θ_B , the light that is reflected from the surface is therefore perfectly polarized as s-polarized light. This situation is depicted in Fig. 4.27. This dependence of reflection on polarization is why polarized sunglasses and polarizing filters for camera lenses (discussed in Section 3.7) work so well. Looking again at Fig. 4.26, it can be seen that, over a wide range of incident angles, the majority of reflected light from a randomly polarized source, such as sunlight, will have s-polarization (where the electric field is perpendicular to the plane of incidence). For the purposes of sunglasses, most of the reflecting surfaces are horizontal, so the primarily s-polarized reflected light will be primarily horizontally polarized. Polarized sunglasses use a polarizing material such as Polaroid sheets to block horizontally-polarized light, which tends to reduce reflections from horizontal surfaces.

The effect is strongest with smooth surfaces such as water (see Fig. 3.14), but reflections from roads and the ground are also reduced. Polarizing filters for camera lenses can be adjusted to block any desired angle of polarization.

Example 4.9 Reflectance calculations

Given: Two scenarios:

1. Light passing from air to a glass lens with $n = 1.5$
2. Light passing from a glass lens with $n = 1.5$ to air

For each scenario, calculate the reflectance R (as an unweighted average of equal amounts of s and p polarization) at these angles of incidence:

- Normal incidence $\theta_1 = 0.0^\circ$.
- Brewster's angle $\theta_1 = \theta_B$.
- The critical angle $\theta_1 = \theta_c$.

Solution: These two scenarios are depicted in Fig. 4.26.

1. Scenario 1.

- Normal incidence. $R_s = R_p = R = \left(\frac{n_1 - n_2}{n_1 + n_2}\right)^2 = 0.04$ or 4%.
- Brewster's angle. $\theta_B = \arctan(1.5/1) = 0.9828 \text{ rad} = 56.31^\circ$. At θ_B , $R_p = 0$ by definition, so only calculate R_s . Using Eq. (4.16), $R_s = 0.147929$, or about 15%, so $R \approx 7.5\%$.
- The critical angle. For $n_2 > n_1$, there is **no** critical angle.

2. Scenario 2.

- Normal incidence. $R_s = R_p = R = \left(\frac{n_1 - n_2}{n_1 + n_2}\right)^2 = 0.04$ or 4%.
- Brewster's angle. $\theta_B = \arctan(1/1.5) = 0.5880 \text{ rad} = 33.69^\circ$. At θ_B , $R_p = 0$ by definition, so only calculate R_s . Using Eq. (4.16), $R_s = 0.147929$, or about 15%, so $R \approx 7.5\%$.
- The critical angle. $\theta_c = \arcsin(1/1.5) = 0.7297 \text{ rad} = 41.81^\circ$. At θ_c , $R_s = R_p = R = 1.0$ by definition, so no need to calculate. $R = 1.0$ or 100%.

Note that at normal incidence and at Brewster's angle, it doesn't matter which material is n_1 and which is n_2 with regard to reflection.

4.6.5 Coherence length

The values of R and T discussed above relate only to the intensity (i.e., magnitude squared) of the light. What about phase effects when light is reflected? When light reflects off a second material with a higher refractive index than the first material, it undergoes a polarity inversion (i.e., a 180° phase shift). In the opposite case, when the second material has a lower refractive index than the first material, the light will reflect in phase. This is an important principle in the field of thin-film optics, antireflection coatings, etc.

When light undergoes multiple reflections between two or more close parallel surfaces, the multiple beams of light generally interfere with one another due to path length differences and phase inversions. The transmission and reflection percentages in this situation depend on the wavelength of the light and the distance between surfaces. This form of interference occurs only

when the surfaces are at distances comparable to or smaller than the light's *coherence length*, which for ordinary white light is only few micrometers or less.¹⁰ An approximation for coherence length is

$$L \approx \frac{2 \ln(2) \lambda^2}{\pi n \Delta\lambda} \quad (4.19)$$

where n is the refractive index of the material through which light is passing, and $\Delta\lambda$ is the approximate spectral width of the light source. A familiar example of such interference between reflections is the observation of iridescent colors seen in a soap bubble or in thin oil films on water. Practical applications include Fabry-Pérot interferometers, antireflection coatings for lenses, and optical filters. A quantitative analysis of these effects is based on the Fresnel equations, but with additional calculations to account for interference.

4.6.6 AR coatings

For a technical user of cameras or other imaging devices, most reflections are undesirable. One ramification of reflection for a camera user is that the fraction of light intensity that is reflected at a boundary never makes it past the boundary, and therefore will never make it to the photodetectors. For example, for incident light arriving at $\theta_1 = 0$, it is easy to see that the Fresnel equations simplify to $R = \left(\frac{n_1 - n_2}{n_1 + n_2}\right)^2$, which makes it easy to perform a "what if" calculation. For the air-glass interface scenario where $n_1 = 1.0$, $n_2 = 1.5$ and $\theta_1 = 0$, it is seen that $R \approx 0.04$, which means 4% of the light is lost to reflection at the boundary, which is not an insignificant amount. This same effect occurs at every boundary in a multi-element lens system, including both the "front" and "rear" boundary of every lens element. This can not only cause significant loss of light intensity available to the photodetectors, but also results in spurious reflections bouncing around inside the optical system, greatly degrading the image contrast and causing undesirable noise spots in an image.

To reduce this effect, anti-reflective (AR) coatings have been developed that incorporate one or more thin films (where the thickness of the coating is typically on the order of $\lambda/4$). Destructive interference of the reflected light (and constructive interference of the transmitted light) greatly reduces R , and allows more light to be transmitted to the photodetectors. The effectiveness of an AR coating is dependent upon both the wavelength and the angle of incidence. The term *coated optics* is often used to describe such AR optics. Essentially all standard optical components (lenses, beam splitters, turning mirrors, etc.) are available with AR coatings, and their use is highly recommended. When looking at a camera lens, the AR coating is usually evident as a bluish (sometime greenish) reflection from the front lens boundary. You can also see this in high quality binoculars and telescopes which use coated optics.

There are many kinds of AR coatings, such as index matching (the oldest kind, first discovered by Lord Rayleigh in 1886), single layer, multilayer, and absorbing. An interesting trivia fact related to AR coatings involves the eye of a moth. The surface of a moth's eyes are covered with a natural nanostructured film which eliminates reflections. This allows the moth to see well in the dark, without reflections from the eyes which would give the moth's location away to predators. The structure consists of a hexagonal pattern of bumps, each roughly 200 nm high and spaced 300 nm center-to-center. This AR coating works because the bumps are smaller than the wavelength of visible light, so the surface appears to have a continuous refractive index gradient between the air and the medium of the eye, which decreases reflection by effectively removing the sudden change in index of refraction seen in a normal air-lens interface. Practical anti-reflective films have been engineered using this effect; this is a form of biomimicry.

¹⁰Coherent light from a laser source has a much longer coherence length.

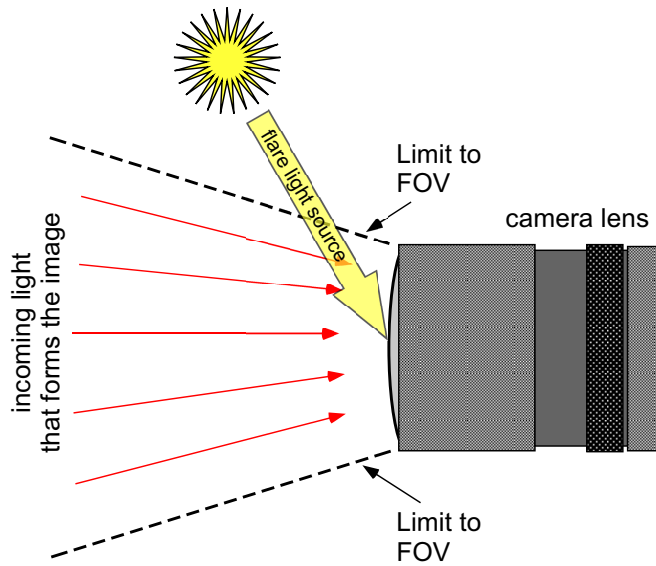


Figure 4.28: Light from outside the FOV can contribute to lens flare.

4.6.7 Lens flare

This section discussing reflection is a good place to mention the phenomenon of *lens flare*. Lens flare is caused when very bright non-image-forming light enters the lens, from inside or sometimes outside the FOV, resulting in internal reflection and scattering from material inhomogeneities in the lens elements. Normally, light from outside the FOV does not contribute to the final image, but if this light is bright enough and it reflects, it may travel an unintended path and reach the FPA sensor. Such a scenario is shown in Fig. 4.28. Lens flare tends to be more of a problem for lenses with more elements, such as zoom lenses. It shows up in two forms: as visible artifacts (often in the shape of the lens aperture opening), and as a haze across all or part of the image. The haze form of lens flare makes an image look “washed out” by reducing contrast and color saturation; it adds light to dark image regions, and adds white to color-saturated regions, thus reducing their saturation. This haze form of flare is also present in biological eyes in bright sunlight.

While some photographers intentionally incorporate lens flare (usually of the artifact form) into their images, technical camera users almost always want to avoid or minimize lens flare. Approaches for controlling lens flare include: use the best AR coated optics you can afford, use prime lenses rather than zoom lenses if possible, use a lens hood (which reduces light from outside the FOV), and control the light source location and coverage if you can (such as by using “barn door” attachments for lights).

4.7 Summary

What are some of the key ideas with regard to basic optics and imaging?

- Calculations such as image plane distance or image size are simplified by the approximations and assumptions of Gaussian optics and the Gaussian lens formula.
- The effects of diffraction, determined largely by the aperture size and shape (and the wavelength of light), cannot be ignored.
- Depth of field defines the region of acceptable sharpness in an image.

- The field of view of a camera or imaging system is determined not just by the optics, but also by the size and shape of the sensor array. The aperture size and shape usually has no influence on the FOV.
- Real-world optics have various aberrations that will cause the minimum blur spot to be larger.
- There are many ramifications to the effects of refraction and reflection, the latter of which is very sensitive to the polarization of light. To control unwanted reflections, including lens flare, use the best AR coated optics you can afford.

Application of these concepts can provide considerable insight into the anticipated performance of a given optical system.

Problems

- 4.1 A camera with a 70 mm lens is used to focus on a 254 mm (per side) cube at a distance of 10 m. Find the linear size the cube's image on the image plane.
- 4.2 If the 70 mm lens is adjusted to an aperture setting of f/4, find the linear value of the three common resolution criteria (Rayleigh, Abbe, and Sparrow).

Chapter 5

Fourier Optics for Analysis and Simulation

FOURIER optics is a particularly powerful and practical method of dealing with design considerations such as apertures, lenses, photodetector size, and spatial sampling. The Fourier approach can even be continued (with a change of domains from space to time) to the electronics associated with obtaining an image from a given sensor system. The classic reference for Fourier optics is the excellent book by Goodman [58], although Wilson [59] can also be quite helpful; a succinct treatment can be found in [18, Chap. 11]. Less theoretical discussions of MTF theory (based upon Fourier optics) can be found in [60–62]. The method is very similar to the Fourier approach for the design and analysis of circuits and systems that is familiar to electrical engineers. The treatment given here is brief and is not intended to be rigorous, but rather to just provide some practical techniques for analyzing or designing an optical system. Applying MTF theory to easily analyze other parts of the camera, such as the sensor array, follows this chapter.

When discussing Fourier optics, it's important to distinguish between two forms of light: coherent versus incoherent light. Coherent light, such as that emitted from laser sources, exhibits wavefronts that stay aligned in phase over long distances, and such propagating light has low divergence. Low divergence is why the spot from a laser pointer on a wall across a large room is still rather small. For coherent light, the electromagnetic field *amplitude* sums directly in calculations. Incoherent light, such as sunlight and that emitted from most common light sources, exhibits a randomized phase of the various wavefronts, and such propagating light has high divergence. That's why the spot from a regular flashlight on a wall across a large room is rather large and spread out. For incoherent light, the electromagnetic field *flux density* (also called irradiance or intensity) sums directly in calculations. With regard to Fourier optics, the difference between coherent and incoherent light comes down to whether we must be concerned with light amplitude (and phase) or light intensity (with no phase term), respectively. This text is primarily concerned with incoherent light (and thus intensity), but Fourier optics as discussed here can be easily adapted to coherent light, as described in [58, 59].

Familiarity with Fourier transforms is assumed here. If needed, Appendix A provides a succinct review.

5.1 Foundation of Fourier optics

5.1.1 Three diffraction regions

Recall the diffraction of light through an aperture discussed in Chapter 4. It was mentioned that a lens was not even necessary to create the diffraction pattern, as shown in Fig. 5.1. What happens to light as it passes through just an aperture, and continues to propagate?

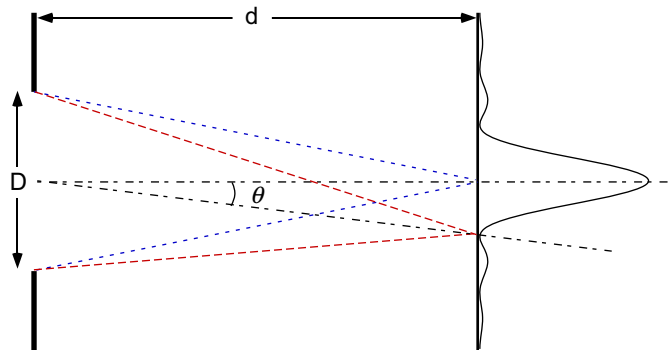


Figure 5.1: Diffraction of light passing through an aperture.

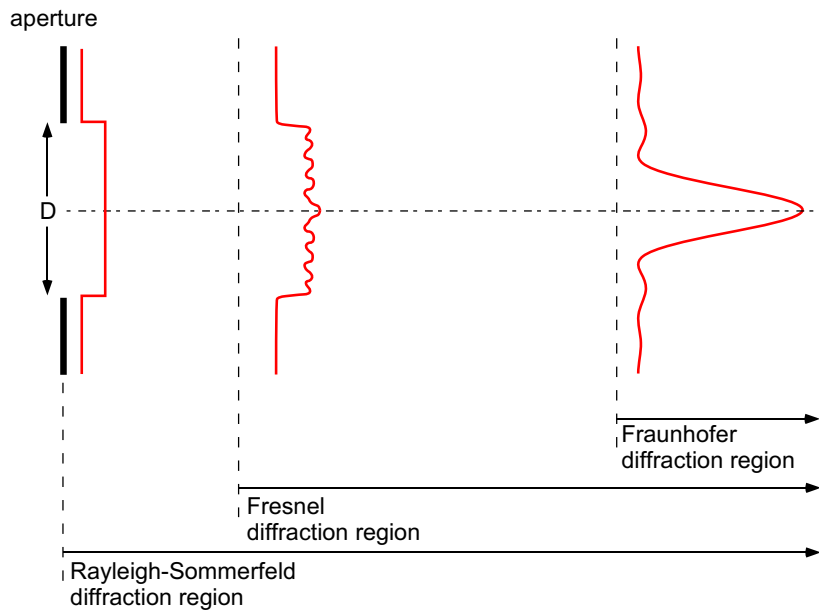


Figure 5.2: The three diffraction regions of light passing through an aperture.

Close to the aperture, the electric field amplitude of the electromagnetic (EM) radiation due to diffraction must be found using the full Rayleigh-Sommerfeld integral solution. This is often a very difficult task; only simple configurations can typically be solved analytically. More complicated configurations require a numerical methods solution. However, don't forget that the Rayleigh-Sommerfeld integrals will provide a correct solution at all distances from the aperture—it's just not an easy method for many situations. A short distance from the aperture, a somewhat simpler method using the Fresnel approximation¹ for diffraction can be used. Very far from the aperture (in the *far field*), the even simpler Fraunhofer approximation for diffraction can be used. These three diffraction regions are depicted in Fig. 5.2.

The Fraunhofer approximation relies on the assumption that only negligible curvature to the wavefronts occurs at this far field distance, so the wavefronts can be treated as planar. This greatly simplifies the methods required for a solution, but depends on distance d being far enough for the light to be considered in the far field. The primary condition for the far field, and thus

¹This is sometimes called the Fresnel-Kirchhoff (or Kirchhoff-Fresnel) approximation.

for Fraunhofer diffraction, is:

$$\frac{D^2}{\lambda d} \ll 1 \quad \text{or} \quad d \gg \frac{D^2}{\lambda} \quad (5.1)$$

where D is the diameter (or largest dimension) of the aperture, λ is the wavelength of light, and d is the distance along the optical axis from the aperture plane to the plane at which the diffraction pattern is observed.

For just an aperture with no lens, the distance to the Fraunhofer region at optical wavelengths is typically on the order of 1000 meters or more. For example, assume $D = 20$ mm for the aperture diameter, and 550 nm for the wavelength of light. In this case, d needs to be much larger than 727 m for light to be in the Fraunhofer region. How much larger is “much larger?” Perhaps 100 times or more,² which means d would need to be at least 72.7 km (or a bit over 45 miles)! If the aperture is ten times smaller, with $D = 2$ mm, then $D^2/\lambda = 7.27$ m, and thus d would need to be at least 727 m for light to be in the Fraunhofer region.

While it seems that long distances are necessary to be able to use the Fraunhofer approximation, it turns out that by inserting a positive lens (or lens system) in the path of the light, the Fraunhofer diffraction region moves to the image plane of the lens (i.e., at distance s_i), which is a much shorter distance (typically less than half a meter).

5.1.2 Aperture functions

Assume light enters the optical system through an aperture and lens, and the lens focuses an image at the image plane. The amplitude transmittance of the aperture can be described mathematically by a simple aperture function $A(x_a, y_a)$, which is an expression of how light is transmitted through or is blocked by the aperture at the aperture plane. For example, an ideal circular aperture, with a radius of r and diameter D , could be expressed as

$$A(x_a, y_a) = \begin{cases} 1 & \sqrt{x_a^2 + y_a^2} \leq r = \frac{D}{2} \\ 0 & \sqrt{x_a^2 + y_a^2} > r = \frac{D}{2} \end{cases} \quad (5.2)$$

where (x_a, y_a) are spatial coordinates at the aperture plane, and the origin of the coordinate system is at the center of the aperture. This function, called a *circ* function, is often defined in polar coordinates to take advantage of the circular symmetry. An ideal rectangular aperture, with a height of D_y , and a width of D_x , could be expressed as

$$A(x_a, y_a) = \begin{cases} 1 & |x_a| \leq \frac{D_x}{2} \text{ AND } |y_a| \leq \frac{D_y}{2} \\ 0 & \text{elsewhere} \end{cases} \quad (5.3)$$

where the notation of x for horizontal and y for vertical axes is used. This function is called a *rect* function. Plots of these two common aperture functions are shown in Fig. 5.3.

If the aperture transmittance is not uniform across the aperture opening, then the EM field emanating from the aperture would have variations in amplitude and phase depending upon the location it came through the aperture. This is easily described by combining the variations into a single complex quantity, having a magnitude term and a phase term, that is called the generalized aperture function. The generalized aperture function is written as

$$A(x_a, y_a) = A_0(x_a, y_a)e^{j\alpha(x_a, y_a)} \quad (5.4)$$

with no change needed to the previous approach. This method will help facilitate the modeling of aberrations later in the chapter.

²Note that antenna designers use a similar rule to determine the far field for much longer wavelengths, but with a more relaxed inequality (i.e., 2 times rather than 100 times). This introduces more error in the approximation, since the wavefronts are less planar at that distance, but it's sufficient for the intended purpose. At optical wavelengths, a factor of 100 times is recommended for the inequality.

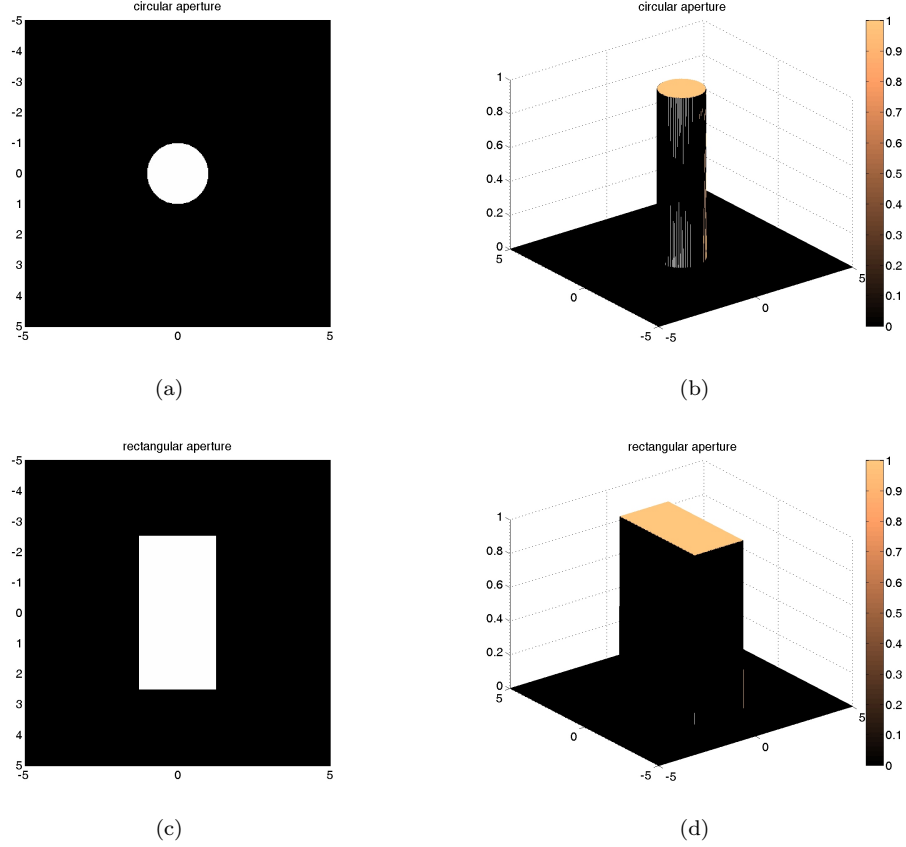


Figure 5.3: Aperture functions. A 2-D circ function is shown in (a), with the associated 3-D version shown in (b). A 2-D rect function is shown in (c), and the associated 3-D version is shown in (d).

5.1.3 Fraunhofer diffraction and Fourier optics

The electric field distribution due to Fraunhofer diffraction of an aperture, at the focal plane of a lens, can be described as

$$E(x, y) = \frac{e^{j(2\pi f t - kR)}}{R} \iint_{\text{Aperture}} \epsilon_A(x_a, y_a) e^{-j\frac{k}{R}(xx_a + yy_a)} dx_a dy_a \quad (5.5)$$

where ϵ_A is the electric field strength per unit area, f is the temporal frequency of the EM radiation, t is time, (x, y) are the spatial coordinates at the image plane, (x_a, y_a) are the spatial coordinates at the aperture plane, $k = 2\pi/\lambda$ (k is often called the *wavenumber*), and R is the distance (sometimes called *range*) from the origin of the aperture plane (i.e., at the center of the aperture) to the point (x, y) at the image plane. The term $e^{j(2\pi f t - kR)}$ simply relates the phase of the electric field at point (x, y) on the focal plane to the phase at the origin of the aperture plane. The $1/R$ term outside the integral accounts for the drop in field amplitude with distance.

At this point, the phase term $e^{j(2\pi f t - kR)}$ isn't of much interest, since it's the relative amplitude distribution of the electric field at the image plane that is of primary importance. In the far field, the value of R is essentially constant for a given image plane at reasonable values of x and y . Thus, the phase term and the $1/R$ term can be lumped into a single scaling constant. This scaling constant, as well as any variations at the aperture in amplitude and phase of the

electric field contained in $\epsilon_A(x_a, y_a)$, can all be incorporated into the magnitude and phase of the previously mentioned generalized aperture function given as Eq. (5.4). Taking advantage of all this consolidation of terms, Eq. (5.5) can be manipulated as

$$E(x, y) = \frac{e^{j(2\pi ft - kR)}}{R} \iint_{\text{Aperture}} \epsilon_A(x_a, y_a) e^{-j\frac{k}{R}(xx_a + yy_a)} dx_a dy_a \quad (5.6a)$$

$$= \int_{-\infty}^{\infty} \int_{-\infty}^{\infty} A(x_a, y_a) e^{-j\frac{2\pi}{\lambda R}(xx_a + yy_a)} dx_a dy_a \quad (5.6b)$$

$$= \int_{-\infty}^{\infty} \int_{-\infty}^{\infty} A(x_a, y_a) e^{-j2\pi(xx_a + yy_a)/\lambda R} dx_a dy_a \quad (5.6c)$$

which is a scaled Fourier transform. A change of variables leads to

$$E(u, v) = \int_{-\infty}^{\infty} \int_{-\infty}^{\infty} A(x_a, y_a) e^{-j2\pi(ux_a + vy_a)} dx_a dy_a \quad \text{where } u = \frac{x}{\lambda R} \text{ and } v = \frac{y}{\lambda R} \quad (5.6d)$$

$$= \boxed{\mathcal{F}\{A(x_a, y_a)\}} \quad (5.6e)$$

where $\mathcal{F}\{\cdot\}$ represents the Fourier transform (in this case, a 2-D Fourier transform). The variables (u, v) used above in Eq. (5.6d) represent linear spatial frequencies measured at the image plane, with the units being the reciprocal of spatial distance but usually referred to as “cycles per unit distance.” Note that there is little standardization among texts regarding which symbols to use for spatial frequencies such as (u, v) shown above. In this book, the symbols (u, v) are used in general for both linear spatial frequencies (in units such as cycles/ μm) and for angular spatial frequencies (in units such as cycles/ μrad). The context of the text should make it clear which type of spatial frequency is being expressed.

Many times, it will be useful to end the progression of Eq. (5.6) at Eq. (5.6c), in which case the expression is in terms of (x, y) , which represent linear spatial coordinates measured at the image plane, with the units being spatial distance. This scaled version of the Fourier transform should not bother the reader. Scaling the exponent in Eq. (5.6c) by the reciprocal of the constants λ and R simply has the effect of “spreading out” or “narrowing in” the resulting shape of the Fourier transform. Specifically, if λ and/or R increase, the shape will spread out at the image plane. It should only take a moment’s thought with regard to physical reality to confirm that this is the effect that would be expected for a longer wavelength or a longer distance from the aperture to the image plane.

The abbreviated mathematical manipulation of Eq. (5.6) was intended to get the reader straight to the very important main point: the field distribution of the Fraunhofer diffraction pattern (at the image plane) is equal to the Fourier transform of the field distribution across the aperture (at the aperture plane). The field distribution across the aperture is the same thing as the aperture function. **This means that the Fraunhofer diffraction pattern is equal to the Fourier transform of the aperture function.** An inverse Fourier transform at this point would return the aperture function.

Take care to note that the derivation is stated in terms of the *field amplitude* of the light. We don’t see field amplitude, and our camera sensors generally don’t record field amplitude. What we see, and what our camera sensors record, is *intensity*. **So the Fraunhofer diffraction pattern that we would see or record at the image plane, called the point spread function (PSF), is actually equal to the magnitude squared of the Fourier transform of the aperture function.** This forms the basis of most practical applications of Fourier optics for typical cameras and imaging sensors. Note that an inverse Fourier transform of the

PSF would *not* return the aperture function, because phase information is lost when converting to intensity.

The translation in space along the optical axis from the aperture plane to the image plane that culminates in Eq. (5.6e) is due to the mathematics describing the propagation of light. A ramification of the translation in space, the change in variables, and the incorporation of scaling constants into the aperture function that are all inherent in this mathematical manipulation is that the specific form of the Fourier transform of the aperture function can be expressed in multiple ways.³ It all depends on which way in which you choose to manipulate the variables, but the general shape of the Fourier transform stays the same. There are four common forms:

1. angular units (sometimes called *angle of diffraction*) measured with respect to the optical axis, usually using the small angle approximation (in radians),
2. angular spatial frequencies (in cycles/radian, cycles/mrad, cycles/ μ rads, etc.),
3. linear spatial coordinates measured at the image plane (in m, mm, μ m, etc.), and
4. linear spatial frequencies measured at the image plane (in cycles/mm, cycles/ μ m, etc.).

While form 4 is implied in Eq. (5.6e), we will find that form 3 from Eq. (5.6c), or form 1 (which is just a variant of form 3) are usually more useful for the purposes of this book when defining a PSF.

The main point of this section was to show that the Fraunhofer diffraction pattern in terms of *intensity*, which is just the magnitude squared of the Fourier transform of the aperture function, is equal to the point spread function (PSF), with regard to incoherent light. The PSF is one of the most important functions used in Fourier optics.⁴

5.1.4 Specific aperture shapes

The two most common aperture shapes in optics, cameras, and imaging devices are circular and rectangular. Beginning with the rectangular aperture, what is the Fourier transform (FT) of an ideal rectangular aperture, with a height of D_x , and a width of D_y , as described by Eq. (5.3)?

One common form of the FT of this rectangular aperture function, expressed in terms of linear spatial coordinates at the image plane (i.e., form 3), is:

$$\mathcal{F}\{A(x_a, y_a)\} = E(x, y) = (D_x D_y) \frac{\sin\left(\frac{D_x \pi x}{\lambda R}\right)}{\left(\frac{D_x \pi x}{\lambda R}\right)} \frac{\sin\left(\frac{D_y \pi y}{\lambda R}\right)}{\left(\frac{D_y \pi y}{\lambda R}\right)} \quad (5.7)$$

where (x, y) are the spatial coordinates at the image plane, λ is the wavelength, and R is the distance from the origin of the aperture plane to the point (x, y) at the image plane.

In the far field, the distance d is very far, as required for the Fraunhofer approximation (if there is no lens), such that $R \approx d$ for reasonable values of x and y . Because of this, we can substitute d in the place of R with little loss of accuracy. If there is a lens, then d is equivalent to s_i as we found in Chapter 4, but we can still substitute it for R . This results in

$$E(x, y) = (D_x D_y) \frac{\sin\left(\frac{D_x \pi x}{\lambda d}\right)}{\left(\frac{D_x \pi x}{\lambda d}\right)} \frac{\sin\left(\frac{D_y \pi y}{\lambda d}\right)}{\left(\frac{D_y \pi y}{\lambda d}\right)} = (D_x D_y) \operatorname{sinc}\left(\frac{D_x x}{\lambda d}\right) \operatorname{sinc}\left(\frac{D_y y}{\lambda d}\right) \quad (5.8)$$

where $\operatorname{sinc}(x)$ is defined as $\frac{\sin(\pi x)}{\pi x}$.

³Wilson provides an excellent explanation of this in [59].

⁴The equivalent to the PSF for coherent light is often called an amplitude spread function, or ASF.

Recall that this result is stated in terms of the field amplitude of the light. What we need is the intensity, which is equal to the magnitude squared of the FT. Let's also combine the scaling factors (i.e., the area of the aperture) into one general scaling factor. From this we obtain

$$I(x, y) = |E(x, y)|^2 = I_0 \operatorname{sinc}^2\left(\frac{D_x x}{\lambda d}\right) \operatorname{sinc}^2\left(\frac{D_y y}{\lambda d}\right) \quad (5.9)$$

where $I_0 = (D_x D_y)^2$. Compare Eq. (5.9) to the result from Chapter 4 for the diffraction pattern due to a rectangular aperture as shown by Eq. (4.4). They are exactly the same.

It can also be shown, with just a bit more effort, that the result of the magnitude squared of the FT of a circular aperture having diameter D is:

$$I(x, y) = I_0 \left[\frac{2J_1\left(\frac{\pi D \rho}{\lambda d}\right)}{\frac{\pi D \rho}{\lambda d}} \right]^2, \quad \rho = \sqrt{x^2 + y^2} \quad (5.10)$$

where function J_1 is a first-order Bessel function of the first kind. This is also exactly the same result from Chapter 4 that was given for the diffraction pattern due to a circular aperture as shown by Eq. (4.3).

The functions expressed in Eq. (5.9) and Eq. (5.10) represent the PSF of an optical system having a rectangular or circular aperture, respectively. The form of both equations is what was earlier called form 3, in that the PSFs are expressed using linear spatial coordinates measured at the image plane.

5.2 PSF

For the purposes of optical design or analysis, we typically express the PSF in linear spatial coordinates (such as mm or μm) measured at the image plane, which is assumed to be normal to the optical axis at distance s_i from the nodal point of the lens. It is sometimes convenient to remove the dependence on the image plane distance s_i by expressing the PSF in angular units (such as mrad or μrad), where the angle is referenced to the optical axis. In any case, once the PSF is known, many straightforward techniques are possible by taking advantage of linear systems theory and the properties of Fourier transforms.

Every optical component (aperture, lens, etc.) has a point spread function (PSF) defined in the spatial domain at the image plane, which describes how an infinitesimally small (yet sufficiently bright) point of light (the optical equivalent of a Dirac delta function) is spread (or smeared) by that component. The PSF (in the spatial domain) of an optical system is very similar to the impulse response (in the time domain) of an electronic system.

A perfect optical component, in the absence of both aberrations and diffraction, would pass an infinitesimally small point of light unchanged. But no such perfect component exists, and diffraction is always present. The PSF of an optical component is convolved in the spatial domain with the incoming light. This means that a perfect component would require a PSF that was a perfect delta function $\delta(x, y)$; how much the true PSF deviates from $\delta(x, y)$ determines how much it smears each point of light. Since diffraction is always present, it provides the limit on how closely a PSF can approach $\delta(x, y)$; any aberrations simply make the PSF deviate even further from the ideal.

In Section 5.1.4, an expression for the PSF of the two most common aperture shapes, circular and rectangular, were shown using linear units. For convenience, those equations are shown in Table 5.1, along with the location of the first zero of the PSF. The equivalent expressions using angular units are shown in Table 5.2. Recall that J_1 is a first-order Bessel function of the first kind.

Table 5.1: Useful equations for the PSF using linear units.

circular aperture PSF	$I(x, y) = I_0 \left[\frac{2J_1\left(\frac{\pi D \rho}{\lambda d}\right)}{\frac{\pi D \rho}{\lambda d}} \right]^2, \quad \rho = \sqrt{x^2 + y^2}$
First zero location	$\rho = 1.22 \frac{\lambda d}{D}$
rectangular aperture PSF	$I(x, y) = I_0 \operatorname{sinc}^2\left(\frac{D_x x}{\lambda d}\right) \operatorname{sinc}^2\left(\frac{D_y y}{\lambda d}\right)$
First zero location	$x = \pm \frac{\lambda d}{D_x}, \quad y = \pm \frac{\lambda d}{D_y}$

Table 5.2: Useful equations for the PSF using angular units.

circular aperture PSF	$I(\theta) = I_0 \left[\frac{2J_1\left(\frac{\pi D \theta}{\lambda}\right)}{\frac{\pi D \theta}{\lambda}} \right]^2$
First zero location	$\theta = 1.22 \frac{\lambda}{D}$
rectangular aperture PSF	$I(\theta_x, \theta_y) = I_0 \operatorname{sinc}^2\left(\frac{D_x \theta_x}{\lambda}\right) \operatorname{sinc}^2\left(\frac{D_y \theta_y}{\lambda}\right)$
First zero location	$\theta_x = \pm \frac{\lambda}{D_x}, \quad \theta_y = \pm \frac{\lambda}{D_y}$

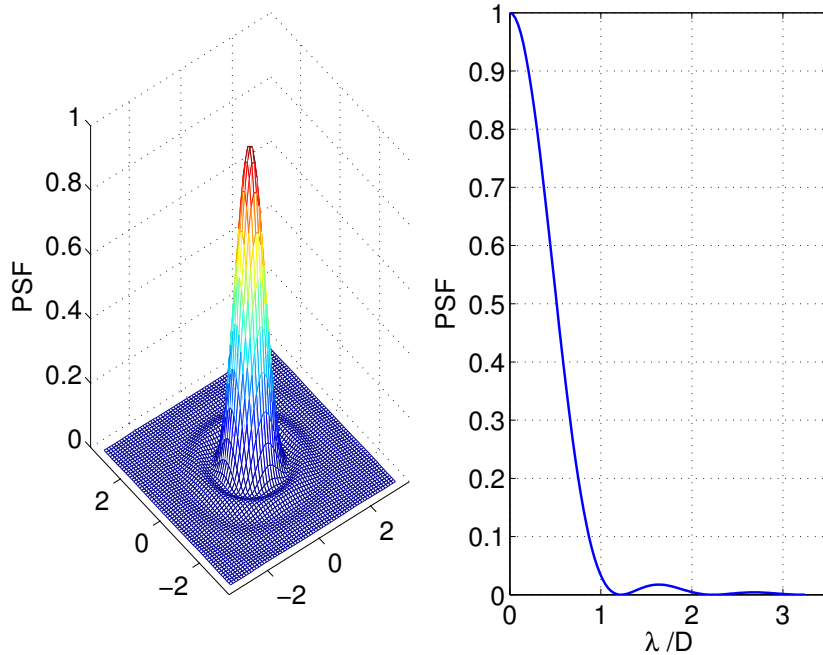


Figure 5.4: The normalized point spread function of a circular aperture is an Airy disk. Angular units of the horizontal axes are radians; to convert from angular to linear units multiply by the image distance $d = s_i$ of the optical system.

Normalized plots of the PSF for a circular aperture are shown in Fig. 5.4; compare this to Fig. 4.3. Assume a point of light $\delta(x_o, y_o)$ having wavelength λ comes from the object plane, passes through a D -diameter circular aperture (and lens), and is focused on the image plane. In order to determine how $\delta(x_o, y_o)$ will appear on the image plane we simply convolve the aperture PSF $h_A(x, y)$, which is an Airy disk, with $\delta(x, y)$ at the image plane. By the sifting property of delta function the result is $h_A(x, y)$, which is the same Airy disk. Thus, the smallest possible blur spot on the image plane due to the aperture is the same Airy disk as we found in Section 4.2, only we can now use the power of the Fourier transform and linear systems theory to more easily extend the analysis. Similar normalized plots of the PSF for a rectangular aperture are shown in Fig. 5.5; compare this to Fig. 4.4.

Example 5.1 Determining the size of the PSF

Given: A 50 mm f/1.4 lens is focused on an object at a distance of $s_o = 3$ m, with the aperture set to f/4. Assume incoherent light at a wavelength of $\lambda = 550$ nm. Find the diameter of the PSF measured two ways: from the first zero of the PSF, and from the half-power point of the PSF. Express the answers in angular units and in linear units.

Solution: A lens has an approximately circular aperture, so the PSF will approximate an Airy disk. From the given f-number, the aperture diameter will be $D = 50/4 = 12.5$ mm. Solving for angular units is easier, since the value of s_i isn't needed. From Table 5.2, the first zero of the Airy disk is at $\theta = 1.22\lambda/D$, so the PSF diameter referenced to the first zero would be $2.44\lambda/D = (2.44)(550 \times 10^{-9})/12.5 \times 10^{-3} = 107.4 \mu\text{rad}$. Recall that the diameter of the Airy disk at the *half-power point*, as shown in Fig. 4.3(a), is approximately λ/D . Therefore, the PSF diameter referenced to the half power point would be $\lambda/D = (550 \times 10^{-9})/12.5 \times 10^{-3} = 44.0 \mu\text{rad}$.

Comparing Table 5.2 to Table 5.1, it's clear that in order to express the answers in linear units, we will need the value of d , which is called s_i in the Gaussian lens formula of Eq. (4.1).

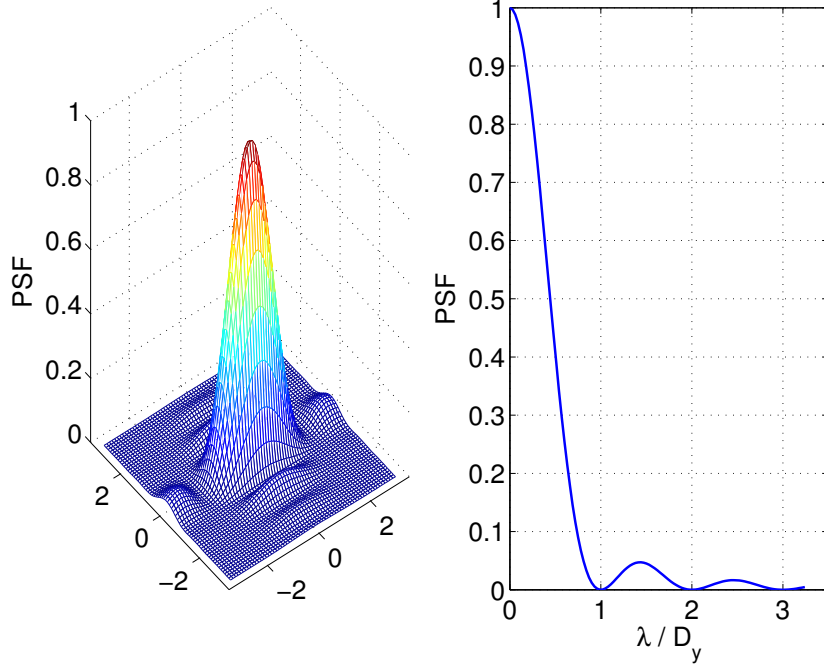


Figure 5.5: The normalized point spread function of a rectangular aperture is a 2-D squared sinc function. Angular units of the horizontal axes are radians; to convert from angular to linear units multiply by the image distance $d = s_i$ of the optical system.

Thus $d = s_i = 1/(1/f - 1/s_o) = 1/(1/50 \times 10^{-3} - 1/3) = 50.85 \times 10^{-3}$ mm. Knowing d , we can completely recalculate using the equation forms given in Table 5.1, or simply multiply the previous answers in angular units by d to obtain the equivalent answers in linear units. Using either approach, the PSF diameter referenced to the first zero would be $5.46 \mu\text{m}$, and the PSF diameter referenced to the half power point would be $2.24 \mu\text{m}$.

The PSF functions given in Chap. 4 that were based on diffraction theory are the same PSF functions found here using Fourier optics methods. The PSF for a circular aperture is an Airy disk, and the PSF for a rectangular aperture is the squared value of a 2-D sinc. Therefore, the discussion in Chap. 4 regarding resolution criteria, particularly Table 4.1, is also valid here.

In general,

$$\text{PSF} = |\mathcal{F}\{A(x_a, y_a)\}|^2 = h_A(x, y). \quad (5.11)$$

If the lens is nonideal, it will also contribute (through convolution) a PSF $h_L(x, y)$ that deviates from a delta function. The PSF $h_L(x, y)$ is determined primarily by the various lens aberrations that are present. The combined PSF of the aperture and the lens is thus $h_{AL}(x, y) = h_A(x, y) * h_L(x, y)$, where the $*$ symbol denotes convolution.⁵ The combined PSF $h_{AL}(x, y)$ is convolved with an ideal image (from purely geometrical optics) to obtain the actual image at the focal plane. If multiple lens elements are used, each lens contributes a PSF via convolution in the same way (unless the lens elements are arranged in such a way as to compensate for each other's aberrations, as discussed in Sections 4.5 and 5.6). Many other image degradations such as misfocus, sensor vibration (relative movement), and atmospheric turbulence can also be modeled with an approximate PSF that contributes, through convolution, to the overall PSF. If specific details regarding the degradation are known, it can sometimes be mitigated through careful image processing, depending upon the noise in the image [44].

⁵In practice, lens aberrations are easier to simulate by adjusting the aperture function, as will be demonstrated later in this chapter.

If you know (or can estimate) the overall optical system PSF, then you can completely characterize the effect of the optical system on any image. This is a very powerful and useful technique. It was mentioned earlier that the PSF is just an optical equivalent of the impulse response associated with an electronic system;; does that mean there an optical equivalent of an electronic system's transfer function?

5.3 OTF, MTF, and CTF

In electronics, recall that the Fourier transform of the impulse response (in the time domain) equals the transfer function (in the frequency domain). Conversely, the inverse Fourier transform of the transfer function yields the impulse response. Convolving any arbitrary input to an electronic system by its impulse response yields the system output given that input. Recall from Fourier transform techniques that convolution in one domain is equivalent to multiplication in the other domain. Thus, multiplying the frequency spectrum of the input to an electronic system by its transfer function yields the frequency spectrum of the output given that input. There is a very similar relationship for optics, which can greatly simplify optical analysis.

5.3.1 The OTF

The Fourier transform of the PSF yields the optical transfer function (OTF). That is, $\text{OTF} = H(u, v) = \mathcal{F}\{h(x, y)\}$, where (u, v) are the spatial frequency coordinates at the focal plane. The PSF is in the spatial domain, and the OTF is in the spatial frequency domain, both at the focal plane. Recalling how we can obtain the PSF using Fourier optics methods, this important relationship can be shown as

$$\begin{aligned}\text{OTF} &= \mathcal{F}\{\text{PSF}\} \\ &= \mathcal{F}\left\{|\mathcal{F}\{A(x_a, y_a)\}|^2\right\},\end{aligned}\quad (5.12)$$

where we neglect aberrations at this point. It's important to remember that the PSF is real (due to the magnitude squared operation to obtain light intensity), but that the OTF is a complex-valued function most often expressed as a magnitude and phase.

5.3.2 The MTF

The magnitude of the OTF is called the modulation transfer function (MTF), and the phase of the OTF is called the phase transfer function (PTF). In equation form, this could be written as $\text{OTF}(u, v) = \text{MTF}(u, v)e^{-j\text{PTF}(u, v)} = \text{MTF}(u, v) \angle \text{PTF}(u, v)$.

For most incoherent imaging systems, we are more interested in the MTF than we are in the PTF. See Fig. 5.6 for a normalized plot of the MTF due only to the PSF of a circular aperture (such as the circular aperture PSF shown in Fig. 5.4).

In the context of the MTF, modulation M is a description of how a sinusoidal pattern of a particular spatial frequency at the object plane can be resolved on the image plane. It quantifies the contrast between the bright (A_{\max}) and dark (A_{\min}) parts of the sinusoidal pattern, as measured at the image plane. Stated another way, modulation is the amplitude of the irradiance variation divided by the average value of the irradiance. The variation is sometimes called the AC value, and the average value is sometimes called the DC value. In equation form, modulation is

$$M = \frac{A_{\max} - A_{\min}}{A_{\max} + A_{\min}} = \frac{2(\text{AC component})}{2(\text{DC component})} = \frac{\text{AC}}{\text{DC}}.\quad (5.13)$$

From Fig. 5.6, you can see that as the spatial frequency increases, the ability of the optical system to resolve the pattern decreases, until at some frequency the pattern cannot be discerned. This has nothing to do with spatial sampling, which hasn't yet occurred! Note the MTF in Fig. 5.6 is

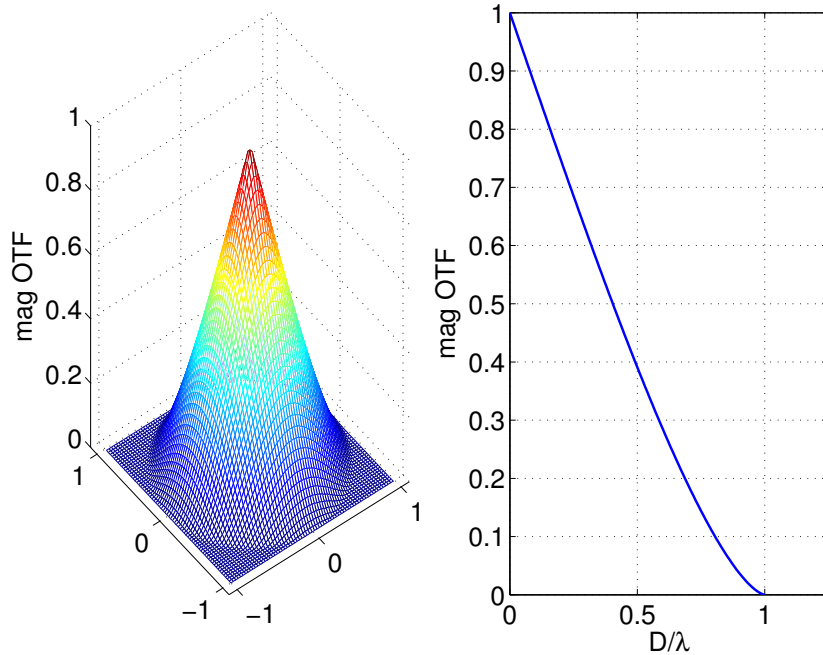


Figure 5.6: The normalized magnitude of the optical transfer function (OTF) of a circular aperture. This magnitude is typically abbreviated as MTF. Angular spatial frequency units of the horizontal axes are cycles/radian; to convert from angular to linear units divide by the image distance $d = s_i$ of the optical system.

zero at $u \geq D/\lambda$; thus D/λ is called the *optical cutoff frequency*, or f_c . However, no real-world optical system can detect a sinusoidal pattern all the way out to f_c ; the practical contrast limit for the MTF is not zero but something higher, depending on the system and the observer. This issue will be revisited later.

Since modulation and the MTF will constitute an important part of many discussions in this text, it makes sense to show figures that may help ensure the concept is fully understood. The values used to calculate modulation are shown as a 1-D plot in Fig. 5.7. The value of M is sometimes called the *modulation depth*. An example of six different values of modulation depth for 1-D sinusoids are shown in Fig. 5.8. These same six values of modulation depth for 2-D sinusoidal images are shown in Fig. 5.9.

The MTF will be an extremely valuable and useful function for analysis of many aspects of a camera or imaging system. In terms of the optics, where the aperture controls the diffraction

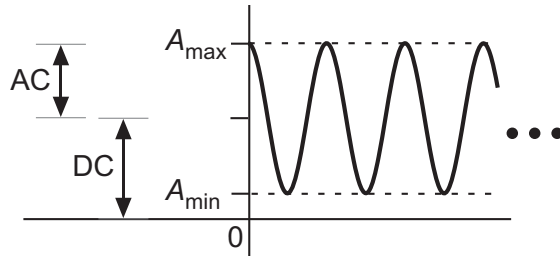


Figure 5.7: Modulation of a sinusoidal pattern is the basis of the MTF, and is defined as $M = (A_{\max} - A_{\min})/(A_{\max} + A_{\min}) = AC/DC$.

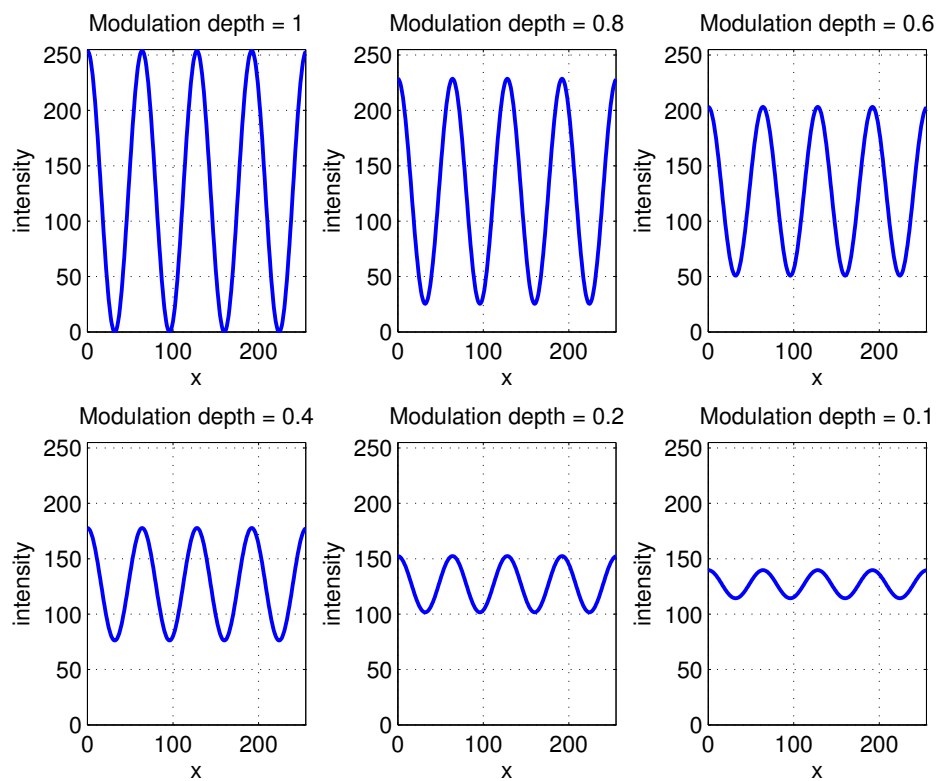


Figure 5.8: Examples of various levels of modulation (i.e., modulation depth) for a sinusoidal image, shown as a 1-D slice.

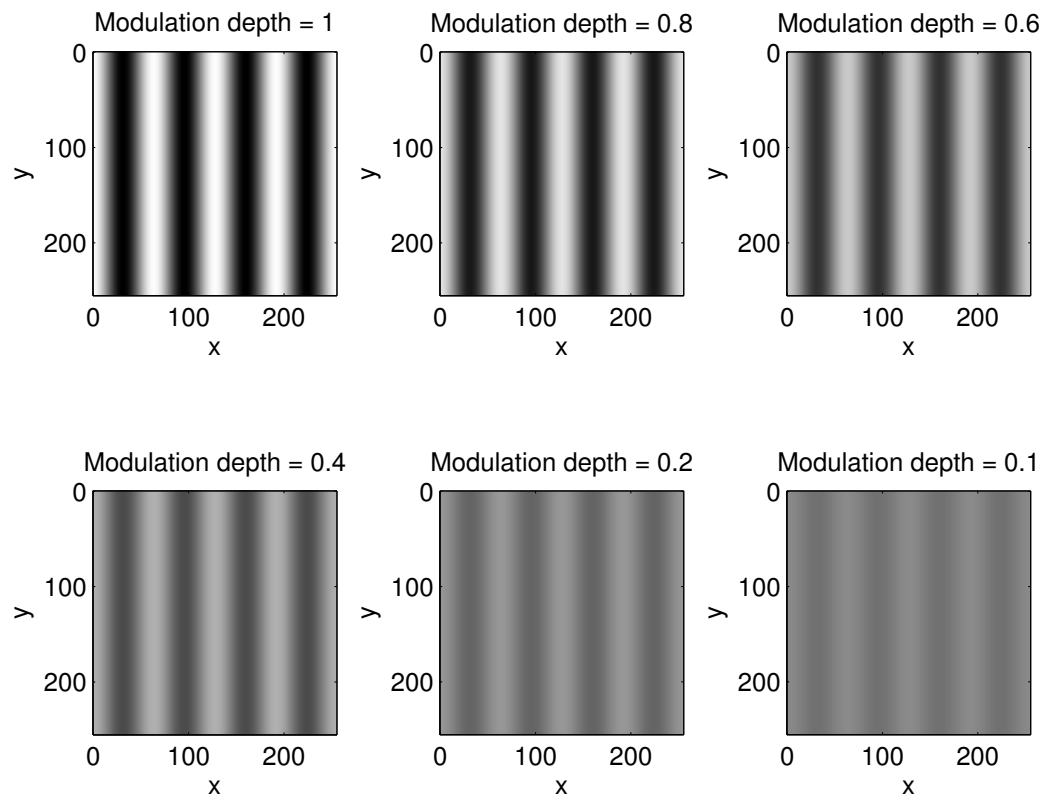


Figure 5.9: Examples of various levels of modulation (i.e., modulation depth) for a sinusoidal image, shown as a 2-D image.

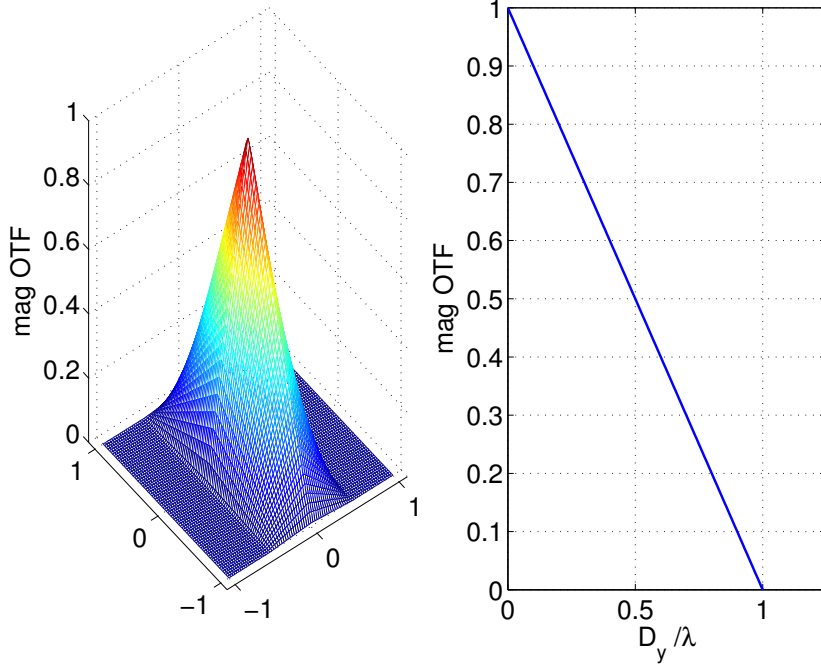


Figure 5.10: The normalized magnitude of the optical transfer function (OTF) of a rectangular aperture. This magnitude is typically abbreviated as MTF. Angular spatial frequency units of the horizontal axes are cycles/radian; to convert from angular to linear units divide by the image distance $d = s_i$ of the optical system.

and aberrations are neglected,

$$\text{MTF} = |\text{OTF}| = |\mathcal{F}\{\text{PSF}\}| = \left| \mathcal{F} \left\{ \left| \mathcal{F} \left\{ A(x_a, y_a) \right\} \right|^2 \right\} \right| \quad (5.14)$$

A plot of the normalized MTF due to a circular aperture was shown in Fig. 5.6. See Fig. 5.10 for a normalized plot of the MTF due only to the PSF of a rectangular aperture (such as the rectangular aperture PSF shown in Fig. 5.5). Notice that the MTF from a rectangular aperture is “triangular” in each axis direction. If this simple shape surprises you, glance at the appendix for Fourier transforms (particularly page 161).

Many plots of MTFs, including many of those in this book, use a normalized frequency axis such that 1.0 is the optical cutoff frequency in that direction. Looking at Fig. 5.6 and Fig. 5.10, it can be seen that the optical cutoff frequency, expressed as a spatial frequency (in angular units of cycles/radian, often abbreviated as cy/rad), is equal to:

$$f_c = \frac{D}{\lambda} \quad \text{for a circular aperture} \quad (5.15)$$

$$f_c = \frac{D_x}{\lambda}, \frac{D_y}{\lambda} \quad \text{for a rectangular aperture, along the appropriate axis direction} \quad (5.16)$$

To convert angular spatial frequencies to linear spatial frequencies at the image plane, *divide* by image distance d . Note that a rectangular aperture, in general, has different cutoff frequencies for u versus v . A comparison of more than just the cutoff frequencies, but also the shape of the MTF for circular versus rectangular apertures, is provided as 1-D plots in Fig. 5.11. No spatial frequency higher than the optical cutoff frequency can be reproduced at the image plane.

It is sometimes convenient to have a closed form equation that describes the 1-D “slice” of the MTFs shown in Fig. 5.11. Let the horizontal axis spatial frequency variable be denoted as

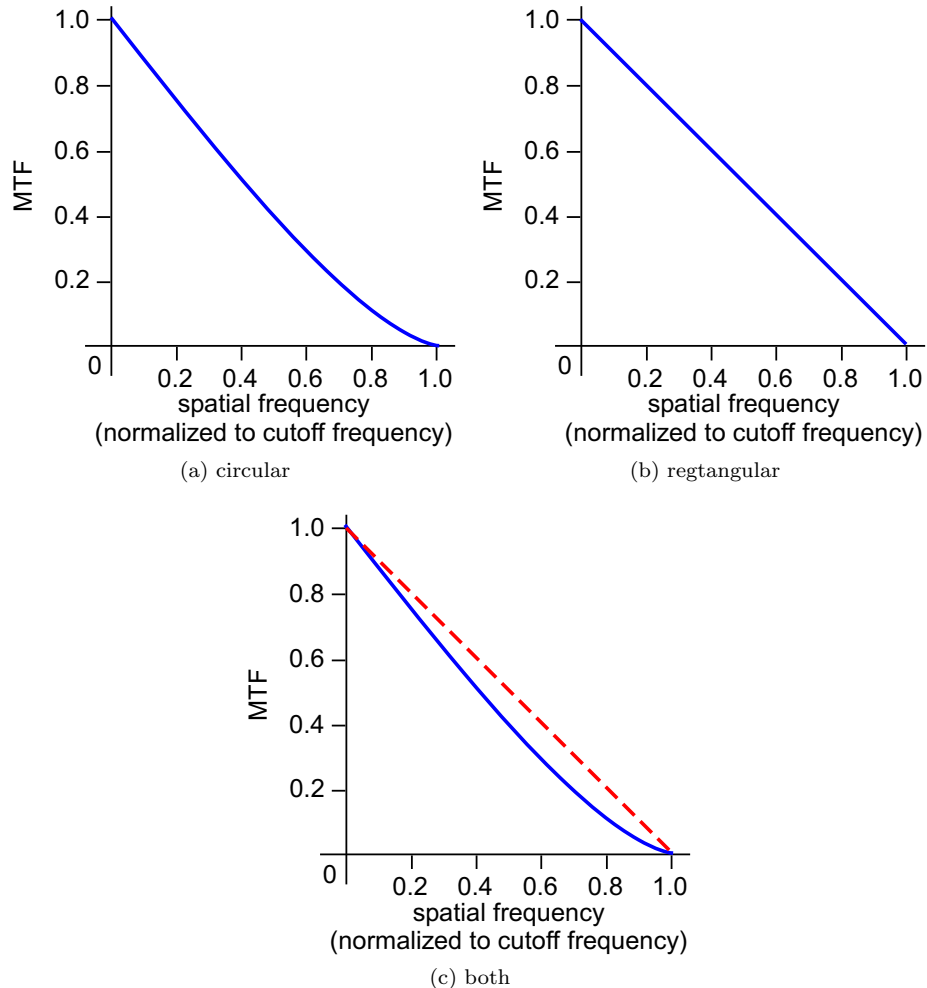


Figure 5.11: Comparison in 1-D of MTFs due to circular and rectangular apertures. The plot of both on the same axes assumes that the diameter of the circular aperture is the same as the size of the opening of the rectangular aperture in the associated direction.

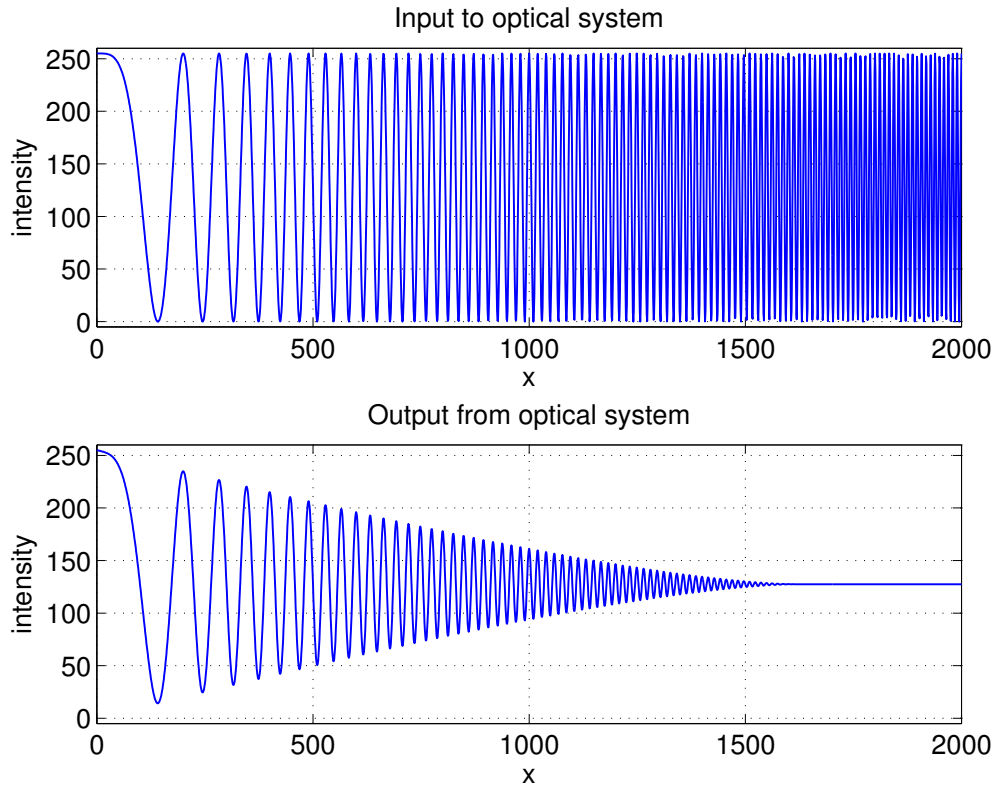


Figure 5.12: Effect of MTF on a chirp pattern, shown in 1-D, in the spatial domain. The point at which the chirp has a spatial frequency equal to the optical cutoff frequency is where $y = 1600$.

\hat{u} , where the “hat” over the u indicates it is normalized with respect to the associated optical cutoff frequency. The equation that describes the 1-D MTF of a circular aperture shown in Fig. 5.11(a), using a normalized frequency axis is:

$$\text{MTF}(\hat{u}) = \frac{2}{\pi} (\arccos(\hat{u}) - \hat{u} \sin(\arccos(\hat{u}))) \quad \text{for } 0 \leq \hat{u} \leq 1 \quad (5.17)$$

$$= \frac{2}{\pi} \left(\arccos(\hat{u}) - \hat{u} \sqrt{1 - \hat{u}^2} \right) \quad \text{for } 0 \leq \hat{u} \leq 1 \quad (5.18)$$

This is obviously a nonlinear equation. The much simpler linear equation that describes the 1-D MTF of a rectangular aperture shown in Fig. 5.11(b), using a normalized frequency axis is:

$$\text{MTF}(\hat{u}) = -\hat{u} + 1 \quad \text{for } 0 \leq \hat{u} \leq 1 \quad (5.19)$$

For either type of aperture, the value of $\text{MTF}(\hat{u})$ for $\hat{u} \geq 1$ is 0.

As an example of how modulation depth of a sinusoidal pattern, the MTF shape, and the optical cutoff frequency interact, assume we have an optical system with a circular aperture to which we provide, at the object plane, a sinusoidal pattern known as a *chirp*. In a chirp pattern, the frequency steadily changes, in this case from low to high in the horizontal direction of the spatial domain. Using a chirp at the object plane we can observe the change in modulation depth for various spatial frequencies at the output of the optical system due to the value of the MTF at those spatial frequencies. This example is shown for the same chirp pattern in 1-D in Fig. 5.12 and in 2-D in Fig. 5.13.

Why bother with the MTF? If the PSF completely defines the system, what's the advantage of using the MTF? For one thing, the concept of a *cutoff frequency* is far easier for most people

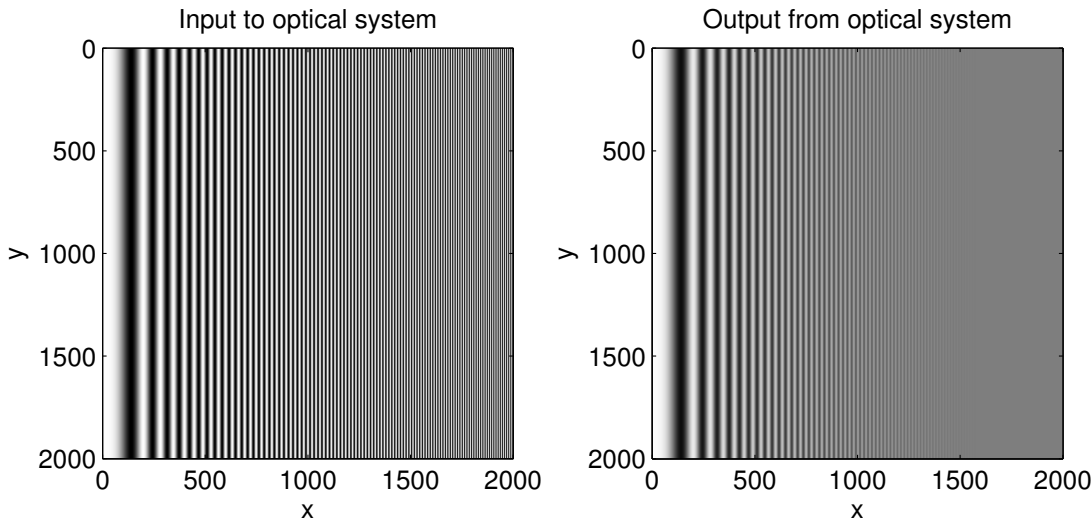


Figure 5.13: Effect of MTF on a chirp pattern, shown in 2-D, in the spatial domain. The point at which the chirp has a spatial frequency equal to the optical cutoff frequency is where $y = 1600$.

to understand in terms of the MTF than trying to relate it to the size of the PSF. Another advantage is that while PSFs of multiple independent components have to be convolved, MTFs of multiple independent components are simply multiplied, which most humans find to be an easier and more intuitive process. For these and other reasons, the use of MTFs to characterize and compare electro-optical systems is widespread in practice.

Example 5.2 Determining the optical cutoff frequency

Given: An optical system has a circular aperture with diameter of $D = 20$ mm. The focal distance is $s_i = d = 100$ mm. Assume incoherent light at a wavelength of $\lambda = 550$ nm. Find the optical cutoff frequency in angular spatial frequency and in linear spatial frequency. Repeat for $D = 2$ mm.

Solution: First, solve for the case of $D = 20$ mm. In angular units, $f_c = D/\lambda = 36.36 \times 10^3$ cy/rad, or 36.36 cy/mrad, which is the more common way to express this value. In linear units at the focal plane, $f_c = D/\lambda d = 364 \times 10^3$ cy/m, or 364 cy/mm, which is the more common way to express this value.

Next, solve for the case of $D = 2$ mm. In angular units, $f_c = D/\lambda = 3.636$ cy/mrad. In linear units at the focal plane, $f_c = D/\lambda d = 36.4$ cy/mm.

5.3.3 The limiting resolution

Knowing the optical cutoff frequency of a particular lens or optical system is very useful, both for comparison to other systems and to assign real-world values to a normalized frequency axis. However, as was mentioned previously, no practical system can resolve spatial frequencies in an object pattern all the way out to the theoretical cutoff frequency. The ability of an optical system to detect details of a scene having various spatial frequencies is limited by how low the contrast (i.e., modulation depth) can be at those frequencies and yet still have the associated image details “show up” in the image. This point of minimum detectable modulation is called by various names, some of the most common being:

- detection threshold,

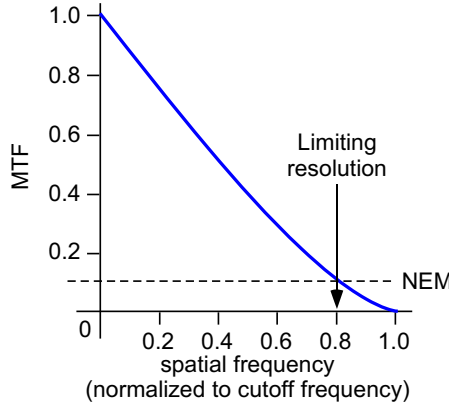


Figure 5.14: Intersection of the MTF and the NEM set the value of the limiting resolution of an optical system. Here the NEM is 10% and the limiting resolution is $0.8f_c$.

- threshold modulation,
- contrast limit,
- noise equivalent modulation (NEM), and
- minimum resolvable contrast (MRC).

While MRC is often used in military imaging system specifications, NEM seems to show up more often in modern literature, so that is what will be used here.

NEM is often defined as the modulation depth needed for the signal-to-noise ratio (SNR) to equal 1.0. This definition of NEM is intended to include noise contributions of the camera electronics, which varies according to the spatial frequency. For now, let's examine a simplified version of NEM that involves only the optics and is constant for all spatial frequencies.

How do we use MTF and NEM together? The *limiting resolution*, in terms of spatial frequency, is where the MTF and the NEM lines intersect. This is shown in Fig. 5.14. Side note: While the Abbe resolution criterion of λ/D could be interpreted as implying that detection is possible down to a modulation depth of zero (since $f_c = D/\lambda$), the Rayleigh resolution criterion of $1.22\lambda/D$ would imply that the detection threshold (i.e., the NEM) would be at a modulation depth of approximately 9% (since Eq. (5.18) evaluated for $\hat{u} = 1/1.22$ is approximately 0.09). This is a realistic value for many real-world systems, which is perhaps another reason for the popularity of the Rayleigh criterion.

What is a typical value for the NEM? As expected, it varies quite a bit from system to system, especially when more than just the optics are considered. A reasonable figure to use as a first guess is 10%. A very good system might have a NEM of 5% or even 2%. A poor system might have a NEM of 20%. Don't forget that NEM, like most things related to optics, is wavelength dependent.

5.3.4 Other methods of comparison

The limit of resolution, being a single number, is easier to specify than the MTF, which is a function of spatial frequency. But the MTF conveys far more information. Consider two systems, A and B, with an identical limit of resolution, as shown in Fig. 5.15(a). While system A and system B have the same limiting resolution, they would provide different image quality. In particular, system B is poorer since it exhibits lower modulation depth at nearly all spatial frequencies. Such a comparison is seldom so clear, however. In Fig. 5.15(b), system A has a lower limiting resolution than system B, but for most of the spatial frequencies system A has a

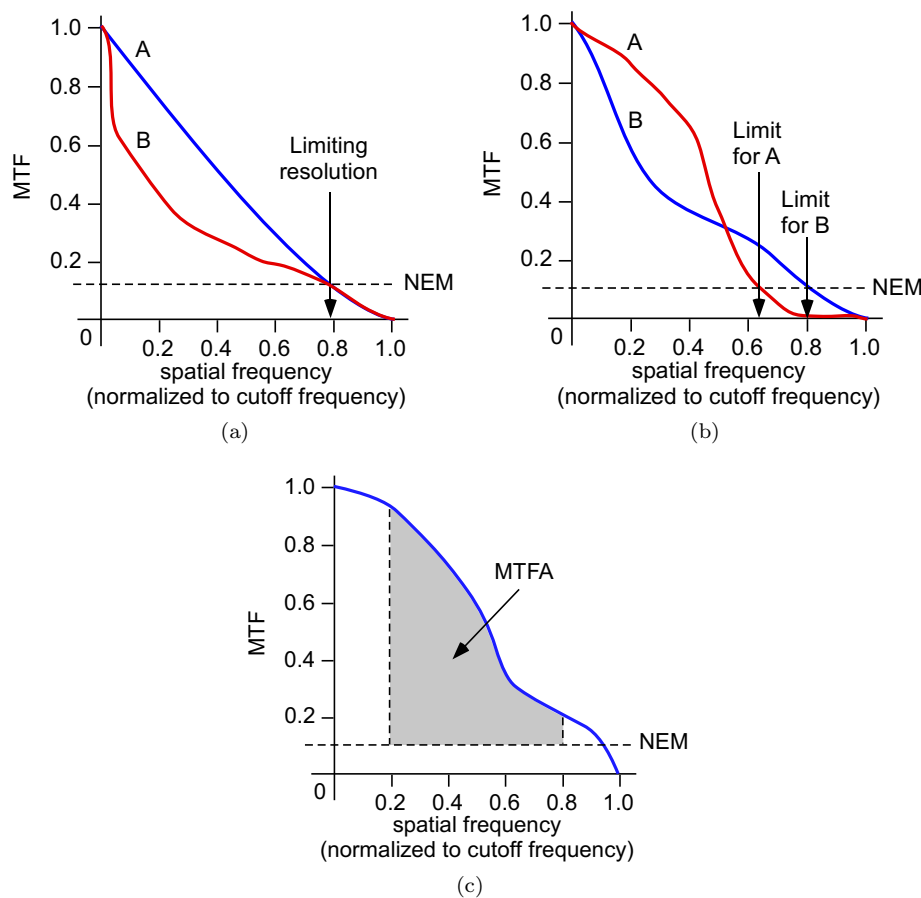


Figure 5.15: Comparing and evaluating optical systems. In (a) and (b), systems are compared by MTFs and by the values of limiting resolution. In (c), a system is evaluated by its MTFA.

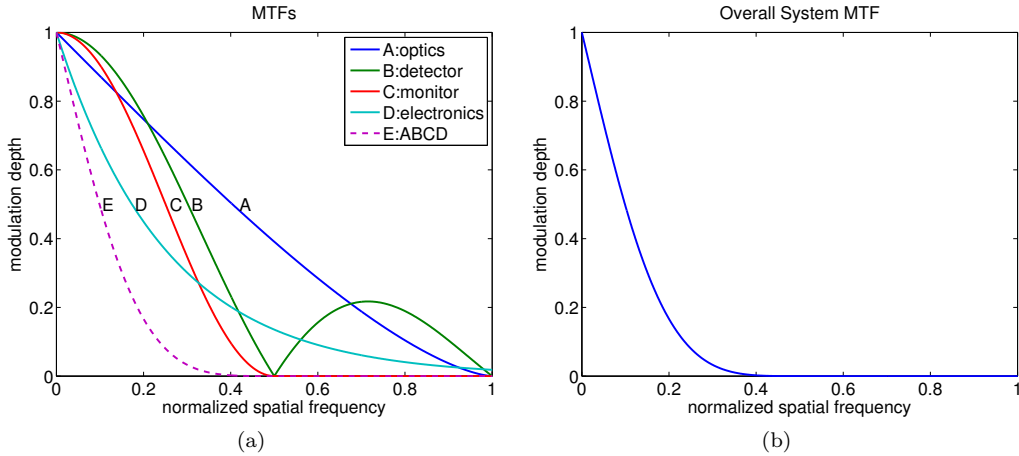


Figure 5.16: In (a), the independent MTFs for subsystems A through D are multiplied to obtain the overall system MTF shown as E. In (b), the system MTF is shown alone. In both subfigures, the spatial frequency axis is normalized with reference to the optical cutoff frequency.

higher modulation depth. Thus, except for high spatial frequencies such as sharp edges in an image, system A would exhibit better image quality.

The *goodness* of an MTF relates to how high the modulation level remains as frequency increases, so some authors use the area under the MTF curve as a figure of merit. Some authors go further and define a quantity called the *MTF area* (MTFA) as the region bounded by the NEM level and the MTF curve, for some particular range of spatial frequencies. An example of this is shown in Fig. 5.15(c), where the range of spatial frequencies of interest for the application under consideration is between 0.2 and 0.8 of f_c .

Remember that an MTF is a 3-D function, so a more precise method than MTFA would be to evaluate a volume under the MTF surface (perhaps called MTFV). For those MTFs that exhibit circular symmetry, an argument can be made that you may only need to evaluate the volume represented by just one quadrant. However, if significant aberrations are involved, the shape of the MTF gets much more complicated. Similar to the limit of resolution, MTFA or MTFV is just a single number, and so it's usefulness only goes so far. Relying heavily on this type of figure of merit is often too simple an approach, and a more application-specific comparison of MTFs may be warranted.

5.3.5 System MTFs

There is a PSF in the spatial domain associated with each component of an imaging system, and each PSF is associated with an MTF in the spatial frequency domain. We combine independent PSFs in the spatial domain through convolution, and we combine independent MTFs in the spatial *frequency* domain through multiplication. We will keep coming back to this concept as we encounter other MTFs (the detector array, for example), but this is a good place to first explore the concept of an overall *system MTF*.

Suppose we have an imaging system that includes optics, a CCD detector array, and various electronics. We also want to display these images on a monitor screen. Each one of these four subsystems will have its own independent MTF. The overall system MTF will be the product of all four of the individual MTFs. This is shown in Fig. 5.16(a). The system MTF is shown alone in Fig. 5.16(b), to emphasize how different the system response can be, even if the optical cutoff frequency is fairly high. While the lens system may be able to image certain fine lines and sharp edges in the object scene, much of this high frequency detail will never show up on the monitor

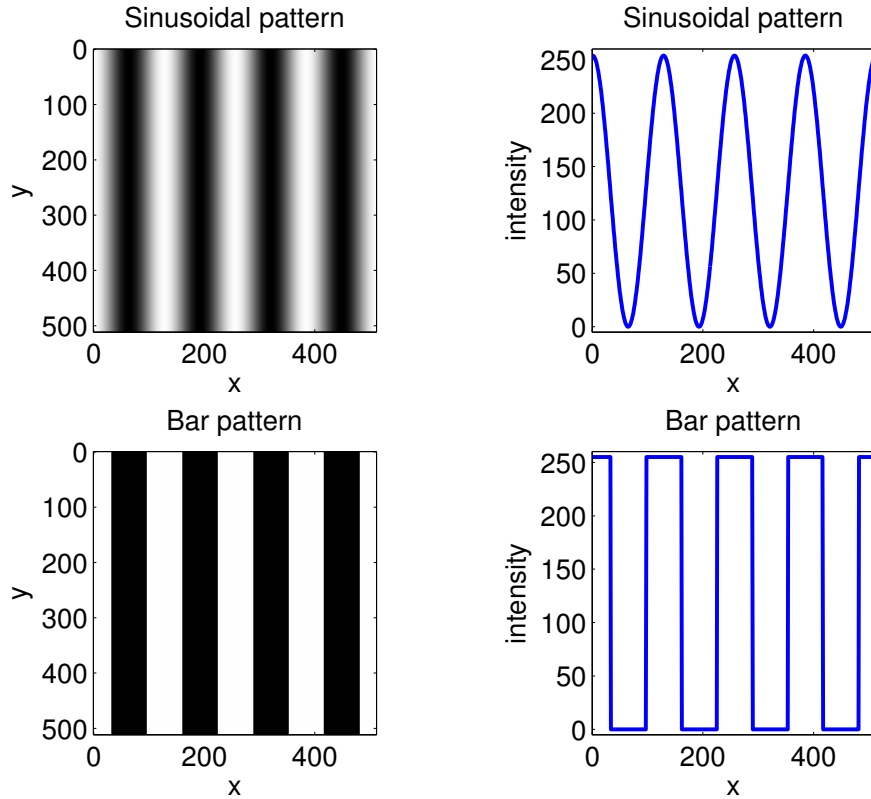


Figure 5.17: Comparison in 2-D and 1-D plots of a sinusoidal pattern and a bar pattern, having the same period and thus the same fundamental frequency.

screen, due to the frequency response of the system MTF.

For this method of obtaining the system MTF to work, the individual MTFs must be independent. This is not true, for example, with lens combinations that compensate for their individual aberrations. In that situation, you need to use the MTF of the lens *combination* as a whole. We will come back to this topic again in a later section.

One rather cumbersome way to empirically measure the overall system MTF of an optical system is to image multiple sinusoidal patterns of various spatial frequencies, and the modulation value could be determined for each of those frequencies. This piecewise data could then be used to estimate the overall MTF. If desired, an inverse Fourier transform of this empirically-derived MTF could then be used to estimate the overall PSF of the imaging system (neglecting the phase term of the OTF). In practice, however, sinusoidal patterns are seldom used.

5.3.6 The CTF

Optical imaging systems are often specified in terms of units such as lp/mm, which stands for line pairs per millimeter, instead of specifying some maximum spatial frequency of a sinusoidal pattern that can be detected. A line pair is a white stripe and black stripe (often called a *bar pattern*), and it is a far easier pattern to produce than an accurate sinusoidal pattern. A comparison of a sinusoidal pattern and a bar pattern is shown in Fig. 5.17. Both patterns have the same period in the spatial domain, and thus the spectrum of both would have the same fundamental frequency (equal to the reciprocal of the period). But while a sinusoid's spectrum has only one frequency (the fundamental), a bar pattern is similar to a square wave and its spectrum consists of the fundamental and all odd harmonics of the fundamental.

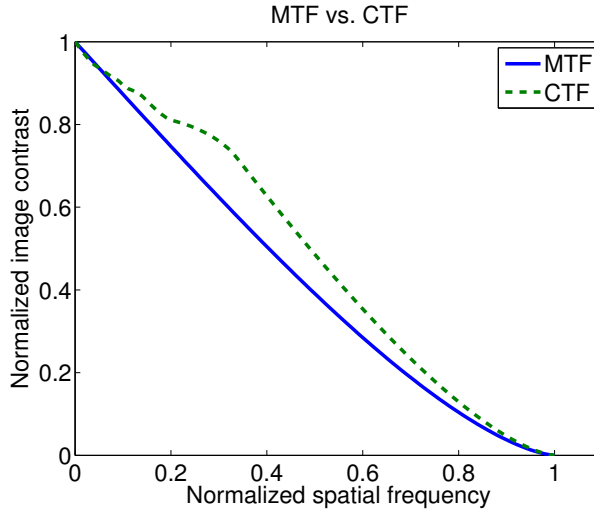


Figure 5.18: Comparison of an MTF with a CTF of a circular aperture.

Because a bar pattern is not sinusoidal, measurements using this pattern do not directly yield the MTF; instead, they yield something called the *contrast transfer function* (CTF). Obtaining the CTF is often easier than obtaining the MTF, but we will usually want to determine the MTF from the CTF. Of course, a bar pattern is to a sinusoidal pattern as a square wave is to a sine wave, so the mathematical conversion between CTF and MTF is well known [63]. Shown in one dimension⁶ for compactness, the relationship is

$$M(u) = \frac{\pi}{4} \left[C(u) + \frac{C(3u)}{3} - \frac{C(5u)}{5} + \frac{C(7u)}{7} - \frac{C(11u)}{11} + \frac{C(13u)}{13} \dots \right], \quad (5.20)$$

where $M(u)$ is the desired MTF value and $C(u)$ is the measured CTF value at a particular spatial frequency u . Note the existence and sign of the odd harmonic terms is irregular; see [63] for details. While the relationship is an infinite series, using just the six terms explicitly shown in Eq. (5.20) will usually provide sufficient fidelity. Fig. 5.18 compares the normalized MTF to the normalized CTF, due only to a circular aperture; note that the CTF tends to overestimate the modulation depth compared to the true MTF.

Even if the CTF is easier to obtain directly than the MTF, the user would still need to image multiple bar patterns of various spatial fundamental frequencies. Empirical resolution testing using this and similar methods have been made somewhat easier by the creation of various test patterns that include a wide range of spatial frequencies. Many test pattern types and variations have been created over the years all over the world, some for photography, some originally for television and video but also used for other types of imaging systems. Many test patterns have fallen out of use and are of historical interest only. A small sample of such test patterns is shown in Fig. 5.19.

Of the test patterns shown in Fig. 5.19, the ISO-12233 test pattern is the newest (the associated ISO standard was adopted in 2000). It was specifically designed to empirically measure the resolution of modern digital cameras, and there are mathematical relationships to obtain the MTF directly from this chart. In addition to using test patterns similar to those shown in Fig. 5.19, other methods have been developed for empirically obtaining the MTF of optics and detector arrays, such as the use of laser speckle patterns [64].

⁶To simplify the discussion at some points, we assume two dimensional functions are separable in Cartesian coordinates. While this may not be exactly true in some situations, the errors caused by this assumption are typically very small [41].

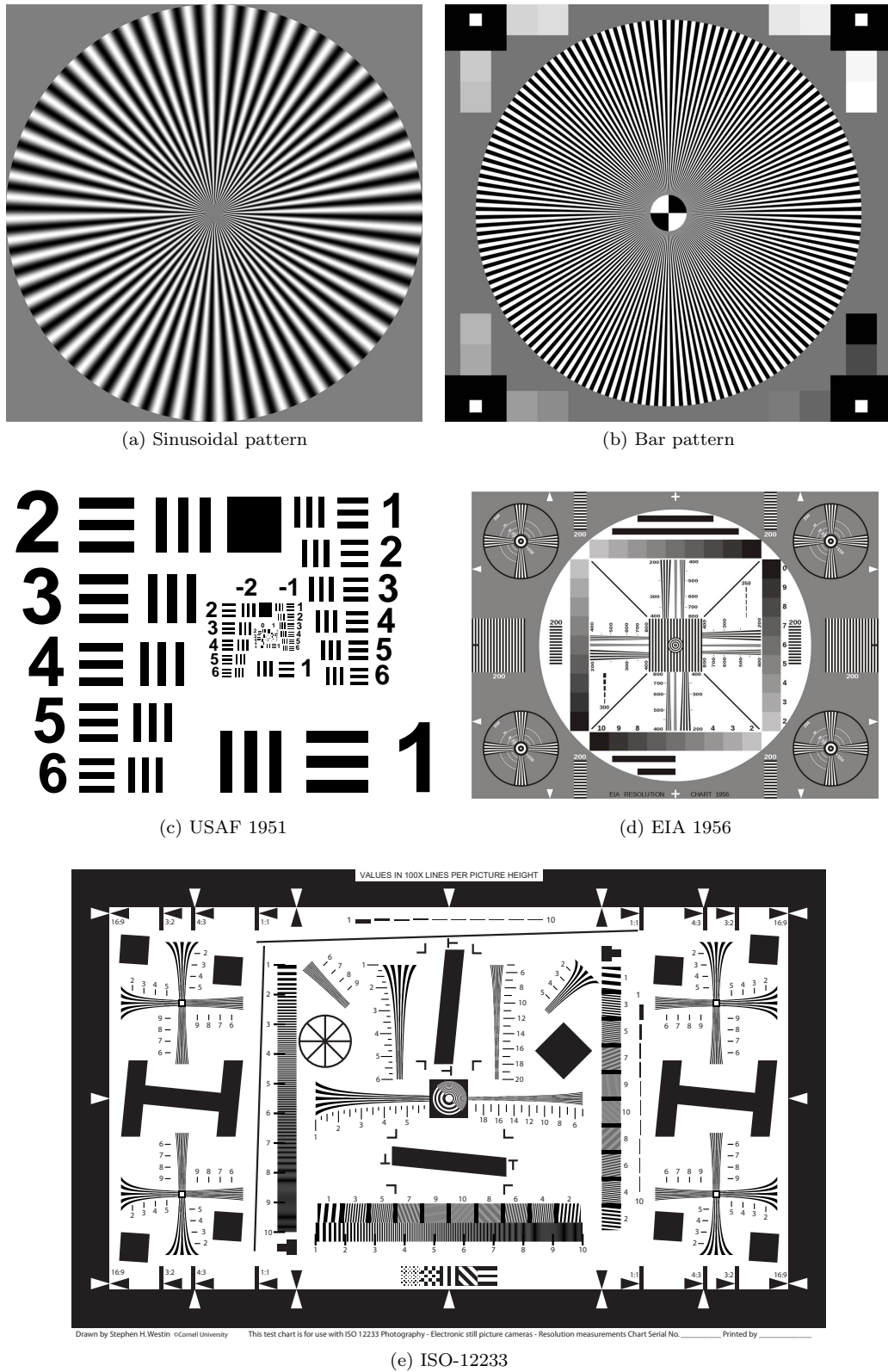


Figure 5.19: Examples of typical test patterns used for still-imaging and video.

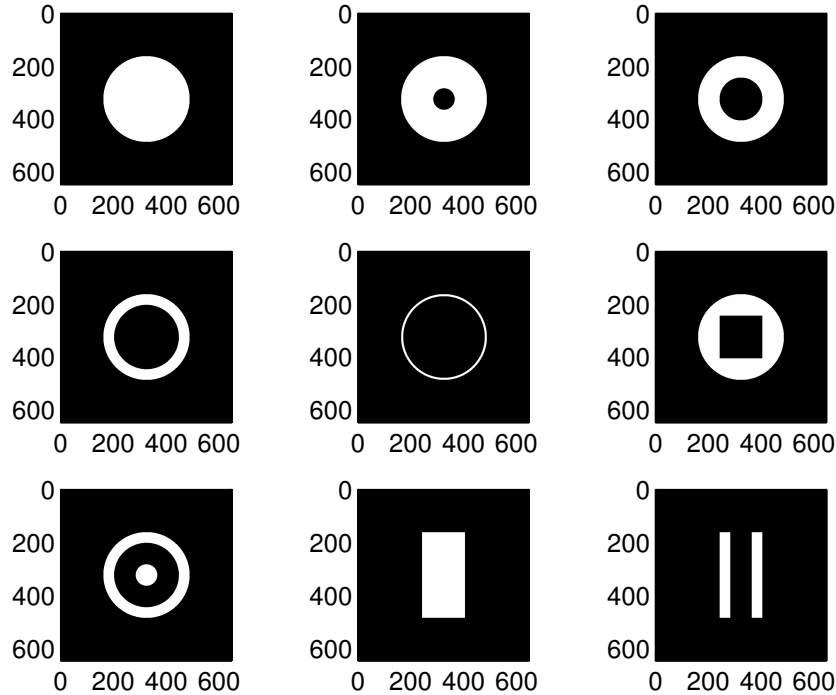


Figure 5.20: Nine apertures, including seven “special” apertures, that can be easily analyzed.

5.4 MTFs of special apertures

So far, this book has concentrated on the MTFs of simple rectangular and circular apertures, which are certainly the most common types of apertures in imaging systems and cameras. What of less common shapes for apertures? If you had to evaluate some more complicated aperture shapes using the Rayleigh-Sommerfeld integrals, even simplifying with the Fraunhofer approximation, the task would be very difficult. Luckily, the methods of Fourier optics will come to our rescue.

Is this concern really necessary? Won’t we almost always have circular apertures and lens shapes? It’s true that for most situations, the ability to handle simple circular and rectangular apertures will be sufficient. But there are exceptions, and not just for custom imaging systems.

One example of a “special” aperture is inherent in the catadioptric lens design, such as the one shown in Fig. 3.8(b). To reduce the size and weight of long telephoto lenses, some manufacturers use a catadioptric design (combining mirrors and lenses). Common sizes for commercial catadioptric lenses are 500 mm f/8 and 600 mm f/8. Catadioptric lenses unavoidably exhibit a variation on the circular aperture that has a circular central obstruction, such that the aperture resembles a doughnut.

Using the Fourier optics approach, any aperture geometry can be quickly evaluated with just a few lines of MATLAB code. Nine apertures are shown in Fig. 5.20; two (upper left, bottom middle) are the normal circular and rectangular apertures. The other seven can be considered “special” apertures. The PSF and MTF of all these apertures are easily determined with the MATLAB code given in Listing C.3.

This is a long program listing (30 plots are generated), but you can extract just the parts you might want. In general, the calculations are just $\text{PSF} = |\mathcal{F}\{A(x_a, y_a)\}|^2$ and $\text{MTF} = |\text{OTF}| = |\mathcal{F}\{\text{PSF}\}|$, performed over and over for the aperture variations. Note that the apertures are formed by combining simple shapes. For example, to form an annular ring aperture such as the upper right of Fig. 5.20, a smaller circular aperture is subtracted from a larger circular aperture.

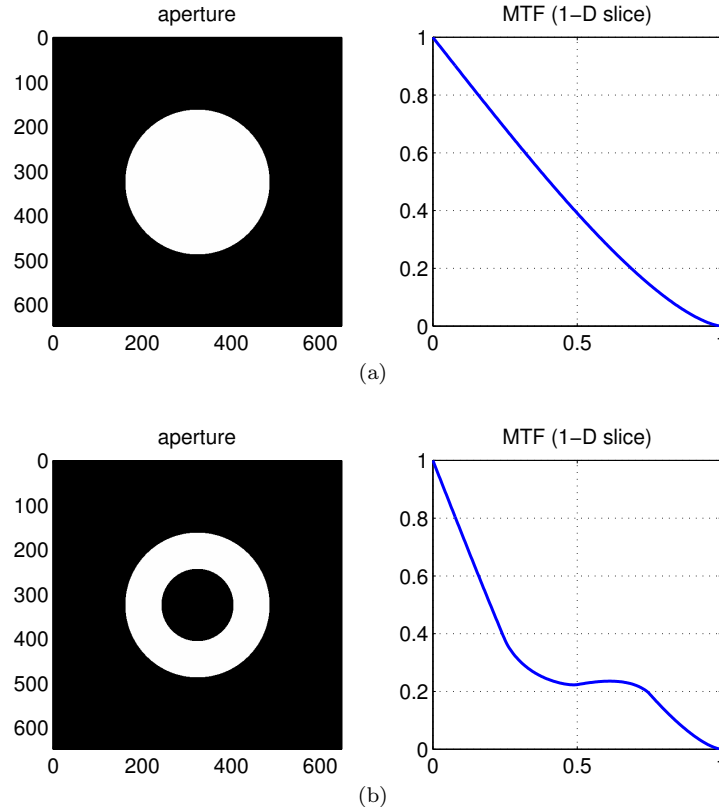


Figure 5.21: In (a), the aperture and associated MTF are shown for a clear circular aperture. In (b), the aperture and associated MTF are shown for an annular ring aperture, where the inner radius of the obstruction is 50% of the outer radius of the opening.

Comparison of the MTF for a normal circular aperture (sometimes called an “open” or “clear” aperture since there is no obstruction), with an annular ring aperture (having a centered, circular obstruction) is shown in Fig. 5.21. The MTFs of all the variations of an annular ring apertures shown in Fig. 5.20 are compared in Fig. 5.22.

A plot similar to that shown in Fig. 5.22 is shown in many optics books, but what very few of those books mention is that the plot isn’t quite correct. Notice the high frequency response for B, C, D, and E all exceed that of A, which is the open circular aperture. The MTF of an open circular aperture must be the upper bound for any circular-shaped aperture at all spatial frequencies. What went wrong in generating the plot? The answer lies in Table 5.3. All the MTFs in Fig. 5.22 were individually normalized to have a modulation depth of 1 at a spatial frequency of 0. However, if all the MTFs are plotted on the same axes, then the normalization factor should be relative to the open aperture of A, since that MTF should be the reference. Redoing Fig. 5.22 in this way produces Fig. 5.23, which correctly shows the relative response for all the MTFs at all the spatial frequencies. While being more correct, Fig. 5.23 suffers from a loss of visible detail in some of the MTFs, especially that of aperture E. That is the likely reason that a plot similar to Fig. 5.22 is the one found in most optics books.

What of the other special apertures? The aperture at the right side middle row of Fig. 5.20 is unusual and is not likely to be seen in practice. It is included here merely to show how simple it is using Fourier optics to determine the PSF and MTF of an arbitrary aperture shape. Since this aperture lacks circular symmetry, a single 1-D plot is insufficient to describe the MTF (or PSF); the program in Listing C.3 will display two 1-D MTF plots (across the u or v axis and across a diagonal) and a full 3-D MTF plot. Just the two 1-D plots are shown here in Fig. 5.24.

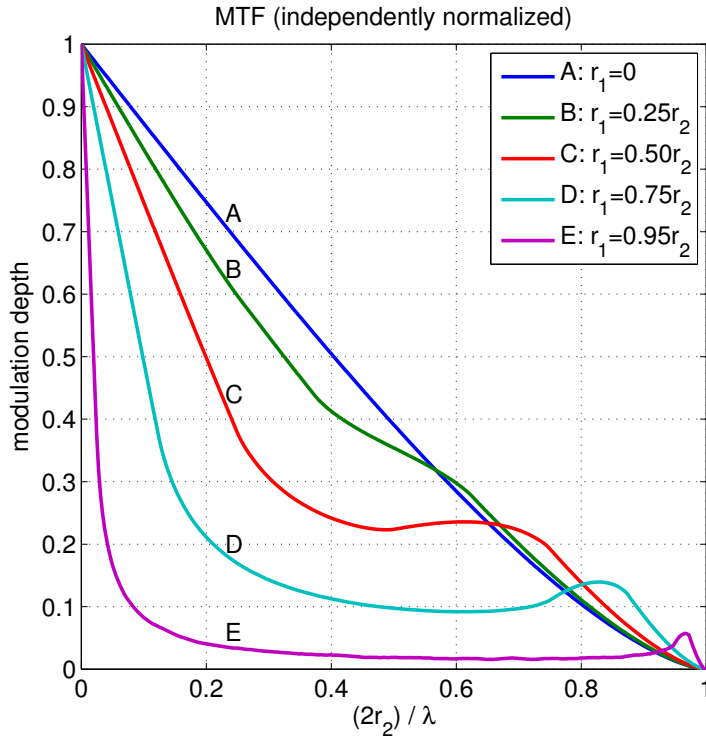


Figure 5.22: MTF comparison of annular ring apertures, where the radius of the center obstruction is r_1 and the radius of the opening is r_2 .

Table 5.3: Comparison of blocked versus clear area for annular ring apertures, where the radius of the center obstruction is r_1 and the radius of the opening is r_2 .

		Area obscured	Area open
A	open	0%	100%
B	$r_1 = 0.25r_2$	16%	84%
C	$r_1 = 0.50r_2$	25%	75%
D	$r_1 = 0.75r_2$	56%	44%
E	$r_1 = 0.95r_2$	90%	10%

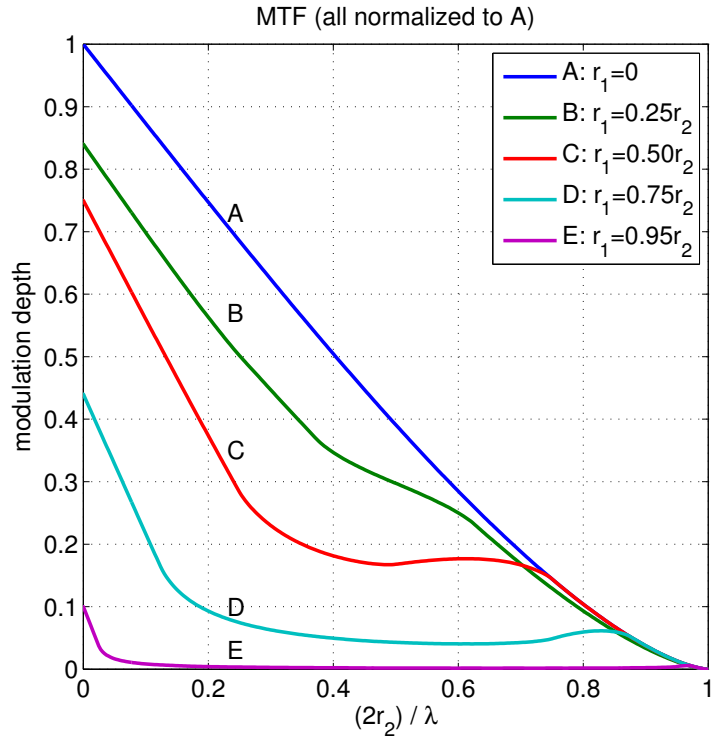


Figure 5.23: MTF comparison of annular ring apertures, where the radius of the center obstruction is r_1 and the radius of the opening is r_2 . All MTFs were normalized relative to A.

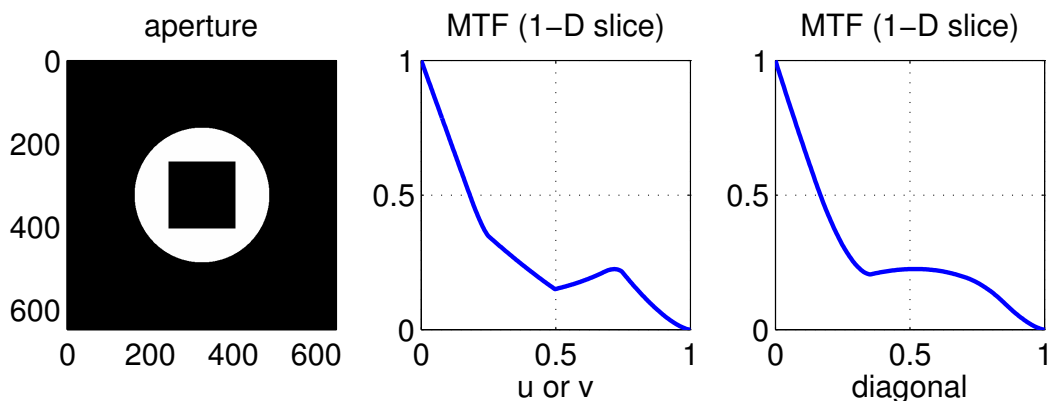


Figure 5.24: A special aperture and two 1-D slices of the associated MTF.

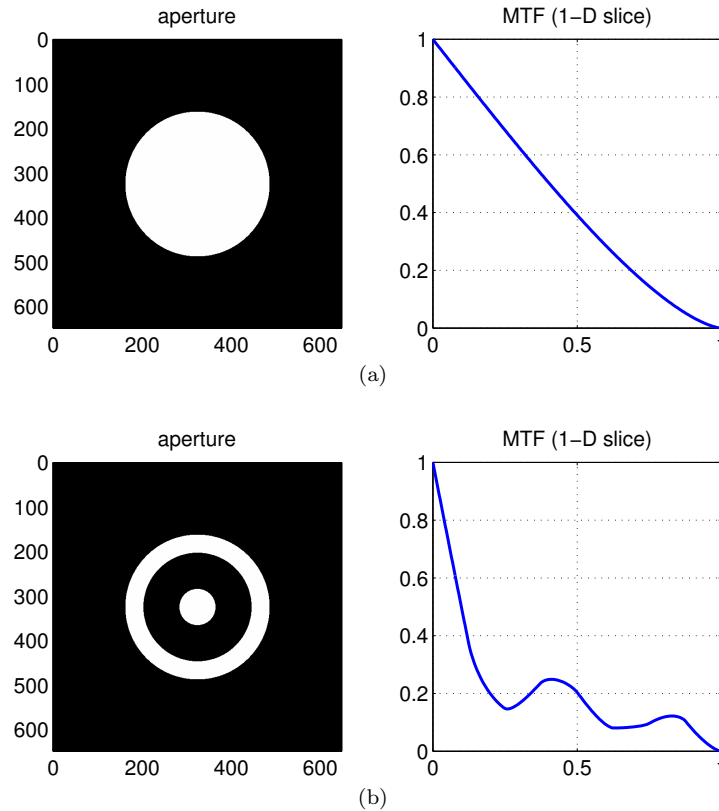


Figure 5.25: In (a), the aperture and associated MTF are shown for a clear circular aperture. In (b), the aperture and associated MTF are shown for a “bullseye” aperture.

The aperture at the lower left of Fig. 5.20 is what might be called a “bullseye” aperture. A comparison with the open circular aperture is shown in Fig. 5.25. The aperture shown at the bottom middle of Fig. 5.20 is a simple rectangular aperture, while the aperture shown at the bottom right of Fig. 5.20 is a two-slit aperture. A comparison of the rectangular aperture with the two-slit aperture is shown in Fig. 5.26.

While it may seem to the reader that these special aperture shapes are unrealistic and only of academic interest, it turns out that certain imaging systems do use some of these aperture shapes for very specific purposes. An example will be provided in the next section on apodization.

5.5 Apodization

Recall that the PSF of common apertures, as seen in Fig. 5.4 and Fig. 5.5, exhibit side lobes (sometimes called “rings” when referring to an Airy disk). While the relative intensity of these side lobes may seem small compared to the peak of the main lobe of the PSF, they still have an effect on the image. This leads to the topic of *apodization*, which translates literally to mean “removing the foot.” In this context, the “feet” are the side lobes, and while we can’t remove them we can reduce them. Apodization is a term used in a variety of technical fields, including optics.

Both amplitude and intensity plots of what we now know as the PSF were shown in Fig. 4.3 and in Fig. 4.4 for circular and rectangular apertures, respectively. It was seen that in the intensity plots, the side lobes were difficult to see, compared to the amplitude plots. Yet it is intensity that our cameras and imaging systems will record. This may mislead the reader into

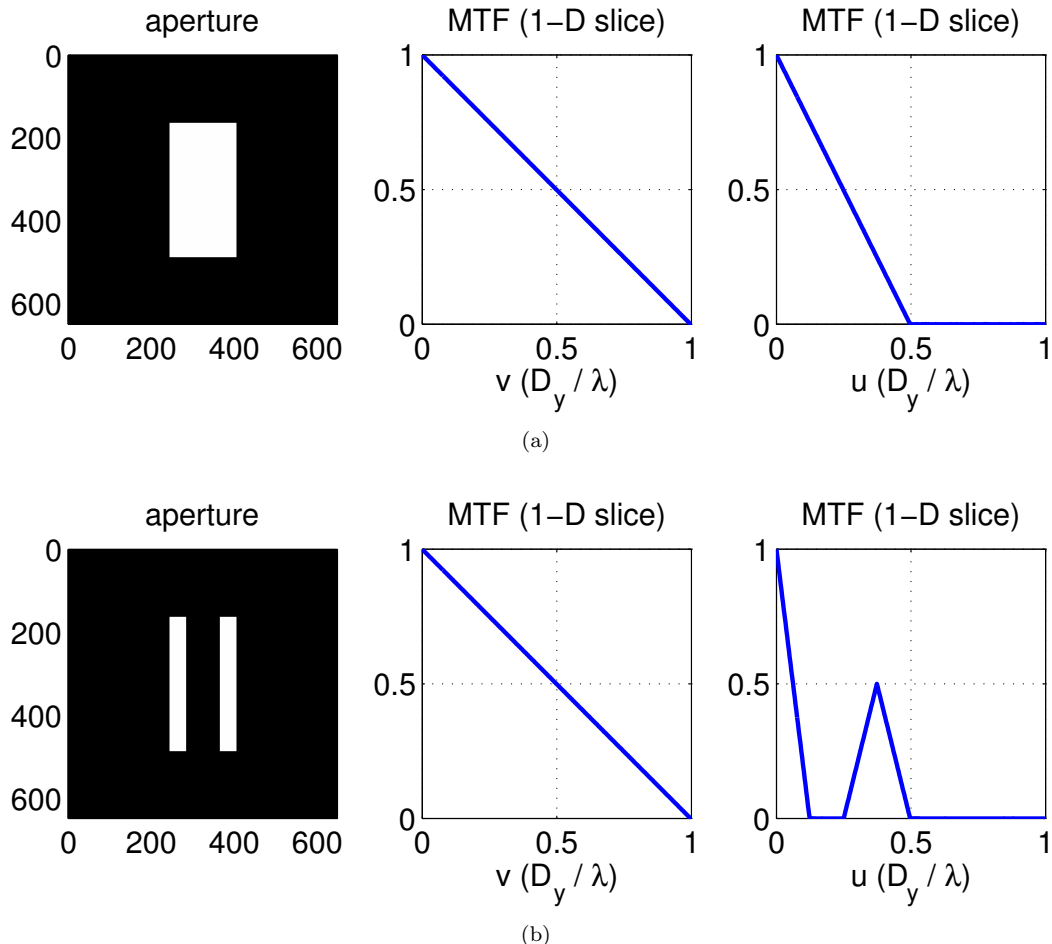


Figure 5.26: In (a), the aperture and associated MTF are shown for a rectangular aperture. In (b), the aperture and associated MTF are shown for a two-slit aperture. The spatial frequency axes are all normalized to the cutoff frequency associated with the larger (vertical) dimension of the apertures.

thinking that such side lobes can always be ignored.

In Figs. 4.3 and 4.4, the simulated camera exposure was set to prevent saturation of the main lobe (the brightest part) in the image. If we allow the main lobe region of the image to become saturated by simulating a longer exposure time, the structure of the side lobes and rings start to become visible in an intensity plot. Let's compare the "no saturation" exposure to an exposure 20 times longer for both a circular and a rectangular aperture. This is shown in Fig. 5.27, where the structure of the side lobes is clearly visible in the longer exposure times. Recall what the acronym PSF implies: every individual point of light in a complex scene at the object plane becomes its own tiny version of the PSF at the image plane. With this in mind, the effect of the side lobes may be better understood.

For some specific imaging applications, the side lobes of the aperture PSF can present a problem. For example, when a telescope is being used to image a binary star system where the stars appear close to one another, but one star is much brighter than the other (e.g., Sirius A and Sirius B in the constellation *Canis Major*), the PSF side lobes due to the bright star can "wash out" and hide the dimmer star. The level of the side lobes in the aperture PSF can be reduced if the transmission characteristics of the aperture are modified. The simplest method for a telescope is to cover the aperture with a glass plate or transparency film that is increasingly opaque (i.e., darker) as the distance gets farther from the center of the aperture. This "gradual rolloff" in the transmission of light through the aperture will reduce the level of the side lobes due to the aperture PSF; a Gaussian or a Hamming rolloff profile is often used in practice. This technique is the optical equivalent the common practice in digital signal processing (DSP) and image processing where a smoothing window⁷ is used to reduce side lobes due to finite-length data. There is no free lunch, however: when you reduce the level of the side lobes, you also unavoidably increase the size (i.e., diameter) of the main lobe.

This dual effect can be easily seen in an example adapted from a DSP text [65] and shown in Fig. 5.28. In this figure, the left plots show a rectangular data window (similar to a rectangular aperture in optics) and a Hamming data window (similar to a rectangular aperture in optics with apodization applied). The right plots are the Fourier transform (and thus the frequency response) of the left plots, so the upper left plot is the expected sinc function. A logarithmic scale (in dB) is used for the vertical axes of the right plots to enhance visibility of the side lobes. The right plots aren't quite equal to PSFs. While the PSF we are familiar with would be the magnitude squared of the Fourier transform, and the horizontal axis would be in spatial units at the image plane, the figures from DSP nevertheless show the exact point to be made here regarding apodization: a window (or aperture) with a "gradual rolloff" will have a Fourier transform (and also a magnitude squared of the Fourier transform) that exhibits lower side lobes but a larger main lobe.

To apply apodization to optics, you change the aperture function from something that is "all or nothing" to something that has a gradual rolloff. In doing so, you will reduce side lobes (or rings) in the PSF of the aperture, which will improve your ability to detect a weak light source close to a strong light source. But you will also widen the main lobe width of the PSF (typically doubling the width), which reduces the spatial resolution of the imaging system. As mentioned before, telescopes can achieve apodization by using a glass plate or transparency at the objective opening, which is the effective aperture of the telescope. This is not as easy for cameras, since the true aperture plane of a lens system is not usually accessible to the user.

Almost all commercial lens systems have an "all or nothing" aperture. One exception is the Minolta/Sony Smooth Trans Focus 135 mm f/2.8 [T4.5] lens. This is a special manual-focus lens design, which accomplishes apodization by utilizing a concave neutral-gray progressively-tinted lens element. The "T" number, or transmission number, differs from the f/# since the apodization filter is in the optical path at all times, reducing the amount of light on the sensor. This special lens is intended for producing a pleasant bokeh, not for imaging a weak source next to a strong source.

⁷Common smoothing windows in DSP include Bartlett, von Hann, Hamming, Blackman, Kaiser, and Dolph.

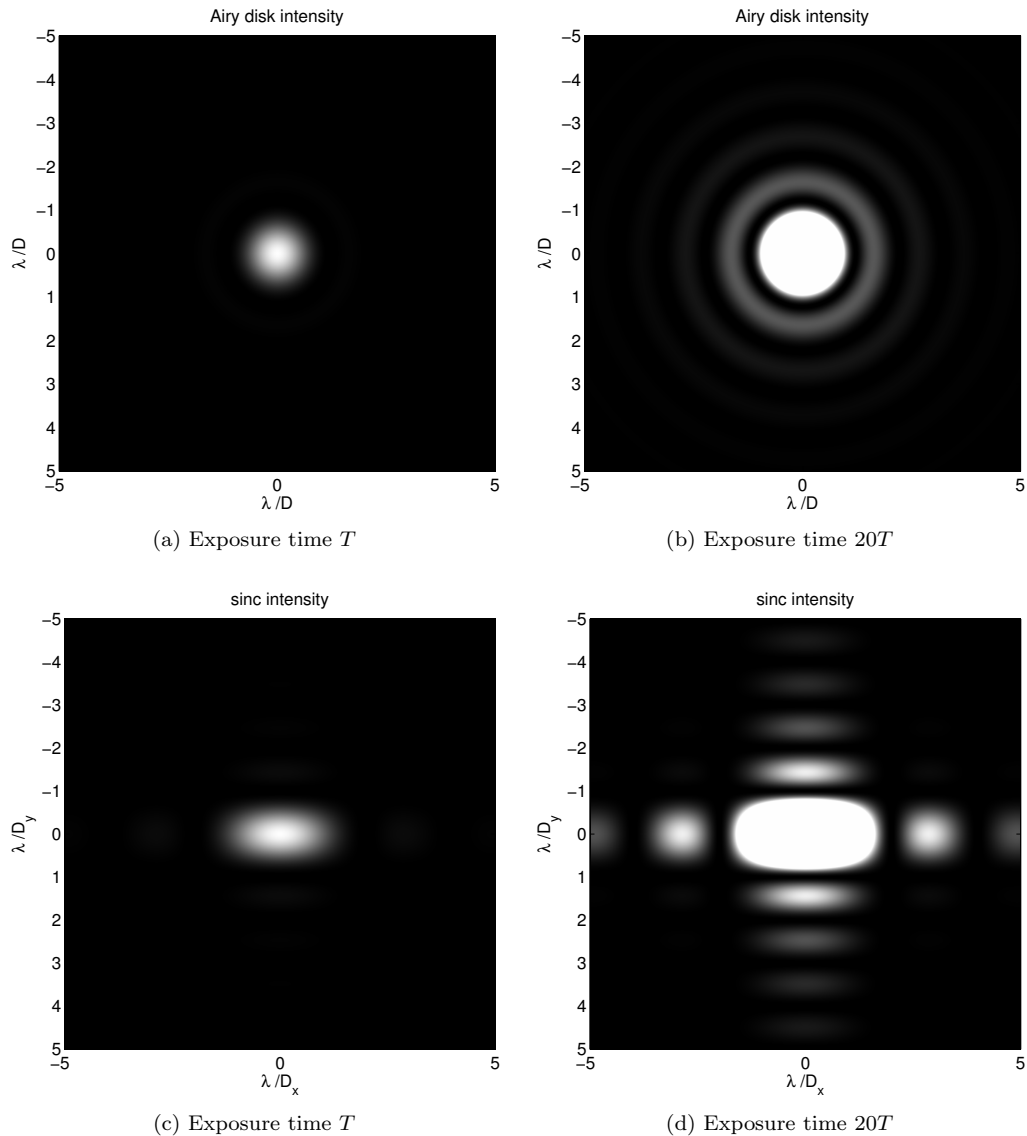


Figure 5.27: Simulated intensity exposures for circular (a,b) and rectangular (c,d) apertures.

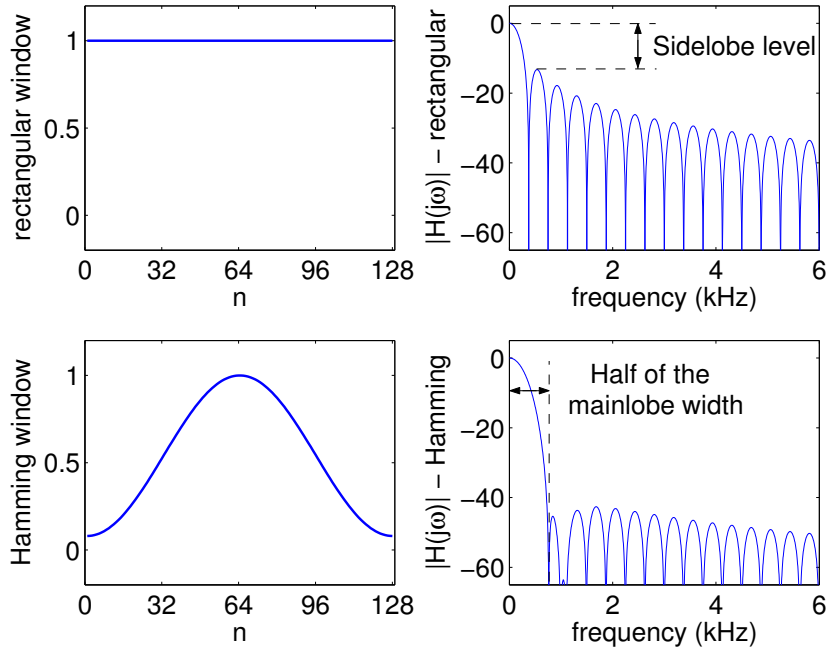


Figure 5.28: From DSP, a comparison of a rectangular window (similar to a rectangular aperture) to Hamming window (similar to a rectangular aperture with apodization applied). Plots on the right side are the Fourier transform of the plots on the left side.

An optics-specific example of apodization is shown in Fig. 5.29, where the apodization function is a normalized 2-D Gaussian. Note that in this example, the diameter of the circular aperture was made half the size of the circular aperture diameter shown in Fig. 5.21(a) and Fig. 5.25(a) to make the PSF main lobe larger and more visible. Comparing the results for the apodized aperture (bottom) to the clear aperture (top), a substantial reduction in the side lobe levels is evident, but the main lobe is approximately twice the width. With regard to the MTFs, the cutoff frequency of the apodized aperture is approximately half that of the clear aperture. These results are typical ramifications of apodization.

You can do the opposite of apodization, by using a “ring aperture” which will make the main lobe of the PSF more narrow, but increase the level of the side lobes. You could think of this as “anti-apodization.” Such ring apertures were shown in Fig. 5.20, and an example of anti-apodization is shown in Fig. 5.30, using what was called aperture E in the earlier discussion. Comparing the results for the anti-apodized aperture (bottom) to the clear aperture (top), a visible reduction in the width of the main lobe is evident, but the level of the side lobes has increased considerably. With regard to the MTFs, the modulation depth of the anti-apodized aperture is low for most spatial frequencies, but there is a visible “bump” at the highest frequencies near the optical cutoff frequency. This would tend to result in an image that has improved spatial resolution (due to the more narrow main lobe of the PSF), with added emphasis on any sharp edges of objects. As a result, this technique is used in microscopy to enhance the visibility of features such as the cellular walls of biological samples.

5.6 Simulating Aberrations

Recall the types of aberrations first described in Section 4.5. We will now offer a particularly powerful way to simulate and explore the effects of aberrations using the techniques of Fourier optics. While most readers of this book are not optical designers, being able to simulate aberra-

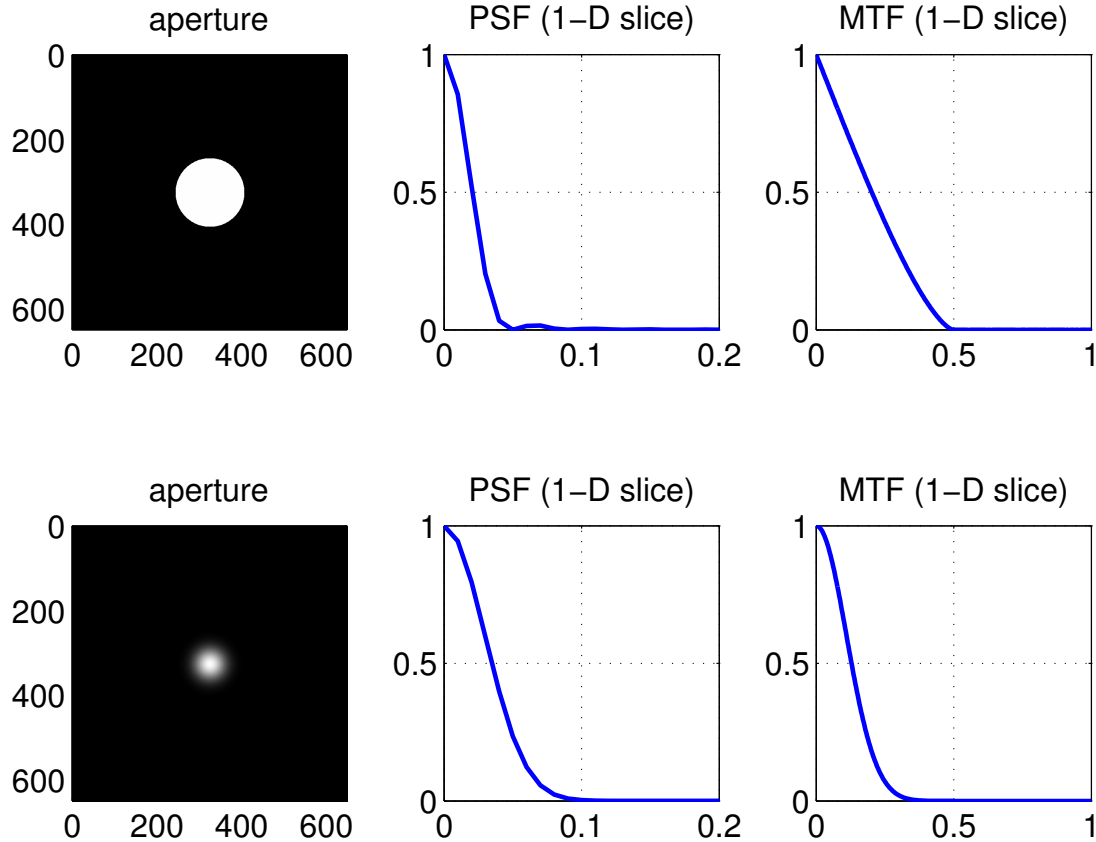


Figure 5.29: Comparison of a clear circular aperture (top) and an equal diameter circular aperture with Gaussian apodization applied (bottom). Spatial frequency axes of the MTF plots are normalized to the optical cutoff frequency for the circular aperture used in Fig. 5.21(a) and Fig. 5.25(a), which is twice the diameter of the aperture used here.

tions permits more informed decisions about optical setups, lens choices, aperture settings, and so forth.

When no aberrations are present, the PSF is real, centered, nonnegative, and symmetric about the optical axis. The MTF is symmetric and monotonically decreasing from a maximum of one at a spatial frequency of zero to a minimum of zero at the optical cutoff frequency. When the optics include significant aberrations, both the PSF and OTF can be complex-valued and asymmetrical. In general, aberrations will broaden the PSF and consequently narrow the OTF, leading to a lower optical cutoff frequency and poorer image quality. An excellent detailed treatment of these effects can be found in Smith [21].

While a larger aperture is preferred for diffraction-limited optics, the presence of aberrations may change that. For example, a larger aperture results in a smaller PSF (and thus better image resolution) and a larger MTF with a higher cutoff frequency (and thus better image quality at a wider range of spatial frequencies). However, a smaller aperture is associated with a reduction in aberrations (and thus higher image quality). This restates the idea of a “sweet spot” aperture size for a given optical system.

While aberrations are typically due mainly to non-ideal lenses, the effects of the various types of aberrations can be more easily simulated by modifying the characteristics of the aperture. If the aperture transmittance is not uniform across the aperture opening, then the field emanating from the aperture would have variations in amplitude and phase depending upon the location at which it came through the aperture. All such aperture transmittance variations can be combined

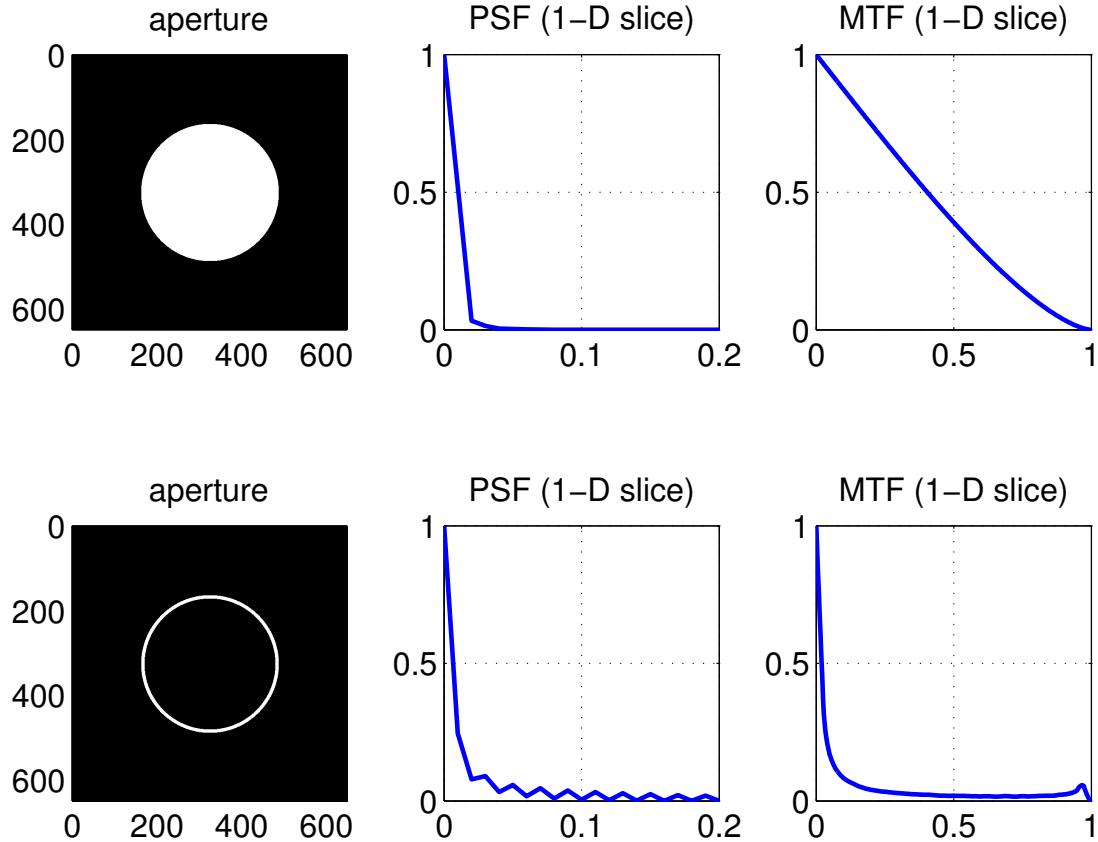


Figure 5.30: Comparison of a circular aperture (top) and a ring aperture (bottom) used for anti-apodization.

into a single complex quantity and written in the form of the generalized aperture function we first showed as Eq. (5.4), and which is shown again below for convenience.

$$A(x_a, y_a) = \underbrace{A_0(x_a, y_a)}_{\text{magnitude}} \underbrace{e^{j\alpha(x_a, y_a)}}_{\text{phase}} \quad (5.21)$$

All the aperture variations depicted in Fig. 5.20 were really just changes to the *magnitude* of the aperture function. To simulate aberrations, we will now make changes to the *phase* of the aperture function, because aberrations manifest themselves as changes to the phase of the wavefronts of light.

5.6.1 Phase function of the aperture

To understand how this technique of altering the phase of the aperture function relates to physical reality, let's discuss the phase of light that is passing through an aperture. Suppose we place a thin, flat, clear glass plate, with parallel faces, in front of the aperture. Assume that the glass plate causes no significant change to the magnitude of the aperture function, and neglect any reflection or absorption, such that the transmission through the glass is $T = 1$. But what of the phase of the aperture function?

If the thickness of the glass is g , and the index of refraction of the glass is n , then the value ng is called the *optical thickness* of the glass. Since $n > 1$, the velocity of light in the glass is slower than the velocity of light in air. That is, the light slows down a bit as it passes through

the glass. In this situation, we say that the light has been *retarded in phase*. How much has it been retarded? The phase shift is:

$$\Delta\alpha = kng = \frac{2\pi}{\lambda}ng, \quad (5.22)$$

and thus the aperture function could be written as:

$$A(x_a, y_a) = A_0(x_a, y_a)e^{j(2\pi/\lambda)ng}. \quad (5.23)$$

Since we assumed that the glass covered the entire aperture, this phase shift is constant over the entire aperture, so there will be no net effect on the diffraction pattern. Thus there will be no change to the PSF, no change to the OTF, and no change to the MTF. Therefore, we can neglect this phase shift.

What if the glass plate is only placed over just some portion of the aperture opening? The phase shift due to the glass is still described by Eq. (5.22), but now it occurs only for a portion of the aperture. This phase difference for light at different regions of the aperture can cause significant changes to the PSF (and thus changes to the OTF and MTF). So we can no longer neglect it.

Take this one step further: what if the phase shift varies across the whole aperture opening? That is, suppose the phase varies over all the (x_a, y_a) points of the opening at the aperture plane? Then the expression of the aperture function becomes:

$$A(x_a, y_a) = A_0(x_a, y_a)e^{j(2\pi/\lambda)\alpha(x_a, y_a)}, \quad (5.24)$$

where, compared to Eq. (5.21), the wavenumber constant $k = 2\pi/\lambda$ has been factored out of the phase function α to make it clearer what is constant and what varies over the aperture. The form of Eq. (5.24) suggests an easy way to incorporate phase variations due to aberrations into the aperture function: simply use $\alpha(x_a, y_a)$.

What about the sign of the phase function $\alpha(x_a, y_a)$? Should we be completely general and expect the phase term of the aperture function to be positive or negative? No! A negative sign to the phase term implies that we have *advanced* the wave instead of retarded it. For example, if we could find some glass with a negative index of refraction,⁸ or somehow “speed up” the velocity of light! It’s highly unlikely you will ever encounter this situation in practice, so assume $\alpha(x_a, y_a) \geq 0$ and that the sign of the phase term will always be positive.

Since aberrations are just deviations in the wavefront from what would be predicted by geometrical optics, we can introduce such wavefront deviations by specifying a particular phase function for the generalized aperture function given by Eq. (5.24). That leads us to the question of how to specify particular types of aberrations as a phase function.

5.6.2 Third-order optics

In Section 4.5, aberrations were described somewhat qualitatively. In order to simulate aberrations and their effects, we need a more quantitative method. There are many ways to mathematically describe optical aberrations; here we’ll take a correct but highly abbreviated approach.

Optics involves, among other things, geometry and trigonometry, where angles are very important. Consider the infinite series representation of sine and cosine of angle x :

$$\sin(x) = x - \frac{x^3}{3!} + \frac{x^5}{5!} - \frac{x^7}{7!} + \frac{x^9}{9!} - \frac{x^{11}}{11!} + \frac{x^{13}}{13!} - \dots \quad (5.25)$$

$$\cos(x) = 1 - \frac{x^2}{2!} + \frac{x^4}{4!} - \frac{x^6}{6!} + \frac{x^8}{8!} - \frac{x^{10}}{10!} + \frac{x^{12}}{12!} - \dots \quad (5.26)$$

⁸Note that some highly specialized materials have been created in the laboratory that exhibit a negative index of refraction, but they are not commonly available.

If we include only the first terms of these equations, then we would have the small angle approximation of $\sin(x) = x$ and $\cos(x) = 1$; this is often called *first-order optics*. It is in this realm that we use geometric optics, ray tracing, Gaussian optics, etc., and in this realm there are no monochromatic aberrations! However, note that chromatic aberrations are present in first-order optics since wavelength dependence cannot be avoided.

If we include the next terms of the infinite series (i.e., the cubed sine terms and the squared cosine terms), then we have what is called *third-order optics*. This is where the primary monochromatic aberrations become evident. For third-order optics, there are five primary types of monochromatic aberrations: spherical, coma, astigmatism, field curvature, and distortion. These were the types discussed in Section 4.5. If we add in the two kinds of chromatic aberration (axial and transverse), then we have seven total types of aberrations to be considered for third-order optics. Third-order optics describe reality with higher fidelity than first-order optics, but the underlying mathematics is more complicated.

As you've probably guessed, you can gain more accuracy by using even higher-order methods by (in effect) including more terms of the infinite series. Calculations involving fifth-order and seventh-order optics are commonly used by some high-end optical design software, such as Zemax. Higher-order types of aberrations are associated with higher-order optics. Fifth-order optics, for example, include additional aberrations, such as oblique spherical aberration and elliptical coma.

For many applications, the gain in accuracy is rather small compared to the vastly increased computational load when dealing with higher-order optics. Therefore, it's usually not worth it to directly consider aberrations of higher-order than those associated with third-order optics. Additionally, the effects of higher-order aberrations tend to be minimized by reducing third-order aberrations. Given all this, we find that the five monochromatic aberrations and the two chromatic aberrations listed above are what most optical designers deal with directly.

5.6.3 Describing aberrations

Just a little history can help put this discussion of aberrations in context. In 1857, the German mathematician Philipp Ludwig von Seidel decomposed the primary (third-order) monochromatic aberrations into five constituent aberrations (spherical, coma, astigmatism, field curvature, distortion); they are now commonly referred to as the five *Seidel aberrations*.⁹ Seidel came up with a method for using a combined polynomial to describe phase deviations due to aberrations, for example:

$$V(r, \theta) = a_{40}r^4 + a_{31}r^3 \cos \theta + a_{22}r^2 \cos^2 \theta + a_{20}r^2 + a_{11}r \cos \theta \quad (5.27)$$

where (r, θ) describe points on the aperture plane in polar coordinates (right hand rule, thumb pointing in the z -direction of propagation, $\theta = 0$ along the x -axis), and the five coefficients shown above describe the level of the five constituent monochromatic aberrations for third-order optics (in the order listed above). Higher-order aberrations can be included in a similar fashion, but the polynomial quickly becomes very complicated.

While Seidel's method is excellent and is still used, it makes it difficult to separate out individual types of aberrations. In 1934, Dutch physicist Frits Zernike extended Seidel's work in a way that, for the first time, allowed a clear mathematical separation between the various types and orders of aberrations.¹⁰ Zernike's orthogonal polynomials, defined on a unit circle, provided a solution to the long-standing problem of the optimum "balancing" of the various aberrations of an optical instrument. Since the 1960's, Zernike's circle polynomials have been widely used in optical design, optical metrology, and image analysis. While this method provides great flexibility, the number of circle polynomials grows with the number of aberrations being described. For example, to describe aberrations out to the equivalent of eleventh-order optics requires 49 Zernike polynomials! Theoretically, there is an infinite number of Zernike polynomials, but only certain ones are commonly used by those interested in optical analysis and design.

⁹The lunar crater *Seidel* is named after him.

¹⁰Zernike won the 1953 Nobel prize in physics for his invention of the phase contrast microscope, and the lunar crater *Zernike* is named after him.

Table 5.4: Monochromatic aberrations associated with third-order optics. Note: the orthonormal representation of the Zernike polynomials is given.

Name	Direction	Zernike polynomial
distortion	x -tilt	$2r \cos \theta$
distortion	y -tilt	$2r \sin \theta$
field curvature/defocus	NA	$\sqrt{3} (2r^2 - 1)$
astigmatism	x	$\sqrt{6} r^2 \cos(2\theta)$
astigmatism	y	$\sqrt{6} r^2 \sin(2\theta)$
coma	x	$\sqrt{8} (3r^3 - 2r) \cos \theta$
coma	y	$\sqrt{8} (3r^3 - 2r) \sin \theta$
spherical	NA	$\sqrt{5} (6r^4 - 6r^2 + 1)$

5.6.4 Using Zernike polynomials

There are a few things to keep in mind when using Zernike polynomials to describe optical aberrations. First, because Zernike polynomials are defined on a unit circle, their use can yield very misleading results if the aperture is not circular. Second, there is a huge amount of inconsistency in the nomenclature, usage, and form related to Zernike polynomials in the literature. Proceed with great care as you read about this topic from different sources. For example, to unambiguously specify a particular Zernike polynomial, you need two index terms, usually called n and m . But how n and m are assigned is not the same across publications. To make matters more difficult, some authors (and optics companies) adopt a single number index convention for Zernike polynomials. But again, the way in which that single index number is assigned is not the same across publications or companies. This is particularly frustrating because there is an international standard (ISO 24157) that includes instructions about how to number Zernike polynomials, but few seem to follow it.

Certain Zernike polynomials can be used to describe optical aberrations as wavefront phase deviations through an aperture, which is exactly what we seek. Table 5.4 provides the most commonly used Zernike polynomials associated with third-order aberrations. In most cases, this is all you need. However, if you need to simulate some higher-order aberrations, example Zernike polynomials are given in Table 5.5.

Note that field curvature and defocus are both modeled the same way, using the same Zernike polynomial. The effect of defocus on an image can be considered to be just a larger amount of field curvature. Defocus is of interest to optometrists and ophthalmologists, since it is used as the model for myopia and hyperopia of the human eye.

These tables were created by scouring half a dozen reference books and a dozen web sites, then resolving all the inconsistencies and nomenclature variations across them. In both Table 5.4 and Table 5.5, index numbers are omitted to avoid confusion. The values of r and θ in the tables are used to describe points on the aperture plane in polar coordinates (right hand rule, thumb pointing in the z -direction of propagation, $\theta = 0$ along the x -axis). Yes, there is even inconsistency in the literature about how to define the polar coordinate system, so this definition is needed here. In general, if the aberration is circularly symmetric (e.g., spherical aberration), there will only be r terms in the polynomial. If the aberration is not circularly symmetric, there will be pairs of polynomials, one with $\cos \theta$ terms (for the x -direction) and one with $\sin \theta$ terms (for the y -direction). But, as expected, what is x and what is y is also not universally agreed upon in the literature. To be consistent with the majority of the literature on Zernike

Table 5.5: Monochromatic aberrations associated with fifth-order and seventh-order optics. Note: the orthonormal representation of the Zernike polynomials is given.

Name	Direction	Zernike polynomial
astigmatism (5 th -order)	x	$\sqrt{10} (4r^4 - 3r^2) \cos(2\theta)$
astigmatism (5 th -order)	y	$\sqrt{10} (4r^4 - 3r^2) \sin(2\theta)$
coma (5 th -order)	x	$\sqrt{8} (10r^5 - 12r^3 + 3r) \cos \theta$
coma (5 th -order)	y	$\sqrt{8} (10r^5 - 12r^3 + 3r) \sin \theta$
spherical (5 th - and 7 th -order)	NA	$\sqrt{7} (20r^6 - 30r^4 + 12r^2 - 1)$

polynomial, x is the horizontal axis, y is the vertical axis, and the origin of the coordinate system (Cartesian or polar) is located at the center of the aperture opening.

For simulation purposes, the orthonormal forms of the Zernike polynomials shown in the tables are usually multiplied by some constant between 0 and 1 to adjust the amount of the particular type of aberration.¹¹ Physically, this constant represents a distance divided by the wavelength, and thus represents the fraction of a wavelength equal to the wavefront error introduced by the aberration. The division by the wavelength comes from the $1/\lambda$ term in the wavenumber $k = 2\pi/\lambda$ shown in the phase term of the aperture function of Eq. (5.24).

5.6.5 Simulated Effects of Aberrations

Now that we have some relatively simple equations to describe aberrations, how do we use them for a simulation? Let's use primary coma in the x -direction as an example. The use of any other aberration simply follows the same technique.

The Zernike polynomial for primary coma in x is given in Table 5.4 as $\sqrt{8} (3r^3 - 2r) \cos \theta$. We insert that into the aperture function:

$$\begin{aligned} A(x_a, y_a) &= A_0(x_a, y_a) e^{j(2\pi/\lambda)d_c[\sqrt{8}(3r^3 - 2r) \cos \theta]} \\ &= A_0(x_a, y_a) e^{j2\pi z_c[\sqrt{8}(3r^3 - 2r) \cos \theta]} \end{aligned} \quad (5.28)$$

where $r = \sqrt{x_a^2 + y_a^2}$, $\theta = \arctan(y_a/x_a)$, and z_c is a constant (usually between 0 and 1) that represents the “amount” of coma, expressed as a fraction of a wavelength.¹² See Listing C.4 for a MATLAB program that implements this simulation. A plot of the magnitude and phase of the aperture function, without and with coma in x (for $z_c = 0.2$), is shown in Fig. 5.31. On the magnitude plot, white is 1 and black is 0. Notice that with no aberration, the phase plot is 0 everywhere. With an aberration, there is an obvious variation in the phase term, as dictated by Eq. (5.28). Because the phase variation includes both positive and negative values, the image plot of the phase term must be scaled such that zero becomes mid-level gray, max positive is

¹¹Values larger than 1 can be used to model very large amounts of aberration.

¹²Don't forget that this is a monochromatic aberration, and so the results of the simulation should be different for different wavelengths.

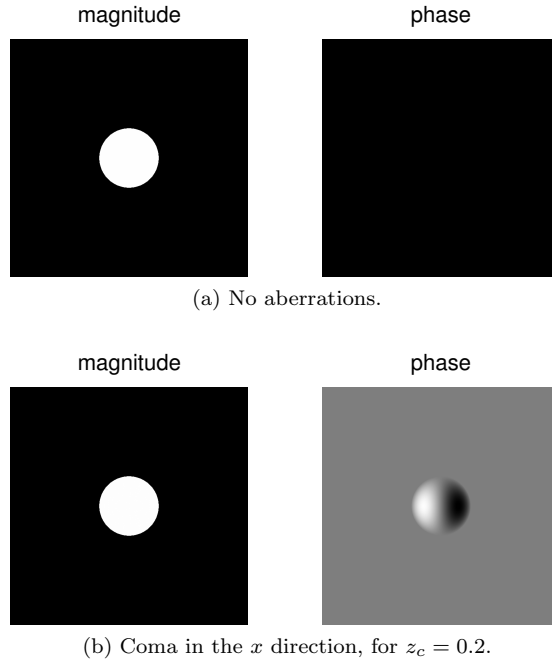


Figure 5.31: A plot of the magnitude and phase of the aperture function for a circular aperture, without and with aberration.

white, and max negative is black. Once the aperture function is defined, the PSF and MTF follow as before: $\text{PSF} = |\mathcal{F}\{A(x_a, y_a)\}|^2$ and $\text{MTF} = |\text{OTF}| = |\mathcal{F}\{\text{PSF}\}|$.

Real-world optical systems usually exhibit more than one type of aberration. Combining various forms using this simulation method is particularly easy. Suppose we wanted to simulate a combination of primary coma in the x -direction and primary astigmatism in the y -direction. The Zernike polynomial for primary coma in x was used in Eq. (5.28); the Zernike polynomial for primary astigmatism in y , from Table 5.4, is $\sqrt{6} r^2 \sin(2\theta)$. The aperture function that combines both types of aberration is:

$$A(x_a, y_a) = A_0(x_a, y_a) e^{j2\pi(z_c[\sqrt{8}(3r^3 - 2r)\cos\theta] + z_a[\sqrt{6}r^2 \sin(2\theta)])} \quad (5.29)$$

where $r = \sqrt{x_a^2 + y_a^2}$, $\theta = \arctan(y_a/x_a)$, z_c is a constant that represents the “amount” of coma, and z_a is a constant that represents the “amount” of astigmatism, with both z_c and z_a expressed as a fraction of a wavelength. Other combinations come to mind: to simulate coma at a 45° angle, simply add equal amounts of x coma and y coma in the phase term. It’s trivial to modify Listing C.4 to simulate any combination of aberrations listed in Table 5.4 and Table 5.5.

Some example PSF and MTF plots that result from simulated aberrations can be very instructive. When plotting such PSFs and MTFs, it’s a good idea to view them several different ways (using different plot types) to be sure you don’t miss some important aspect of the functions. For example, MATLAB provides the ability to easily generate 1-D line plots, 2-D image and contour plots, and 3-D mesh and surface plots. High-end optical design software can produce similar plots, if you have it available. Each type of plot has its advantages for visualizing certain aspects of a PSF or MTF. In the figures that follow, none of the plot axes have been normalized, to keep the discussion general. The axis units are not intended to have any physical significance, other than the fact that the PSFs are plotted in the spatial domain and the MTFs are plotted in the spatial frequency domain. However, the *relative* size of one PSF to another, or of one MTF to another, is a valid comparison using these generalized units.

A 1-D plot, across the x -axis, that compares the non-aberrated PSF with the PSF associated

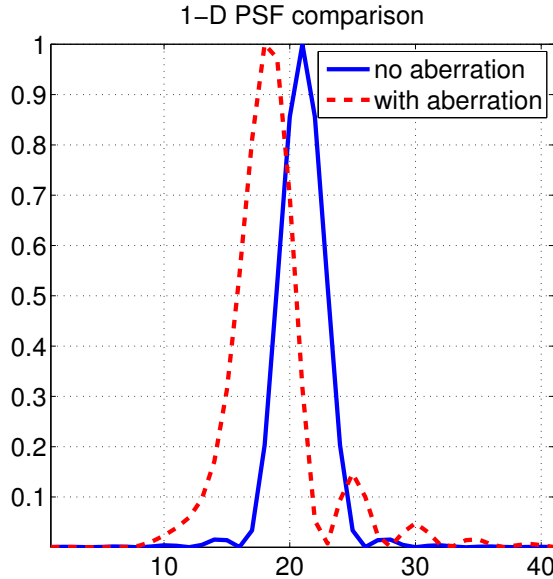


Figure 5.32: Comparison along the x -axis of PSFs without and with coma in the x direction.

with coma in x for $z_c = 0.2$ (i.e., 2/10 of a wavelength aberration) is shown in Fig. 5.32. Notice the aberrated PSF is no longer centered, is asymmetrical (with a “tail” of side lobes in the x direction), yet the main lobe is approximately the same width at the half-power point. Given the characteristics of coma shown in Fig. 4.19, which showed coma in the y direction, this resulting PSF should make sense. The associated MTFs, provided as two 1-D plots across the horizontal u -axis (associated with the x -axis) and across the vertical v -axis (associated with the y -axis), are shown in Fig. 5.33. The non-aberrated and aberrated MTFs are both symmetrical about the origin (since the PSFs were both real), and the optical cutoff frequency is approximately the same for both, since the width of the PSF main lobe was nearly the same for the non-aberrated and aberrated PSFs. However, the non-centered, asymmetrical PSF associated with coma definitely changes the MTF. Spatial frequencies in the middle region between zero and the cutoff frequency show reduced modulation depth. The u -axis plot shows this effect to a much greater degree, which is to be expected since the coma was in the x direction. Another way to look at the PSF and MTF comparison is by “looking down” on these 3-D functions as 2-D contour plots, shown in Fig. 5.34. This type of plot is an excellent way to observe the overall effect of the coma aberration.

A similar series of plots for spherical aberration, for $z_s = 0.2$ (i.e., 2/10 of a wavelength aberration), is instructive. A 1-D plot, across the x -axis, that compares the non-aberrated PSF with the PSF associated with spherical aberration is shown in Fig. 5.35. Notice the aberrated PSF is still centered and symmetrical (due to the circular symmetry of spherical aberration), yet the main lobe is much wider at the half-power point. The associated MTFs, provided as two 1-D plots across the horizontal u -axis (associated with the x -axis) and across the vertical v -axis (associated with the y -axis), are shown in Fig. 5.36. The non-aberrated and aberrated MTFs are both symmetrical about the origin (since the PSFs were both real), but the optical cutoff frequency of the aberrated case is much lower, since the width of the PSF main lobe was much wider. Spatial frequencies in the middle region between zero and the cutoff frequency also show greatly reduced modulation depth. Looking down at the PSF and MTF functions as 2-D contour plots is shown in Fig. 5.37. This type of plot is an excellent way to observe the much larger PSF and the much smaller (lower cutoff frequency) MTF that is associated with spherical aberration.

When different types of aberrations are combined, the PSF and MTF functions can become

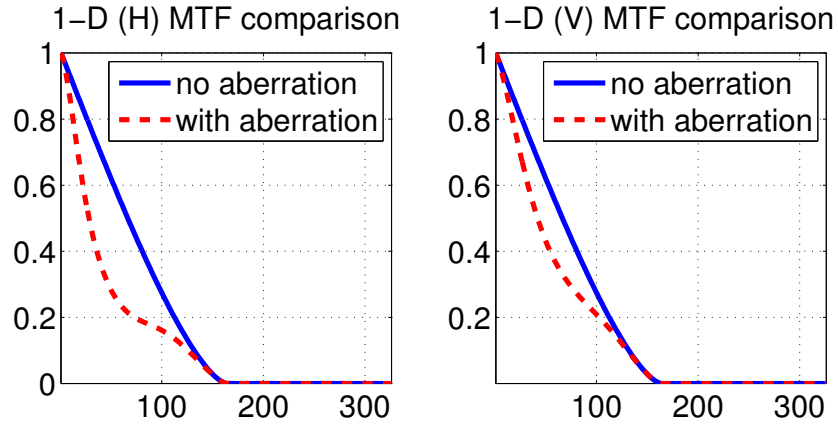


Figure 5.33: Comparison along the horizontal u -axis (left subplot, associated with the x -axis) and across the vertical v -axis (right subplot, associated with the y -axis) of the MTFs without and with coma in the x direction.

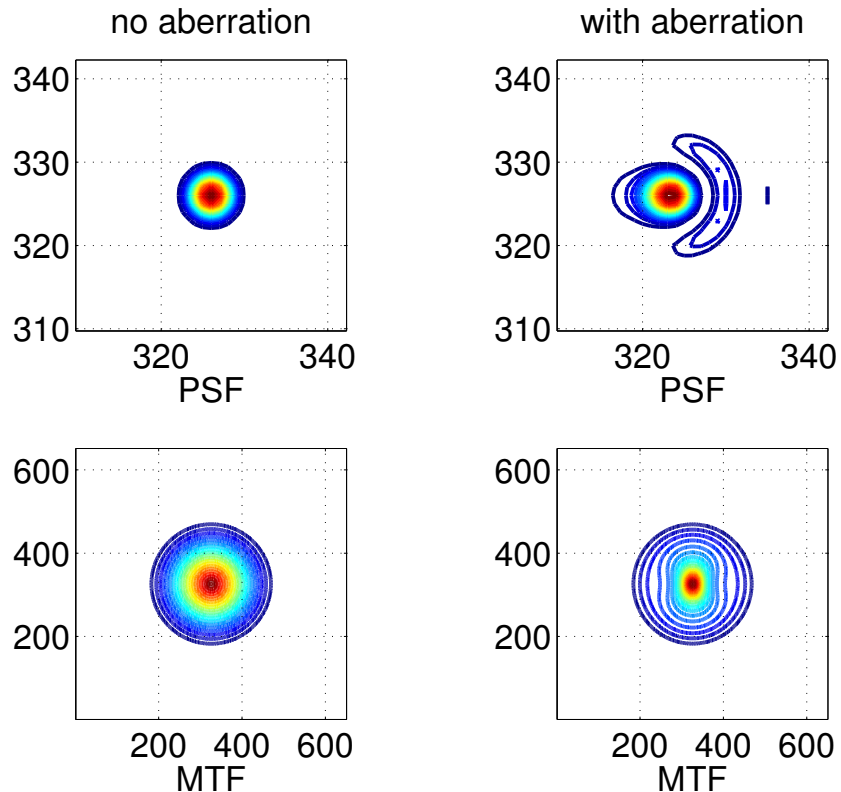


Figure 5.34: Comparison contour plots of the PSFs and MTFs without and with coma in the x direction. Note that to show sufficient detail, the PSF plots (top row) are “zoomed in” compared to the scale shown for the MTF plots (bottom row).

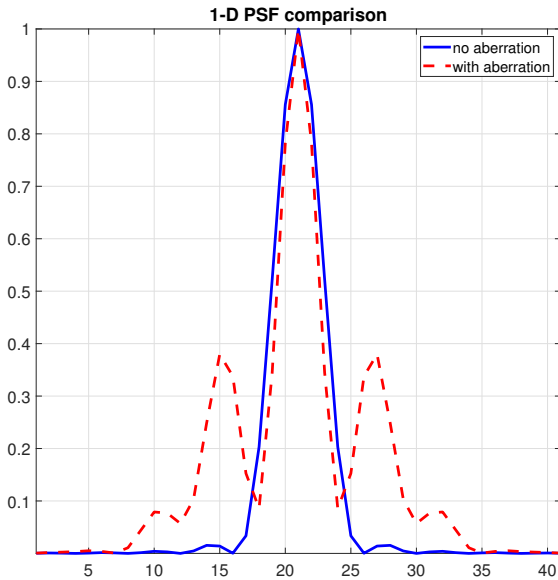


Figure 5.35: Comparison along the x -axis of PSFs without and with spherical aberration.

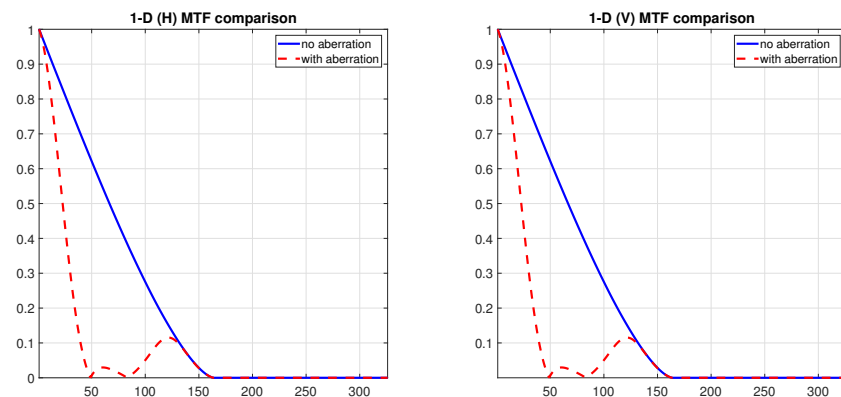


Figure 5.36: Comparison along the horizontal u -axis (left subplot, associated with the x -axis) and across the vertical v -axis (right subplot, associated with the y -axis) of the MTFs without and with spherical aberration.

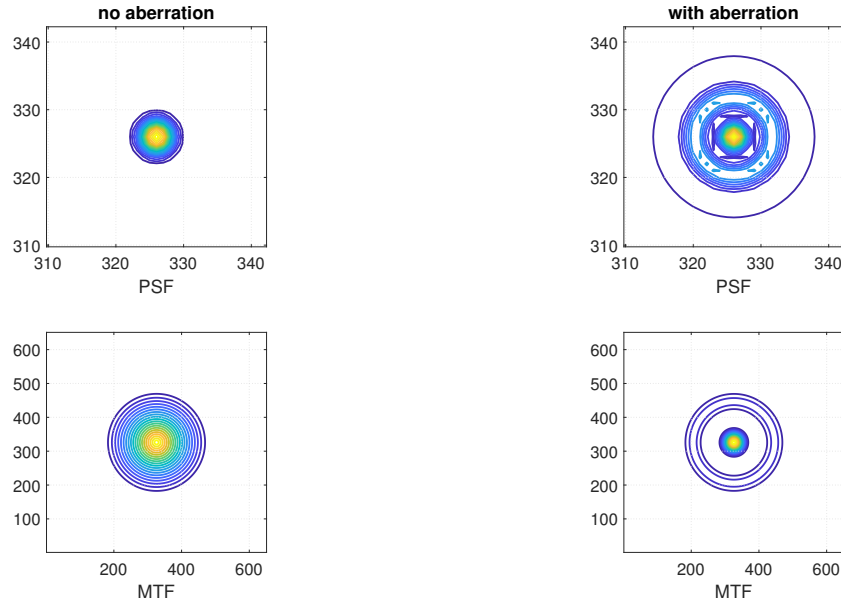


Figure 5.37: Comparison contour plots of the PSFs and MTFs without and with spherical aberration. Note that to show sufficient detail, the PSF plots (top row) are “zoomed in” compared to the scale shown for the MTF plots (bottom row).

quite complex. The combination of coma in x and astigmatism in y described by Eq. (5.29) and evaluated for $z_c = 0.2$ and $z_a = 0.2$ (i.e., 2/10 of a wavelength aberration contributed by each type of aberration) is a good example, and is shown in Fig. 5.38.

In general, the effect of all aberration types (individually and in combination) are proportional to the size of the aperture. Smaller apertures show less effect from aberrations. The simulation methods described here make it particularly easy to test that concept by simulating the same amount of aberration, but with different aperture sizes.

Notice that the presence of one or more aberrations typically made the PSF larger and possibly asymmetrical, and consequently made the MTF smaller, with reduced modulation depth for certain spatial frequencies and perhaps a lower optical cutoff frequency. Any asymmetries in the PSF yielded variations in modulation depth for the MTF between the horizontal spatial frequencies and the vertical spatial frequencies. No aberration will ever make the PSF smaller or increase the modulation depth for a particular spatial frequency. The PSF and MTF associated with the diffraction-limited open aperture is the theoretical bound for the best result possible with normal optics, and while you can only approach this level of performance, it does provide a good point of comparison for a real-world system.

Only the MTF, and not the PTF (phase transfer function), was shown for the simulations (although the program from Listing C.4 displays both). This is because it’s difficult to infer much directly from PTF plots. However, the PTF does affect the image quality.

Knowledge of the aberrated PSF and MTF provides insight into the anticipated effects some level of aberration would have on an image. The simulation can be taken even further, if desired. Comparing Fourier optics to digital signal processing or image processing, one could think of the OTF as a filter function in the frequency domain. The spectrum of a test image could be multiplied¹³ by the OTF “filter” to yield the resulting non-ideal image that would result from using aberrated optics. Because the OTF “filter” has real and imaginary components, the phase of the OTF (i.e., the PTF) will have an effect on the image, not just the MTF as implied by many texts. If you prefer to consider such a “filtering” operation in the spatial domain, then the

¹³You would perform multiplication point-by-point, not as matrix multiplication.

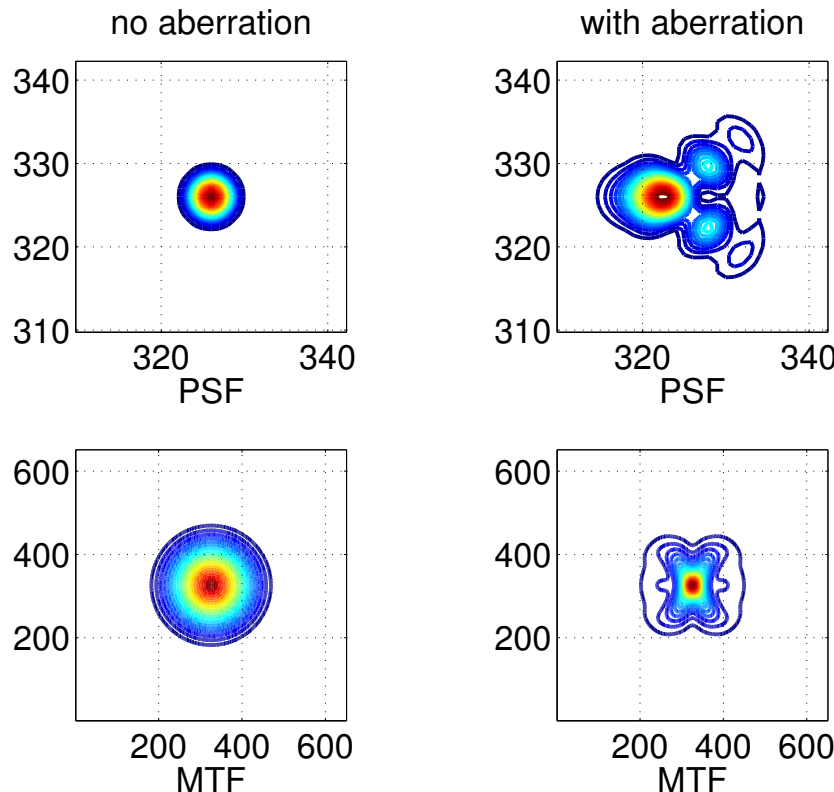


Figure 5.38: Comparison contour plots of the PSFs and MTFs without and with a combination of coma in x and astigmatism in y . Note that to show sufficient detail, the PSF plots (top row) are “zoomed in” compared to the scale shown for the MTF plots (bottom row).

PSF serves as the impulse response of the filter. Therefore, the spatial domain image would be convolved with the PSF to yield the resulting non-ideal image due to aberrated optics. If done properly,¹⁴ either method should provide the same result (aberrations reduce image quality), but many people seem to find multiplication in the frequency domain easier to understand. The availability of mathematical tools such as the FFT makes this option very easy to accomplish.

So far, this discussion has only mentioned in detail the five primary (i.e., Seidel) monochromatic aberrations, with the simulations performed at a single wavelength. What about chromatic aberration, which is also present? In general, chromatic aberration manifests itself as a defocus effect from one wavelength to another, since the optical system’s focal length changes from one wavelength to another. Simulating this manually, even with a tool as powerful as MATLAB, is certainly possible but can be tedious. Some of the visible effects of chromatic aberration, such as color fringing at object edges, are difficult to simulate properly. High-end commercial optical design software is better suited to these sorts of simulations. If this next level of simulation is needed, the reader may want to investigate packages such as Zemax OpticStudio (by Radian Zemax, LLC; see <http://zemax.com/>), Code V (by Synopsis OSG; see <http://optics.synopsys.com/codev/>), ASAP (by Breault Research Organization, Inc.; see <http://www.breault.com/>), or OSLO (by Sinclair Optics, Inc.; see <http://www.sinopt.com/>). There are some “freeware” packages also available, but they tend to be less capable than the commercial products.

The simulation techniques described in this section certainly allow the reader to take a more

¹⁴Frequency domain methods require zero padding to avoid circular convolution errors. Consult any good image processing text such as [44].

quantitative approach to dealing with aberrations. The few examples shown here do not span the full range of effects that aberrations can cause. In general, aberrations can not only reduce the cutoff frequency, they can also cause contrast reversals, cause zero contrast bands to appear below the cutoff frequency, and generally reduce image quality. A proposed quantitative measure of aberrated image quality that can be expressed as a single number is the *Strehl ratio*, which is the ratio of the volume integral of the aberrated two-dimensional MTF to the volume integral of the associated diffraction-limited MTF [21]. However, just as the single numbers that specify the optical cutoff frequency or the limiting resolution don't tell the whole story, use of only the Strehl ratio may also be insufficient in many situations.

When discussing aberrations, it is important to recall from the earlier discussion in Section 4.5 that optical components which are not separated by a diffuser of some sort may compensate for the aberrations of each other—hence the term *corrected* optics. Otherwise, the MTFs of individual system components are all cascaded by multiplication.

The concept of *aberration tolerance* should be considered: how much aberration is acceptable within the system requirements? In Ref. [21], Smith advises that most imaging systems can withstand aberration resulting in up to one-quarter of a wavelength of optical path difference from a perfect (i.e., ideal) reference wavefront, without a “noticeable effect” on image quality. High-quality optics available today typically achieve this goal [22].

5.7 Summary

How can you put the techniques of Fourier optics to best use?

- Define the aperture function for simulating an open aperture of a given maximum size, with no aberrations. This will provide your diffraction-limited point of comparison.
- Once the aperture function is defined, the PSF and MTF are calculated using the relationships: $\text{PSF} = |\mathcal{F}\{A(x_a, y_a)\}|^2$ and $\text{MTF} = |\text{OTF}| = |\mathcal{F}\{\text{PSF}\}|$.
- This provides the best possible PSF and MTF, and the highest optical cutoff frequency. You can now connect the simulation to physical reality and actual units by remembering $f_c = D/\lambda$ cy/rad in angular units or $f_c = D/\lambda d$ cy/m in linear units. At this point, you may also want to apply one of the common resolution criteria. Compare all this to your known system requirements.
- Then start introducing aberrations of various types and amounts, and if appropriate also reduce the aperture size, each time comparing aspects of the PSF and MTF to the original diffraction-limited point of comparison, and checking everything against your known system requirements.
- Repeat this for multiple wavelengths as needed to represent the anticipated illumination source, and also to investigate potential effects of chromatic aberrations.

These techniques allow you to better understand the underlying tradeoffs in your optical system, along with the effects of aberrations. They also allow you to search for an optimal aperture size for a given amount of aberration, balancing the effect of aperture size on the PSF and MTF with the effect on aberrations.

Problems

- 5.1 A camera with a 70 mm lens is adjusted to an aperture setting of f/4, and is set to focus at a distance of 10 m. Assume no aberrations. Find the width of the PSF at the half power point in linear units. How does this compare to the three common resolution criteria?
- 5.2 For the same camera and setup, find the optical cutoff frequency in linear units.

Chapter 6

Imaging Sensors

Up until now, this book has concentrated on the optical aspects of forming an image. But the primary optical system of a camera or imaging device serves just one purpose: to gather light and bring the desired scene to an acceptably sharp focus on the photodetectors. It is the photodetectors that sense the light, and transduce the incident photons into a usable voltage that can be captured and eventually result in a digital image. This chapter concentrates on that next step in image formation: the operation of the imaging sensors. The discussion that follows is intentionally generic and not specific to a particular sensor technology such as charge-coupled device (CCD), complementary metal-oxide semiconductor (CMOS), or charge injection device (CID), unless such a distinction is particularly helpful. For more specific details regarding imaging sensors for digital cameras, consult the references [35, 40, 42, 66–70]. In particular, reference [35] and the references cited in that book, provide an excellent resource for more in-depth details than are appropriate here.

The previous chapter provided a particularly powerful method of using Fourier techniques to perform simulation and analysis of optical systems. This chapter will extend those techniques in such a way that we can use them to simulate and analyze the sensor array and its closely associated subcomponents. For obvious reasons, the name “Fourier optics” may not be appropriate here, even though the underlying techniques are basically the same. Many authors use a more general name, such as *MTF analysis*, when non-optical components are involved.

The reader should be warned that the specific details of how to treat some of the effects of the sensor array on image formation are not universally agreed upon by all authors, and this may lead to confusion if the reader is referring to multiple sources. In this chapter, we will define a multi-part “MTF” associated with the sensor array that permits the same powerful mathematical techniques from the last chapter to be used here. However, strictly speaking, there can be no *true MTF* for any sampling device such as a sensor array (for reasons we shall briefly discuss in the appropriate section). Because of this, some authors recommend alternatives (such as the Sampled Imager Response (SIR) function proposed by Vollmerhausen et al. in [41]). The results associated with using a metric such as the SIR function instead of an MTF can be quite good, and the reader is encouraged to investigate such methods. But the downside is that such methods tend to make the analysis considerably more complicated. The author of this book tends to agree with Holst, who in [39] admits to the mathematical limitations of applying pure MTF theory to a sampling device such as a CCD array, then says, “In spite of these disclaimers, an imaging system is treated as quasilinear over a restricted operating region to take advantage of the wealth of mathematical tools available.” Basically, the benefit of extending MTF analysis techniques to sensor arrays outweighs the inexactitude of the method, and the results have proven to be very close to reality. A detailed treatment of using MTF analysis for sampled image systems can be found in [71].

The majority of the time, we use 2-D sensor arrays to acquire the digital image, so that type of sensor is to be assumed in this chapter unless otherwise specified. This chapter includes sections

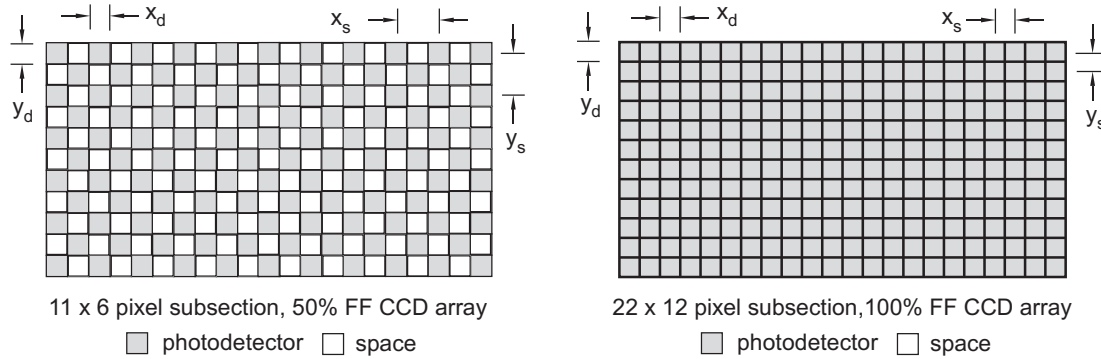


Figure 6.1: Rectangular subsections of two example focal plane arrays with square photodetector areas (i.e., $x_d = y_d$). Left: 50% fill factor. Right: 100% fill factor.

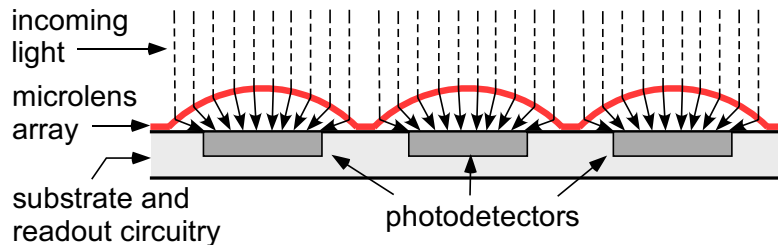


Figure 6.2: Simplified illustration of how a microlens array can greatly increase the effective fill factor of a sensor array. Not shown is the possible existence of a color filter array and an optical low pass filter, which would occupy layers between the microlens array and the photodetectors.

that briefly discuss 1-D linear arrays and single-detector scanning imagers. The discussion in this chapter spans both still-image cameras and video cameras. Chapter 7 will discuss differences between these two types of cameras.

Assuming a scene is imaged with acceptable sharpness at the focal plane, the next step is to use some photosensitive devices to convert the light energy to electrical energy. One of the most common techniques is to use a rectangular (2-D), planar array of photodetectors at the focal plane; this is generically called a focal plane array (FPA). Relative sizes of FPA sensors used in popular consumer cameras were given in Table 4.2 and Figure 4.14. See Fig. 6.1 for a simplified diagram of a small subsection of a generic FPA, where x_d and y_d represent the size of the photosensitive area in the x and y directions respectively. The center-to-center distance between photodetectors is x_s and y_s ; this is sometimes called the detector *pitch*. The *fill-factor* (FF) of the array is defined as the ratio of the photosensitive area (i.e., the active detector area) to the total array area over an appropriate region (with dimensions usually having an even multiple of x_s and y_s per side) of the FPA.¹ In Fig. 6.1, a fill factor of 50% (where $x_s = 2x_d$ and $y_s = 2y_d$) is shown on the left, and a fill factor of 100% (where $x_s = x_d$ and $y_s = y_d$) is shown on the right.

While some real-world FPAs have a physical FF that approaches 100%, constraints such as the chip real estate needed for readout electronics used in certain sensor technologies can significantly reduce the area available for the photosensitive detector region. In that case, most modern FPAs use a microlens array on the surface of the chip to direct light away from the “dead zone” and into the detector region, resulting in an *effective* fill factor of 90% or higher. This is illustrated in Fig. 6.2. Use of a microlens array implies that the values of x_d , y_d , x_s ,

¹Note that while many authors define a 2-D fill factor similar to this based on a ratio of areas, others define only a 1-D fill factor in each dimension (horizontal and vertical). Be a careful reader.

and y_s mentioned previously should be the effective values rather than the physical values. It should be noted that even with a microlens array, the color filter arrays (CFA) used for some color cameras can appear to limit the FF to 50% for green and 25% for red and blue, but due to spectral overlap of the filters, the true effect of the CFA is more complicated. This will be discussed in more detail at the appropriate place. For the majority of FPAs, the FF is the same in each dimension for a given color, and most often the individual photodetector shape is square even though the full FPA dimensions are typically rectangular.

Use of the FPA introduces two categories of changes to the image:

1. non-sampling effects, such as the spatial integration of light over the finite photosensitive area of each photodetector, and
2. the spatial sampling of the continuous image provided by the optics.

We first discuss the non-sampling effects, then address the ramifications of spatial sampling, using a Fourier optics type of approach where PSFs and MTFs can be defined. For compactness, a one dimensional approach is often used to simplify the diagrams and equations where appropriate for the discussion that follows; however, don't forget that the sensor array under consideration here is a 2-D device.

6.1 Non-sampling effects of the FPA

6.1.1 Blurring due to detector size

Each photodetector site (sometimes called a *pixel*) of the FPA must have a large enough photosensitive area to capture a sufficient number of photons to obtain a usable signal above the noise floor.² This finite area results in spatial integration which produces a blurring (i.e., smearing) effect on the image. In the most common case, the sensitivity of the photodetector is relatively constant over the entire photosensitive area, so the sensitivity distribution of the FPA is just a rectangular (sometimes called *tophat* or *flattop*) function with a width determined by the size of the photosensitive area in the given dimension for the individual photodetectors. We seek the effective PSF of the array, which will lead to the associated OTF, which will lead to the MTF. As with optics, the PSF is determined by what happens when an “impulse” of light falls on the FPA.

Suppose three separate impulses of light fall on an FPA, as shown in Fig. 6.3. Each photodetector site performs spatial integration (similar to averaging) of the light that falls within its boundary; this has a definite blurring effect. For example, the two impulses falling on the same photodetector site (row 1, column 1) cannot be resolved as separate points of light. The output associated with that location will be twice as high compared to only one impulse falling on the location, but that's all. Furthermore, information about *where* a point of light falls within a photosensitive area (such as the impulse falling on the upper right corner of the photodetector at row 4, column 3) is lost; only the amount of light captured for that particular row and column of the FPA is recorded.

What does that imply for the impulse response (i.e., PSF) of the FPA due to the detector size? If we consider aberration-free optics, then the impulse of light at the object plane becomes an Airy disk (due to diffraction) on the FPA at the focal plane, where it is spatially integrated across the entire area of the photodetector site. The Airy disk is thus blurred into a flattop (i.e., rectangular) pulse, as shown in Fig. 6.4. Therefore, the PSF of the FPA must be a rectangular pulse with dimensions in x and y equal to the effective dimensions of a single photodetector site. If no microlens array is present, the effective dimensions are the same as the physical dimensions of the photodetector.

The OTF of the FPA due to the detector size is the Fourier transform of the PSF due to the effective detector size, and as just discussed, that PSF is a rectangular function (often called

²A short discussion of low-light techniques was given in Section 3.8.

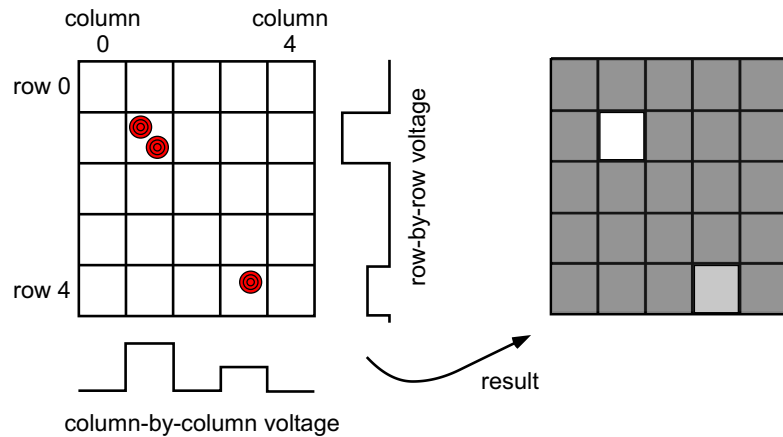


Figure 6.3: Simulated effect of three impulses of light (shown as Airy disks in red) falling on an FPA. The two impulses falling on the same photodetector site at row 1, column 1 will not be resolved as separate points of light.

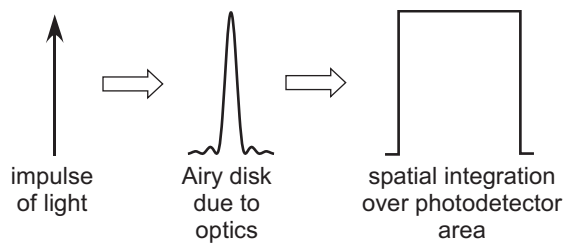


Figure 6.4: Process of an impulse of light entering a camera lens and falling on an FPA.

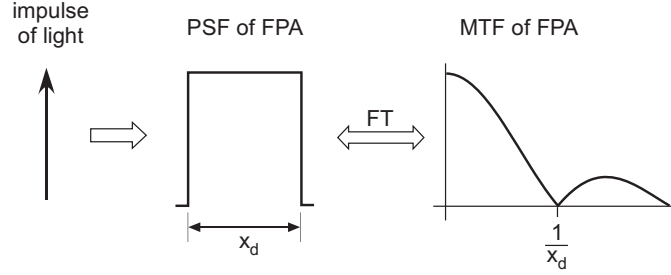


Figure 6.5: The impulse response, or PSF, of the FPA is a rect function, so the MTF is the magnitude of a sinc function.

a rect function). The Fourier transform of a rect function is the well-known sinc function.³ The MTF is the magnitude of the OTF. Thus, the MTF of the FPA is the magnitude of the associated sinc. In 1-D, the x -axis in the spatial domain corresponds to the u -axis in the spatial frequency domain, so the 1-D MTF due to the detector size in this direction is:

$$\text{MTF}_{\text{det}}(u) = \left| \frac{\sin(\pi x_d u)}{\pi x_d u} \right| = |\text{sinc}(x_d u)| , \quad (6.1)$$

where x_d is the size of the photosensitive area in the x direction. A diagram of this 1-D relationship is depicted in Fig. 6.5. Note that in Fig. 6.5, only the magnitude of the FT (i.e., the MTF) is shown, to keep the figure from being too cluttered, but the reader should understand that the double arrow representing a FT pair would also include the phase of the FT on the right side of the arrow. A similar 1-D relationship is used for the y and v direction. For locations not on the x or y axes, MTF values would need to be calculated using the full 2-D sinc equation, which is:

$$\text{MTF}_{\text{det}}(u, v) = \left| \frac{\sin(\pi x_d u)}{\pi x_d u} \frac{\sin(\pi y_d v)}{\pi y_d v} \right| = |\text{sinc}(x_d u) \text{sinc}(y_d v)| . \quad (6.2)$$

A 2-D versus 1-D plot of this MTF is shown in Fig. 6.6, where the 2-D MTF plot is shown for the common case of square photodetectors (i.e., $x_d = y_d$).

While the sinc function extends out to infinity along the spatial frequency axes (so that technically there is no true cutoff frequency for this MTF), it is common in practice to consider the MTF of an FPA as significant only up to the first zero of the sinc magnitude, which defines the boundary of the main lobe. The extent of the main lobe of the MTF on the 2-D (u, v) spatial frequency plane can be more clearly seen when the MTF is plotted as an image, as shown in Fig. 6.7. The first zero of the sinc magnitude, and thus the effective cutoff frequency associated with this MTF, is at $u = \pm 1/x_d$ and $v = \pm 1/y_d$. Thus a larger photosensitive area may gather more light, but results in the cutoff frequency occurring at a lower spatial frequency, which implies there would be more blurring in the image. Note that the units of spatial frequency in Eq. (6.1) and Eq. (6.2) for the MTF of an FPA are linear units (e.g., cycles/meter); when optical MTFs were previously discussed, angular units were often used. Conversion is easy: angular spatial frequency divided by the distance to the image plane s_i of the optical system equals linear spatial frequency at the image plane, assuming the small angle approximation holds.

Note that the detector MTF discussed so far depends only upon the physical dimensions of the photosensitive area of a single photodetector in the sensor array. This assumes all active photodetectors have the same area, which should be true for almost any FPA (neglecting any flaws in the array). The spacing between detectors and the overall size of the array do not contribute to the MTF; how they affect the image will be discussed later. This detector MTF has the largest non-sampling effect on the overall image quality that is due to the FPA, and

³The definition of the sinc function used in this book is $\text{sinc}(x) = (\sin(\pi x))/(\pi x)$. Some physics and optics books omit the π term. See the MATLAB function `sinc`.

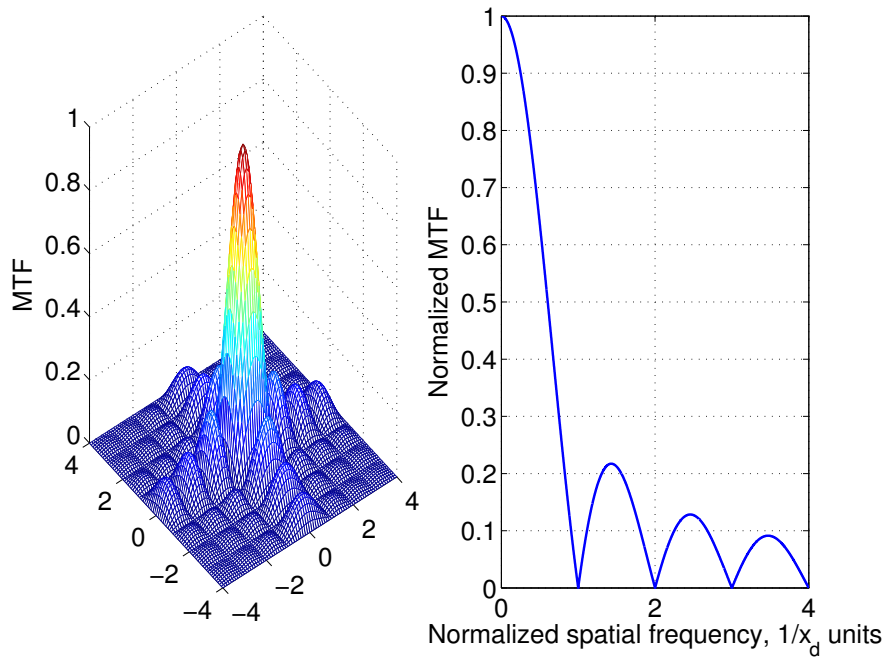


Figure 6.6: Normalized detector MTF of a typical focal plane array with a square photosensitive area, where $x_d = y_d$. The spatial frequency units of the horizontal axes are the reciprocal of the spatial dimension of a single photodetector in that direction, as in $1/x_d$ or $1/y_d$.

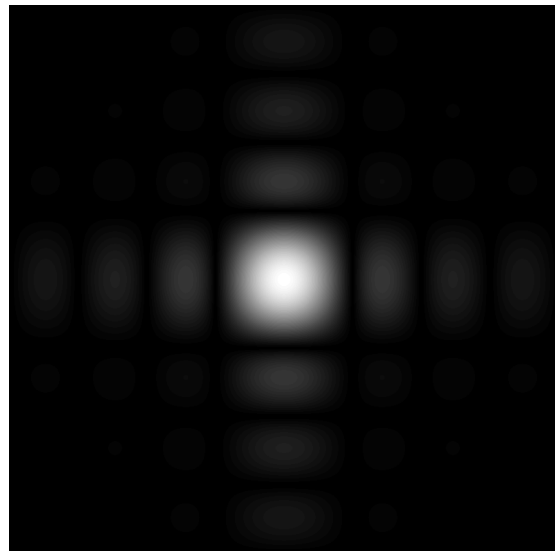


Figure 6.7: Image plot of the detector MTF on the 2-D (u, v) spatial frequency plane for a typical focal plane array with a square photosensitive area, where $x_d = y_d$. The origin of the spatial frequency axes is at the center of the image.

therefore many authors stop here. But there are many other ways in which the FPA affects the image. How much farther you “drill down” and include other FPA-related effects is dependent upon the needs of your specific application. What are some of these other effects?

6.1.2 Other FPA blurring effects

Image blurring by the FPA may come from sources in addition to the spatial integration of the photodetector area. Typically these other sources affect the image far less, and are often neglected. Two sources of blurring mentioned in several references are diffusion and charge transfer efficiency.

A certain amount of image blurring can occur in the FPA due to the phenomenon of diffusion. Photons are converted to electrons by the individual photodetectors in the sensor array, each in their own “well,” where the electrons accumulate before being read out. The “random walk” of electrons in the FPA substrate can result in some small number of electrons that are generated in one detector’s well ending up in another detector’s well. This undesirable diffusion of electrons is a form of blurring, because light that fell on one detector site may cause an increase in electrons at an adjoining detector site. This blurring effect can be characterized in the form of an MTF [68, 72]. Shown in 1-D for simplicity, this MTF is:

$$\text{MTF}_{\text{diff}}(u) = \frac{1 - \frac{e^{-\alpha L_D}}{1 + \alpha L(u)}}{1 - \frac{e^{-\alpha L_D}}{1 + \alpha L_{\text{Diff}}}}, \quad \text{where} \quad L(u) = \frac{L_{\text{Diff}}}{\sqrt{1 + (2\pi L_{\text{Diff}} u)^2}} \quad (6.3)$$

and α is the (strongly) wavelength-dependent photon absorption coefficient, L_D is the depletion width, and L_{Diff} is the diffusion length for the FPA. In general, $\text{MTF}_{\text{diff}}(u) = \text{MTF}_{\text{diff}}(v)$.

In typical real-world applications using modern sensor arrays, the blurring effect of diffusion in the FPA is negligible at visible wavelengths. At longer wavelengths, such as with infrared imagers, the blurring effect of diffusion cannot be ignored.

Another FPA-related phenomenon that can induce image blurring is *charge transfer efficiency* (CTE). As charge moves across the sensor array, some of the charge gets “left behind,” causing a blurring effect. This can be expressed as an MTF [35, 67]. This blurring effect is highly directional, specifically in the direction of the charge transfer. If the direction of charge transfer is along the direction of the x -axis, then

$$\text{MTF}_{\text{CTE}}(u) = \exp \left\{ -N(1 - \epsilon) \left[1 - \cos \left(2\pi \frac{u}{u_N} \right) \right] \right\} \quad (6.4)$$

where N is the number of charge transfers, ϵ is the CTE, and μ_N is the Nyquist frequency. The value of the Nyquist frequency is one-half the sample frequency; thus in the x -direction it is $\mu_N = 1/(2x_s)$. Due to the nature of the sensor designs, CTE is typically not an issue with CMOS sensors, only CCD sensors. As $\epsilon \rightarrow 1$, the MTF has less and less effect on the image. For most modern CCD arrays using buried-channel transfers, a consumer-grade device might have $\epsilon > 0.9999$ and $N < 1500$, while a scientific-grade device might have $\epsilon > 0.999999$ and N that might exceed 5000. Thus for many applications, blurring from CTE of a CCD array can often be ignored [35, 40, 67].

Note that the finite size in each dimension of the entire FPA implies an additional effect that should at least be mentioned. This is not really a blurring effect in the spatial domain, but rather a “blurring” effect upon the *frequency domain* representation of a scene imaged by the FPA. Imaging with a finite size array is the same as multiplying (in the spatial domain) a finite-sized rectangular window with an infinitely large array. This is equivalent to convolving (in the frequency domain) a sinc with the ideal frequency domain representation of the image. Thus the resulting effect is a slight broadening of individual frequency components, and the rise of side lobes around each frequency component, in the spectrum of the image. Since the main

lobe width of this sinc along a given axis is inversely proportional to the size of the FPA along that axis, and the FPA is typically very large compared to the size of an individual photodetector or the spacing between photodetectors, this effect is very small and is usually ignored for most camera and imaging systems. But it's good to know that the effect is there.

The discussion so far assumes that the amount of light is reasonable for the FPA. If the light level is very low, noise from effects such as dark current will render the image unusable. A brief discussion of low-light imaging was given in Section 3.8. If the light level is too high, individual photodetector sites of the FPA will “overflow” with electrons created by the incident photons and the intensity of the image will saturate, which may also render the image unusable. Overflow is sometimes called blooming. The number of electrons each photodetector site can collect is often called the *well capacity*, which is dependent upon factors such as the type of photosensitive material, area of the photodetector site, applied voltage, and array architecture.

As a simple example, an individual photodetector site in a fairly typical silicon-based CCD array has a well capacity of approximately 1500 electrons/ μm^2 [35]. An FPA intended for scientific imaging might have a pixel size of $26 \times 26 \mu\text{m}$, and thus an associated well capacity of approximately one million electrons per pixel. An FPA in a cellular phone camera, on the other hand, may have pixels as small as $1.4 \times 1.4 \mu\text{m}$, with an associated well capacity of approximately 2940 electrons per pixel. The specific effect resulting from overflow is dependent upon the particular FPA type (e.g., CCD, CMOS, CID), and implementation (e.g., frame transfer, interline transfer, existence of overflow or antibloom drains, etc.).

If the light level is too low or too high, there are three main ways to adjust it: change the optics (such as changing the aperture size or using a neutral density filter), change the sensing (such as changing the shutter speed or the ISO sensitivity of the FPA), or change the illumination. Often some combination of all three is used. Adjusting the optics has already been covered; the other two methods will be covered in later parts of the book.

6.2 Sampling effects of the FPA

What of the effect of spatial sampling? The fact that the continuous image brought to a focus by the optics is then spatially sampled by the individual photodetector sites (i.e., pixels) of the FPA has unavoidable ramifications that must be understood and accounted for by the serious user of digital cameras or other imaging systems.

6.2.1 Mathematical description of sampling

A commonly used mathematical description of image sampling is to convolve the combined point spread function of all the non-ideal aspects of the imaging system (optics, sensor array, and associated electronics) with an ideal continuous image source, followed by sampling via an ideal basis function such as a train of delta functions [41, 73, 74]. Thus for an image source sampled in the x direction,

$$g[n] = [h(x) * f(x)] \sum_{n=0}^{N-1} \delta(x - nx_s) \quad (6.5)$$

where $g[n]$ is the discrete-space sampled image result, $h(x)$ is the combined point spread function of all the non-ideal effects, $f(x)$ is the ideal continuous-space image, N is the number of pixels in the x direction, and x_s is the center-to-center spacing of the photodetectors. Sampling in the y direction has a similar form. The tophat PSF due the FPA (such as depicted by Fig. 6.5) would contribute to the overall $h(x)$ in Eq. (6.5). But what of the effect of sampling itself? Since x_s is the spatial sampling interval, then $F_s = 1/x_s$ is the spatial sampling frequency. From the sampling theorem, we can conclude that any spatial frequencies sampled by the FPA that are higher than one-half the sampling frequency, or $F_s/2 = 1/2x_s$, will be aliased (a brief review of

sampling and aliasing is provided in Appendix B). With no dead space between detectors (i.e., a fill factor of 100%, where $x_d = x_s$), the first zero of the FPA's MTF due to the detector size occurs at F_s , so the FPA will respond to spatial frequencies well above $F_s/2$, which means that some aliasing is extremely likely. Lower fill factors exacerbate the potential for aliasing, since a larger center-to-center detector spacing for a given detector size (i.e., $x_s > x_d$) lowers the spatial sampling frequency. Aliasing will be explored again in this chapter but in more detail, after MTF contributions of additional factors are discussed.

Example 6.1 Optics and sensor array

Given: This problem provides the reader with an opportunity to put together several of the concepts presented so far. Given a digital camera setup, with following parameters:

- CMOS array: pixels are $10 \mu\text{m} \times 10 \mu\text{m}$, with “tophat” response, spaced $15 \mu\text{m}$ apart (pitch) in each dimension.
- Optical system focal length is 150 mm.
- Optical system circular aperture diameter is 30 mm.
- The wavelength of interest is assumed to be 550 nm.
- Assume the object of interest is effectively at optical infinity.
- Assume that aberrations are negligible.

Determine the following values:

- The cutoff spatial frequency (based on the MTF of the optics), given in linear units at the image plane.
- The cutoff spatial frequency (based on the MTF of FPA detector size only), given in linear units at the image plane.
- The Nyquist frequency (one-half the sample frequency) due to the spatial sampling of the FPA.
- The overall system limiting frequency, based on the previous answers only.
- Is this a diffraction-limited system?

Solution: Using the various relationships presented so far, the desired values can be determined in a straightforward manner. Since the object is at infinity, distance $d = s_i$ can be assumed to be the focal length.

- The optical cutoff frequency is found from Eq. (5.16), modified for linear units: $f_c = \frac{D}{\lambda d}$. Thus $f_c = 30 \times 10^{-3} / [(550 \times 10^{-9})(150 \times 10^{-3})] = 363.64 \times 10^3 \text{ cy/m}$ or 363.64 cy/mm . The optics are assumed to be circularly symmetric, so the same cutoff frequency applies to the u and v axes.
- The detector cutoff frequency is usually taken to be the first zero of the sinc function that represents the MTF due to the FPA detector size. From the previous discussion, the first zero of the sinc (along the u axis) occurs at $1/x_d = 1/(10 \times 10^{-6}) = 100 \times 10^3 \text{ cy/m}$ or 100 cy/mm . Since the pixels are square, the same cutoff frequency exists along the v axis.
- The Nyquist frequency is one-half the spatial sampling frequency. The spatial sampling frequency along the x axis is $u_s = 1/x_s = 1/(15 \times 10^{-6}) = 66.7 \times 10^3 \text{ cy/m}$ or 66.7 cy/mm . Therefore, the Nyquist frequency for the u axis is 33.3 cy/mm . Since the same pitch occurs along the y -axis as the x -axis, this same Nyquist frequency exists along the v axis.

- The overall limiting frequency is the lowest frequency of the three, which in this case is the Nyquist frequency of 33.3 cy/mm in each direction.
 - Since the optical cutoff frequency due to diffraction is not the limiting frequency, the system is not a diffraction-limited system.
-

6.2.2 Sampling is not LSI

The possibility of aliasing is not the only effect we need to consider with regard to spatial sampling of an image. Simple examples from a 1-D sampling simulation in the x direction can make the point visually. In this simulation, a 1-D sinusoidal pattern will be applied to a 500 μm long 1-D section of a sensor array. The size x_d of the individual detectors (i.e., pixels) is 50 μm each, with a 100% fill factor, so there is no “dead space” between pixels. This means that the sampling interval x_s is also 50 μm , and the associated sampling frequency is $u_s = 1/(50 \mu\text{m}) = 0.020 \text{ cy}/\mu\text{m}$ or 20 cy/mm. (Don’t confuse u , the spatial frequency variable associated with the x direction, with μ , which is the abbreviation for the 10^{-6} unit multiplier.) For four different positions of the sinusoidal pattern, the simulation shows what response individual pixels would have, and calculates the modulation depth. Suppose the sinusoidal pattern has a period of 200 μm , which means each cycle of the sinusoid is sampled by four pixels. This exceeds the minimal sampling of two samples per cycle, so no aliasing will occur. In spatial frequency terms, the frequency of the sinusoid is $u_0 = 1/(200 \mu\text{m})$ or 5 cy/mm which is equal to $u_0 = 0.25u_s$. This scenario is depicted in Fig. 6.8. Notice how different positions of the sinusoid (relative to the pixel locations) result in very different pixel values, and different modulation depths.

The simulation is repeated for a sinusoidal pattern that has a period of 100 μm , which means each cycle of the sinusoid is sampled by two pixels. This is equal to the minimal sampling of two samples per cycle, so again no aliasing will occur. In spatial frequency terms, the frequency of this sinusoid is $u_0 = 1/(100 \mu\text{m})$ or 10 cy/mm which is equal to $u_0 = 0.5u_s$. This scenario is depicted in Fig. 6.9. Once again, different positions of the sinusoid (relative to the pixel locations) result in very different pixel values, and different modulation depths.

The very important ramification of the result shown in Figs. 6.8 and 6.9 is that sampling is *not* shift invariant, so a sampler such as an FPA cannot be a linear shift invariant (LSI) device. This is the fundamental reason why it is not mathematically correct, in a strict rigorous treatment, to use MTF theory or any of our familiar linear systems theory tools with an FPA or with any sampling device—it violates the LSI (or LTI, for time signals) constraint. Does this mean we cannot use the powerful tools of MTF theory with the FPA? What shall we do?

We could just give up (not acceptable!). We could pretend this effect isn’t there (not recommended). We could use a different method, such as the SIR function of Vollerhausen et al. [41]. The SIR method would require us to keep track of the relative phase of the image versus the FPA, which increases the complexity of our calculations considerably. Or, we could define an additional “MTF” term that attempts to account for the expected differences in modulation depth according to the relative position of the sinusoidal pattern on the FPA, as recommended by Boreman and others [35, 39, 60]. This last method treats the relative position of the pattern on the FPA as a uniformly distributed random variable with respect to the sampling locations, and determines an additional MTF term that is the average of all the MTFs that would result from all the possible positions of the pattern. This stochastic approach is the method used in this book, as it allows us continue to use the same basic techniques we’ve been using for Fourier optics, while accounting for the lack of shift invariance when sampling.

How do we define this additional MTF term related to sampling? Boreman recommends that the random positioning of the pattern be uniformly distributed over a distance of one sampling interval in a given direction. The variations in modulation depth such as those observed in Figs. 6.8 and 6.9 will just repeat if the pattern moves farther than one sampling interval, and

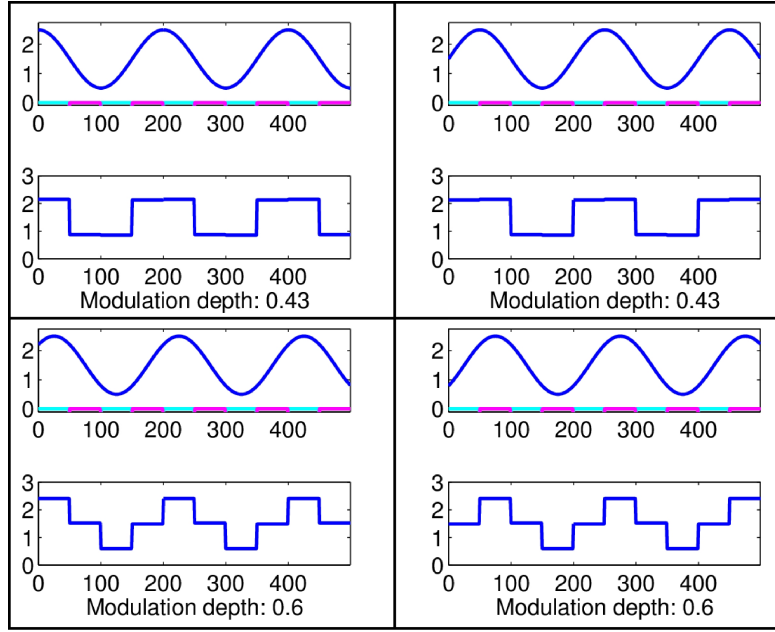


Figure 6.8: A spatial sampling scenario where $u_0 = 0.25u_s$. Horizontal units are given in μm , and each pixel is $50 \mu\text{m}$ across. Each of the four quadrants shows two subplots: the upper subplot shows the sinusoid and the pixel locations, and the lower subplot shows the simulated pixel outputs. Each quadrant shows the sinusoid in a different position relative to the pixel locations.

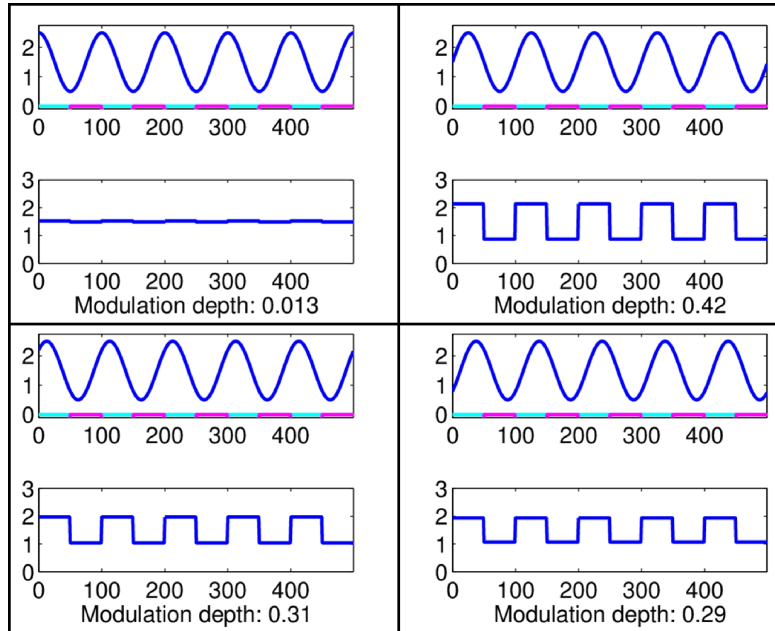


Figure 6.9: A spatial sampling scenario similar to Fig. 6.8, except here $u_0 = 0.5u_s$.

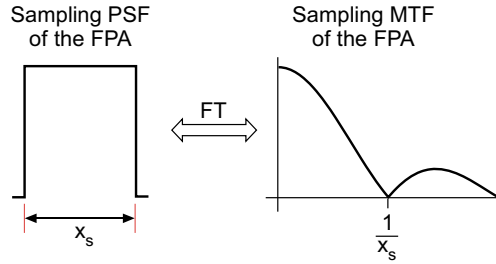


Figure 6.10: The PSF and associated MTF that accounts for variations in modulation depth due to random, unpredictable changes in position of the image relative to the pixel locations.

any given position within a sampling interval is equally probable. Thus the “impulse response,” or PSF, due to sampling is just a rectangular function with a width equal to the sampling distance in that direction. This PSF shape is familiar, and the associated MTF we’ll call the “sampling MTF” will be the magnitude of the FT of the sampling PSF. In 1-D (for simplicity,) this is:

$$\text{PSF}_{\text{samp}}(x) = \text{rect}\left(\frac{x}{x_s}\right) \quad (6.6)$$

$$\text{MTF}_{\text{samp}}(u) = \left| \frac{\sin(\pi x_s u)}{\pi x_s u} \right| = |\text{sinc}(x_s u)| \quad (6.7)$$

and a figure showing this PSF and MTF should also look familiar; see Fig. 6.10.

Note that the FPA has more than one MTF term we must consider. Even if we can neglect some of them, such as the MTFs associated with diffusion and with charge transfer efficiency, the contributions of the two MTFs related to the detector size described by Eq. (6.1) and the sampling effect described by Eq. (6.7) must be combined. As mentioned before, the correct method to combine multiple independent MTFs is through multiplication. Since the sampling MTF changes according to the fill factor, it’s instructive to show combined MTFs for two different fill factors, as shown in Fig. 6.11.

Most newer monochrome camera FPAs, and FPAs associated with 3-chip color cameras, have a FF of between 90% and 100%, depending upon the particular FPA design. A single-chip color camera FPA, with a Bayer color filter array (CFA), appears to have a maximum FF of approximately 50% (for green wavelengths only), which will be evident when we discuss CFAs in more detail in an upcoming section. As we will see in that section, the actual effective FF due to a CFA is somewhat complicated. For general use of a camera with random scenes to be imaged, the sampling MTF certainly affects the performance of the camera, and should be taken into account as shown above.

It is important to note that in certain testing scenarios, the effects of the sampling MTF can be inadvertently canceled out! How can this happen? In many test setups, when characterizing a camera with a static test pattern, the relative position of the test pattern and camera are usually adjusted to yield the highest modulation depth. Setting up a test in this way removes the random positioning aspect of the image, and eliminates the sampling MTF from the result. This may be why the ramifications of the non-LSI aspects of sampling on the overall MTF is often forgotten. Test results thus obtained would tend to overestimate the performance of the camera for use with other types of scenes. One way to include sampling MTF effects in the test results is by using a test pattern that includes a “random noise” type of test target.

6.2.3 Aliasing

At this point, we need to return to the concept of aliasing and the Nyquist frequency. As previously defined, the Nyquist frequency (also called “fold-over frequency” in some books)

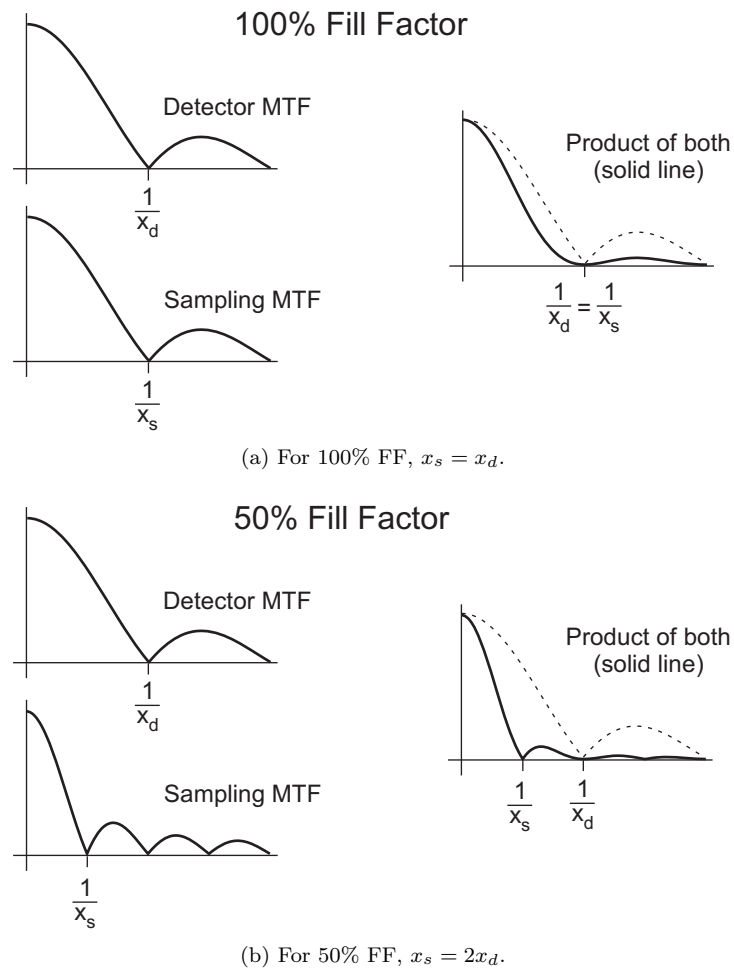


Figure 6.11: Combined MTFs for the FPA.

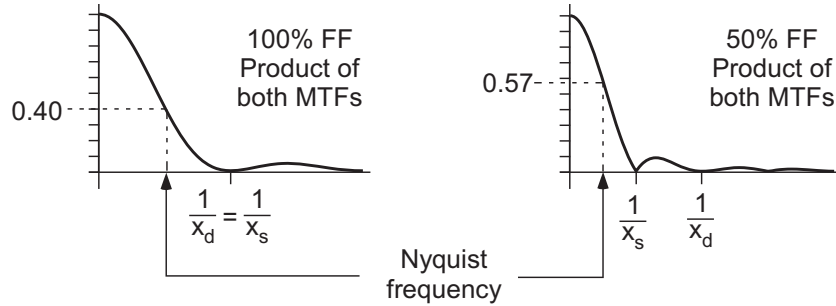


Figure 6.12: Combined MTFs for the FPA, with the Nyquist frequency shown.

is one-half the sample frequency. Any spatial frequency in an image that is higher than the Nyquist frequency will be aliased. Where is the Nyquist frequency with respect to the combined MTFs we have just seen? The sample frequency is determined solely by the sample interval. For example, in the x -direction the sample frequency would be $u_s = 1/x_s$, and the associated Nyquist frequency would be $u_N = 1/(2x_s)$. The Nyquist frequency is shown in Fig. 6.12, for both 100% FF and 50% FF examples.

Notice that in the 50% FF case, the MTF is still relatively high at the spatial frequency where aliasing begins, but for the 100% FF case MTF is almost 30% lower (that is, $(0.57)(0.7) \approx 0.40$). Empirical evidence with FPAs shows that, without any additional anti-aliasing filter, aliasing is fairly objectionable with a 50% FF but acceptable to most viewers with a 100% FF. Because of this, cameras using FPAs that achieve a FF approaching 100%, such as many modern monochrome FPAs, do not need to employ an anti-aliasing filter on the FPA. For these cameras, the low-pass filtering effect of the detector MTF (due to spatial integration over the detector area), combined with the sampling MTF, is usually sufficient.⁴ For single FPA color cameras, using a color filter array such as a Bayer pattern, the FF is much less than 100%, and therefore the addition of some form of anti-aliasing filter to the FPA is typically needed for these cameras. This is even more of an issue because humans find aliasing of color images far more objectionable than aliasing of monochrome images. Note that for this type of camera, only green will have the highest FF of at least 50%, whereas red and blue FF can be as low as 25% FF for certain wavelengths. This will be discussed in more detail in Section 6.3.1.

6.2.4 Anti-aliasing

For those cameras that need some additional form of anti-aliasing (AA) for the FPA, the obvious question is “how do we do it?” Anti-aliasing implies a low-pass filter effect, where any spatial frequencies above the Nyquist frequency are substantially reduced in intensity. This low-pass filtering must be done optically, before the image is spatially sampled by the FPA.

The MTF associated with the optics of the lens system and aperture (such as shown in Fig. 5.11) represent a low-pass effect, but the cutoff frequency is often too high, has a too gradual (nearly linear) “roll-off,” and changes with any change in the aperture size, so its general utility for optical anti-aliasing is poor. That means we may need to place something else in front of the FPA (but under the microlens array) to perform the optical anti-aliasing function.

The most common method of creating an optical anti-aliasing filter is to use two (or more) thin layers of a birefringent material (such as quartz or lithium niobate) to create an optical low-pass filter (OLPF) [60, 75]. Birefringent materials are sensitive to polarization, and essentially exhibit two different indices of refraction for horizontally versus vertically polarized light (or any two polarizations in quadrature). The assumption is that incoming light is either randomly polarized or circularly polarized, so that there is roughly an equal amount of horizontally versus

⁴Aliasing will still be present in most images, but its effects will not be perceived as objectionable by most viewers.

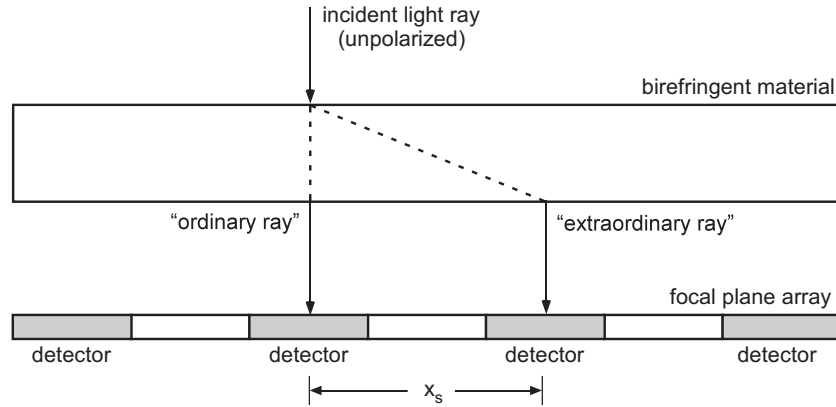


Figure 6.13: A single birefringent layer splits each incoming unpolarized light ray into two outgoing polarized light rays. The two outgoing rays are polarized in quadrature to each other, and are separated in this figure by a distance of x_s .

vertically polarized light. This is one reason why old-style linear polarization filters intended for film cameras can cause problems with modern digital cameras.

With a single birefringent layer, an incoming impulse of light gets “split in two” as it passes through the layer, due to the two different indices of refraction. Thus a single point from the object plane gets mapped to two points on the image plane. How can this result in the equivalent of an OLPF and thus provide an AA effect? An exaggerated, idealized 1-D diagram along the x -axis, as shown in Fig. 6.13, will help show the basic concept. The distance between the two points on the image plane that result from the ordinary and extraordinary rays is a function of the type of material, the thickness of the material, and the wavelength of the light.⁵ In the example shown in Fig. 6.13, the distance between the two points on the image plane is exactly x_s , or equal to the sampling interval. Therefore, the impulse response (or PSF) of this filter is two delta functions, spaced x_s apart. This can be described mathematically as

$$h_{\text{filter}}(x) = \frac{1}{2} [\delta(x) + \delta(x - x_s)], \quad (6.8)$$

where the $1/2$ term is for conservation of energy. The OTF of this filter is the FT of the PSF:

$$\text{OTF}_{\text{filter}}(u) = \mathcal{F}\{h_{\text{filter}}(x)\} = \frac{1}{2} (1 + e^{-j2\pi x_s u}), \quad (6.9)$$

which can be found easily by using the shift property of the FT and superposition. A MATLAB plot of this complex-valued OTF is shown in Fig. 6.14. The bottom plot of Fig. 6.14 depicts the MTF of the single birefringent layer. Note that the response drops rapidly to zero at $1/2x_s$, which is the Nyquist frequency. The fact that the response rises again for frequencies above the Nyquist frequency will be of no consequence. As we will see, the response of the birefringent layer from 0 to $1/2x_s$ will provide the low pass effect we need for anti-aliasing.

While the bottom plot of Fig. 6.14 depicts the MTF graphically, we desire to have an equation for this MTF. One way to obtain a simple form of the MTF is to use Euler’s formula and simple trigonometric identities as shown below.

⁵For most materials used for cameras, the wavelength dependence of birefringence (in the visible range of light) is very small and can be ignored [75]. Thus the distance between the two points on the image plane is approximately the same for all wavelengths.

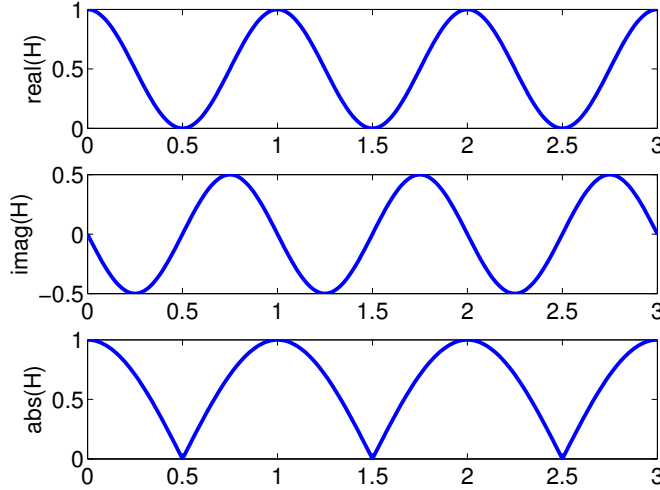


Figure 6.14: The OTF associated with Fig. 6.13, where the distance between the ordinary and extraordinary rays is x_s . The horizontal axes are spatial frequency, labeled in $1/x_s$ units. The bottom plot is the magnitude of the OTF (i.e., the MTF).

$$\text{OTF}_{\text{filter}}(u) = \frac{1}{2} (1 + e^{-j2\pi x_s u}) = \frac{1}{2} (1 + \cos(2\pi x_s u) - j \sin(2\pi x_s u))$$

$$\begin{aligned} \text{MTF}_{\text{filter}}(u) &= |\text{OTF}_{\text{filter}}(u)| = \frac{1}{2} \sqrt{(1 + \cos(2\pi x_s u))^2 + (-j \sin(2\pi x_s u))^2} \\ &= \frac{1}{2} \sqrt{(1 + 2 \cos(2\pi x_s u) + \cos^2(2\pi x_s u)) + \sin^2(2\pi x_s u)} \\ &= \frac{1}{2} \sqrt{(1 + 2 \cos(2\pi x_s u) + 1)} = \frac{1}{2} \sqrt{(2 + 2 \cos(2\pi x_s u))} \\ &= \sqrt{\frac{1}{2} + \frac{1}{2} \cos(2\pi x_s u)} = \left| \cos\left(2\pi \frac{x_s}{2} u\right) \right| \end{aligned}$$

This MTF provides an OLPF in one direction. At least one more layer is needed to provide a complete 2-D anti-aliasing solution.

Putting this together, let's look at the product of all three main MTFs associated with a 50% FF FPA, shown in 1-D for clarity (see Fig. 6.15). Showing just the final MTF result as a single plot in Fig. 6.16 provides better detail regarding the level of modulation at various spatial frequencies. Figure 6.16 shows that potential aliasing due to frequencies above the Nyquist frequency is greatly reduced when an OLPF is used that has the first null at $1/2x_s$. But Fig. 6.16 shows something else: due to a relatively gradual roll-off of the OLPF, the level of modulation for frequencies somewhat below the Nyquist frequency, which we don't want to filter out, is lower than desired. This would result in images where sharp edges are somewhat blurred and some fine detail would be lost; this may be too much filtering for many imaging applications.

As an alternate approach to that shown in Fig. 6.13, a thinner birefringent layer could be used where the distance between the two points on the image plane due to the ordinary and extraordinary rays is exactly $x_s/2$, or equal to one-half the sampling interval, as suggested by [60, 75]. This variation of Fig. 6.13 is shown in Fig. 6.17. This approach means that the extraordinary ray shown in Fig. 6.13 would fall on “dead space” (a place where there was no detector), which at first glance implies that approximately half of the light intensity would be lost. However, another incoming ordinary ray is just as likely to fall on the “dead space” and the associated extraordinary ray would then fall on a detector. When the distance between the two points on the image plane due to the ordinary and extraordinary rays is exactly $x_s/2$, the

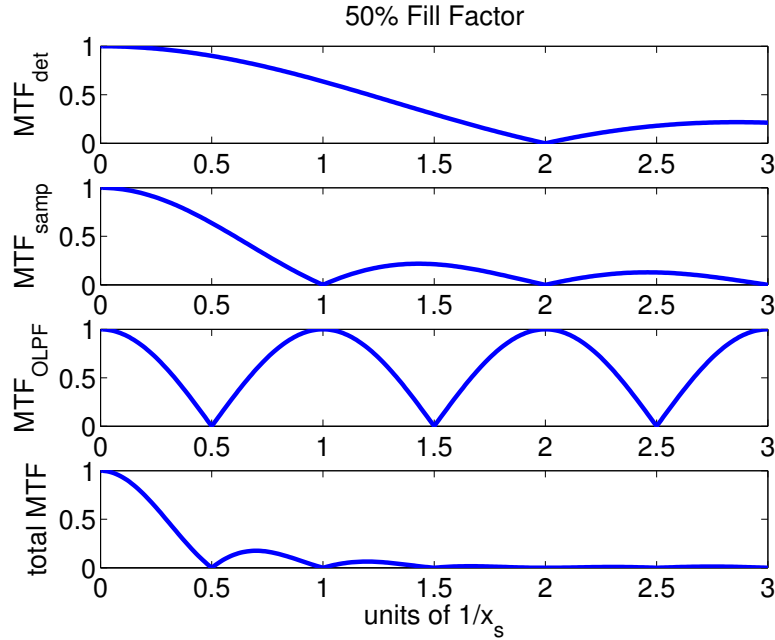


Figure 6.15: The individual MTFs and the product of all three at the bottom, where the distance between the ordinary and extraordinary rays of the OLPF is x_s . The horizontal axes are spatial frequency, labeled in $1/x_s$ units. The Nyquist frequency is thus labeled as 0.5.

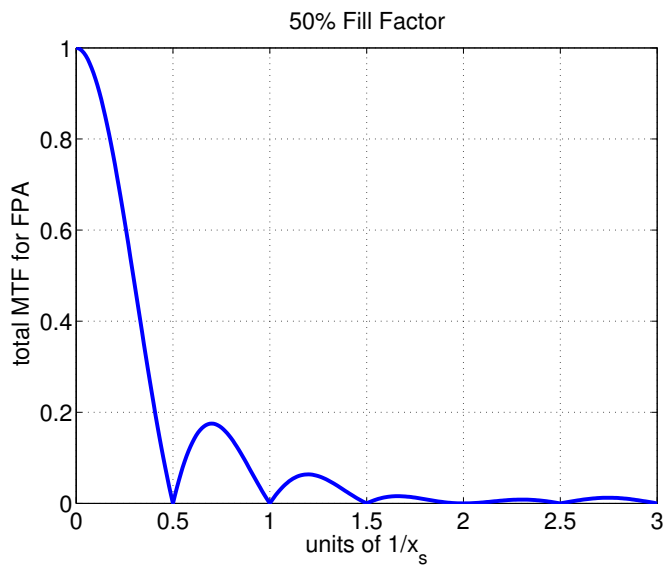


Figure 6.16: The combined MTF for a 50% FF FPA, where the distance between the ordinary and extraordinary rays of the OLPF is x_s . The horizontal axes are spatial frequency, labeled in $1/x_s$ units. The Nyquist frequency is thus labeled as 0.5.

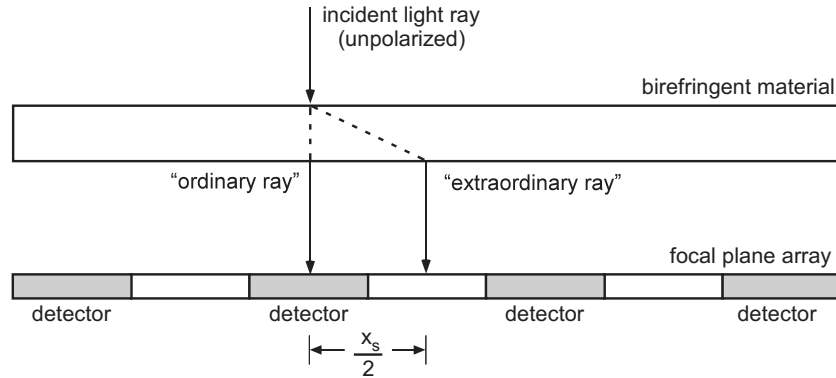


Figure 6.17: A variation on Fig. 6.13, where the two outgoing rays are separated by a distance of $x_s/2$.

PSF and MTF of the 1-D filter would be

$$h_{\text{filter}}(x) = \frac{1}{2} \left[\delta(x) + \delta(x - \frac{x_s}{2}) \right], \quad \text{MTF}_{\text{filter}}(u) = \left| \cos(2\pi \frac{x_s}{4} u) \right|. \quad (6.10)$$

The first null of the MTF will now occur $u_s = 1/x_s$, which is twice the Nyquist frequency (i.e., the first null is at the spatial sampling frequency).

How will this alternate approach change the MTF result? A plot similar to Fig. 6.15 is shown in Fig. 6.18. This approach will provide sharper images, at the expense of more aliasing. A comparison of the two OLPF approaches to a 100% FF with no OLPF and to a 50% FF with no OLPF is shown in Fig. 6.19. Using a spacing of x_s for the OLPF provides the best reduction of aliasing, but at the cost of some image sharpness. Using a spacing of $x_s/2$ for the OLPF provides improved sharpness, at the expense of more aliasing. A very interesting result is the

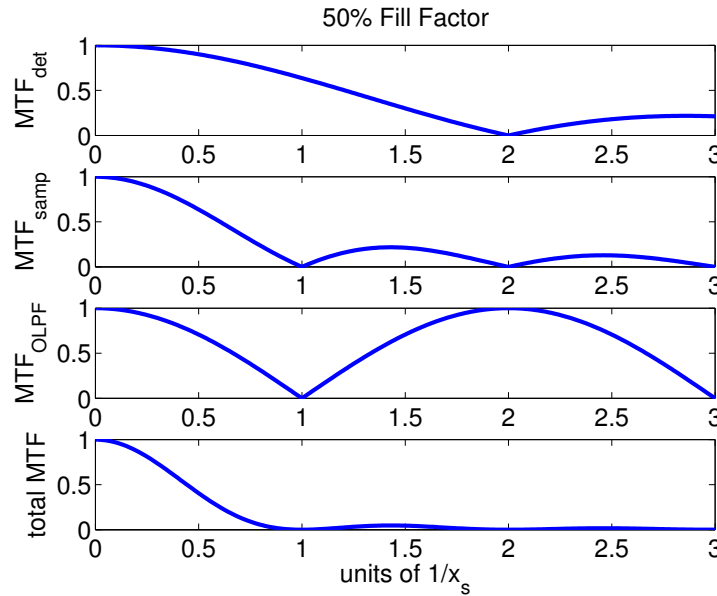


Figure 6.18: The individual MTFs and the product of all three at the bottom, where the distance between the ordinary and extraordinary rays of the OLPF is $x_s/2$. The horizontal axes are spatial frequency, labeled in $1/x_s$ units. Their Nyquist frequency is thus labeled as 0.5.

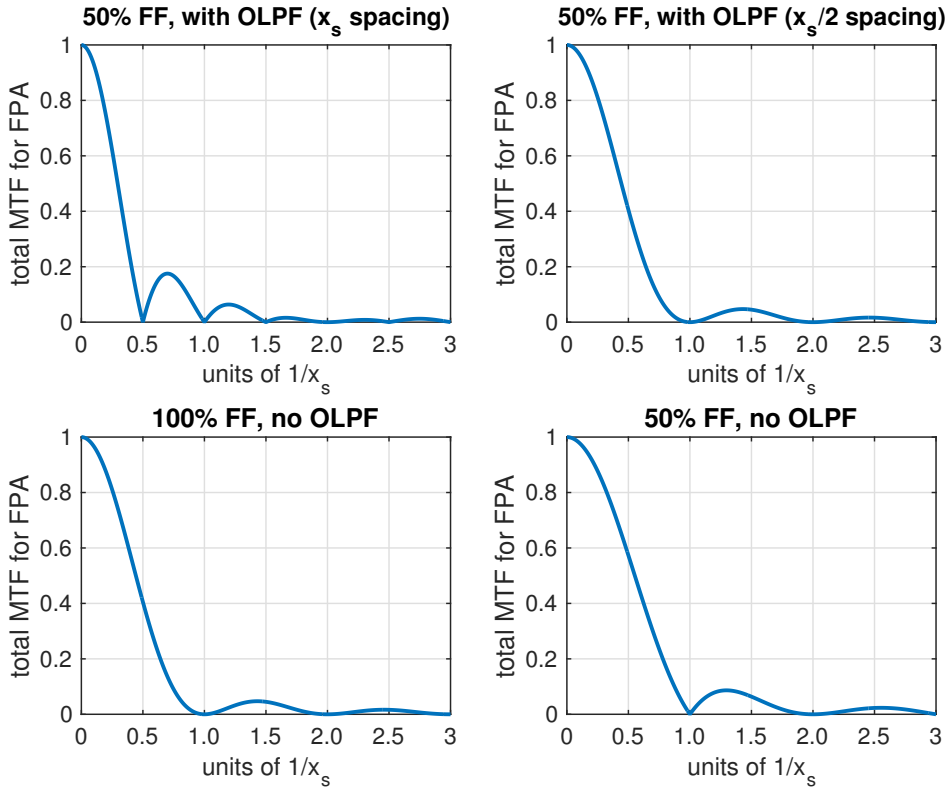


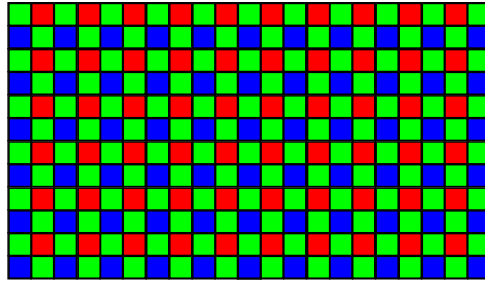
Figure 6.19: A comparison of the two OLPF approaches for 50% FF (top) to no OLPF for 100% FF and 50% FF (bottom). The horizontal axes are spatial frequency, labeled in $1/x_s$ units. The Nyquist frequency is thus 0.5 on the horizontal axes.

50% FF sensor with an OLPF having a spacing of $x_s/2$ compared to a 100% FF sensor having no OLPF; the MTFs are essentially identical (they can be plotted right on top of one another with no discernible difference). Recall that the modulation level of 0.4 at the Nyquist frequency for a 100% FF sensor was deemed to have an acceptable level of aliasing by most general purpose users. Therefore, the 50% FF sensor with an OLPF having a spacing of $x_s/2$ might also be expected to be acceptable. Lastly, the 50% FF sensor with no OLPF shows a high degree of aliasing (modulation of 0.57 at the Nyquist frequency), which is likely to be objectionable to many users.

For very compact cameras, such as those in mobile phones, two thin birefringent layers may be too bulky. In that case, manufacturers may instead use optical gratings to create what is commonly called a grating optical low-pass filter, or GOLF. While thinner, the GOLF approach generally results in an inferior MTF compared to an OLPF.

It may seem as if the author is being evasive by showing different OLPF approaches, such as a spacing of x_s versus a spacing of $x_s/2$ for the ordinary and extraordinary rays. Which is “right” for a digital camera? While the “right” choice is always application dependent, this is a particularly frustrating situation where different camera manufacturers can make very different choices, yet consider those choices to be closely guarded trade secrets. This proprietary information is not released to the public, although some enterprising users have disassembled particular camera models and found a variety of approaches similar to those discussed here.

If a microlens array can achieve nearly 100% FF for an FPA, why even worry about an OLPF? As will be discussed in Section 6.3.1, use of a color filter array (CFA) can greatly reduce the fill factor for a particular wavelength, and may require the use of an OLPF. As will be



subsection of a 100% FF CCD array with a
Bayer mosaic filter pattern for a color camera

Figure 6.20: A single FPA for a color camera using a Bayer mosaic color filter array (CFA). Note there are twice as many green filters in each dimension than red or blue filters.

seen, the use of an OLPF for color cameras is currently a controversial topic, with no universally agreed-upon “right” answer.

6.3 Color Imaging: Single FPA Methods

There is no such thing as a true “color FPA” in the strict sense. A sensor array simply detects light intensity across a some range of wavelengths. An example of this was shown in Fig. 2.6. Additional wavelength-selective elements or other special design aspects must be added to provide the ability to distinguish the individual colors necessary for producing a color image. An FPA is not inexpensive, so a great deal of design effort has gone into creating cameras that can produce color images with just a single FPA.

6.3.1 Color Filter Arrays

One of the most common methods used to distinguish color is to add a color filter array (CFA) in front of the FPA sensor. While various patterns of CFAs have been proposed, the oldest (since the mid-1970’s) and still most widely used CFA pattern is the Bayer mosaic⁶ shown in Fig. 6.20 [76]. The CFA limits the wavelengths allowed for a particular pixel location on the FPA to just one band of red, green, or blue.

Two things should be immediately evident from Fig. 6.20. First is that there are twice as many green pixels in the Bayer CFA as there are red or blue; this is to account for the greater sensitivity of human vision to green. Specifically, humans gather more detail about an image from wavelengths in the green range than any other wavelengths. The Bayer pattern is sometimes referred to as an RGBG pattern. The second thing to notice is that the FF is no longer 100% for a particular color, as shown in Fig. 6.21. In fact, based on a 2×2 pixel area, the FF appears to be 50% for green, and 25% for both blue and red. However, the true FF for a particular wavelength is more complicated than that.

An absolute FF of 50% for green wavelengths and 25% for both blue and red wavelengths would require that the “pass band” of the three color filters had no overlap, and would imply “brick wall” filter responses that are impossible to build. In fact, the characteristics of typical filters used for a Bayer CFA have considerable overlap, as depicted in Fig. 6.22. For example, light energy at approximately $\lambda = 518$ nm (bluish-green) would be accepted equally well by both the blue and the green pixel locations on the FPA. Looking at Fig. 6.20, this implies an effective FF of 75% for this wavelength. Note that even the response of the red filter is not insignificant for this wavelength.

⁶The Bayer mosaic is named after Bryce E. Bayer (pronounced BYE-er), a Kodak research scientist who created it in 1974 and received a U.S. patent for it in 1976.

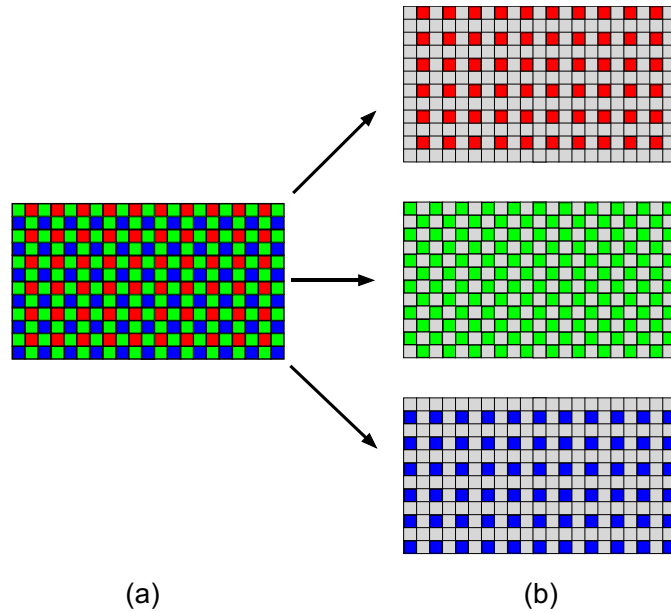


Figure 6.21: A Bayer mosaic CFA results in a sparse sampling grid for each color.

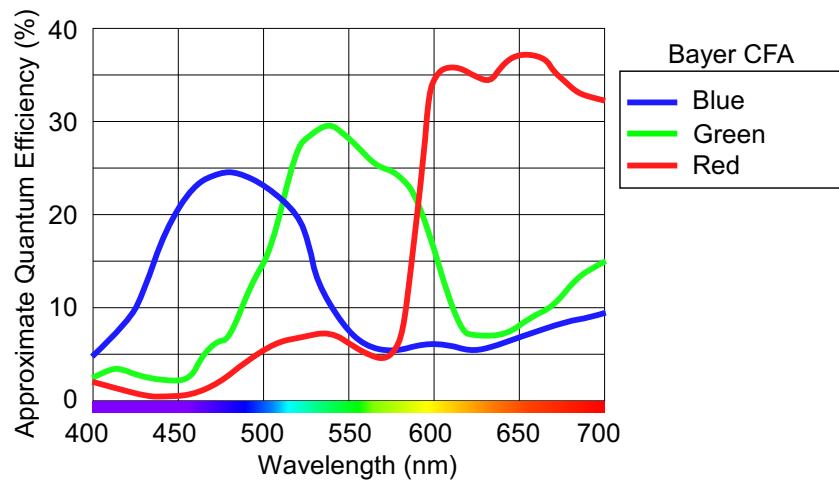


Figure 6.22: Typical filter responses for a Bayer mosaic color filter array (CFA). Note there are significant regions of overlap.

A similar argument can be made for light energy at approximately $\lambda = 585$ nm (yellow), which is accepted equally well by the red and green pixels. In fact, much of the light energy spanning the range of wavelengths from approximately 475 to 625 nm (with the exception of the range from approximately 540 to 570 nm) will have a higher effective FF than might be inferred from Fig. 6.20. A higher FF means a higher effective spatial sampling frequency, and thus a higher Nyquist frequency, resulting in less aliasing. On the other hand, bluish-purple light at $\lambda = 450$ nm would only be accepted by a blue pixel, and reddish-orange light at $\lambda = 625$ nm would only be accepted by a red pixel, and therefore both have an effective FF of only 25%. Note also from Fig. 6.22 that the quantum efficiency of the three filters is not equal, nor does it match the relative color sensitivity of human vision depicted in Fig. 2.6; this is just one reason why color correction is typically performed in the camera electronics that follow the FPA sensor.

Some other CFA mosaic patterns that have been proposed as alternatives to the Bayer RGBG pattern include RGBW (where W stands for white, meaning a clear filter that passes all colors) that Kodak introduced, RGE (where E stands for emerald, a modification of some of the green filters), CYGM (cyan, yellow, green, and magenta), and some other variants such as the EXR and X-Trans filter arrays by Fujifilm. However, the standard Bayer pattern is by far the most common CFA used today.

The use of a CFA, and the overlap of the filter responses for many wavelengths, makes it very difficult to know the actual spatial sampling frequency (which is related to the effective fill factor) for a specific wavelength. The most common approach is to ignore the overlap of certain wavelengths for the CFA, and base the analysis on just two cases: one for the middle of the green band of wavelengths and one for the middle of the blue and red bands of wavelengths. As seen in Fig. 6.21(b), the center-to-center spacing of all pixel locations in the horizontal and vertical directions is two times the pixel size in that direction regardless of color. That is, $x_s = 2x_d$ and $y_s = 2y_d$ for red, green, and blue. Therefore, the sampling MTFs in the horizontal and vertical directions for all colors is assumed to have a cutoff frequency half that of the cutoff frequency associated with the detector MTF, as shown in Fig. 6.11 for the 50% FF case. It is when one considers the diagonal direction that the differences between green and red/blue become evident.

From Fig. 6.21(b), the green *diagonal* center-to-center spacing is seen to be $\sqrt{2}$ times the horizontal or vertical pixel size, whereas the red and blue diagonal center-to-center spacing is $2\sqrt{2}$ times the horizontal or vertical pixel size. Thus for green, the effective cutoff frequency associated with the sampling MTF for the diagonal direction is *higher* (by a factor of $1/1.414$ versus $1/2$) compared to the sampling MTF cutoff frequency for either the horizontal or vertical directions. On the other hand, for red or blue, the effective cutoff frequency associated with the sampling MTF for the diagonal direction is *lower* (by a factor of $1/2.828$ versus $1/2$) compared to the sampling MTF cutoff frequency for either the horizontal or vertical directions. While this analysis should not be taken as an exact solution, it confirms the impression given by Fig. 6.21(b) that overall, green outperforms red or blue when a CFA is used. This conclusion matches empirical image results for color cameras using CFAs.

The practical ramifications of the reduction in FF due to the CFA is that the effective spatial sampling frequency is lower than for monochrome, especially for red and blue, which greatly increases the chance for aliasing in the image. For example, consider a sharp edge associated with an object in an image. The Fourier transform of an edge contains many frequencies, and the sharper the edge, the more important the higher frequencies are. If these higher frequencies are filtered out by an OLPF, the edge will appear softer and less sharp. If no OLPF is used, some of the higher frequencies will likely alias. Because different colors have different diagonal spatial sampling frequencies due to the CFA, they will alias at different frequencies, and the aliasing artifacts that appear in the image at the object's edge (especially diagonal edges) will show coloration that has little to do with the actual object (generically called "false color"). This is one reason observers find color aliasing so objectionable. Therefore, most color cameras that use a single FPA with a CFA employ an OLPF to reduce the possibility of aliasing.

Another problem with a CFA is the phenomenon of color crosstalk, which also causes false color. If a very small spot of white light happens to fall on just a red pixel, the white spot will

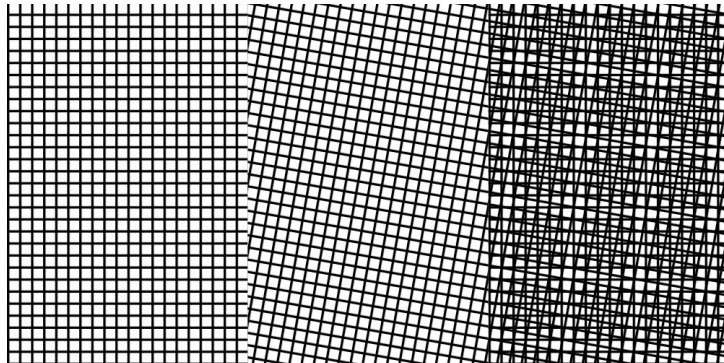


Figure 6.23: Moiré pattern (right) created by superimposing two grids (left and middle).

appear red in the image. The same type of error would occur for the green or blue pixels. For this reason, the spatial extent of the smallest blur spot on the image plane needs to span at least four pixels. This can be achieved with the use of an OLPF, and lends more credence to the use of an OLPF for a camera using a CFA to obtain color information [35].

A digital imaging problem that can occur with any FPA, but is exacerbated when a CFA is used, is the creation of a moiré pattern. This occurs when two similar patterns are superimposed on each other with a slight rotation or misalignment between them, and a third undesirable pattern appears as an artifact. A simple monochrome example is shown in Fig. 6.23. In the context of digital image formation, one pattern would exist at the object plane and is brought to focus at the image plane, and the other “pattern” is the rectangular grid of the FPA itself, also at the image plane. When the pitch of a pattern at the image plane is very close to the pitch (i.e., spacing) of the pixels on the FPA, the appearance of a moiré pattern is likely. With a CFA, the moiré pattern takes on a form of false colors which greatly increases the distracting nature of this artifact. Once again, use of an OLPF greatly reduces the likelihood of moiré patterns.

From the previous discussion, it may seem as if an OLPF should always be used if a CFA is used with a single FPA to create a color image. However, this is a controversial topic among some users today. As can be seen from Fig. 6.19, the intended low pass effect of the OLPF reduces the level of modulation at higher spatial frequencies compared to no OLPF for a given FF and x_s . This has the unavoidable effect of reducing sharpness in the image, and some camera users strenuously object to any loss of sharpness no matter how small, even if the previously described problems of aliasing, color crosstalk, and moiré patterns are more pronounced.

In response to this, some single-FPA cameras that use a CFA are now available without the slight reduction in sharpness caused by an OLPF. For example, the Nikon D800 and the D800E are identical cameras except the latter has no OLPF effect. It would not be correct to say the D800E has “no OLPF.” It actually has two birefringent layers, as does the D800, but in the D800E the second layer “undoes” the effect of the first layer. In the D800, the first layer blurs horizontally, and the second layer blurs vertically, giving the desired 2-D blurring effect. In both cameras, an IR-reduction filter layer is used between the two birefringent layers (recall from Fig. 2.6 that most FPAs are very sensitive in the IR). There are also web sites that will guide a user through the removal of the OLPF for a specific DSLR camera, the Canon 5D Mark III, but in so doing the user also loses the IR filter and the dust reduction system for the FPA sensor.⁷ No IR filter results in “IR contamination” that can cause undesirable color shifts in some images or even result in well-capacity overflow.

Many users still prefer to have an OLPF, and the cynics among them believe the “no OLPF” issue has been pushed mainly as a marketing strategy to sell cameras. That being said, the real-

⁷Most DSLRs have a dust reduction system that is activated for a few moments upon either power-down or power-up of the camera. The system vibrates the front of the FPA at an ultrasonic frequency, “shaking off” dust particles from the sensor. Without it, you may need to have the sensor professionally cleaned periodically.

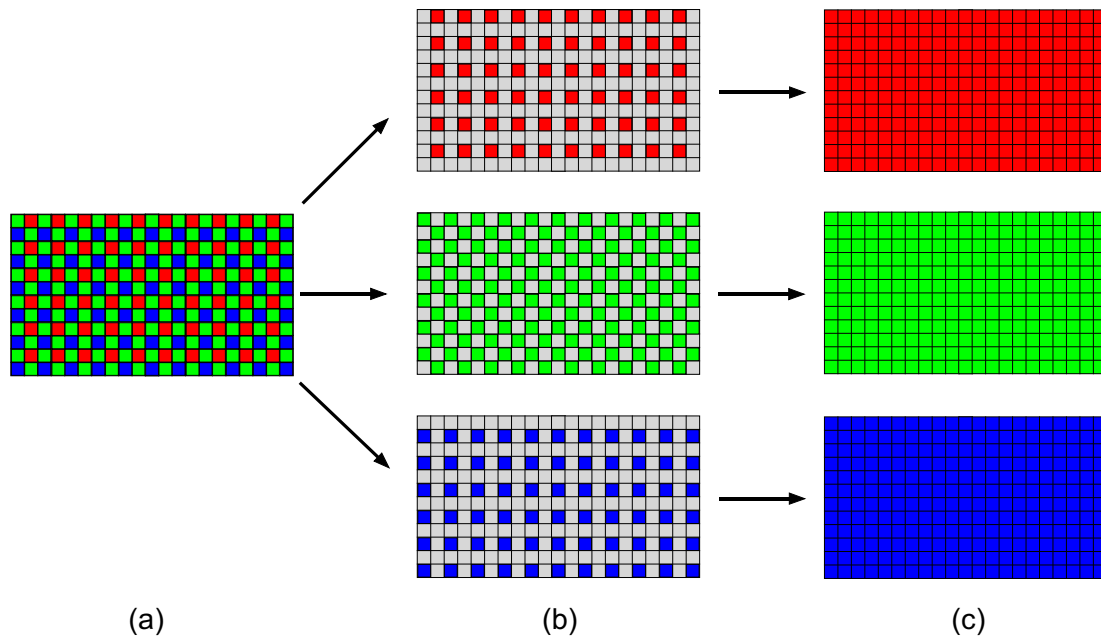


Figure 6.24: An FPA with a Bayer mosaic color filter array (a) produces sparsely sampled color planes (b), to which a demosaicing interpolation algorithm must be applied to obtain the needed R, G, and B color planes at full resolution (c).

world need of an OLPF becomes less important as the pitch of the FPA grows smaller, which is a trend in consumer-grade digital cameras. Smaller pitch means a shorter distance between pixels, which means a higher spatial sampling frequency and thus a higher Nyquist frequency. For general purpose photography, typical images obtained with these small-pitch sensors may not have much spatial frequency content high enough to cause problems such as aliasing, color crosstalk, and moiré patterns if no OLPF is used. For technical users of digital cameras, there is no “typical image,” so this probably doesn’t apply. Furthermore, scientific-grade cameras tend not to have such a small pitch, as larger pixel sizes are preferred to obtain higher sensitivity and greater well-capacity.

Whether or not an OLPF is used, a color camera using a CFA produces sparsely-sampled color planes (see Fig. 6.24), which must be converted into three full-resolution color planes in order to create a standard color image. To achieve this, the camera needs to apply what is called a demosaicing interpolation algorithm to obtain the needed R, G, and B color planes at full resolution. Similar to the specific details of the OLPF implementation, the details related to the demosaicing techniques used by various manufacturers are closely guarded proprietary secrets. Such demosaicing algorithms are much more sophisticated than just simple (bilinear, bicubic, etc.) interpolation algorithms familiar to image processing experts. Commercial demosaicing algorithms include other aspects, such as edge detection, adaptive interpolation in the presence of edges, high-boost filtering, and so on. The general overall effect of the interpolation process is that of a low pass filter (i.e., blurring), but a sharpening filter is typically used to try to mitigate the blurring caused by the interpolation.

The demosaicing interpolation algorithm is not performed on or by the FPA, but rather by electronics that follow the FPA, so we will put off any more detailed discussion of that for now.

6.3.2 Color Without a CFA

The previous discussion showed that while the use of a CFA is a relatively simple, inexpensive technique for obtaining a color image from a single FPA, and is the method used in the vast

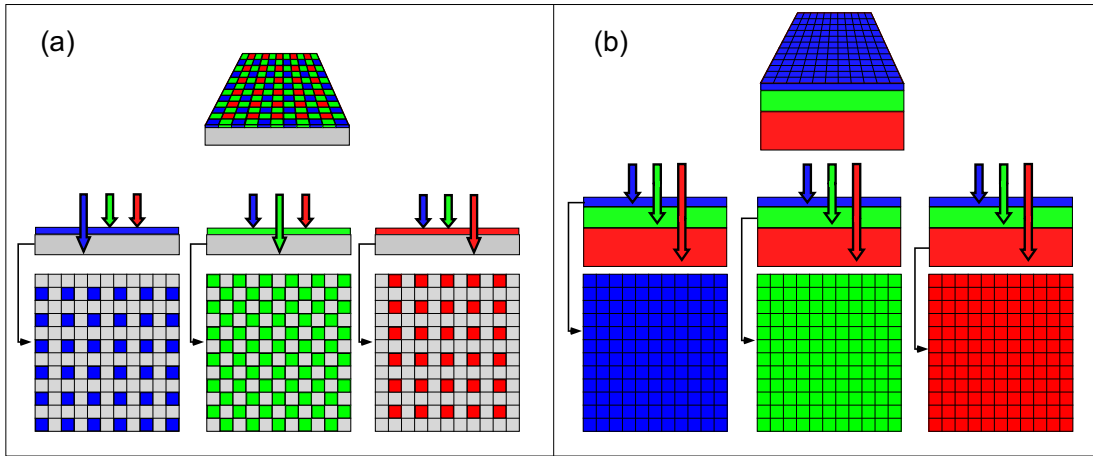


Figure 6.25: Simplified comparison of an FPA using a Bayer mosaic color filter array (a) versus an FPA using “stacked” layers (b), such as the Foveon X3 sensor.

majority of consumer-grade color cameras, using a CFA results in several problems that are only partially mitigated by using an OLPF. An alternate method for a single FPA camera to provide color information is to take advantage of the fact that different wavelengths have different penetration depths in the sensor material (longer wavelengths have deeper penetration depths). By using a three-layer “stack” of detectors, and a layer-specific readout method, the need for a color filter array and the associated demosaicing interpolation algorithm is eliminated, as shown in Fig. 6.25. The three full-resolution color planes are directly created by this type of sensor. Because a CFA is not present, color crosstalk and color moiré patterns are essentially eliminated, and aliasing is greatly mitigated since the effective fill factor for all three colors can approach 100%. For these reasons, an OLPF is typically not used with this type of FPA sensor. A commercial product that uses this approach is the Foveon X3 sensor found in cameras manufactured by Sigma.⁸

While it may appear that the stacked approach is completely superior, there are always trade-offs. For example, the readout method to get the signals off the FPA chip is more complicated for a stacked sensor. Also, while demosaicing interpolation is not needed for stacked sensors, the color differentiation is less sharp than with CFA designs, and this requires non-trivial signal processing to produce color images in a standard color space (such as RGB or YCbCr). This required processing can increase color noise in low-light situations. There is also some ambiguity with regard to specifying pixel counts: for example, Sigma usually reports the sum of pixel locations in all three layers. Thus a Foveon sensor reported to have 14.1 megapixels (MP) produces a final color image with a resolution of 2688×1769 pixels, which is a 4.7 MP image, not a 14.1 MP image. Empirical tests by independent users report that a 14.1 MP Foveon sensor is roughly equivalent in qualitative image detail to an 8 MP Bayer CFA sensor when using JPEG compression for images and about as good a 10 MP Bayer CFA sensor when using native RAW image format. These reports also indicate the Foveon sensor may not be well suited to low light imaging, compared to a Bayer CFA sensor.

While the stacked approach, such as that used in the Foveon sensor, may appear to have the potential to outperform the Bayer CFA approach, this potential has yet to translate into widespread commercial success. Any possible technological superiority of a stacked versus CFA approach has yet to be proved, and many other factors help decide commercial success of a product. The Betamax versus VHS videotape competition is a classic example of marketing overcoming a technological advantage. As of this writing, every camera manufacturer except

⁸The Foveon technology was purchased by Sigma, and at this writing this technology has not been licensed to any other camera manufacturer.

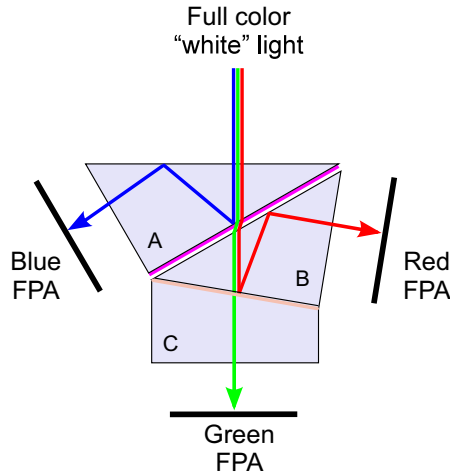


Figure 6.26: A 3-FPA arrangement for a color camera using a Phillips-type trichroic prism.

one (Sigma) uses some type of CFA to produce color images from a single FPA. To obtain higher quality color images than is possible with a single FPA, an alternate approach is to use three independent FPA sensors.

6.4 Color Imaging: Three FPA Method

This section describes a method of obtaining color images that allows nearly 100% FF for all colors, avoids the use of a CFA, essentially eliminates the need for an OLPF, has as good or better color separation as the best CFA (and much better than a stacked sensor), and needs no demosaicing interpolation algorithm or color space processing algorithm. This method uses three independent FPAs that are each dedicated to one of the primary colors red, green, or blue. The colors are typically separated with a device such as a trichroic (i.e., three color) prism and each color is directed to the proper FPA. A 3-FPA arrangement using a Phillips-type trichroic prism is shown in Fig. 6.26.

There several desirable attributes for a color separation prism, including

- equal path lengths of the light for all three colors,
- invariance to polarization of the incoming white light, and
- an image with the same orientation for all three colors.

While not perfect, the Phillips-type trichroic prism shown in Fig. 6.26 is one popular method that approaches these design goals. The transmission efficiency of the prism technique is very high, so the total light gathered by all three FPAs using this approach is significantly greater than if a beam splitter and filtering approach were used.

Given all the advantages of a 3-FPA method listed in the first paragraph of this section, why doesn't every camera use this technique? The advantages are counterbalanced by significant disadvantages, including: much higher cost (two additional FPAs plus the high precision prism); much greater size, weight, and power consumption; and more sensitivity to misalignment of the optical paths due to physical shock.

For these reasons, and the fact that the image quality of single FPA/CFA combinations has become quite good, there are no currently available still-image cameras (such as a DSLR) that use the 3-FPA method.⁹ Only high-end video (i.e., "camcorder") and television cameras,

⁹It's been reported that Sony made a small number of very bulky 3-CCD still-image analog cameras in the 1990's, that recorded images on to magnetic disks.

which typically use much lower pixel-count sensor arrays, use a 3-FPA design. Historically, most of these video cameras used CCD sensors, rather than CMOS sensors, and the term “3CCD camera” became synonymous with this type of video camera (even if, today, the camera may actually use three CMOS sensors). Essentially all broadcast television cameras are of the 3CCD type, not just for image quality reasons but also because a 3CCD camera provides more options for how the luma and chroma can be sampled for certain video signal formats (discussed more fully in Chapter 7).

6.5 Color versus Monochrome Imaging

Many users of digital cameras assume that color cameras are somehow “better” than monochrome cameras. However, for many technical applications where distinguishing color is not critical, a monochrome camera can almost always provide superior image quality. There is no CFA and typically no OLPF, there are no filter or prism losses, no potential alignment issues (as in a 3-FPA design), a higher fill factor, greater sensitivity, wider dynamic range, and lower weight/power. Cost should be lower, but often is not.

Unfortunately, because the market for monochrome cameras is relatively small compared to color cameras, the availability and selection of monochrome cameras has been steadily shrinking over the years. Most of the commercially available monochrome cameras today are video cameras (yet video introduces more complications compared to still-image cameras). There are no currently available monochrome DSLR cameras of which the author is aware. However, as of this writing, Leica markets a monochrome version (the “Monocrom”) of its excellent model M digital still-image camera (for around \$8,000 USD), and at least one company (LDP, LLC) will convert a standard color still-image camera to monochrome (or to UV-only or IR-only).

Note that most color cameras have a “black and white” setting, but this provides none of the advantages of a true monochrome camera. In fact, if a monochrome image is desired using a color camera, better results can almost always be obtained by taking the original image as color and using postprocessing software to convert to monochrome. As always, the user must explicitly disclose all computer-based manipulations of any image used as data for research.

6.6 1-D Linear Detector Arrays

Not all digital cameras use a 2-D rectangular FPA for a sensor, although that is by far the most common variant. A significant category of digital cameras, appropriate for certain specialized applications, is called a “line scan” camera (as opposed to the more common “area scan” cameras). As the name implies, a line scan camera utilizes a sensor that is a 1-D linear array of detectors (i.e., pixels) such that a single “line” or row of an image is recorded at a given instant in time. Usually, either the camera or more commonly the object to be imaged moves at a constant rate (orthogonal to the long dimension of the sensor array), and a 2-D image (i.e., a frame) is formed by collecting a certain number of lines for each image frame. A simple comparison of an area scan camera versus line scan camera is shown in Fig. 6.27. A line scan camera typically outputs a continuous video signal at some standard frame rate; it is not a still-image camera. Area scan cameras can be either still-image or video.

Line scan cameras are most often found in machine vision applications of industrial processes, such as inspecting a product during or after manufacture. There are some specific reasons for using a line scan camera for this type of scenario. For example, line scan cameras are much less affected by motion blur compared to an area scan camera, so the relative motion between the camera and the object plane can be much higher. Illumination is also much easier; it’s generally difficult to maintain constant, even illumination of a wide 2-D area. With a line scan camera, only a small, narrow region must be properly illuminated. A line scan camera is typically less expensive than an area scan camera, primarily because a 1-D sensor array costs less than an equivalent resolution 2-D sensor array. However, a line scan camera will also need external

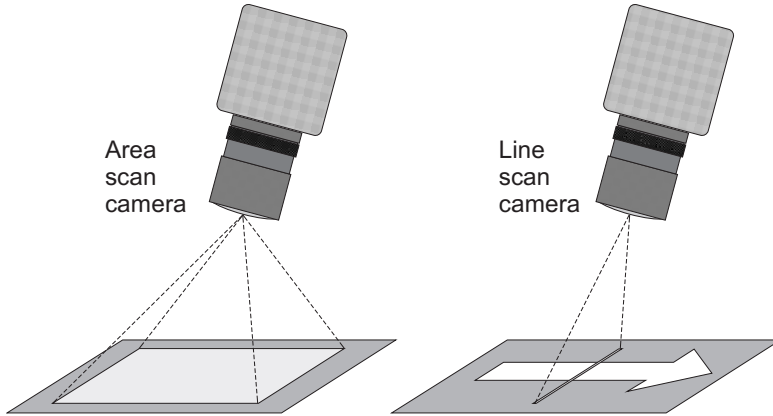


Figure 6.27: Comparison of an area scan camera imaging a fixed object plane, and a line scan camera imaging a moving object plane.

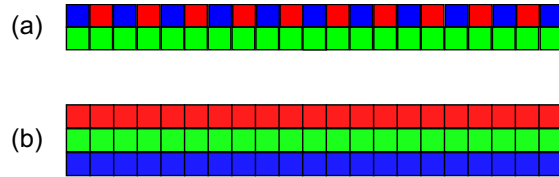


Figure 6.28: Two methods of using a color filter array to extract color information with a line scan camera. (a) Bilinear. (b) Trilinear. A third method uses a trichroic prism similar to that shown in Fig. 6.26.

synchronization and timing signals to ensure the 2-D image frame is created properly, and this will add somewhat to the system cost.

Line scan cameras may be monochrome or color. To distinguish color information, some line scan cameras use a color filter array approach, using two (called bilinear) or three (called trilinear) physically adjacent 1-D arrays of detectors (as shown in Fig. 6.28). More expensive color line scan cameras use a trichroic prism and three separate 1-D arrays of detectors with no color filters (since the prism separates the wavelengths), in a manner similar to that shown in Fig. 6.26. As with the color cameras using a single 2-D FPA, the color filter array approach is less expensive than the trichroic prism approach but it has technical drawbacks. Because the multiple rows of a bilinear or trilinear array do not image exactly the same spatial location, there is some alignment error. If the camera's optical axis is not perpendicular to the plane of relative movement (such as the 15 degree angle depicted in Fig. 6.27), then the object distance s_o is also different for each row of the array, which exacerbates the problem. In general, if the application permits the use of a monochrome line scan camera, use one. They are cheaper and introduce fewer potential problems than a color camera.

When users require higher and higher relative velocity between the camera and object plane (for example, to increase the throughput of a manufacturing process), the integration time of light on a given photodetector becomes less and less. For the same illumination, this results in a darker image, with a lower signal to noise ratio. While a user can often increase the brightness of the illumination up to a certain point, camera manufacturers now offer design variations that provide greater light sensitivity. A simple, inexpensive approach is to double the number of rows and simply sum the output from both rows as if it were a single row. This approach causes some blurring in the direction of motion due to the larger effective pixel size, but approximately doubles the light gathering of the camera. For even higher sensitivity, a more sophisticated, and more costly, approach is a time delay integration (TDI) line scan camera where many rows are

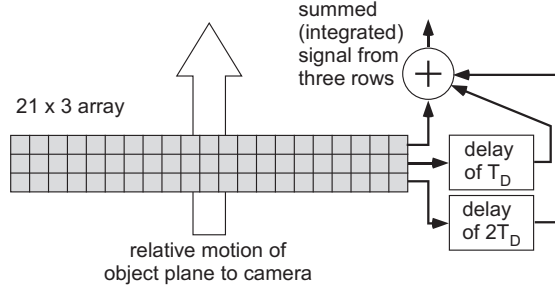


Figure 6.29: Simplified diagram of a line scan TDI approach for increasing light sensitivity.

summed but using time delays to mitigate the blurring.

A highly simplified example of the TDI approach is shown in Fig. 6.29. The amount of time delay is determined by the relative velocity of the camera and the object plane. At time t_0 , the bottom row of the array in Fig. 6.29 is imaging a certain location on the object plane. Due to the relative motion of the object plane, at time $t_0 + T_D$, the middle row is imaging that same location, and at time $t_0 + 2T_D$ the top row is imaging that same location. When the three rows are summed using the appropriate time delays as shown in Fig. 6.29, the light sensitivity is effectively tripled but with essentially no blurring (unless there is some other time-varying change at the object plane during the total integration time). To keep the figure simple, the required timing synchronization clock signals were not shown. While Fig. 6.29 depicted only three rows, actual TDI line scan cameras use many rows for integration. In (column, row) format, some example array sizes of currently available TDI line scan cameras range from 2048×48 , 4096×96 , all the way up to $12k \times 256$. More rows used for integration means more light sensitivity, but also means more sensitivity to any mismatch between the relative object plane velocity and the time delays. A TDI line scan camera with 96 rows can reportedly withstand up to a 4% error between the object plane velocity and the time delays without any significant degradation (blurring) of the image.

Estimates of the sensor-related MTFs for a line scan camera are treated differently for the two spatial domain axis. Along the “long” axis of the 1-D sensor array (which usually corresponds to the horizontal image axis, which here is called the x -axis), both the detector MTF and the sampling MTF contributions are essentially the same as was discussed for 2-D FPA (i.e., area scan) cameras. Along the axis of relative motion between the camera and object plane (which usually corresponds to the vertical image axis, which here is called the y -axis), the method of determining the detector MTF is unchanged, but the sampling MTF estimate depends upon the relative velocity, setup geometry, and acquisition time of each “line” in an image frame. A longer time between “snapshots” of a row means the object plane has moved farther due to its constant velocity. This linear translation of the object plane is mapped back to a linear spatial distance on the image plane at the 1-D sensor array, and this determines the effective sampling distance y_s . The discussion that follows is for a simple monochrome line scan camera; the reader can infer how to apply the same basic ideas to a color and/or TDI line scan cameras.

For reasons that will become evident, a popular setup for line scan cameras is such that the motion-induced sampling distance y_s is equal to one-half the physical dimension in the y direction of a single pixel. For example, if the linear array is made up of a 1-D line of square pixels such that $x_d = y_d = d$, with a 100% fill factor in the x -direction, then the sampling distances would be $x_s = d$ and $y_s = d/2$. This scenario, using a single 1-D sensor array for a line scan camera, is shown in Fig. 6.30.

In this scenario, the x -axis MTFs are

$$\text{MTF}_{\text{det}}(u) = |\text{sinc}(du)| \quad \text{MTF}_{\text{samp}}(u) = |\text{sinc}(du)|, \quad (6.11)$$

which both have a cutoff frequency of $1/d$, so the combined MTF (i.e., the product of the two)

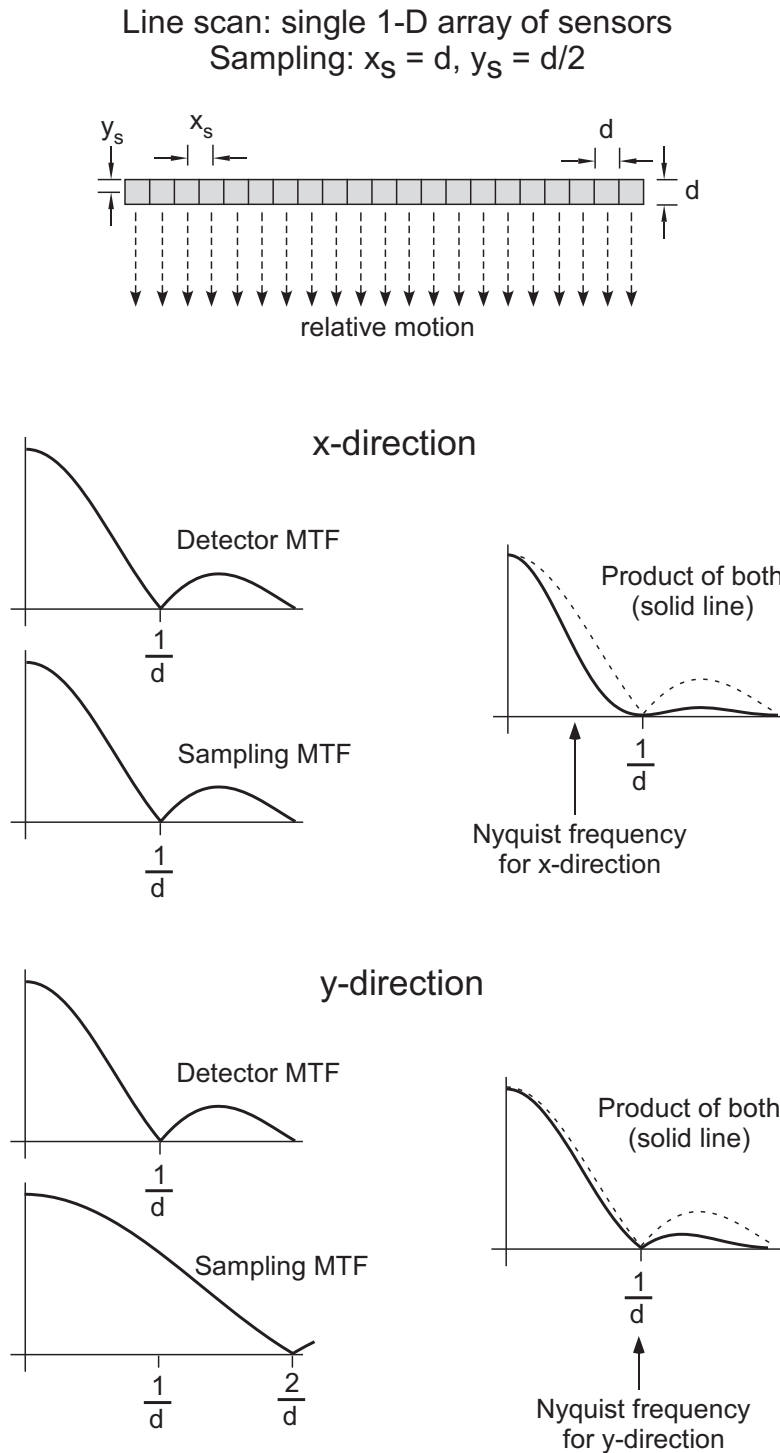


Figure 6.30: Simplified diagram of a line scan camera using a single 1-D array of sensors. The sampling intervals are $x_s = d$ and $y_s = d/2$, where d is the dimension of a single square pixel in the sensor array.

is

$$\text{MTF}_{both}(u) = |\text{sinc}(du)|^2, \quad (6.12)$$

which has a cutoff frequency of $1/d$ and the Nyquist frequency is $1/2d$. See the upper plots of Fig. 6.30. Conversely, the y -axis MTFs are

$$\text{MTF}_{det}(v) = |\text{sinc}(dv)| \quad \text{MTF}_{samp}(v) = \left| \text{sinc}\left(\frac{d}{2}v\right) \right|. \quad (6.13)$$

In this case, the detector MTF has a cutoff frequency of $1/d$, but the sampling MTF has a cutoff frequency of $2/d$, which means the Nyquist frequency is $1/d$. The combined MTF (i.e., the product of the two) is

$$\text{MTF}_{both}(u) = \left| \text{sinc}(dv) \text{sinc}\left(\frac{d}{2}v\right) \right|, \quad (6.14)$$

which has a cutoff frequency of $1/d$ and the Nyquist frequency is also $1/d$. See the lower plots of Fig. 6.30.

The practical ramification of this setup is that while there can be some aliasing in the x -direction (the MTF is 0.4 at the Nyquist frequency), potential aliasing has been nearly eliminated in the y -direction. When some camera manufacturers became aware of this commonly used setup for line cameras, they introduced a variation on the line camera sensor that could achieve essentially equivalent MTFs in both directions. This is accomplished by using two staggered 100% FF 1-D sensor arrays as shown in Fig. 6.31. This arrangement requires some additional image processing (by the camera electronics) to properly combine the signals from the two staggered rows into one image row.

In this scenario, the sampling distances would be $x_s = d/2$ and $y_s = d/2$, and the x -axis MTFs are

$$\text{MTF}_{det}(u) = |\text{sinc}(du)| \quad \text{MTF}_{samp}(u) = \left| \text{sinc}\left(\frac{d}{2}u\right) \right|, \quad (6.15)$$

for which the detector MTF a cutoff frequency of $1/d$, and the sampling MTF has a cutoff frequency of $2/d$. The combined MTF is

$$\text{MTF}_{both}(u) = \left| \text{sinc}(du) \text{sinc}\left(\frac{d}{2}u\right) \right|, \quad (6.16)$$

which has a cutoff frequency of $1/d$ and the Nyquist frequency is also $1/d$. See the upper plots of Fig. 6.31. The y -axis MTFs are essentially the same, equal to

$$\text{MTF}_{det}(v) = |\text{sinc}(dv)| \quad \text{MTF}_{samp}(v) = \left| \text{sinc}\left(\frac{d}{2}v\right) \right|. \quad (6.17)$$

As before, the detector MTF has a cutoff frequency of $1/d$, but the sampling MTF has a cutoff frequency of $2/d$, which means the Nyquist frequency is $1/d$. The combined MTF is

$$\text{MTF}_{both}(u) = \left| \text{sinc}(dv) \text{sinc}\left(\frac{d}{2}v\right) \right|, \quad (6.18)$$

which has a cutoff frequency of $1/d$ and the Nyquist frequency is also $1/d$. See the lower plots of Fig. 6.31. For this setup, aliasing is nearly eliminated in both the x and y directions, at the expense of a more expensive sensor and a little more image processing by the camera electronics.

The previous discussion about MTFs covered only two possible setups of line scan cameras; many others are possible. Some users today seem to shy away from line scan cameras, even when the application seems perfectly suited to them, due to unfamiliarity. While the analysis is just slightly more involved, excellent results can be obtained and the user should not ignore this type of camera.

Line scan: two staggered 1-D arrays of sensors
Sampling: $x_s = d/2$, $y_s = d/2$

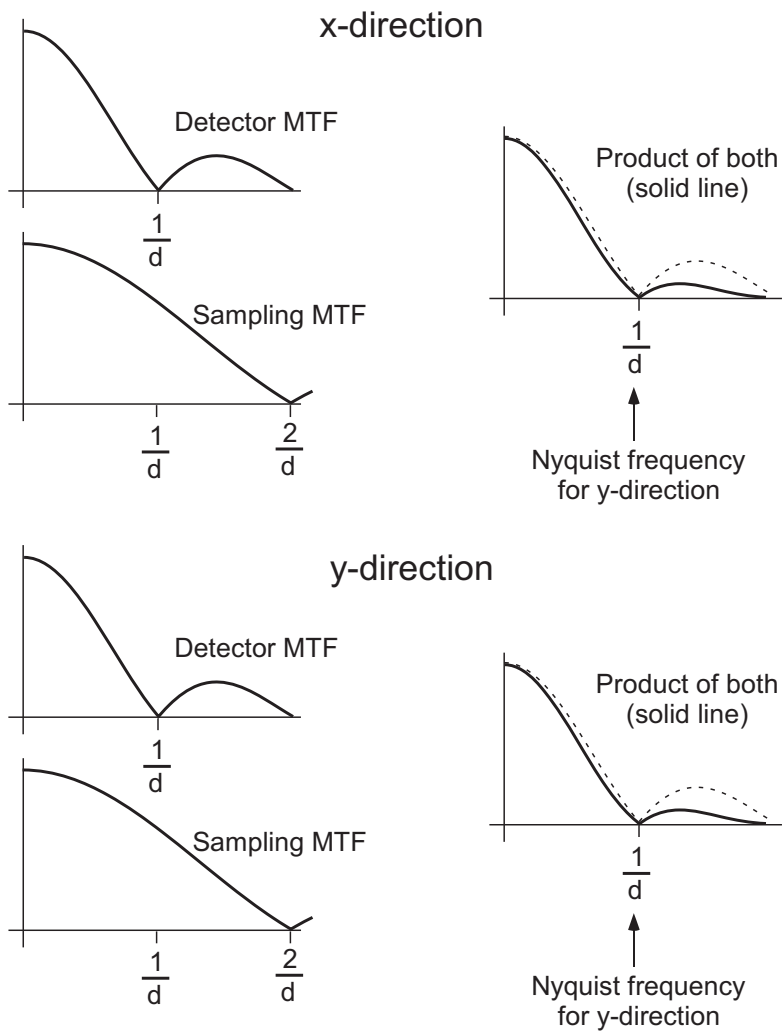
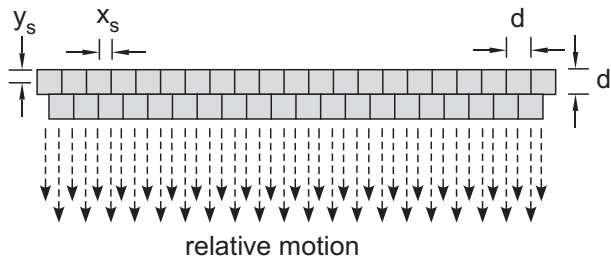


Figure 6.31: Simplified diagram of a line scan camera using two staggered 1-D arrays of sensors. The sampling intervals are $x_s = d/2$ and $y_s = d/2$, where d is the dimension of a single square pixel in the sensor array.

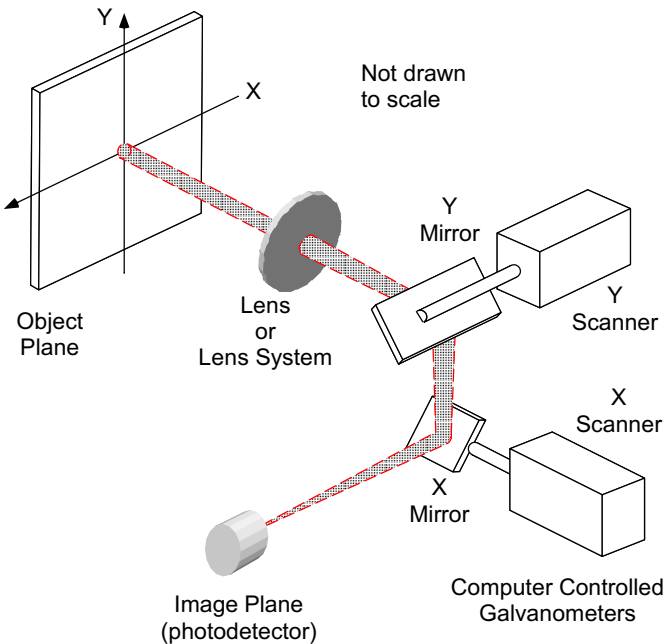


Figure 6.32: Simplified diagram of an XY scanning system used to acquire a 2-D image using a single photodetector.

6.7 Single Detector Scanning

Sometimes the imaging system is not a traditional camera, but for one reason or another must be a custom system designed and built for a very specific application. The variations and possibilities for this are nearly endless, but this section briefly discusses one such custom setup: single detector scanning.

In a single detector scanning system, only one photodetector is used and a 2-D image is created through manipulation of the optical path through which light is received. A simplified diagram of this type of optical setup is shown in Fig. 6.32. Note that the partially rotating mirrors can direct the light path to originate from any point on the object plane, within the designed FOV.

In a typical raster scan technique, the X mirror sweeps across the horizontal FOV while the Y mirror remains fixed. Some number of samples are obtained from the photodetector for each horizontal row, which can be thought of as the number of horizontal “pixel” locations. At the end of the horizontal scan, a blanking signal is applied to the photodetector while the X mirror quickly resets to the beginning of the horizontal sweep, and the Y mirror increments vertically by one row, and the process is repeated. The number of vertical increments within the FOV dictates the number of vertical “pixel” locations. At the end of the vertical FOV, the Y mirror quickly resets to the beginning of the vertical sweep during the appropriate blanking interval. Note that the converging lens or lens system will invert the direction of light path travel compared to the direction of mirror movement.

There are *many* variations on this basic idea. Sometimes, the illumination at the object plane is provided by a laser source that is coupled into the same light path using a beamsplitter; for example, this technique is used for a scanning laser ophthalmoscope (SLO) to image the retina. Sometimes one or both of the mirrors are cylindrical multi-sided designs, and instead of sweeping back and forth, they rotate in only one direction (this allows faster manipulation of the light path).

Estimating the MTF of such an arrangement follows from the previous discussions. The

detector MTF is found in the same way, based on the physical dimensions x_d and y_d of the photodetector that result in spatial integration. The sampling MTF is determined by the effective distance between “pixel” locations at the object plane that are determined from the sampling rate of the photodetector, movement of the mirrors, and the optical geometry. These object plane pixel locations are then mapped back to a fictitious 2-D image plane using the focal length of the lens and the object plane distance, to yield an effective value of x_s and y_s in linear units at the image plane.

6.8 Nontraditional Sensors: Biomimetic Fly Eye

While all cameras are, in some way, a form of biomimetic design (i.e., based partly upon biological form or function), as mentioned in Section 2.3, some optical designs deviate significantly from a traditional camera. One example of this is a fly eye vision sensor, based upon the compound eye of *Musca domestica*, the common housefly [5, 6, 77, 78].

The housefly has two compound eyes, as shown in Fig. 6.33(a), that are each composed of approximately 3,000 individual structures called ommatidia. Each optically-isolated ommatidium is comprised of a nearly hexagonal corneal facet lens (approximately $25\ \mu\text{m}$ across) at the surface, followed by a cone-shaped lens that is the primary focusing element, ending in a pack of eight photoreceptors arranged along seven optical axes (two photoreceptors near the center of the ommatidium are coaxial). The seven optical axes have overlapping quasi-Gaussian angular sensitivity to light, as depicted for three axes in Fig. 6.33(b), and in the first neural layer (prior to the brain) the house fly implements what is called neural superposition on the visual information. One important result of this is what has been called *motion hyperacuity*, which means the fly eye can detect object movement at increments just a tiny fraction of the physical spacing of the optical axes. This hyperacuity is one of the main reasons the artificial fly eye vision sensor was designed and built; the optical front end of one prototype for this sensor is shown in Fig. 6.33(c).

Research has shown that the fly eye vision sensor is extremely sensitive to motion in a wide range of lighting and contrast scenarios, and can be fabricated to be much smaller, lighter in weight, and consume much less power than a traditional CCD or CMOS type of camera that might be used in a similar application. However, this type of sensor does not produce a traditional 2-D image. The optics intentionally blur the incoming light to achieve the overlapping fields of view (thus the cutoff frequency of the optical MTF is rather low), and the signals from the multiple optical axes are combined in various ways (mimicking neural superposition) to extract specific information such as movement, edge location, flow field vectors, etc. Since a traditional

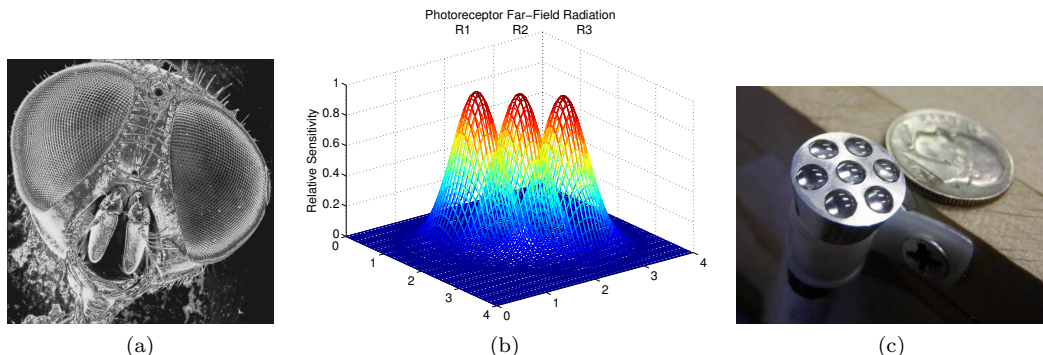


Figure 6.33: Compound eyes of the common house fly (a) have overlapping quasi-Gaussian angular sensitivity (b) over the FOV of each individual optical axis. The optical front end of an artificial vision sensor that mimics this is shown in (c), next to a U.S. dime for comparison.

2-D image is not created by this sensor, the discussion for this book ends here. But this sensor provides a good example of the sheer diversity of imaging setups that may be encountered in practice.

The previous sections have discussed various MTF considerations for a 2-D rectangular FPA, a 1-D linear FPA, a single detector imaging system, and one example of a biomimetic vision sensor. To determine the overall sensor MTF for other imaging methods, use the basic theory presented in this chapter. For a specific discussion of the MTF associated with a coherent fiber optic bundle in a hexagonal pattern, or the effective MTF when using microdither (i.e., microscan) techniques on sparse sensor arrays, see Boreman's text [60]. The discussion now turns from mainly spatial considerations to temporal considerations related to the FPA.

6.9 Shutters and Temporal Effects

6.9.1 Global Shutter versus Rolling Shutter

6.9.2 Shutter Speed

The effects of spatial sampling imposed by the FPA were introduced in Section 6.2. Users must also consider how temporal sampling, with respect to the detector array, will affect the image. For cameras that take static (i.e., still) images, the primary temporal aspect is simply the light integration time (sometimes called shutter speed) of the FPA. This can be implemented electronically by the rate at which the voltage readout from the FPA (and FPA reset) is achieved, or in more traditional camera designs by a physical shutter which opens to admit light on to the FPA for some specified period of time. Note that obtaining a still image in this way results in just a single temporal “sample,” therefore temporal aliasing is not an issue. Video cameras, which record a sequence of many images (called frames), are subject to temporal aliasing. This topic will be discussed in the next chapter.

Higher-end digital cameras allow more complete user control over the shutter speed, and may permit a fastest shutter speed of 1/4000 of a second (in consumer-grade cameras) or 1/16000 of a second (in professional-grade camera) or even less as technology advances. These cameras usually provide a wide range of shutter speeds from fastest to slowest, often with each setting twice the duration of the previous one to be equivalent to an aperture change of one full f-stop larger. The longest shutter time is a setting where the shutter stays open until the user manually closes it again (sometimes called the *bulb* setting for historical reasons).

Faster shutter speeds allow blur-free capture of faster events (see Fig. 6.34), but the shorter integration time also means less light (see Fig. 6.35). As mentioned previously, the aperture and the shutter speed together determine what is called the “exposure” of light on the FPA. But changing the aperture also affects the depth of field (DOF) as well. Photographers often manipulate the combination of aperture and shutter speed to achieve a desired artistic effect; technical camera users typically have other considerations.

Sometimes a user wishes to capture a challenging image with both very bright AND very dark regions, and it's often the case that all the various available combinations of aperture and shutter speed result in either some underexposed regions or some overexposed regions of the image. Some newer digital cameras provide a possible solution: high dynamic range (HDR) imaging. When the HDR setting is selected, the camera takes multiple images (usually three) each at a different exposures, then digitally merges them all into a single HDR image. An example is shown in Fig. 6.36. This is not the same as manual or semi-automated “exposure bracketing,” in which multiple exposures are used, and the single best image is then selected. Be careful: using HDR techniques, you have to worry about all the shutter times, not just one, and if the image changes significantly during the time it takes to obtain the three exposures the method is rendered useless.

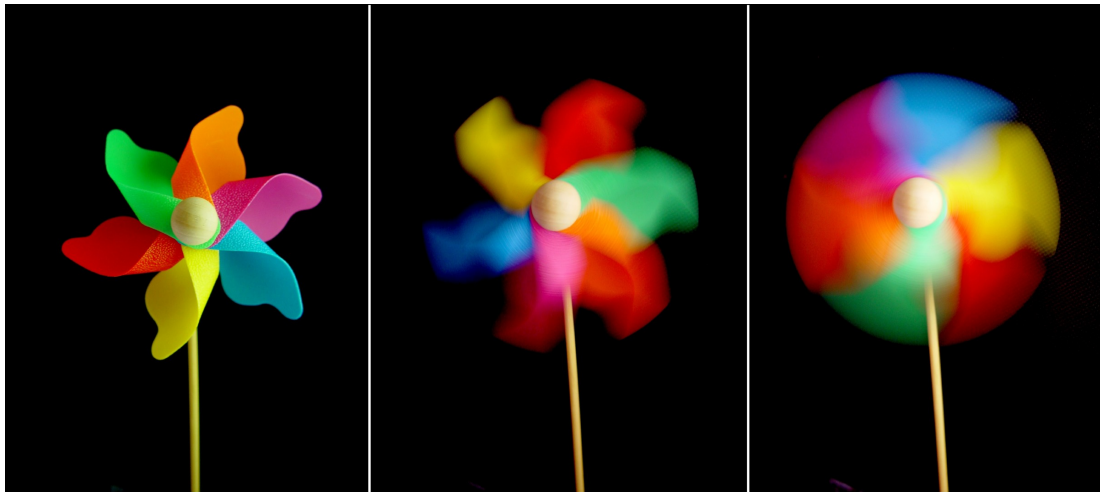


Figure 6.34: Effect of shutter speed on motion blur in an image of a rotating pinwheel. The pinwheel has the same rotational velocity in all three images. The three images were taken with relative shutter speeds of fast (left), medium (center), and slow (right), with the aperture adjusted to maintain the same exposure. [79]



Figure 6.35: Effect of shutter speed (with aperture fixed) on the exposure of an image. The scene is of Greenwich, London (UK) at night, and the green laser beam emitted by the Greenwich observatory to indicate the Greenwich meridian can be seen. The image was taken from the Thames River path, facing the observatory from the north-west. The five images were taken with relative shutter speeds of faster (left) to slower (right). [80]



Figure 6.36: High dynamic range (HDR) image (top) and the three source images (bottom) from which it was created. [81]

6.9.3 Sensitivity to Light

While shutter speed and aperture size together determine the exposure, there is a third aspect that affects exposure: the sensitivity of the FPA to light. The FPA sensitivity is expressed by a method inherited from older film cameras, where the sensitivity to light of photographic film was rated by a number often called the “speed” of the film on one of many scales that were defined over the years. Two of the most widely used of these include the linear ASA scale and the logarithmic DIN scale. The worldwide standard today is the ISO scale, which combined both ASA and DIN scales in 1974. Thus the ISO scale has both linear and logarithmic numbers, expressed for example, as ISO 100/21°, where 100 is the linear number and 21° is the logarithmic number. Often, the logarithmic number is omitted, such that ISO 100 really means ISO 100/21°.

A higher number means the film is more sensitive to light; the higher the number, the “faster” the film. A doubling of the sensitivity to light is represented by a doubling of the speed value on the linear scale, and by adding 3° on the logarithmic scale. Thus film rated as ISO 200/24° is twice as sensitive to light as film rated as ISO 100/21°. ISO 200/24° film can use a shutter speed twice as fast as ISO 100/21° film with the same aperture to obtain the same exposure (or the same shutter speed with one f-stop smaller aperture size).¹⁰ Note that this relationship starts to break down at very fast or very slow shutter speeds, a phenomenon called *reciprocity error*. Higher speed film produces an image that has more noise-like “grain” evident in it.

Modern digital cameras use a very similar rating method, sometimes called the *exposure index* (EI) but more often called the ISO setting. While somewhat arbitrary, and with some variance between manufacturers, in general an ISO setting for a digital camera provides a similar lightness to an image as could be expected from film with the same ISO rating, given the same shutter speed and aperture. The user can adjust the sensitivity of the FPA by setting the ISO number, which essentially adjusts the gain of the amplification stage in the sensor readout electronics. As with film, higher sensitivity is accompanied by greater noise in the resulting image. A typical general-use ISO setting is 100, which provides a reasonable compromise between light sensitivity and image noise for general purpose daylight photography. A setting of ISO 200 or 400 is more suitable for nighttime or indoor photography. However, the sensors and associated electronics in modern digital cameras have far surpassed photographic film in terms of sensitivity to light. Cameras are available (as of 2014) with ISO equivalent speeds of up to 409600, a number that would be unimaginable for conventional film photography. More powerful embedded processors in the cameras, as well as more advanced noise reduction software techniques, allow this amount of gain and processing to be executed the moment the photo is captured, allowing usable images to be obtained that would have been too time consuming to process with earlier generations of digital camera hardware, and impossible with film cameras.

6.9.4 Video Cameras

Video cameras, discussed in more detail in the next chapter, don’t have a readily adjustable shutter speed as still image cameras do. Instead, they have a fixed frame rate (such as 30 frames per second), with higher-priced video cameras having a choice of various common frame rates (e.g., 24, 25, 30, 48, 50, 60 fps). One frame is a single fixed image that is part of a sequence of images. The actual exposure time per frame may be some fraction of the total frame time, but as with frame rate this is typically fixed for the duration of a particular video sequence. Given that, how do video cameras control exposure? The aperture can be changed, with the unavoidable ramifications to DOF and diffraction. Video cameras can also dynamically adjust the ISO setting, which affects the noise characteristics of the images obtained. The next chapter will provide more details regarding video cameras.

¹⁰Remember that a smaller aperture size means a larger f-number. An f-number of f/2 is one f-stop smaller, and thus provides half the light, of an f-number of f/4.

6.9.5 Relative Motion

6.9.6 Vibration

6.10 Summary

When considering temporal effects, the camera user must consider available illumination, and the speed of events (including movements and vibration) to be recorded, when determining an appropriate shutter speed and ISO number for a digital camera. This chapter, combined with the two previous chapters, presented an overview of optics and photodetectors in a practical way for the express purpose of allowing the reader to intelligently choose an appropriate digital camera for a particular purpose, or for analyzing data taken by a digital camera. Repetitive calculations based on the techniques provided can be made easily using a numerical analysis program such as MATLAB®, which can also provide highly insightful plots. More extensive optical analysis, simulation, and design can be achieved with a program designed specifically for optics, such as Zemax. Tools such as MATLAB and Zemax are extremely valuable for this purpose, can save a great deal of time, and help avoid dead ends for potential design approaches.

At the risk of oversimplification, a particularly handy, “back of the envelope” figure of merit for an imaging system, that is easy to calculate and takes into account both optics and the detector array, is $F\lambda/d$, where F is the f-number discussed in Section 4.2, λ is the wavelength of light under consideration, and d is the detector size of one element (i.e., pixel) of the FPA in the given direction [38,39]. With this figure of merit, $F\lambda/d < 1$ results in a detector-limited system, and $F\lambda/d > 1$ results in an optics-limited system. When $F\lambda/d \geq 2$, there is no spatial aliasing possible, but this condition may result in too much image blur. See Holst [38,39] for more detail, but keep in mind that this single number as a figure of merit provides only a top-level glimpse into the performance of the camera system.

Chapter 7

Video Cameras versus Still-Image Cameras

B^{LAH, blah}

7.1 Video: a Time Sequence of Still Images

7.1.1 Frame Rate versus Shutter Speed

7.1.2 Motion Aliasing in Video

7.2 Video formats

7.2.1 Interlaced versus Progressive Scan

7.2.2 Formats Derived from Broadcast standards

7.2.3 Modern Digital Video Formats

7.3 Special Case of Cinematic Video

Video cameras don't have a shutter speed per se; rather they have a frame rate, which is the time between each image frame that makes up the video stream. The units are frames per second or fps. A faster frame rate has the same ramifications for capturing faster events and for light exposure as does a faster shutter speed. But since video also captures motion, temporal sampling has another aspect that must be considered. If the frame rate is too slow, the motion may be aliased when the video is viewed. Television viewers have seen this phenomenon when the wheels of a car in the video seem to slow down or even turn backwards as the car speeds up—this is an example of temporal aliasing due to an insufficient frame rate. Frame rate is usually proportional to the cost of the camera, with 30 fps being common, 200 fps readily available, and over 1000 fps possible for specialized, high-end video cameras. Note that video cameras usually use a fixed frame rate, and control the exposure entirely by adjusting the aperture and/or the light sensitivity of the FPA.

Another issue should be considered with regard to video cameras. There are many video format standards, but two primary categories of video format are interlaced scan or progressive scan. See Fig. 7.1 for a side-by-side example. While most digital video cameras today are progressive scan, where an entire frame is created row-by-row in one pass at the speed of the frame rate, there are still many video cameras that use an interlaced scan standard. Originally

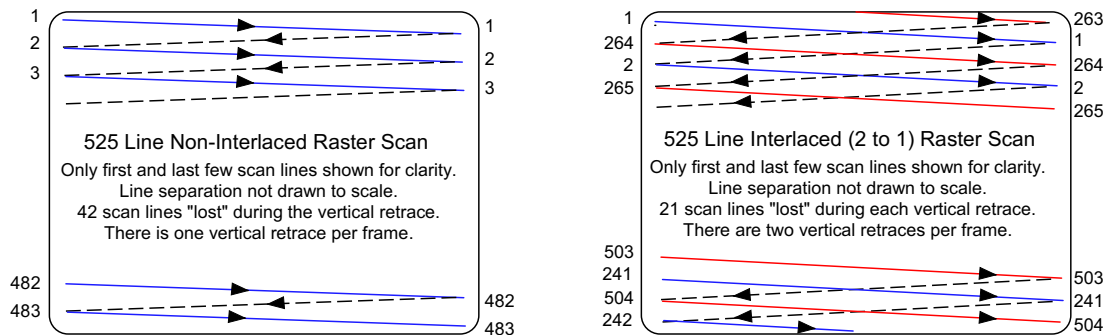


Figure 7.1: Progressive scan (left) and interlaced scan (right) for a 525-row video format.

developed to conserve the bandwidth needed for analog television signals, interlaced scan builds a frame in a two-step process. During one-half of a frame period, the odd-numbered rows are created first (collectively called the odd field), then during the next half-frame period the even-numbered rows are created (collectively called the even field). Thus it takes two fields to create a full frame, and the field rate is twice as fast as the frame rate. Due to the persistence of human vision, this provides a *perception* of a frame rate twice the actual frame rate, yet requires only about half the bandwidth that would be required for a progressive scan frame rate equal to the interlaced scan field rate. NTSC (North America, ≈ 60 fields per second, ≈ 30 frames per second) and PAL (Europe, 50 fields per second, 25 frames per second) are two common older interlaced video standards. But interlaced scan is not dead; the relatively new high definition television standard called ATSC supports both interlaced and progressive scan modes. Only CRT displays and some plasma displays can directly display interlaced video; other displays must use a deinterlacing algorithm to convert to progressive scan. If using a video camera that employs an interlaced format, the user must take into account the effect this has on both spatial sampling (due to every other row being sampled for each field) and temporal sampling (due to the difference between the field rate and the frame rate).

Chapter 8

Camera Electronics and Interfaces

UNDERSTANDING how the optics and imaging sensors influence any digital images acquired is a fundamental requirement for anyone who wishes to intelligently use digital cameras. However, it is also important to understand the various camera types and how the choice of camera can shape the problem domain for digital imaging.

8.1 Image acquisition electronics

8.1.1 MTF Due to Hardware

8.1.2 MTF Due to Demosaicing Interpolation Algorithms

The Fourier approach is commonly used in the design and analysis of electronic circuits and systems. The terminology is only slightly different between optical and electronic systems: the point spread function is similar to the impulse response, and the optical transfer function is similar to the transfer function. While optical system designers look mainly at the magnitude of the optical transfer function, electronic systems designers usually are concerned with both the magnitude and phase of the transfer function. Electronics operate in the time domain, whereas optics operate primarily in the spatial domain.¹ If it is desirable to maintain the link to the spatial domain as one analyzes the associated image acquisition electronics, then one can map time to space. For example, assume the FPA data is typically read out row by row (i.e., horizontal readout). The spatial samples from the FPA are sent to the readout electronics at a certain temporal rate T_s . Knowing x_s , the center-to-center distance between detectors on a row of the FPA, one can map the spatial distance associated with one temporal sample, across the row. The readout then shifts down to the next row, and that distance is y_s , the center-to-center distance between detectors on a column of the FPA. Whether this space-to-time mapping is useful depends upon the application.

While many modern camera and imaging systems use a digital interface to pass data to the computer, recording, and/or display devices, there are still many older (and some newer special purpose) systems that make use of an analog interface at some point in the signal chain. This requires special consideration. A common example is the relatively inexpensive analog video camera (such as RS-170, RS-330, NTSC, CCIR, PAL, or SECAM) that processes (i.e., modulates) the output from the FPA into a specific analog video format to be carried by a cable to the

¹As previously discussed, optics and imaging systems also have an implied time domain aspect, in terms of how an image changes over time. The most obvious example of this is video, which is a time sequence of static images taken at some *frame rate*. Any motion detection or object tracking also implies that the time axis must be considered.

computer, whereupon a specialized analog-to-digital converter (called a frame grabber)² turns the analog image data into discrete digital pixel data. Two issues are predominant: bandwidth and resampling. The analog bandwidth B allocated to the video signal³ puts a limit on the horizontal resolution the camera can provide (regardless of the number of photodetectors on the FPA) such that the varying analog voltage level in the video signal cannot have more than $2B$ independent values per second [19]. The resampling that occurs (the first sampling was at the FPA, the second at the frame grabber) almost always means that a pixel of digital image data has no direct correspondence to a particular photodetector location on the FPA. For some applications, this can have serious ramifications to how the image data can be reliably interpreted.

How the interface between optical analysis and electronic analysis is handled is up to the camera designer and the particular application, but the process warrants significant thought to avoid erroneous conclusions.

8.2 Digital versus analog interface

8.2.1 RS-170 and Variants

8.2.2 External Interfaces: CameraLink, Firewire, USB, and Variants

8.2.3 Internal Interfaces: MIPI Standards

8.3 Other factors related to cameras

²There are optional frame grabbers for digital cameras, without the A/D circuitry.

³Knowledge of the video signal specifics, such as scan rate, blanking interval, and bandwidth must be known.

Chapter 9

Lighting and Illumination

B^{LAH, blah}

- 9.1 Achieving Even Illumination
- 9.2 Ramifications of Illumination Wavelengths
- 9.3 Ramifications of Illumination Power Source
- 9.4 Image Noise and Flicker Due to Illumination

Chapter 10

Image File Storage and Compression

B^{LAH, blah}

- 10.1 Internal Image Formats
- 10.2 RAW versus Compressed
- 10.3 Compression Overview
 - 10.3.1 Lossless versus Lossy
 - 10.3.2 JPEG
- 10.4 Recommendations

Chapter 11

Watermarks for Digital Images

B^{LAH, blah}

- 11.1 Definition and Purpose of Watermarks
- 11.2 Visible versus Invisible
- 11.3 Robust versus Fragile
- 11.4 Ramifications for Research Data
- 11.5 Special Topic: Steganography

Chapter 12

Simulating and Testing a Digital Imaging System

B^{LAH, blah}

Camera calibration is typically needed [82].

12.1 Software Tools to Support Simulation

12.2 MATLAB and a Fourier Optics Approach

12.3 Recommendations

Appendices

Appendix A

Review of Fourier Transforms

ONE of the powerful tools covered in this book is Fourier optics (sometimes more generally called *MTF theory* to reflect the reality that this same tool can be applied to camera components other than just optics). However, to understand Fourier optics or MTF theory, one needs to be familiar with the basics of the Fourier transform (FT). For those readers who may be a bit rusty in this area, this appendix provides a brief overview of the main ideas. For more detail than provided here, see references such as [45, 83, 84].

We begin by reviewing the 1-D continuous FT, then the 1-D discrete FT (DFT). We then review the 2-D continuous FT and the 2-D DFT. The review changes back and forth between the time domain (using the variable t) and the spatial domain (using the variable x or y) for the FT, to show that it is just a simple change of units.

A.1 The 1-D Continuous Fourier Transform

The equations that define the 1-D continuous-time FT (and its inverse), using the frequency variable f (rather than the radian frequency variable $\omega = 2\pi f$ popular with some authors), are given by:

$$F(f) = \int_{-\infty}^{\infty} f(t)e^{-j2\pi ft} dt \quad (\text{A.1})$$

$$f(t) = \int_{-\infty}^{\infty} F(f)e^{j2\pi ft} df. \quad (\text{A.2})$$

If, instead of the time domain we wanted to use the spatial domain along the x -axis, and u as the spatial frequency variable associated with the x -axis, the equations would be:

$$F(u) = \int_{-\infty}^{\infty} f(x)e^{-j2\pi ux} dx \quad (\text{A.3})$$

$$f(x) = \int_{-\infty}^{\infty} F(u)e^{j2\pi ux} du. \quad (\text{A.4})$$

Note that a $1/2\pi$ factor for the FT pair, as seen in some books, is only needed if radian frequency such as ω is used, where $\omega = 2\pi f$.

A.1.1 Properties

It is helpful at this point to recall a few of the very helpful fundamental properties of Fourier analysis.

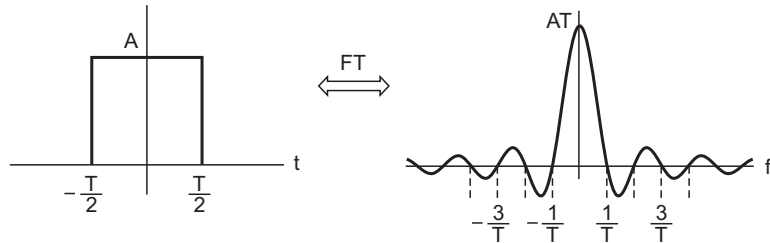
- A periodic function in one domain is paired with a discrete function in the other domain.

- An aperiodic function in one domain is paired with a continuous function in the other domain.
- If you “squeeze” in one domain, you will “spread” in the other domain (sometimes called the *reciprocal spreading property*).
- Convolution in one domain is multiplication in the other domain.
- A shift in one domain is paired with a phase term in the other domain.
- The FT of a real signal results in an even function of magnitude and an odd function of phase.

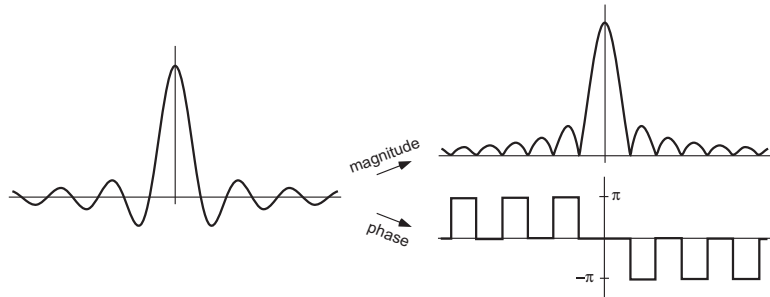
A.1.2 Fourier Transform Pairs

There are some fundamental FT pairs that are important to understanding MTF theory. Rather than show the equations, figures will be shown in the belief that they are better at helping develop (or refresh) one’s intuition about FT’s in general.

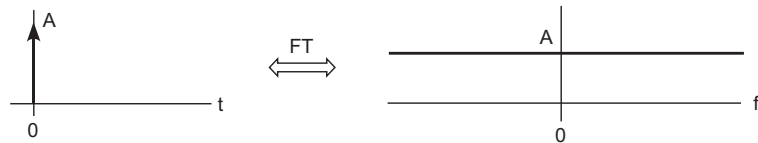
One of the most important FT pairs involves what is called a rect function and a sinc function, shown below.¹



Note that the result of a FT is, in general, complex not real. Many times, the complex result is expressed as magnitude and phase, rather than real and imaginary parts.



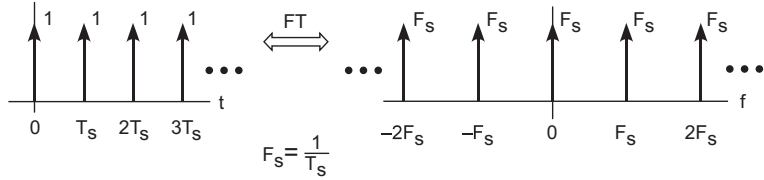
Another important FT pair involves the Dirac delta function.



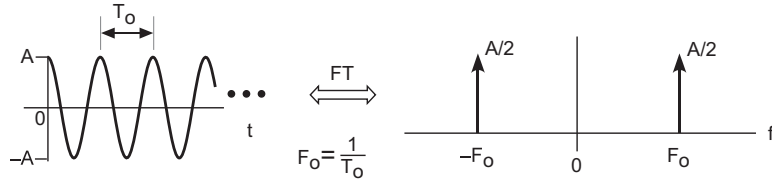
While the FT pair of a delta function and a constant (i.e., DC) value is important, there is a related FT pair that is very helpful to understanding sampling. This pair involves the FT of an infinite “train” of Dirac delta functions, spaced equally apart. This FT pair is such that an

¹The most common definition of the sinc function, $\text{sinc}(x) = \sin(\pi x)/\pi x$, is assumed in this text.

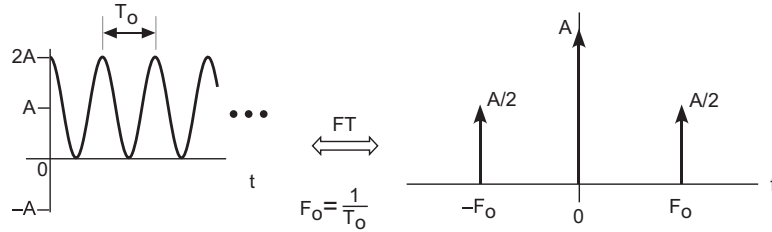
infinite “train” of Dirac delta functions in one domain is associated with infinite “train” of Dirac delta functions in the other domain. An important aspect to note is the spacing in each domain, and the amplitude scale factors. This is shown for the situation where the time domain is our independent variable, but the spatial domain version is quite similar.



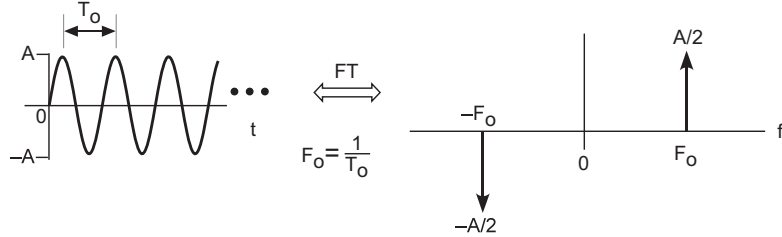
An important FT pair is the one that involves a sinusoid. The simplest is the FT of the cosine with zero phase shift, since the frequency domain phase response is zero everywhere.



Note that a pure sinusoid has a zero mean (i.e., DC) value, thus it should be no surprise that there is no component at zero hertz. If we add a DC value to the cosine from before, the DC term shows up in the spectrum, as expected, at a frequency of zero hertz.

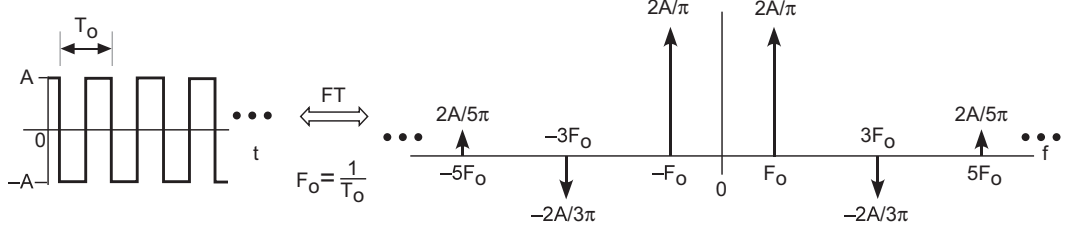


The difference between a cosine and a sine is a shift in the positive t (or x , or y) direction of $1/4$ wavelength. This means the phase response of the sine’s spectrum must be different from the cosine. The figure below implies a phase of zero when the delta function is positive, and a phase of π radians (180 degrees) when the delta function is negative.

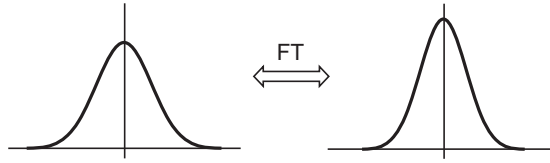


The theory behind the Fourier series explains that waveforms of any complexity may be created by summing an infinite number of pure sinusoids of appropriate frequency, magnitude, and phase. Fourier transforms can be used to demonstrate the same principle. For example, to form a square wave, we must sum an infinite number of sinusoids of the appropriate magnitude and phase, having frequencies equal to all the odd harmonics of the fundamental frequency of the square wave. If the period of the square wave is T_0 , then the fundamental frequency is $F_0 = 1/T_0$, and the odd harmonics (including the fundamental) will be $\pm F_0, \pm 3F_0, \pm 5F_0, \dots$ and so

on. The phase of each frequency component will be either zero or π , which can be depicted as either a positive or negative delta function. Given all this, the spectrum that results from the FT of the square wave should show components at the odd harmonic frequencies, which can be seen below.



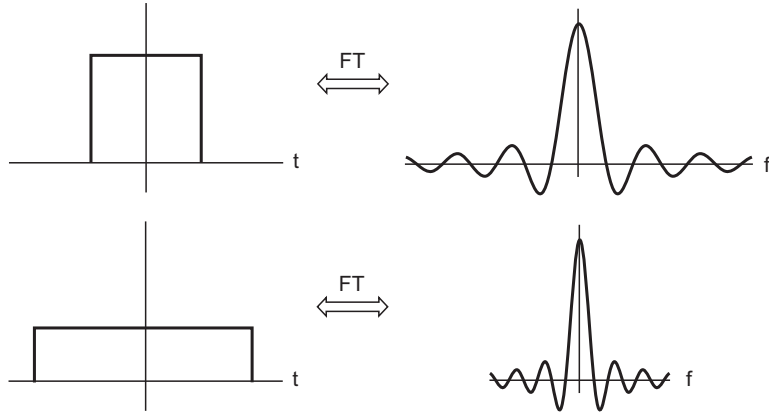
One of the most interesting functions with regard to its FT is the Gaussian, in that the FT of a Gaussian is another Gaussian!



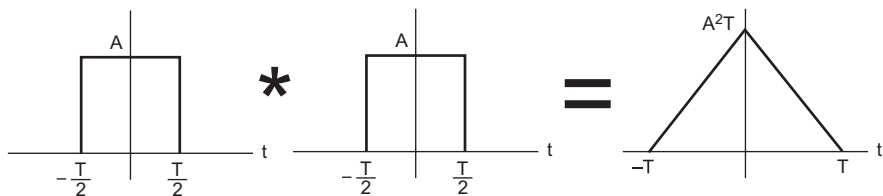
This is a FT pair for which the equation form of the pair is handy to have available, so it is provided below.

$$h(t) = \frac{1}{\sigma\sqrt{2\pi}} Ae^{-\frac{1}{2}(\frac{t}{\sigma})^2} \iff H(f) = Ae^{-2(\pi\sigma f)^2} \quad (\text{A.5})$$

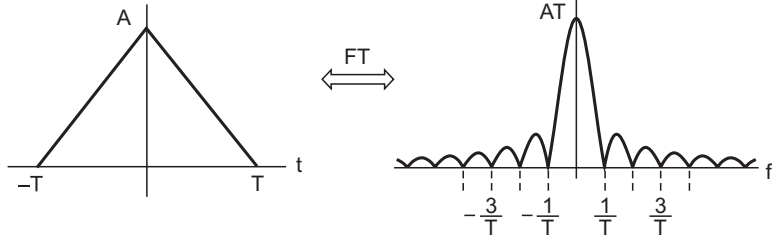
Note that from the relative location of the standard deviation σ on both sides of Eq. (A.5), the reciprocal spreading property can be inferred. That is, if the width of the Gaussian (as determined by σ) in one domain increases, the width of the Gaussian in the other domain decreases. The same property can be shown quite easily for the rect \Leftrightarrow sinc FT pair.



If we convolve a rect function in the time domain with another (identical) rect function in the time domain, we will get a triangular function, as shown below.



Recalling that the FT of a rectangular pulse is a sinc, and also that convolution in one domain is multiplication in the other domain, it should come as no surprise that the FT of a triangular function is a squared sinc function.



This brief review of the 1-D continuous Fourier transform should provide the foundation needed to better understand Fourier optics and MTF theory. When dealing with optics, the FT is considered to be continuous. But the FT is typically calculated on a computer, which evaluates not the continuous FT but the discrete FT.

A.2 The 1-D Discrete Fourier Transform

The discrete FT, usually abbreviated as DFT, is most often calculated using one of many varieties of fast algorithms generically called a *Fast Fourier Transform*, or FFT. Keep in mind that the FFT is just a fast way to calculate the DFT. A “brute force” calculation of the DFT is almost never done, since the FFT is so much faster.

The equations that define the 1-D DFT pair along the x -axis in the spatial domain, using the spatial frequency variable u , are given by:

$$F(u) = \sum_{x=0}^{M-1} f(x)e^{-\frac{j2\pi ux}{M}} \quad \text{for } u = 0, 1, 2, \dots, M-1 \quad (\text{A.6})$$

$$f(x) = \frac{1}{M} \sum_{u=0}^{M-1} F(u)e^{\frac{j2\pi ux}{M}} \quad \text{for } x = 0, 1, 2, \dots, M-1 \quad (\text{A.7})$$

Many authors write these equations in a more general way, where n is substituted for x (or for t), and k is substituted for u (or for f). Some useful aspects to note about the DFT:

- If you provide M data points as input to the DFT, you will get M data points for the output. No more, no less.
- The output data points of a DFT are complex numbers, even if the input points were real. Often in the context of this book we are most interested in just the magnitude, or the magnitude squared, of the output.
- If you take the DFT of real data, and then immediately take the inverse DFT, the result will be complex, not real, due to the limited precision of the computer. Most likely the imaginary components will be very small, but they will be nonzero. If your knowledge of the problem domain tells you the correct result must be real, you can probably discard the imaginary components.
- The $1/M$ scale factor can be included in either the forward or the inverse DFT (or use a $\sqrt{1/M}$ factor in both); different authors have different preferences.

Other helpful relationships of the DFT involve the sample period, sample frequency, and frequency resolution of the DFT. For temporal sampling, the relationships are:

$$F_s = \frac{1}{T_s} \quad \text{and} \quad \Delta f = \frac{1}{MT_s} = \frac{F_s}{M} \quad (\text{A.8})$$

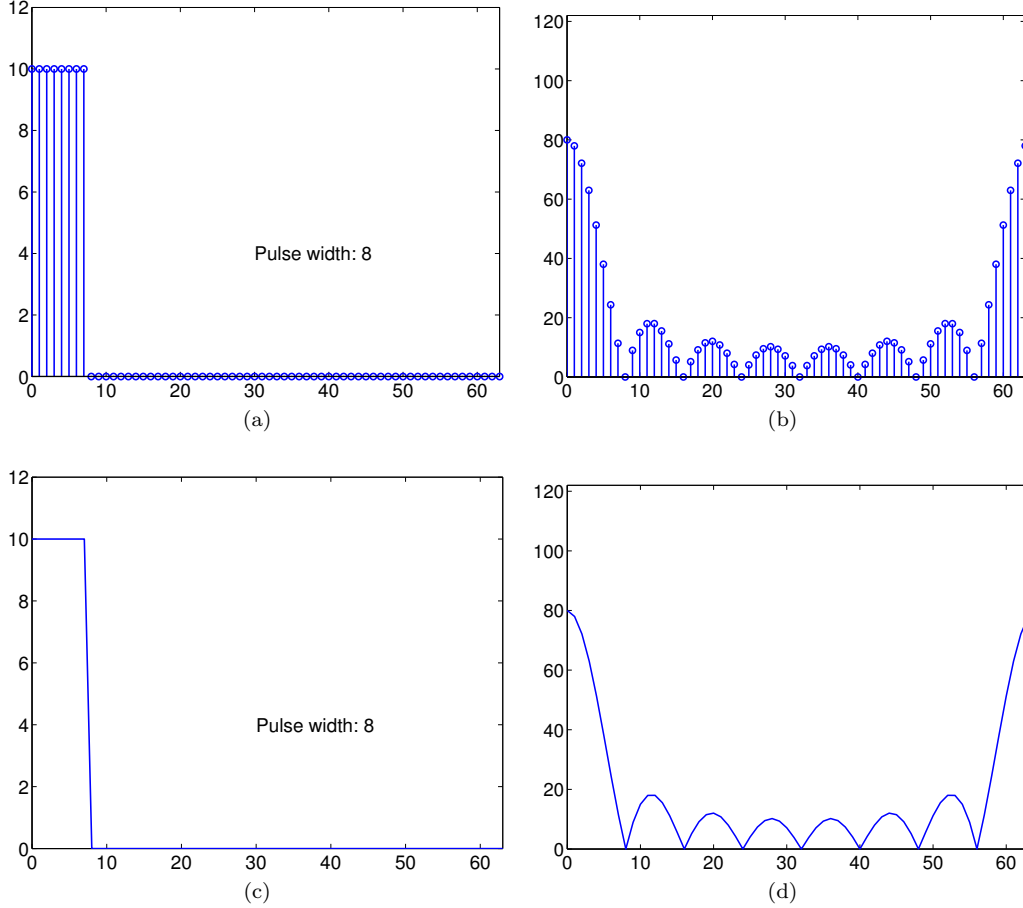


Figure A.1: Graphs of 64 samples of an 8-sample-wide discrete rectangular pulse (a) and the magnitude of the associated DFT (b), plotted with the `stem` command in MATLAB. The same two graphs are shown in (c) and (d), using the `plot` command.

For spatial sampling, the equivalent relationships (assuming the x -axis) are:

$$u_s = \frac{1}{\Delta x} \quad \text{and} \quad \Delta u = \frac{1}{M \Delta x} = \frac{u_s}{M} \quad (\text{A.9})$$

For temporal sampling, the value T_s is the time between samples, and for spatial sampling, Δx is the linear distance (along the x -axis) between samples. The values F_s and u_s are the respective sampling frequencies. The values Δf and Δu specify the frequency resolution of the DFT. For example, in the case of temporal sampling, the samples are spaced T_s seconds apart. If these are provided as input points to the DFT, then the output points from the DFT will be spaced Δf Hz apart. In the case of spatial sampling, if the samples are spaced Δx mm apart and are provided as input points to the DFT, then the output points from the DFT will be spaced Δu cycles/mm apart.

Some simple examples showing DFT results (via the `FFT` command in MATLAB) can be instructive. We will create the equivalent of a rect signal, where the total number of points is $M = 64$, all equal to zero except the first 8 points. This is shown in Fig. A.1(a), and the magnitude of the associated DFT is shown in Fig. A.1(b). Note the discrete nature of the data is made obvious by use of the MATLAB `stem` command, whereas the `plot` command draws a line that connects all the points, the latter of which can often provide better insight into the “shape” of the spectrum.

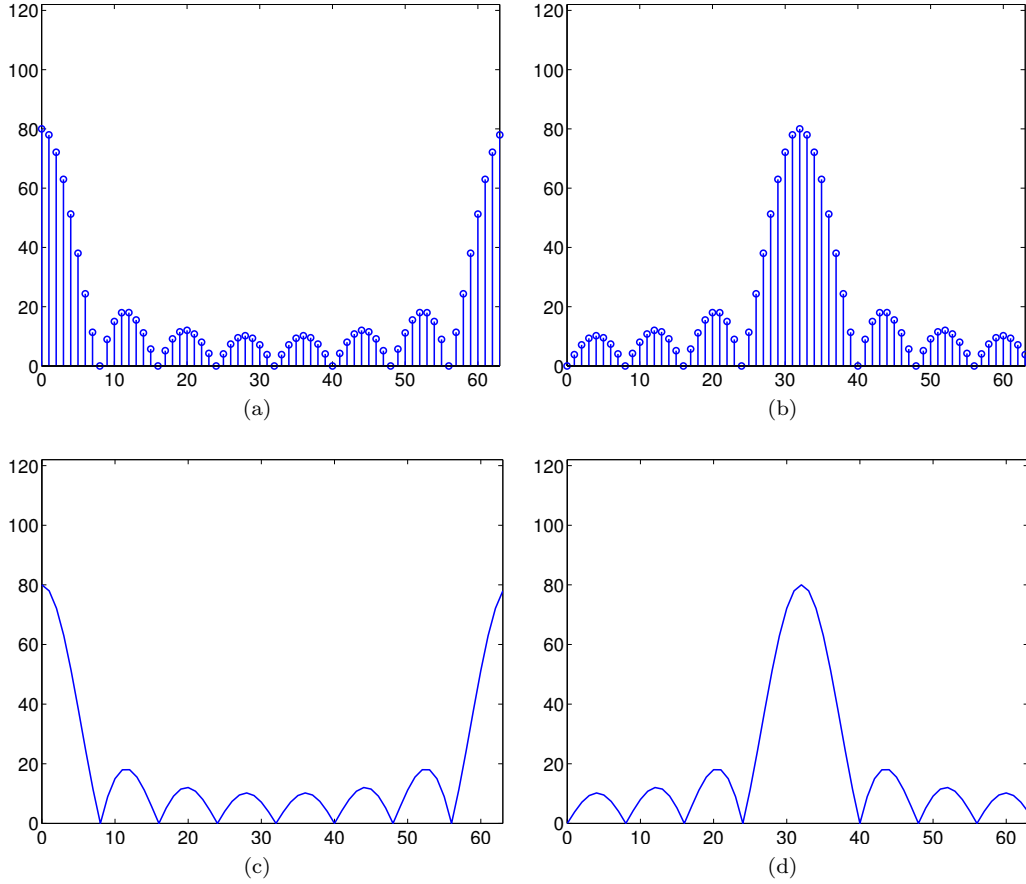


Figure A.2: The magnitude spectrum of the rectangular pulse shown in Fig. A.1. In (a) and (c), the natural ordering of the DFT output is shown. In (b) and (d), the “flipped” version is shown.

As expected from the earlier section on continuous FTs, a rect pulse having an amplitude A and a pulse width T has a spectrum in the shape of a sinc with a main lobe height of AT . But notice that the ordering of the spectrum values from a DFT may seem “flipped” compared to the plots shown for continuous FTs. This is because the normal output order from a DFT is: DC value first, then the positive frequency components increasing in frequency until the halfway point (where the frequency is equivalent to both $\pm F_s/2$), followed by the most negative frequency component and then “counting up” until the very last point is the least negative frequency component. This ordering is simply due to the way the DFT is calculated.

Some people prefer to reorder the output so that the DC point is in the middle, the negative frequencies on the left, and the positive frequencies are on the right, so that the spectrum better matches the spectra typically shown for continuous FTs. This can easily be accomplished; the two most common ways are:

1. multiply the input data by $(-1)^n$, where n is the sample number, just *before* taking the DFT; or
2. use the `fftshift` command in MATLAB on the DFT output, just *after* taking the DFT.

Use only one of the two methods; either one will “flip” the spectrum as desired. The first method can be used with any programming language; the second is for MATLAB only. As an example, Fig. A.2 shows the magnitude spectrum both without and with such a “flip.” Such a “flip”

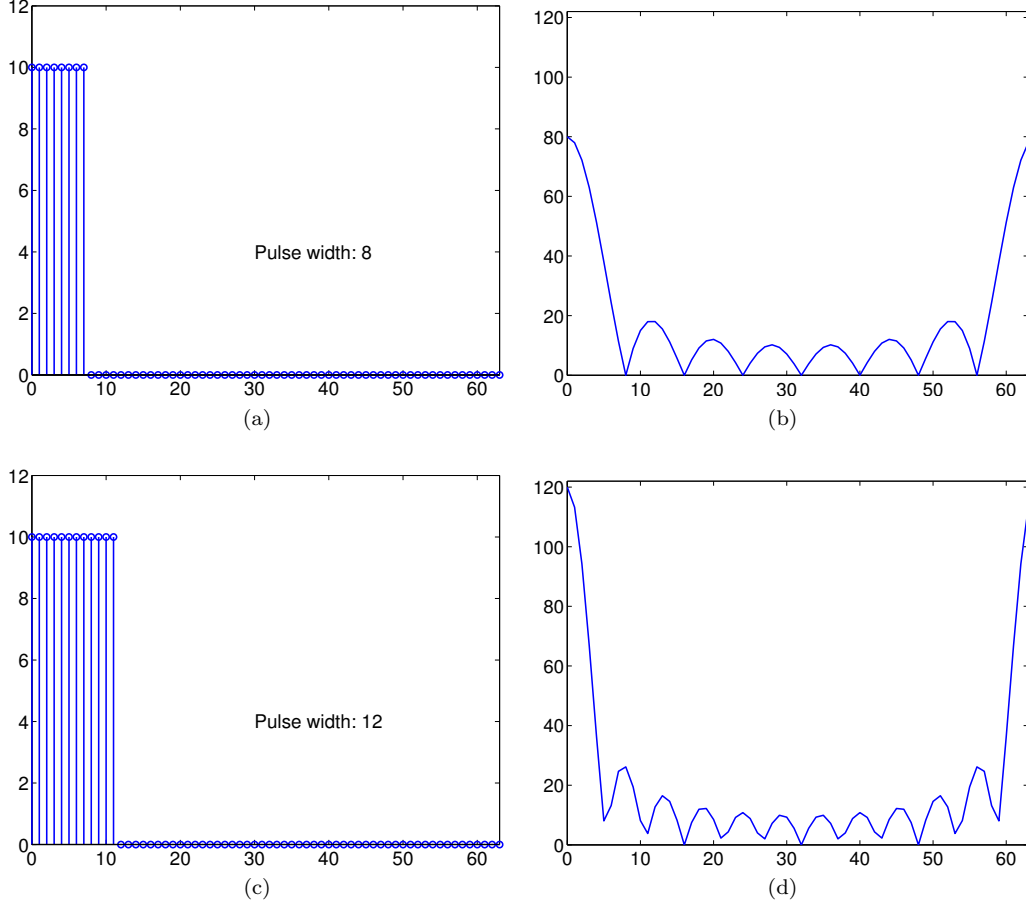


Figure A.3: Discrete rectangular pulses of width 8 and 12, and the magnitude of the associated DFTs.

is very common for 2-D spectra, as it helps most people to more easily interpret the spectral “image.”

Looking at Fig. A.1(a) or (c), another difference between continuous and discrete signals can be seen. Continuous signals (in the time or space domain) can be defined as centered about zero, and the FT of such a symmetric signal will typically have a fairly trivial phase response of zero (and π if negative terms are present in the spectrum). However, the first data point of a discrete signal always starts at $n = 0$; one cannot specify a discrete signal in “negative time” as one can when mathematically defining a continuous signal. That’s why the width 8 rectangular pulse in Fig. A.1(a) or (c) starts at $n = 0$ and ends at $n = 7$. The main ramification of this is that the DFT spectrum will always have a nontrivial phase term to reflect a “shift” compared to a zero-centered continuous signal. However, in the majority of the work with Fourier optics and MTF theory, only the magnitude spectrum is of interest. Only in certain situations is the phase term examined.

If one remembers the special ordering of the DFT output, and the presence of a nontrivial phase term (if phase is of interest), and the relationships given in Eq. (A.8) and Eq. (A.9), then the examples given for the continuous FT can be applied to the DFT. For example, compare two pulse widths for a rect function as shown in Fig. A.3. As seen earlier, a rect pulse having an amplitude A and a pulse width T has a spectrum in the shape of a sinc with a main lobe height of AT . But what is also evident in Fig. A.3 is the reciprocal spreading property: the

wider pulse width has a more narrow spectrum. Other properties of the FT apply as well to the DFT. Some adjustment is sometimes needed when reinterpreting continuous FT understanding for the DFT. For example, for the continuous FT of a width $t = T$ rect function, the “zeros” between the lobes of the sinc are spaced $f = 1/T$ apart. This is also true for the DFT, but if the horizontal axis of the spectrum is labeled not by frequency but just with the integer number of the output data point (which is often the case), then Eq. (A.8) comes in handy. You can see that a scaling factor of the number of data points M is needed, so that the “zeros” between the lobes of the sinc, in terms of the integer number of the output data points, will be spaced M/T apart. Looking at Fig. A.3, you can confirm that the “zeros” are spaced at $64/8 = 8$ for the width 8 rect, and the “zeros” are spaced at $64/12 = 5.33$ for the width 12 rect.

Some important things to keep in mind when comparing the DFT to the continuous FT include the following statements.

- The input is, by definition, discrete (i.e., sampled or created on a computer) not continuous.
- There is no such thing as symmetry about $t = 0$.
- You can only get zero phase by using some mathematical tricks.
- Changing the number of data samples by just one can change the result more than you might expect.
- The input data sequence supposedly repeats infinitely outside the given samples.
- The frequency axis for the continuous FT is continuous, from $-\infty$ to $+\infty$, whereas the frequency axis for the DFT is discrete (i.e., values exist only at certain points), and is bound to the finite range of $-F_s/2$ to $+F_s/2$, which means there is “warping.”
- Outside the range of $-F_s/2$ to $+F_s/2$, the DFT frequency spectrum repeats infinitely, with each “copy” spaced F_s apart.
- The convolution \Leftrightarrow multiplication duality is complicated by circular convolution if appropriate zero padding is not used.
- Other: The DFT exhibits *frequency leakage*, responds well to smoothing windows for the data, exhibits *frequency bias* when no smoothing window is used, and responds well to zero padding of the data to obtain higher *effective* frequency resolution.

None of this is true for the continuous FT. Space does not permit a detailed explanation of all these points, but nonetheless they are important for knowledgeable use of the DFT beyond simple examination of signal spectra. Like it or not, if you evaluate a FT on a computer, you are actually calculating a DFT. If more detail is needed, consult one of the references.

A.3 The 2-D Continuous Fourier Transform

Expanding the 1-D continuous FT to a 2-D continuous FT is straightforward. Using common spatial domain variables, the equations are:

$$F(u, v) = \int_{-\infty}^{\infty} \int_{-\infty}^{\infty} f(x, y) e^{-j2\pi(ux+vy)} dx dy \quad (\text{A.10})$$

$$f(x, y) = \int_{-\infty}^{\infty} \int_{-\infty}^{\infty} F(u, v) e^{j2\pi(ux+vy)} du dv. \quad (\text{A.11})$$

Time domain signals are typically 1-D, so when discussing 2-D functions the spatial domain is usually more appropriate.

Orthogonality of the axes make the 2-D FT separable into the product of two 1-D FTs in theory, and that is how many analyses are performed in practice. However, when analyzing digital cameras it is common to have an optical MTF which is separable in polar coordinates, and a sensor array MTF which is separable in rectangular coordinates. A combined MTF of optics and sensor is, strictly speaking, not separable in either coordinate system, but the error resulting from assuming separability is often rather small. Vollerhausen et al. provide a good treatment of this [41].

A.4 The 2-D Discrete Fourier Transform

When evaluating the Fourier transform of a 2-D signal or function on a computer, it is the DFT, not the continuous FT, that is calculated. Recall that the Fast Fourier Transform (FFT) is just a fast way to calculate the DFT; the DFT and FFT outputs are identical. The equations that define the 2-D DFT pair for spatial domain signals are:

$$F(u, v) = \sum_{x=0}^{M-1} \sum_{y=0}^{N-1} f(x, y) e^{-j2\pi(\frac{ux}{M} + \frac{vy}{N})} \quad (\text{A.12})$$

for $u = 0, 1, 2, \dots, M - 1$ and $v = 0, 1, 2, \dots, N - 1$

$$f(x, y) = \frac{1}{MN} \sum_{u=0}^{M-1} \sum_{v=0}^{N-1} F(u, v) e^{j2\pi(\frac{ux}{M} + \frac{vy}{N})} \quad (\text{A.13})$$

for $x = 0, 1, 2, \dots, M - 1$ and $y = 0, 1, 2, \dots, N - 1$

The frequency resolution in 2-D follows the same relationship as the 1-D case.

$$\Delta u = \frac{1}{M\Delta x} \quad \text{and} \quad \Delta v = \frac{1}{N\Delta y} \quad (\text{A.14})$$

Centering the DC point of the 2-D spectrum is accomplished in a similar fashion to the 1-D case. In any programming language, you can use

$$\text{DFT} \left\{ f(x, y)(-1)^{x+y} \right\} = F \left(u - \frac{M}{2}, v - \frac{N}{2} \right), \quad (\text{A.15})$$

or you can use the `fftshift` command in MATLAB on the DFT output.

The 1-D rect function already discussed is an important one in Fourier analysis, as is the 2-D version of the rect. The 2-D rect, in general, is rectangular rather than square, and is a useful model for various aspects of a sensor array in a digital camera. Another 2-D function, the circ, is a circularly symmetric “pulse” that is a useful model for various aspects of the optics used in a digital camera. Note that a 1-D circ would be indistinguishable from a 1-D rect, so the circ function is generally only defined in 2-D.

Since these two functions, the rect and the circ, are so valuable in applying Fourier analysis to digital cameras, an example of these functions and their respective magnitude spectra may be helpful. These are shown in Fig. A.4, where the peak values of the spectra have been normalized to unity.² The reciprocal spreading property is evident in Fig. A.4(a) and (b); the smaller direction of the rect is associated with a wider direction of the sinc.

This concludes the brief review of the Fourier transform.

²When plotting 2-D functions in MATLAB, commands such as `mesh` and `surf` are very handy.

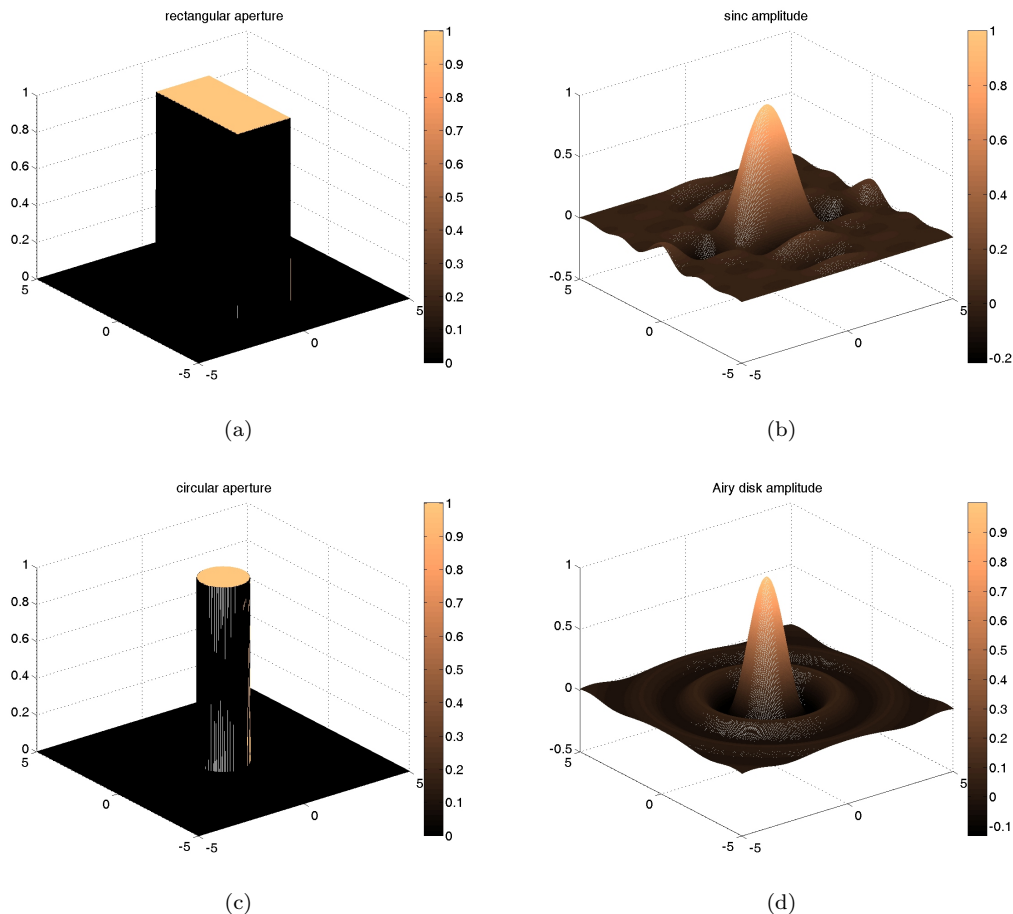


Figure A.4: A 2-D rect function is shown in (a), and the normalized magnitude of the associated 2-D DFT (a 2-D sinc function) is shown in (b). A 2-D circ function is shown in (c), and the normalized magnitude of the associated 2-D DFT (an Airy disc function) is shown in (d).

Appendix B

Review of Analog-to-Digital Conversion

IT is important to understand the process of analog-to-digital conversion (ADC) when using almost any digital device, including digital cameras. The end-to-end process involves three main steps: sampling, quantizing, and encoding. Most people seem to understand the ADC process best when explained for samples taken along one dimension (1-D) of a signal at regular time intervals (i.e., temporal sampling). It is then easier to adapt the same ideas to samples taken at regular points in space (i.e., spatial sampling), and then further extend the concept to 2-D spatial sampling. It is 2-D spatial sampling, along the rows and columns of the sensor array, which is most often of interest when analyzing digital cameras and imaging.

This appendix provides a brief overview of the basic analog-to-digital conversion process for those readers who can benefit from a top-level refresher. The discussion is conceptual and general in nature, rather than specifically describing any particular circuitry that performs the ADC conversion. For more details, the reader should consult references such as [83–85]

B.1 Sampling

Suppose we have a simple analog signal that varies in voltage as time progresses. The voltage at any instant in time can be any amplitude value (within the limits of the equipment); this is called *continuous in amplitude*. The signal voltage can be measured at any instant in time; this is called *continuous in time*. The original analog signal is thus continuous both in amplitude and in time, and this is depicted in Fig. B.1(a). At specific, regularly spaced instants in time shown in Fig. B.1(b), the value of the signal is obtained, resulting in the samples shown in Fig. B.1(c).

After sampling, the sampled signal is still continuous in amplitude, but no longer continuous in time. Since the samples only exist at discrete points in time, the sampled signal shown in Fig. B.1(c) is referred to as being *discrete in time*. A few points should be made about Fig. B.1.

The time interval between samples, shown as T_s in the figure, is called the *sample period*, and usually has the units of seconds. Every T_s seconds, a sample is obtained, and these are the only points in time at which the sampled signal exists. The *sample frequency*, a very useful value, is defined as $F_s = 1/T_s$, and has the units of hertz. Some data sheets use samples per second (or sps) as the units for sample frequency, although strictly speaking this is not correct since the units of T_s are not seconds per sample.

The sampling implied by Fig. B.1(b) is what is called *ideal sampling*, since the time during which a sample is taken is an impossibly short time. Thus the upward arrows in Fig. B.1(b) can be thought of as Dirac delta functions. In reality, taking a sample requires some finite length of time called a *sample aperture*, and if a detailed analysis is needed this may be taken into account using well-known methods. To protect against the signal amplitude changing much during the

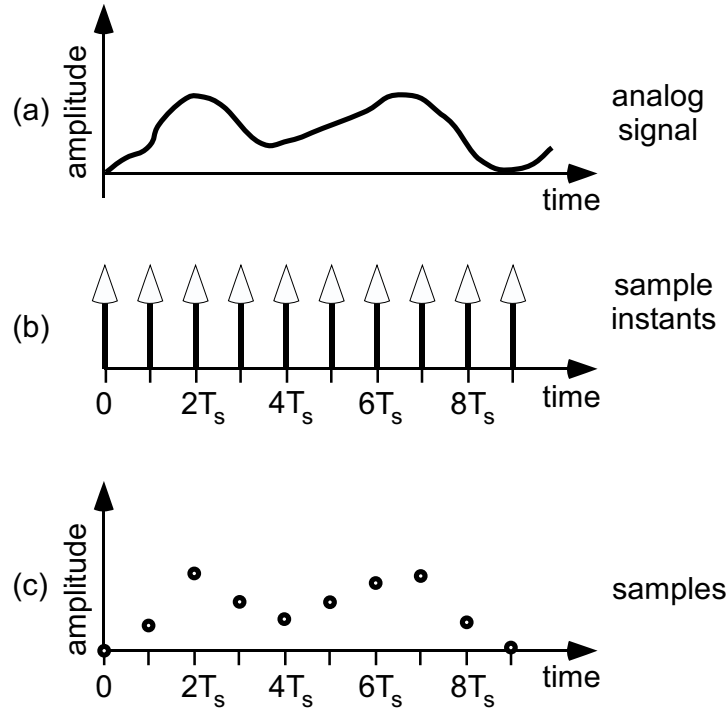


Figure B.1: The sampling process. The analog signal in (a) is sampled at points in time shown in (b), resulting in the sample values shown in (c). The sample period is T_s , and thus the sample frequency is $F_s = 1/T_s$.

sample aperture, a *sample and hold* circuit may be used to effectively “freeze” the sample value over the duration of the sample aperture. For the purposes of this discussion, we assume ideal sampling.

Looking at Fig. B.1, you can see that if the signal changed quickly between samples, those changes would be “missed” by the sampling process. Thus the sample period must be short enough to “catch” all the important variations in the signal amplitude. Another way of saying this is that we must sample “fast enough” to catch all the signal changes. To show the effect of not sampling fast enough, Fig. B.2 shows two sinusoids that are sampled with the same sample period.

The top signal in Fig. B.2 is sampled fast enough to catch all the changes in the signal, and the signal that can be reconstructed just from the samples is essentially the same as the original signal. The bottom signal in Fig. B.2, on the other hand, is higher in frequency and is not sampled fast enough to catch all the variations. An attempt to reconstruct the signal, based only upon the samples, results in a signal having much lower frequency than the original. This is an example of the phenomenon called *aliasing*. Once aliasing has occurred, it cannot be “undone” except in very rare situations.¹

A frequency-domain approach is another way to examine the concept of sampling and aliasing that some people find more intuitive. The condition of making the sample period short enough to catch all the changes in the signal is the same as saying that the sample frequency must be high enough to account for all the important frequencies in the spectrum of the signal. This concept is demonstrated in Fig. B.3.

The magnitude spectrum of the original analog signal is shown in Fig. B.3(a); the highest frequency present in the original signal is shown as f_h . The act of sampling a signal results in

¹A quadrature mirror filter pair when used in a two-band filter bank for subband coding is one of those rare situations when aliasing can be cancelled out.

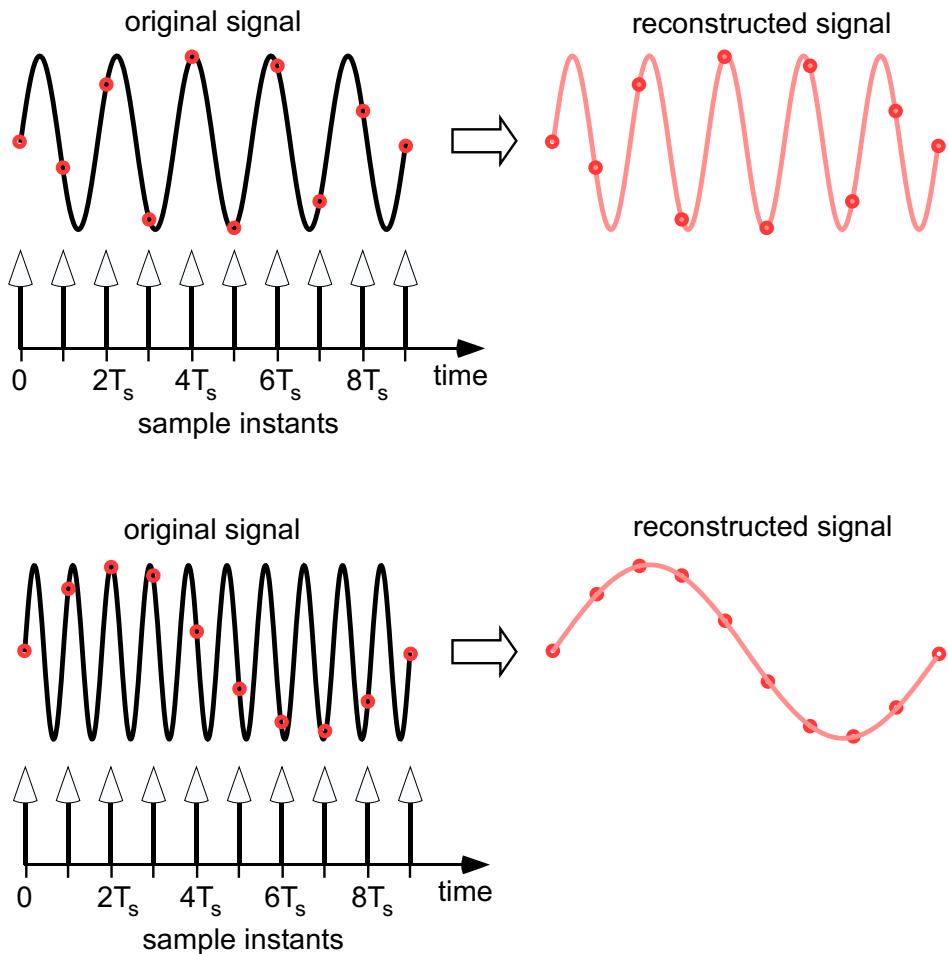


Figure B.2: The sampling process shown for two different frequency sinusoids. The top signal is sampled fast enough, but the bottom signal is not.

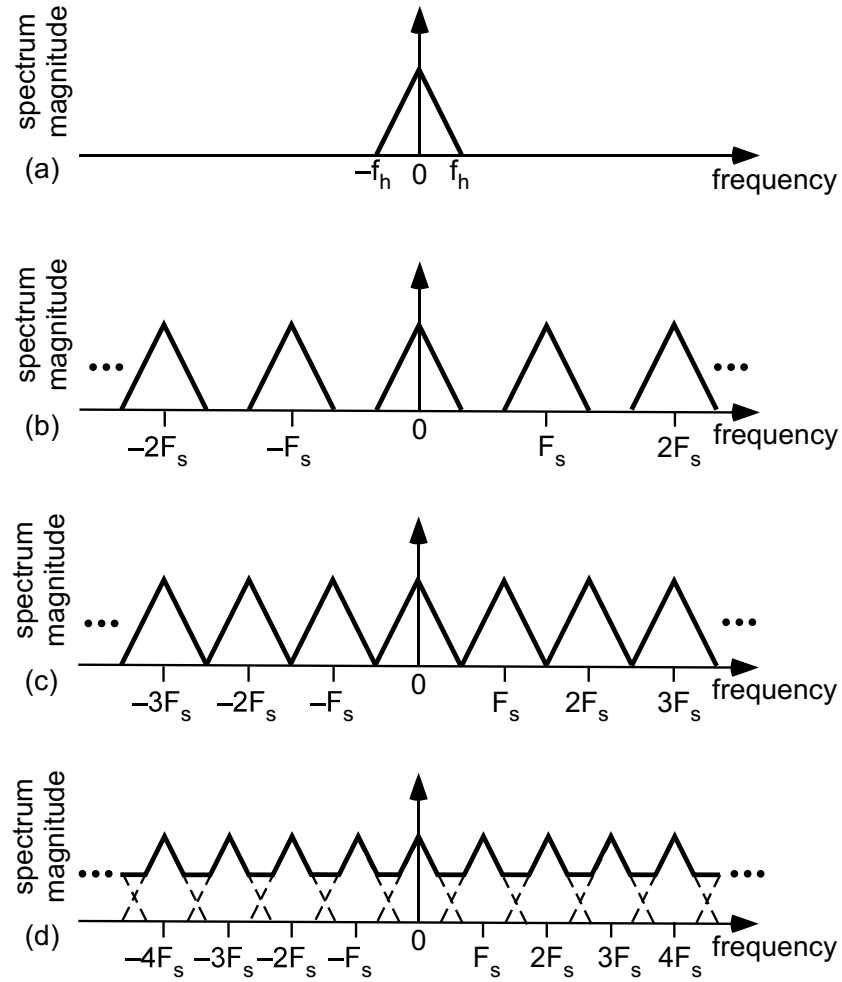


Figure B.3: The sampling process in the frequency domain. The magnitude spectrum of the original signal is shown in (a); the highest frequency present in the signal is f_h . The frequency domain result is shown for over sampling (b), critically sampling (c), and under sampling (d).

an infinite number of “copies” of the original spectrum appearing, with the copies spaced apart by a distance of F_s . This result is shown for over sampling (when $F_s > 2f_h$) in Fig. B.3(b), critically sampling (when $F_s = 2f_h$) in Fig. B.3(c), and under sampling (when $F_s < 2f_h$) in Fig. B.3(d). Note how distorted the spectrum becomes in Fig. B.3(d), when F_s is not high enough. Frequencies from adjacent copies of the spectrum overlap and mix together, and once mixed cannot be “unmixed.” This a frequency domain way to explain the same *aliasing* concept that was shown in Fig. B.2.

When aliasing occurs, some frequencies in the original signal will appear to be lower frequency signals. If the sampling frequency is F_s , and a particular “true” frequency in the original signal is f_o , then if $F_s/2 < f_o < 3F_s/2$, the aliased version of that frequency, what we’ll call f_a , will be

$$f_a = \frac{1}{2}F_s - \left(f_o - \frac{1}{2}F_s \right) = F_s - f_o. \quad (\text{B.1})$$

Note that if $f_o = F_s$ (or any integer multiple of F_s), then $f_a = 0$. From Eq. B.1, it appears that as f_o increases above F_s will become negative.² But recall that for real signals, we always have

²This is the cause in movies and TV of car and wagon wheels sometimes seeming to be spinning “backwards.”

positive and negative pairs of frequency components. Therefore, in the case of f_o just exceeding F_s , the negative member of the pair will have aliased “up” into the positive side of the frequency axis! A quick sketch can help you verify that for yourself. The aliased frequency will always show up in the range of $-F_s/2$ to $+F_s/2$.

What if f_o is even higher than $3F_s/2$? It’s straightforward to show that if $3F_s/2 < f_o < 5F_s/2$, then the aliased frequency f_a will show up at $f_a = 2F_s - f_o$. Continuing the pattern further, if $5F_s/2 < f_o < 7F_s/2$, then the aliased frequency f_a will be $f_a = 3F_s - f_o$. And so on...

The phenomenon of aliasing can be avoided by adhering to the well-known *sampling theorem*: ensure the sampling frequency is equal to or greater than two times the highest frequency in the signal being sampled (i.e., $F_s \geq 2f_h$).³ Historically, the sampling theorem is attributed to the works of Claude Shannon and Harry Nyquist (who worked together at Bell Laboratories in the USA), but was also independently discovered by John Whittaker (in the UK), and by Vladimir Kotelnikov (in Russia), and often bears one or more of these names in the literature.

The result of trying to recover the original signal (called reconstruction), by using an ideal low pass filter on the sampled signal, is shown in Fig. B.4. Note that the correct spectrum is recovered for the oversampled and critically sampled cases, but only a distorted spectrum (due to aliasing) is possible for the undersampled case. Of course, ideal low pass filters such as the one shown at the top of Fig. B.4 are unattainable in practice. Real-world filters do not have a vertical “brick wall” transition between the passband frequencies and the rejected frequencies. For a more realistic low pass filter to properly recover the original spectrum, the oversampled case is recommended.

B.2 Quantizing

By the end of the ADC process, we will need to be able to represent each sample as a binary value, each having the same number of bits, and this means we can’t allow the samples to remain continuous in amplitude. Samples that are continuous in amplitude would need an infinite number of bits to represent the infinite number of possible amplitude values. Therefore, we have to restrict the samples to a finite number of allowed amplitude values, called *quantization levels*. The number of bits n that we define for representing each of the samples determines the number of quantization levels k , such that $k = 2^n$. For example, if $n = 8$, then there are $k = 256$ quantization levels to which the sample amplitudes will be restricted. In the interests of clarity, we will use an example with only 8 quantization levels, which implies we will eventually use $n = 3$ bits per sample. This is shown in Fig. B.5.

The red circular markers shown in Fig. B.5(b) are restricted to the 8 allowed quantization levels. Note that a rounding quantizer is assumed, so that if the true sample value is located at a point greater than halfway between two levels, the quantized value will be the higher level.⁴ At this point in the ADC process, the samples are now discrete in both amplitude and time. To simplify the notation, we follow the common convention of showing the horizontal axis in Fig. B.5(b) not as a time axis, but rather an axis that labels each sample by its number in the sequence of samples.

It’s important to note that the quantization process results in quantized samples whose values are not quite the same as many of the original samples. For example, the true value of sample 3 in Fig. B.5(b) is between quantization levels 1 and 2, yet the quantized sample is assigned the value of quantization level 2. The difference between the true value of sample 3 and the quantized value of sample 3 is called the *quantization error*; this error manifests itself as noise added to

³This assumes what is called “low-pass sampling,” where the signal to be sampled exists from DC (or a very low frequency) up to some upper frequency f_h . There is also the case of “bandpass sampling” where aliasing can either be avoided or be taken advantage of using specific sample frequencies where $F_s < 2f_h$. Some communications systems, such as certain software defined radio designs, often use this technique.

⁴There are also truncating quantizers, that always force the quantized value to nearest lower quantization level.

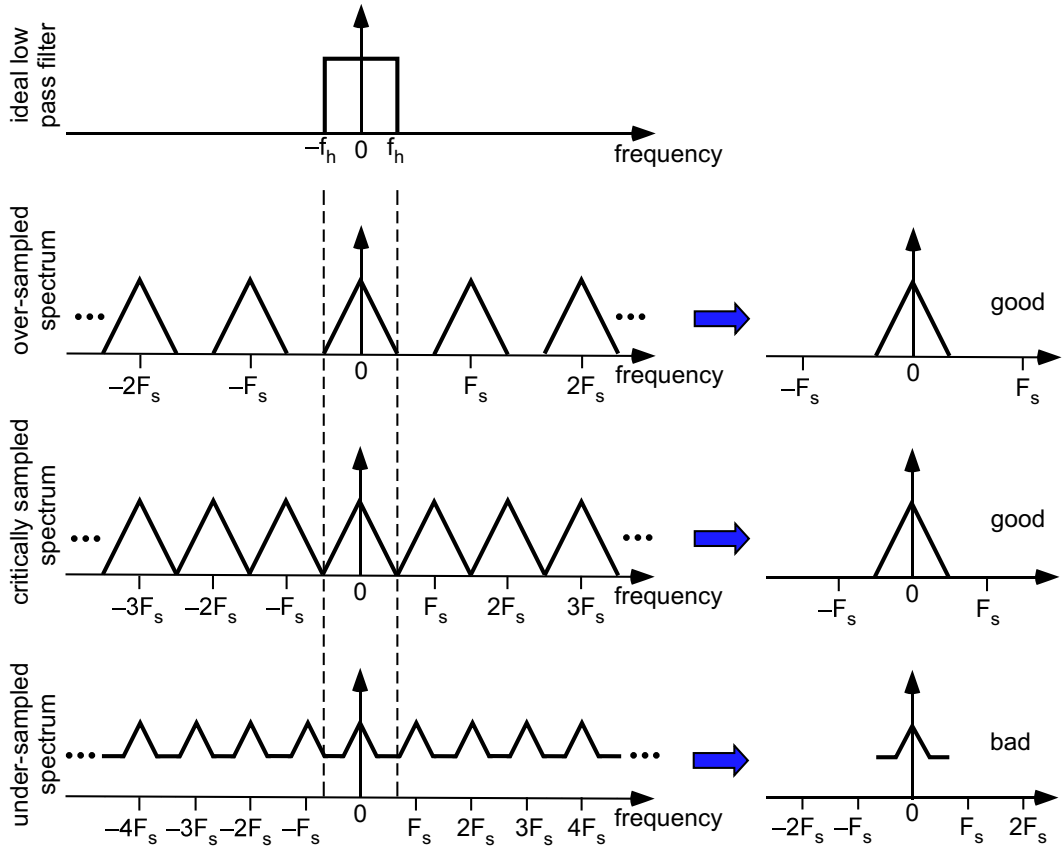


Figure B.4: Reconstruction of a sampled signal using a low pass filter, shown in the frequency domain. The highest frequency present in the magnitude spectrum of the original analog signal was f_h , which is used as the cutoff frequency of the ideal low pass filter shown at the top. The frequency domain result is shown for over sampling, critically sampling, and under sampling. Aliasing is evident in the under-sampled case.

the signal as part of the ADC process. How much noise? We skip the relatively straightforward derivation in the interests of brevity, and show only the result [83]. For an analog-to-digital converter (ADC) that takes n -bit samples, it can be shown that the signal-to-quantization-noise ratio, in decibels, is

$$\text{SQNR}_{\text{dB}} = 6.02n + 10.79 - 20 \log_{10} \left(\frac{R_{\text{FS}}}{\sigma_x} \right), \quad (\text{B.2})$$

where R_{FS} is the full-scale voltage range of the ADC (which is typically a fixed value), and σ_x is the standard deviation of the input signal (in volts), representing the square root of the signal power, or variance σ_x^2 , in watts.⁵ SQNR_{dB} as shown is a power ratio; that is, it represents the ratio of the signal power to the quantization noise power, in decibels. Note that certain signal processing techniques, such as noise shaping, can result in a somewhat higher SQNR_{dB} than what is predicted by Eq. (B.2).

A higher value of SQNR_{dB} is better (less noise, more signal), therefore the more bits per sample the less quantization noise will be introduced in the ADC process for a given signal power. A handy rule of thumb that is obvious from Eq. (B.2) is that each additional bit per sample results in approximately a 6 dB increase in the theoretical signal-to-quantization-noise

⁵For example, the standard deviation of a sinusoid is just its RMS value.

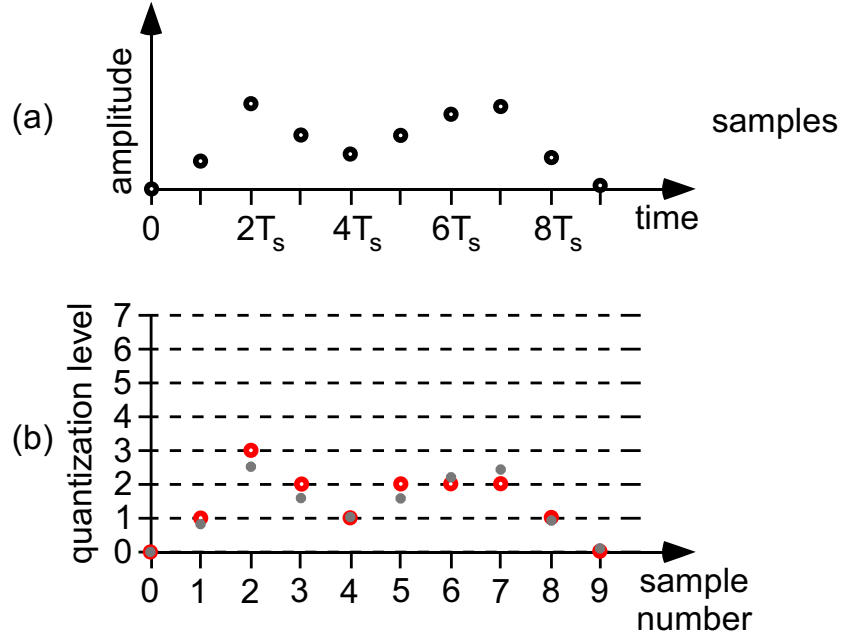


Figure B.5: The quantization process. The continuous amplitude samples shown in Fig. B.1(c) are shown above in (a). In (b), the small gray markers are the original samples, and the larger red markers are the quantized samples that are restricted to the 8 quantization levels shown. A rounding quantizer is assumed.

ratio. Keep in mind that the SQNR is just one of multiple contributors to the overall signal-to-noise (SNR) ratio.

The resolution of the ADC is closely tied to the $k = 2^n$ quantization levels, in that the full-scale voltage range of the ADC, abbreviated R_{FS} , is divided up into k possible voltage levels. Thus the voltage resolution is $\delta = R_{FS}/2^n$. Using the $n = 3$ bit, $k = 8$ quantization levels shown in Fig. B.5(b) as an example, suppose the minimum voltage value at quantization level 0 is -1 V, and the maximum voltage value at quantization level 7 is $+1$ V, then $R_{FS} = 2$ V and the resolution is $\delta = 2/8 = 250$ mV. This can be seen more clearly in Fig. B.6. The resolution δ is the smallest amount of voltage change in the input that is guaranteed to produce a change in the binary number that represents the sample; changes in the input voltage of less than δ will go undetected in the ADC process. Note that in certain cases, this may deviate by a factor of two at either extreme of R_{FS} , as shown in Fig. B.6(b). For reasons that will become evident, δ is often called the LSB resolution of the ADC, where LSB stands for least significant bit. Note that it is also common to express resolution of an ADC just as the number of bits per sample n , which is independent of R_{FS} . Another value that may be of interest is the effective number of bits (ENOB), which is less than or equal to n . An increase of one effective bit of resolution will increase the overall SNR of the digitized signal by 6 dB, assuming the resolution is limited by the ADC process.

If the LSB voltage resolution needs to be smaller for a given application (so that smaller voltage changes can be detected), either the full-scale voltage range of the ADC must be reduced, or the number of bits per sample must be increased, or both. However, R_{FS} is usually constrained by the minimum and maximum anticipated values of the input signal. The number of bits per sample is usually dictated by the particular ADC chip selected.

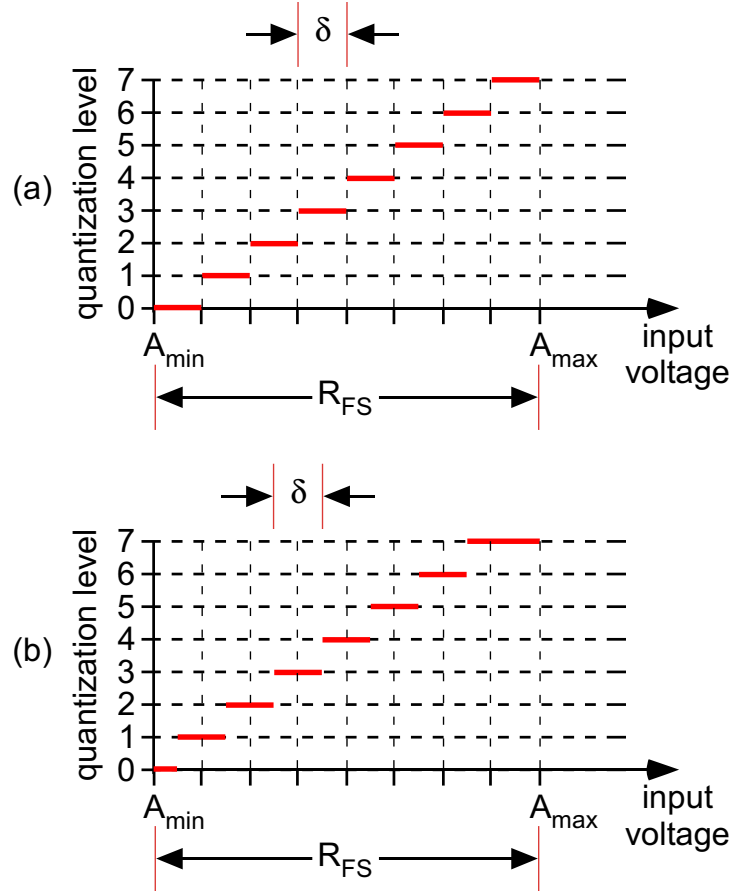


Figure B.6: The voltage resolution δ of the quantization process for a 3-bit ADC. A truncating quantizer is implied by (a), whereas a rounding quantizer is implied by (b).

B.3 Encoding

After the sampling step, the analog signal is discrete in time. After the quantization step, the analog signal is also discrete in amplitude. The final step is to assign a unique binary code to each quantization level, so that each sample can be assigned the appropriate binary number.

The simplest case is when the quantization levels represent values from zero to some maximum positive voltage. In this situation, the most common code consists of unsigned binary integers. If the quantization levels must represent both negative and positive numbers, the most common code consists of signed binary integers using the two's complement format.⁶ For the case of positive and negative numbers, the labels for the quantization levels (such as 0 to 7 as shown in Fig. B.5(b) on the left) are often given positive and negative values to make the encoding more obvious. Both of these encoding schemes are shown in Table B.1 for a 3-bit per sample ADC. Note that the two's complement method results in a slight asymmetry between the positive and negative extremes of the range, since zero is considered positive.

For general purpose signal processing, the signed method is more common, since in general signals will have both positive and negative values. For digital imaging and image processing, the unsigned method is more common, since the samples typically represent light intensity values,

⁶The two's complement of a binary number can be found by complementing every bit then adding one. Another method is to start with the LSB and, working to the left, keep the value of all the bits including the first 1 encountered, then complement all the remaining bits to the left.

Table B.1: An example of binary codes assigned to quantization levels for the encoding step of a 3-bit per sample ADC process.

unsigned quantization level	unsigned binary integer	signed quantization level	signed binary integer
7	111	3	011
6	110	2	010
5	101	1	001
4	100	0	000
3	011	-1	111
2	010	-2	110
1	001	-3	101
0	000	-4	100

which are always nonnegative.

As an example, refer to Fig. B.5 and the unsigned (left) half of Table B.1. The sequence of 10 quantized samples shown in Fig. B.5(b), referred to only by the associated quantization level, would be: 0, 1, 3, 2, 1, 2, 2, 2, 1, 0. Using the unsigned binary integer encoding of Table B.1, this becomes: 000, 001, 011, 010, 001, 010, 010, 010, 001, 000. It is this last sequence, the binary numbers, that is the output of the ADC process.

The three steps described (sampling, quantizing, and encoding) are presented as separate discussions for better clarity of the overall explanation. In the actual circuitry inside an ADC chip, the implementation of these steps is generally not nearly so separated. There are also many different ways to perform the ADC function, such as flash (also called parallel or direct conversion), successive-approximation, integrating (either single-slope or dual-slope), sigma-delta (also called delta-sigma), and others. Each type of ADC has its own tradeoffs of performance and price, but that discussion is beyond the scope of this Appendix.

B.4 Extending the Concepts to 2-D Spatial Sampling

Quantizing and encoding are essentially the same for 1-D or 2-D applications of the analog-to-digital conversion process. It is only how sampling is accomplished that changes. The discussion up to now has assumed that samples are taken at regular intervals of time, which is more formally called *temporal sampling*. If we sample a single 2-D image that is frozen in time, we typically sample at regular intervals in space across the rows and columns of an arbitrary rectangular coordinate system. Sampling at regular intervals in space is called *spatial sampling*, and if we sample both rows and columns, it is 2-D spatial sampling. This is the type of sampling accomplished by the sensor array in a digital camera. If the images that are sampled come from a time sequence of images, such as with a video stream, then we are performing both temporal and spatial sampling.

In spatial sampling, the units of the sample period are typically linear units (such as millimeters) or angular units (such as milliradians). Likewise, the units of spatial frequency are cycles per mm or cycles per mrad. Other than the difference in units, all the concepts discussed in this appendix apply to spatial sampling just the same as they do for temporal sampling. To avoid aliasing, at least two samples per period are needed. This is another way of saying that the spatial sampling frequency must be at least twice the frequency of the pattern being sampled. Note that if the distance between sample points along the x -axis is different than the distance between sample points along the y -axis, then the sample frequency will be different in those two directions.

If an image is sampled in such a way that aliasing occurs, periodic patterns will show up as if they are lower in spatial frequency than they really are. For example, suppose we digitize the image of a horizontally-varying sinusoidal pattern (the pattern is constant vertically), as shown in Fig. B.7. This artificial pattern was chosen to simplify the discussion. Assume the sensor was a 128×128 array of “pixels” that spatially sampled the image. The axis convention used here is one that is common in image processing, where (x, y) equates to the (row, column) convention of linear algebra. This means that x is the vertical axis, y is the horizontal axis, and the origin is in the upper left corner.

In Fig. B.7(a), the period of the sinusoid is 16 pixels, and the image correctly shows 8 cycles of the sinusoidal pattern across the image width. In Fig. B.7(b), the period of the sinusoid is 2 pixels, and the image correctly shows 64 cycles of the pattern across the image width. At 2 samples per period, this is the highest frequency pattern that can be imaged without aliasing. In Fig. B.7(c), the period of the sinusoid is 0.75 pixels, and due to aliasing the image does not show the correct 171 cycles of the sinusoidal pattern across the image width. In Fig. B.7(d), the period of the sinusoid is 0.08 pixels, and due to aliasing the image does not show the correct 1,600 cycles of the sinusoidal pattern across the image width. Notice that aliasing results in an image displayed in which the apparent spatial frequency of the pattern is lower than reality.

Since most images are not truly bandlimited, patterns with frequencies higher than twice the spatial sampling frequency often are present. Thus aliasing often occurs in real-world images. This may or may not be objectionable, depending upon the specific application. What is most important is for the user to be aware of the concepts covered in this Appendix, and how they may affect the validity of any image data.

The reader may wonder about how many bits per sample (often called bits per pixel) are typical for a digital camera. While in a standard “true color” image, each of the red, green, and blue image planes use 8-bits per pixel for a total of 24-bits per pixel, that is *not* the number of bits for the ADC. The 8-bits per color plane comes after considerable processing of the RAW image data by the electronics inside the camera. The actual ADCs used by the FPA sensor chip are commonly 12 or 14 bits per pixel, and unless RAW data is specifically selected by the user this is most often intentionally reduced (again, by the electronics inside the camera) to 8-bits per pixel to be compatible with the JPEG compression standard. Refer to your camera’s user guide for specific details.

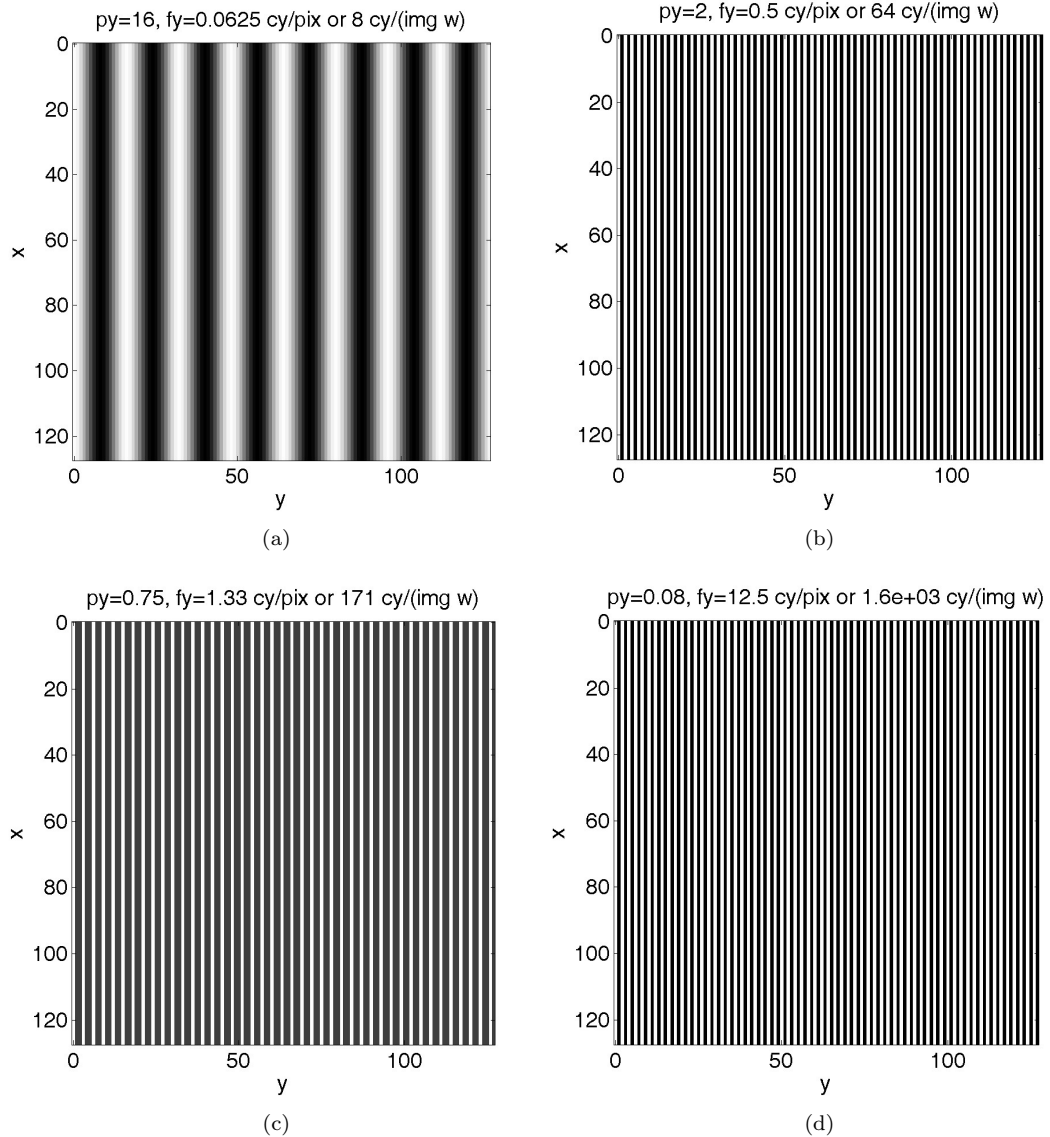


Figure B.7: Simulated result of spatially sampling different sinusoidal patterns with a 128×128 sensor array. The horizontal period of the pattern was (a) 16 pixels, (b) 2 pixels, (c) 0.75 pixels, and (d) 0.08 pixels. Aliasing is visible in (c) and (d).

Appendix C

Example MATLAB programs

THIS appendix provides a small collection of MATLAB programs that demonstrates how various useful calculations, simulations, and analyses associated with cameras and imaging systems can be performed, and how many of the figure plots in this book were created. Some speed optimizations for MATLAB have not been used in an attempt to make the code more understandable.

Listing C.1: Calculates depth of field (DOF).

```
1 function DOF=dof_calc(f,N,c,so)
2 % Calulates hyperfocal distance and depth of field
3 %
4 % Input is focal length, f-number, CoC, and focus distance.
5 % CoC for 35 mm camera is 0.029 mm,
6 % for Canon APS-C is 0.018 mm, etc.
7 %
8 % Copyright 2013 Cameron H.G. Wright
9 %
10 % remove semicolon to print hyperfocal distance to the screen
11 H=f^2/(N*c) + f ;
12
13 if so >= H
14     DOF=inf;
15 else
16     DOF=(2*H*so^2)/(H^2 - so^2);
17 end
18
19 % remove semicolon to print DOF distance to the screen
20 DOF;
21
return
```

Listing C.2: Calculates field of view (FOV).

```
1 function fov_calc(H,V,f,so)
2 % Calulates field of view
3 %
4 % Input is horizontal and vertical sensor dimensions,
5 % lens focal length, and focus distance.
6 %
7 %
```

```

% Copyright 2013 Cameron H.G. Wright
9
11 % calculate si
11 si=1/((1/f)-(1/so));
13 % calculate angular FOV
14 alphaH=2*atan(H/(2*si));
15 alphaV=2*atan(V/(2*si));
17 % convert to degrees
18 aHd=alphaH*180/pi;
19 aVd=alphaV*180/pi;
21 % calculate linear FOV at so
22 FOVh=alphaH*so;
23 FOVv=alphaV*so;
25 str1=sprintf('%s\n', ' radians degrees linear');
26 str2=sprintf('Horizontal FOV: %g %g %g\n', alphaH,aHd,FOVh);
27 str3=sprintf('Vertical FOV: %g %g %g\n', alphaV,aVd,FOVv);
29 disp([str1 str2 str3])
31 return

```

Listing C.3: Calculates PSF and MTF of special apertures.

```

function mtf_special()
1 % creates plots of the MTF for various aperture geometries
2 % starts with circ, then goes on to annular rings and such
3 %
4 % includes functions ip_dispsc() and gaussian() in this file
5 % for portability purposes
6 %
7 % copyright (c) 2013 Cameron H. G. Wright
8

10 XX=3.24; % max extent of spatial domain coordinates
11 x=-XX:0.01:XX; % vector for spatial domain range
12 xn=x/XX; % normalized vector for easy plotting of spatial
13 % frequencies
14 N=length(x);
15 k=0:N-1; % integer vector for plotting purposes only
16 x0=(N+1)/2; % index in vector x where zero is located
17 y=x;
18 x2=x.^2; % precalculate for radii
19 y2=x2; % precalculated for radii
20 r0=XX/2; % largest radius I'll use for circular apertures
21
22 % for rectangular symmetry, create X and Y meshgrids
23 [X1,Y1]=meshgrid(x);
24

26 % for circular symmetry, pre-build radii--saves a lot of CPU time

```

```

r=zeros(N); % preallocates an NxN matrix of zeros
28 for i=1:N
    for j=1:N
        r(i,j)=sqrt(x2(i) + y2(j)); % build matrix of radii
    end
32 end

34 % define indices for a diagonal line from ctr to corner
% used for a certain plot later
36 pd=find(X1>=0 & Y1>=0 & X1==Y1);
xd=r(pd);

38 % circular aperture
40 a1=zeros(N);
p=find(r<r0); % p contains all the indices where the test is true
42 a1(p)=1;

44 % note for PSF and MTF, use fftshift to recenter the FFT result
psf1=(abs(fftshift(fft2(a1))).^2); % calculate PSF
46 psf1=psf1/max(max(psf1)); % normalize the PSF

48 mtf1=(abs(fftshift(fft2(psf1)))); % calculate the MTF
mtf1=mtf1/max(max(mtf1)); % normalize the MTF
50

52 % annular ring, r=0.25*r0, area 16% blocked, 84% open
a2=zeros(N);
p=find(r<r0*0.25);
54 a2(p)=1;
a2sv=a2; % save this for later
56 a2=a1-a2;

58 psf2=(abs(fftshift(fft2(a2))).^2);
psf2=psf2/max(max(psf2)); % normalize
60

62 mtf2=(abs(fftshift(fft2(psf2)))); % calculate the MTF
mtf2=mtf2/max(max(mtf2)); % normalize

64 % annular ring, r=0.5*r0, area 25% blocked, 75% open
a3=zeros(N);
66 p=find(r<r0*0.5);
a3(p)=1;
68 a3sv=a3; % save this for later
a3=a1-a3;
70

72 psf3=(abs(fftshift(fft2(a3))).^2);
psf3=psf3/max(max(psf3)); % normalize

74 mtf3=(abs(fftshift(fft2(psf3)))); % calculate the MTF
mtf3=mtf3/max(max(mtf3)); % normalize
76

78 % annular ring, r=0.75*r0, area 56% blocked, 44% open
a4=zeros(N);
p=find(r<r0*0.75);

```

```

80 a4(p)=1;
a4=a1-a4;

82 psf4=(abs(fftshift(fft2(a4))).^2);
84 psf4=psf4/max(max(psf4)); % normalize

86 mtf4=(abs(fftshift(fft2(psf4)))); 
mtf4=mtf4/max(max(mtf4)); % normalize

88 % annular ring, r=0.95*r0, area 90% blocked, 10% open
90 a5=zeros(N);
p=find(r<r0*0.95);
92 a5(p)=1;
a5=a1-a5;

94 psf5=(abs(fftshift(fft2(a5))).^2);
96 psf5=psf5/max(max(psf5)); % normalize

98 mtf5=(abs(fftshift(fft2(psf5)))); 
mtf5=mtf5/max(max(mtf5)); % normalize

100 % square inside a circle
102 a6=zeros(N);
p=find(abs(X1) < XX/4 & abs(Y1) < XX/4);
104 a6(p)=1;
a6=a1-a6;

106 psf6=(abs(fftshift(fft2(a6))).^2);
108 psf6=psf6/max(max(psf6)); % normalize

110 mtf6=(abs(fftshift(fft2(psf6)))); 
mtf6=mtf6/max(max(mtf6)); % normalize

112 % a rectangular aperture
114 a0=zeros(N);
p=find(abs(X1) < XX/4 & abs(Y1) < XX/2);
116 a0(p)=1;

118 psf0=(abs(fftshift(fft2(a0))).^2);
psf0=psf0/max(max(psf0)); % normalize

120 mtf0=(abs(fftshift(fft2(psf0)))); 
mtf0=mtf0/max(max(mtf0)); % normalize

124 % two slits
a7=zeros(N);
126 p=find(abs(X1) < XX/8 & abs(Y1) < XX/2);
a7(p)=1;
128 a7=a0-a7;

130 psf7=(abs(fftshift(fft2(a7))).^2);
psf7=psf7/max(max(psf7)); % normalize
132

```

```

134 mtf7=(abs(fftshift(fft2(psf7))));  

134 mtf7=mtf7/max(max(mtf7)); % normalize  
  

136 % ring inside a ring  

136 a8=zeros(N);  

138 a8=a4+a2sv;  
  

140 psf8=(abs(fftshift(fft2(a8))).^2);  

140 psf8=psf8/max(max(psf8)); % normalize  
  

142 mtf8=(abs(fftshift(fft2(psf8))));  

144 mtf8=mtf8/max(max(mtf8)); % normalize  
  

146 % a Gaussian aperture for apodization, but chop to equal aperture a10  

146 % dimensions  

148 sd=0.25; mn=0;  

148 a9=gaussian(r,mn,sd);  

150 a9=a9/max(max(a9)); % set peak back up to 1 if needed, depends on sd  

150 a9=a9.*a3sv; % chope to diameter used for a10  
  

152 psf9=(abs(fftshift(fft2(a9))).^2);  

154 psf9=psf9/max(max(psf9)); % normalize  
  

156 mtf9=(abs(fftshift(fft2(psf9))));  

156 mtf9=mtf9/max(max(mtf9)); % normalize  
  

158 % small circular aperure  

160 a10=a3sv;  
  

162 psf10=(abs(fftshift(fft2(a10))).^2);  

162 psf10=psf10/max(max(psf10)); % normalize  
  

164 mtf10=(abs(fftshift(fft2(psf10))));  

166 mtf10=mtf10/max(max(mtf10)); % normalize  
  

168 % figure plotting code  

170 % close open figures, intialize counter  

172 close all;  
  

174 % To hardcode the font size globally, use:  

174 set(0,'DefaultAxesFontSize',24);  

176 set(0,'DefaultTextFontSize',24);  

176 set(0,'DefaultLineWidth',4)  
  

178 % set values to use large figure windows  

180 scrsz = get(0,'ScreenSize'); % get the screen size  

180 % Vista and Win7 have a 31 pixel task bar at bottom  

182 Los=10; % left offset  

182 Bos=55; % bottom offset  

184 Ros=20; % right offset  

184 Tos=145; % top ofset

```

```

186 FigPos=[scrsz(1)+Los scrsz(2)+Bos scrsz(3)-Ros scrsz(4)-Tos];
188 figure(1)
set(gcf,'Position',FigPos,'visible','off')
set(1,'DefaultAxesFontSize',18);
subplot(331)
192 ip_dspsc(a1)
subplot(332)
194 ip_dspsc(a2)
subplot(333)
196 ip_dspsc(a3)
subplot(334)
198 ip_dspsc(a4)
subplot(335)
200 ip_dspsc(a5)
subplot(336)
202 ip_dspsc(a6)
subplot(337)
204 ip_dspsc(a8)
subplot(338)
206 ip_dspsc(a0)
subplot(339)
208 ip_dspsc(a7)

210 figure(2)
set(gcf,'Position',FigPos,'visible','off')
212 ip_dspsc(a1)
title('aperture')

214 figure(3)
set(gcf,'Position',FigPos,'visible','off')
mesh(X1,Y1,psf1)
218 axis tight
title('PSF')

220 figure(4)
set(gcf,'Position',FigPos,'visible','off')
mesh(k,k,mtf1)
224 axis tight
title('MTF')

226 figure(5)
set(gcf,'Position',FigPos,'visible','off')
plot(xn,mtf1((N+1)/2,:)) % 1-D slice down the middle
230 axis([0 1 0 1])
title('MTF (1-D slice)')
232 ylabel('modulation depth')
xlabel('D / \lambda')

234 figure(6)
set(gcf,'Position',FigPos,'visible','off')
ip_dspsc(a2)
238 title('aperture')

```

```
240 figure(7)
241 set(gcf,'Position',FigPos,'visible','off')
242 mesh(k,k,psf2)
243 axis tight
244 title('PSF')

246 figure(8)
247 set(gcf,'Position',FigPos,'visible','off')
248 mesh(k,k,mtf2)
249 axis tight
250 title('MTF')

252 figure(9)
253 set(gcf,'Position',FigPos,'visible','off')
254 plot(xn,mtf2((N+1)/2,:)) % 1-D slice down the middle
255 axis([0 1 0 1])
256 title('MTF (1-D slice)')
257 ylabel('modulation depth')
258 xlabel('D / \lambda')

260
261 figure(10)
262 set(gcf,'Position',FigPos,'visible','off')
263 subplot(1,2,1)
264 ip_dispse(a1)
265 title('aperture')
266 subplot(1,2,2)
267 plot(xn,mtf1(x0,:)) % 1-D slice down the middle
268 title('MTF (1-D slice)')
269 axis([0 1 0 1])
270 axis square
271 grid on

272
273 figure(11)
274 set(gcf,'Position',FigPos,'visible','off')
275 subplot(1,2,1)
276 ip_dispse(a2)
277 title('aperture')
278 subplot(1,2,2)
279 plot(xn,mtf2(x0,:)) % 1-D slice down the middle
280 title('MTF (1-D slice)')
281 axis([0 1 0 1])
282 axis square
283 grid on

284
285 figure(12)
286 set(gcf,'Position',FigPos,'visible','off')
287 subplot(1,2,1)
288 ip_dispse(a3)
289 title('aperture')
290 subplot(1,2,2)
291 plot(xn,mtf3(x0,:)) % 1-D slice down the middle
```

```

292 title('MTF (1-D slice)')
293 axis([0 1 0 1])
294 axis square
295 grid on
296
297 figure(13)
298 set(gcf,'Position',FigPos,'visible','off')
299 subplot(1,2,1)
300 ip_dispse(a4)
301 title('aperture')
302 subplot(1,2,2)
303 plot(xn,mtf4(x0,:)) % 1-D slice down the middle
304 title('MTF (1-D slice)')
305 axis([0 1 0 1])
306 axis square
307 grid on
308
309 figure(14)
310 set(gcf,'Position',FigPos,'visible','off')
311 subplot(1,2,1)
312 ip_dispse(a5)
313 title('aperture')
314 subplot(1,2,2)
315 plot(xn,mtf5(x0,:)) % 1-D slice down the middle
316 title('MTF (1-D slice)')
317 axis([0 1 0 1])
318 axis square
319 grid on
320
321 figure(15)
322 set(gcf,'Position',FigPos,'visible','off')
323 mesh(k,k,mtf5)
324 axis tight
325 title('MTF')
326
327
328 % Comparison
329 % while it seems that obscured aperture MTFs exceed the clear
330 % aperture MTF for certain frequencies, this is just an artifact of
331 % the independent normalization process
332 figure(16)
333 set(gcf,'Position',FigPos,'visible','off')
334 plot(xn,mtf1(x0,:),xn,mtf2(x0,:),xn,mtf3(x0,:),xn,mtf4(x0,:),xn,mtf5(
335     [+]x0,:))
336 title('MTF (independently normalized)')
337 axis([0 1 0 1])
338 axis square
339 grid on
340 legend('A: r_1=0','B: r_1=0.25r_2','C: r_1=0.50r_2','D: r_1=0.75r_2',
341     '[+]'E: r_1=0.95r_2')
342 text(0.23,0.73,'A')
343 text(0.23,0.64,'B')
344 text(0.23,0.44,'C')

```

```

344 text(0.23,0.2,'D')
345 text(0.23,0.06,'E')
346 ylabel('modulation depth')
347 xlabel('(2r_2) / \lambda')

348 % Comparison
349 % in this plot, the normalization process is all in terms of
350 % the unobscured aperture
351 figure(17)
352 set(gcf,'Position',FigPos,'visible','off')
353 plot(xn,mtf1(x0,:),xn,0.84*mtf2(x0,:),xn,0.75*mtf3(x0,:),xn,0.44*mtf4
      [+] (x0,:),xn,0.1*mtf5(x0,:))
354 title('MTF (all normalized to A)')
355 axis([0 1 0 1])
356 axis square
357 grid on
358 legend('A: r_1=0','B: r_1=0.25r_2','C: r_1=0.50r_2','D: r_1=0.75r_2',
      [+] 'E: r_1=0.95r_2')
359 text(0.23,0.73,'A')
360 text(0.23,0.57,'B')
361 text(0.23,0.35,'C')
362 text(0.23,0.1,'D')
363 text(0.23,0.03,'E')
364 ylabel('modulation depth')
365 xlabel('(2r_2) / \lambda')

366

367 figure(18)
368 set(gcf,'Position',FigPos,'visible','off')
369 subplot(1,3,1)
370 ip_dispse(a6)
371 title('aperture')
372 subplot(1,3,2)
373 plot(xn,mtf6(x0,:)) % 1-D slice down the middle
374 title('MTF (1-D slice)')
375 axis([0 1 0 1])
376 axis square
377 grid on
378 xlabel('u or v')
379 subplot(1,3,3)
380 plot(xd/XX,mtf6(pd)) % 1-D slice diagonal
381 title('MTF (1-D slice)')
382 axis([0 1 0 1])
383 axis square
384 grid on
385 xlabel('diagonal')

386 figure(19)
387 set(gcf,'Position',FigPos,'visible','off')
388 mesh(k,k,mtf6)
389 axis tight
390 title('MTF')

```

```

394 figure(20)
395 set(gcf,'Position',FigPos,'visible','off')
396 subplot(1,3,1)
397 ip_dspsc(a0)
398 title('aperture')
399 subplot(1,3,2)
400 plot(xn,mtf0(:,x0)) % 1-D slice down the middle
401 title('MTF (1-D slice)')
402 axis([0 1 0 1])
403 axis square
404 grid on
405 xlabel('u (D_x / \lambda)')
406 subplot(1,3,3)
407 plot(xn,mtf0(x0,:)) % 1-D slice down the middle
408 title('MTF (1-D slice)')
409 axis([0 1 0 1])
410 axis square
411 grid on
412 xlabel('v (D_x / \lambda)')

414 figure(21)
415 set(gcf,'Position',FigPos,'visible','off')
416 subplot(1,3,1)
417 ip_dspsc(a7)
418 title('aperture')
419 subplot(1,3,2)
420 plot(xn,mtf7(:,x0)) % 1-D slice down the middle
421 title('MTF (1-D slice)')
422 axis([0 1 0 1])
423 axis square
424 grid on
425 xlabel('u (D_x / \lambda)')
426 subplot(1,3,3)
427 plot(xn,mtf7(x0,:)) % 1-D slice down the middle
428 title('MTF (1-D slice)')
429 axis([0 1 0 1])
430 axis square
431 grid on
432 xlabel('v (D_x / \lambda)')

434 figure(22)
435 set(gcf,'Position',FigPos,'visible','off')
436 mesh(k,k,mtf7)
437 axis tight
438 title('MTF')

440 figure(23)
441 set(gcf,'Position',FigPos,'visible','off')
442 subplot(1,2,1)
443 ip_dspsc(a8)
444 title('aperture')
445 subplot(1,2,2)
446 plot(xn,mtf8(x0,:)) % 1-D slice down the middle

```

```
448 title('MTF (1-D slice)')
449 axis([0 1 0 1])
450 axis square
451 grid on

452 figure(24)
453 set(gcf,'Position',FigPos,'visible','off')
454 mesh(k,k,mtf8)
455 axis tight
456 title('MTF')

458 figure(25)
459 set(gcf,'Position',FigPos,'visible','off')
460 subplot(2,2,1)
461 ip_dispse(a9)
462 title('aperture')
463 subplot(2,2,2)
464 plot(x,a9(x0,:)) % 1-D slice down the middle
465 title('aperture (1-D slice)')
466 axis([0 XX 0 1])
467 axis square
468 grid on
469 subplot(2,2,3)
470 plot(x,psf9(x0,:)) % 1-D slice down the middle
471 title('PSF (1-D slice)')
472 axis([0 XX 0 1])
473 axis square
474 grid on
475 subplot(2,2,4)
476 plot(xn,mtf9(x0,:)) % 1-D slice down the middle
477 title('MTF (1-D slice)')
478 axis([0 1 0 1])
479 axis square
480 grid on

482 figure(26)
483 set(gcf,'Position',FigPos,'visible','off')
484 mesh(X1,Y1,psf9)
485 axis tight
486 title('PSF')

488 figure(27)
489 set(gcf,'Position',FigPos,'visible','off')
490 mesh(k,k,mtf9)
491 axis tight
492 title('MTF')

494 figure(28)
495 set(gcf,'Position',FigPos,'visible','off')
496 subplot(2,2,1)
497 ip_dispse(a10)
498 title('aperture')
499 subplot(2,2,2)
```

```
500 plot(x,a10(x0,:)) % 1-D slice down the middle
501 title('aperture (1-D slice)')
502 axis([0 XX 0 1])
503 axis square
504 grid on
505 subplot(2,2,3)
506 plot(x,psf10(x0,:)) % 1-D slice down the middle
507 title('PSF (1-D slice)')
508 axis([0 XX 0 1])
509 axis square
510 grid on
511 subplot(2,2,4)
512 plot(xn,mtf10(x0,:)) % 1-D slice down the middle
513 title('MTF (1-D slice)')
514 axis([0 1 0 1])
515 axis square
516 grid on

517 figure(29)
518 set(gcf,'Position',FigPos,'visible','off')
519 subplot(2,4,1)
520 ip_dispse(a10)
521 title('aperture')
522 subplot(2,4,2)
523 plot(x,a10(x0,:)) % 1-D slice down the middle
524 title('aperture (1-D slice)')
525 axis([0 XX 0 1])
526 axis square
527 grid on
528 subplot(2,4,3)
529 plot(x,psf10(x0,:)) % 1-D slice down the middle
530 title('PSF (1-D slice)')
531 axis([0 0.2 0 1])
532 axis square
533 grid on
534 subplot(2,4,4)
535 plot(xn,mtf10(x0,:)) % 1-D slice down the middle
536 title('MTF (1-D slice)')
537 axis([0 1 0 1])
538 axis square
539 grid on
540 subplot(2,4,5)
541 ip_dispse(a9)
542 title('aperture')
543 subplot(2,4,6)
544 plot(x,a9(x0,:)) % 1-D slice down the middle
545 title('aperture (1-D slice)')
546 axis([0 XX 0 1])
547 axis square
548 grid on
549 subplot(2,4,7)
550 plot(x,psf9(x0,:)) % 1-D slice down the middle
551 title('PSF (1-D slice)')
```

```
axis([0 0.2 0 1])
554 axis square
grid on
556 subplot(2,4,8)
plot(xn,mtf9(x0,:)) % 1-D slice down the middle
558 title('MTF (1-D slice)')
axis([0 1 0 1])
560 axis square
grid on
562 % for centered title of subplot groups
txt=['Example of apodization'];
564 annotation(gcf,'textbox','String',txt,'Position',[0 0 1 1],...
    'LineStyle','none','HorizontalAlignment','center');

566 figure(30)
568 set(gcf,'Position',FigPos,'visible','off')
subplot(2,4,1)
570 ip_dispsc(a1)
title('aperture')
572 subplot(2,4,2)
plot(x,a1(x0,:)) % 1-D slice down the middle
574 title('aperture (1-D slice)')
axis([0 XX 0 1])
576 axis square
grid on
578 subplot(2,4,3)
plot(x,psf1(x0,:)) % 1-D slice down the middle
580 title('PSF (1-D slice)')
axis([0 0.2 0 1])
582 axis square
grid on
584 subplot(2,4,4)
plot(xn,mtf1(x0,:)) % 1-D slice down the middle
586 title('MTF (1-D slice)')
axis([0 1 0 1])
588 axis square
grid on
590 subplot(2,4,5)
ip_dispsc(a5)
592 title('aperture')
594 subplot(2,4,6)
plot(x,a5(x0,:)) % 1-D slice down the middle
title('aperture (1-D slice)')
596 axis([0 XX 0 1])
axis square
598 grid on
599 subplot(2,4,7)
600 plot(x,psf5(x0,:)) % 1-D slice down the middle
title('PSF (1-D slice)')
602 axis([0 0.2 0 1])
axis square
604 grid on
subplot(2,4,8)
```

```

606 plot(xn,mtf5(x0,:)) % 1-D slice down the middle
607 title('MTF (1-D slice)')
608 axis([0 1 0 1])
609 axis square
610 grid on
611 % for centered title of subplot groups
612 txt=['Example of anti-apodization'];
613 annotation(gcf,'textbox','String',txt,'Position',[0 0 1 1],...
614   'LineStyle','none','HorizontalAlignment','center');

616 % uncomment print commands to save EPS figure files of the plots
617
618 % print -depsc2 -f1 spec_ap
619
620 % print -depsc2 -f10 mtf_ring00
621 % print -depsc2 -f11 mtf_ring25
622 % print -depsc2 -f12 mtf_ring50
623 % print -depsc2 -f13 mtf_ring75
624 % print -depsc2 -f14 mtf_ring95
625 % print -depsc2 -f16 mtf_ring-comp
626 % print -depsc2 -f17 mtf_ring-comp2
627
628 % print -depsc2 -f20 mtf_rect
629 % print -depsc2 -f21 mtf_2slit
630 % print -depsc2 -f23 mtf_bullseye
631 % print -depsc2 -f29 mtf_apodization
632
633 % show figure plots on screen one by one
634 for i=1:30
635   figure(i)
636   pause
637 end
638
639
640 % The font settings are persistent until you restart MATLAB
641 % To reset manually, use:
642 % %%%%%%%%
643 % reset default figure properties %%%%%%%
644 set(0,'DefaultAxesFontSize','remove');
645 set(0,'DefaultTextFontSize','remove');
646 set(0,'DefaultLineLineWidth','remove')
647 % %%%%%%%%
648
649 end
650 % end of program
651
652
653
654 function ip_dispssc(A)
655 % simplified routine to display 8-bit gray scale images
656 % scales image to full range of display
657 % Syntax: ip_dispssc(A)
658 % where A is an image matrix, typically uint8

```

```

% This is similar to using imagesc
660 %
661 %
662 % Copyright 2004-2008 Cameron H. G. Wright
663 %
664 L=256;
665 L1=L-1;
666 A=double(A); % just in case
667 minA=min(min(A));
668 A=A-minA; % shift
669 maxA=max(max(A));
670 if maxA~=0
671     A=A*L1/maxA; % compress or expand
672 end
673 [X Y]=size(A);
674 % switch X and Y for image coordinates
675 image(0:Y-1,0:X-1,A)
676 axis ij
677 axis equal
678 axis tight
679 colormap(gray(L))
680 end

681
682 function y = gaussian(x,mn,sd);
683 %GAUSS Returns the value of the Gaussian (i.e. Normal)
684 % GAUSS(x,mn,sd) returns the Gaussian of x with
685 % mean mn and standard deviation sd.
686 %
687 % If only one argument is given,
688 % mn is set to 0 and sd is set to 1.
689 %
690 % Cameron H.G. Wright, 1993
691
692 if (nargin == 1)
693     mn = 0;
694     sd = 1;
695 end
696 a = 1/(sd * sqrt(2 * pi));
697 b = ((x - mn).^2)/(2 * sd^2);
698 y = a * exp(-b);
699 end

```

Listing C.4: Calculates PSF and MTF of circular aperture, with and without coma aberration.

```

function mtf_coma()
2 % creates plots of PSF, MTF, and PTF of a circular aperture with and
3 % without coma aberration for a lens system
4 %
5 % includes functions ip_dispsc() in this file
6 % for portability purposes
7 %
8 % copyright (c) 2013 Cameron H. G. Wright

```

```

%%%%%%%%%%%%%%%
12 % set aperture radius, as a fraction of max possible radius
% keep it to 0.5 or less for well behaved calculations
14 RR=0.25;
% set the amount of aberration, as a fraction of a wavelength
16 % a nice simulation is with zc=0.2
zc=0.2;
%%%%%%%%%%%%%%%
18

20 XX=3.25; % max extent of spatial domain coordinates
x=-XX:0.01:XX; % vector for spatial domain range
22 xn=x/XX; % normalized vector for easy plotting of spatial
    [+]
frequencies
N=length(x);
24 k=0:N-1; % integer vector for plotting purposes only
x0=(N+1)/2; % index in vector x where zero is located
26 k0=x0;
y=x; % not really needed but provides a bit more clarity
28

30 % set the radius to use for the circular apertures
r0=XX*RR;
32
34 % create X and Y meshgrid arrays
[X1,Y1]=meshgrid(x,y);

36 % for circular symmetry, pre-build radii--saves a lot of CPU time
r=zeros(N); % preallocates an NxN matrix of zeros
38 r = sqrt(X1.^2 + Y1.^2);

40 % create matrix of angles
theta=atan2(Y1,X1);
42

44 % circular aperture, no aberrations
a1=zeros(N); % preallocate NxN
46 a1(r<r0)=1; % set to one where r<r0

48 %
    [+]
    [+]
% now add the coma in x aberration to that aperture
50 coma=zeros(N); % preallocate NxN
coma=sqrt(8)*(3*(r.^3) - 2*r).*cos(theta);
52 a1a=zeros(N); % preallocate NxN
a1a=a1.*exp(j*2*pi*zc*coma); % set level of aberration to zc
    [+]
wavelengths
54 %
    [+]
    [+]
56 % commence Fourier optics fun!

```

```

58 % for perfect circular aperture
60 % note for PSF and MTF, use fftshift to recenter the FFT result
61 psf1=(abs(fftshift(fft2(a1))).^2); % calculate PSF
62 psf1=psf1/max(max(psf1)); % normalize the PSF

64 otf1=fft2(psf1);
65 mtf1=fftshift(abs(otf1)); % calculate the MTF, shift to center
66 myscale=max(max(mtf1));
67 mtf1=mtf1/myscale; % normalize the MTF
68 ptf1=angle(otf1); % unwrap does not help here

70
71 % for aberrated circular aperture
72 % note for PSF and MTF, use fftshift to recenter the FFT result
73 psf1a=(abs(fftshift(fft2(a1a))).^2); % calculate PSF
74 psf1a=psf1a/max(max(psf1a)); % normalize the PSF

76 otf1a=fft2(psf1a);
77 mtf1a=fftshift(abs(otf1a)); % calculate the MTF, shift to center
78 myscale=max(max(mtf1a));
79 mtf1a=mtf1a/myscale; % normalize the MTF
80 ptf1a=angle(otf1a); % unwrap does not help here

82

84 % figure plotting code

86 % close open figures, intialize counter
87 %close all; % MATLAB complains when using "close all" with hidden
88 % figures
89 % use method below
90 set(0,'ShowHiddenHandles','on')
91 delete(get(0,'Children'))

92 % To hardcode the font size globally, use:
93 set(0,'DefaultAxesFontSize',18);
94 set(0,'DefaultTextFontSize',18);
95 set(0,'DefaultLineWidth',3)

96
97 % set values to use large figure windows
98 scrsz = get(0,'ScreenSize'); % get the screen size
99 % Vista and Win7 have a 31 pixel task bar at bottom
100 Los=10; % left offset
101 Bos=55; % bottom offset
102 Ros=20; % right offset
103 Tos=145; % top ofset
104 FigPos=[scrsz(1)+Los scrsz(2)+Bos scrsz(3)-Ros scrsz(4)-Tos];

106
107 Fig=0; % initialize figure counter
108 Fig=Fig+1;

```

```

110 figure(Fig)
111 set(gcf,'Position',FigPos,'visible','off')
112 subplot(121)
113 ip_dspsc(abs(a1))
114 title('magnitude')
115 subplot(122)
116 ip_dspsc(angle(a1))
117 title('phase')
118 % for centered title of subplot groups
119 txt=['Aperture, no aberration'];
120 annotation(gcf,'textbox','String',txt,'Position',[0 0 1 1],...
121 'LineStyle','none','HorizontalAlignment','center');

122 Fig=Fig+1;
123 figure(Fig)
124 set(gcf,'Position',FigPos,'visible','off')
125 subplot(121)
126 mesh(abs(a1))
127 axis tight
128 axis square
129 title('magnitude')
130 subplot(122)
131 mesh(angle(a1))
132 axis tight
133 axis square
134 title('phase')
135 % for centered title of subplot groups
136 txt=['Aperture, no aberration'];
137 annotation(gcf,'textbox','String',txt,'Position',[0 0 1 1],...
138 'LineStyle','none','HorizontalAlignment','center');

139 Fig=Fig+1;
140 figure(Fig)
141 set(gcf,'Position',FigPos,'visible','off')
142 subplot(121)
143 ip_dspsc(abs(a1a))
144 title('magnitude')
145 subplot(122)
146 ip_dspsc(unwrap(angle(a1a)))
147 title('phase')
148 % for centered title of subplot groups
149 txt=['Aperture, with aberration'];
150 annotation(gcf,'textbox','String',txt,'Position',[0 0 1 1],...
151 'LineStyle','none','HorizontalAlignment','center');

152 Fig=Fig+1;
153 figure(Fig)
154 set(gcf,'Position',FigPos,'visible','off')
155 subplot(121)
156 mesh(abs(a1a))
157 axis tight
158 axis square
159 title('magnitude')

```

```

164 subplot(122)
165 mesh(unwrap(angle(a1a)))
166 axis tight
167 axis square
168 title('phase')
169 % for centered title of subplot groups
170 txt=['Aperture, with aberration'];
171 annotation(gcf,'textbox','String',txt,'Position',[0 0 1 1],...
172   'LineStyle','none','HorizontalAlignment','center');

173 Fig=Fig+1;
174 figure(Fig)
175 set(gcf,'Position',FigPos,'visible','off')
176 mesh(psf1)
177 axis tight
178 axis square
179 title('PSF, no aberration')

180 Fig=Fig+1;
181 figure(Fig)
182 set(gcf,'Position',FigPos,'visible','off')
183 mesh(psf1a)
184 axis tight
185 axis square
186 title('PSF, with aberration')

187 Fig=Fig+1;
188 figure(Fig)
189 set(gcf,'Position',FigPos,'visible','off')
190 plot(psf1(k0,k0-20:k0+20)) % 1-D zoomed in
191 grid on
192 axis tight
193 axis square
194 title('1-D PSF, no aberration')

195 Fig=Fig+1;
196 figure(Fig)
197 set(gcf,'Position',FigPos,'visible','off')
198 plot(psf1a(k0,k0-20:k0+20))
199 grid on
200 axis tight
201 axis square
202 title('1-D PSF, with aberration')

203 Fig=Fig+1;
204 figure(Fig)
205 set(gcf,'Position',FigPos,'visible','off')
206 plot(psf1(k0,k0-20:k0+20),'b-')
207 hold on
208 plot(psf1a(k0,k0-20:k0+20),'r--')
209 grid on
210 axis tight
211 axis square

```

```

216 legend('no aberration','with aberration')
217 title('1-D PSF comparison')
218
219 Fig=Fig+1;
220 figure(Fig)
221 set(gcf,'Position',FigPos,'visible','off')
222 [C,h]=contour(psf1,20,'LineWidth',2);
223 %clabel(C,h); % tends to take away too much countour line
224 axis tight % may not want this for contour plots
225 axis square
226 title('PSF, no aberration')
227 grid on
228
229 Fig=Fig+1;
230 figure(Fig)
231 set(gcf,'Position',FigPos,'visible','off')
232 [C,h]=contour(psf1a,20,'LineWidth',2);
233 %clabel(C,h); % tends to take away too much countour line
234 axis tight % may not want this for contour plots
235 axis square
236 title('PSF, with aberration')
237 grid on
238
239 Fig=Fig+1;
240 figure(Fig)
241 set(gcf,'Position',FigPos,'visible','off')
242 mesh(mtf1)
243 axis tight
244 axis square
245 title('MTF, no aberration')
246
247 Fig=Fig+1;
248 figure(Fig)
249 set(gcf,'Position',FigPos,'visible','off')
250 [C,h]=contour(mtf1,20,'LineWidth',2);
251 %clabel(C,h); % tends to take away too much countour line
252 %axis tight % may not want this for contour plots
253 axis square
254 title('MTF, no aberration')
255 grid on
256
257 Fig=Fig+1;
258 figure(Fig)
259 set(gcf,'Position',FigPos,'visible','off')
260 mesh(ptf1)
261 axis tight
262 axis square
263 title('PTF, no aberration')
264
265 Fig=Fig+1;
266 figure(Fig)
267 set(gcf,'Position',FigPos,'visible','off')
268 mesh(mtf1a)

```

```

axis tight
270 axis square
title('MTF, with aberration')

272 Fig=Fig+1;
274 figure(Fig)
set(gcf,'Position',FigPos,'visible','off')
276 [C,h]=contour(mtf1a,20,'LineWidth',2);
%clabel(C,h); % tends to take away too much countour line
278 %axis tight % may not want this for contour plots
axis square
280 title('MTF, with aberration')
grid on

282 Fig=Fig+1;
284 figure(Fig)
set(gcf,'Position',FigPos,'visible','off')
286 mesh(ptf1a)
axis tight
288 axis square
title('PTF, with aberration')

290 Fig=Fig+1;
292 figure(Fig)
set(gcf,'Position',FigPos,'visible','off')
294 plot(mtf1(k0,k0:N))
grid on
296 axis tight
axis square
298 title('1-D (H) MTF, no aberration')

300 Fig=Fig+1;
302 figure(Fig)
set(gcf,'Position',FigPos,'visible','off')
plot(mtf1a(k0,k0:N))
304 grid on
axis tight
306 axis square
title('1-D (H) MTF, with aberration')

308 Fig=Fig+1;
310 figure(Fig)
set(gcf,'Position',FigPos,'visible','off')
312 plot(mtf1(k0,k0:N),'b-')
hold on
314 plot(mtf1a(k0,k0:N),'r--')
grid on
316 axis tight
axis square
318 legend('no aberration','with aberration')
title('1-D (H) MTF comparison')

320 Fig=Fig+1;

```

```

322 figure(Fig)
323 set(gcf,'Position',FigPos,'visible','off')
324 plot(mtf1(k0:N,k0))
325 grid on
326 axis tight
327 axis square
328 title('1-D (V) MTF, no aberration')

330 Fig=Fig+1;
331 figure(Fig)
332 set(gcf,'Position',FigPos,'visible','off')
333 plot(mtf1a(k0:N,k0))
334 grid on
335 axis tight
336 axis square
337 title('1-D (V) MTF, with aberration')

338 Fig=Fig+1;
339 figure(Fig)
340 set(gcf,'Position',FigPos,'visible','off')
341 plot(mtf1(k0:N,k0),'b-')
342 hold on
343 plot(mtf1a(k0:N,k0),'r--')
344 grid on
345 axis tight
346 axis square
347 legend('no aberration','with aberration')
348 title('1-D (V) MTF comparison')

350 Fig=Fig+1;
351 figure(Fig)
352 set(gcf,'Position',FigPos,'visible','off')
353 subplot(121)
354 plot(mtf1(k0,k0:N),'b-')
355 hold on
356 plot(mtf1a(k0,k0:N),'r--')
357 grid on
358 axis tight
359 axis square
360 legend('no aberration','with aberration')
361 title('1-D (H) MTF comparison')
362 subplot(122)
363 plot(mtf1(k0:N,k0),'b-')
364 hold on
365 plot(mtf1a(k0:N,k0),'r--')
366 grid on
367 axis tight
368 axis square
369 legend('no aberration','with aberration')
370 title('1-D (V) MTF comparison')

372 Fig=Fig+1;
373 figure(Fig)

```

```

set(gcf,'Position',FigPos,'visible','off')
376 subplot(221)
[C,h]=contour(psf1,20,'LineWidth',2);
378 %clabel(C,h); % tends to take away too much countour line
%axis tight % may not want this for contour plots
380 axis square
title('no aberration')
382 xlabel('PSF')
grid on
384 subplot(222)
[C,h]=contour(psf1a,20,'LineWidth',2);
386 %clabel(C,h); % tends to take away too much countour line
%axis tight % may not want this for contour plots
388 axis square
title('with aberration')
390 xlabel('PSF')
grid on
392 subplot(223)
[C,h]=contour(mtf1,20,'LineWidth',2);
394 %clabel(C,h); % tends to take away too much countour line
%axis tight % may not want this for contour plots
396 axis square
xlabel('MTF')
398 grid on
400 subplot(224)
[C,h]=contour(mtf1a,20,'LineWidth',2);
402 %clabel(C,h); % tends to take away too much countour line
%axis tight % may not want this for contour plots
404 axis square
xlabel('MTF')
grid on
406 Fig=Fig+1;
408 figure(Fig)
set(gcf,'Position',FigPos,'visible','off')
410 subplot(221)
[C,h]=contour(psf1,20,'LineWidth',2);
412 %clabel(C,h); % tends to take away too much countour line
axis tight % may not want this for contour plots
414 axis square
title('no aberration')
416 xlabel('PSF')
grid on
418 subplot(222)
[C,h]=contour(psf1a,20,'LineWidth',2);
420 %clabel(C,h); % tends to take away too much countour line
axis tight % may not want this for contour plots
422 axis square
title('with aberration')
424 xlabel('PSF')
grid on
426 subplot(223)
[C,h]=contour(mtf1,20,'LineWidth',2);

```

```

428 %clabel(C,h); % tends to take away too much countour line
429 axis tight % may not want this for contour plots
430 axis square
431 xlabel('MTF')
432 grid on
433 subplot(224)
434 [C,h]=contour(mtf1a,20,'LineWidth',2);
435 %clabel(C,h); % tends to take away too much countour line
436 axis tight % may not want this for contour plots
437 axis square
438 xlabel('MTF')
439 grid on
440
441
442 % If you want to save figures as EPS files
443 % print -depsc2 -f1 ap_circ
444
445
446 for i=1:Fig
447   figure(i)
448   pause
449 end
450
451
452 % The font settings are persistent until you restart MATLAB
453 % To reset manually, use:
454 % %%%%%%%%
455 set(0,'DefaultAxesFontSize','remove');
456 set(0,'DefaultTextFontSize','remove');
457 set(0,'DefaultLineLineWidth','remove')
458 % %%%%%%%%
459
460 return
461 % end of program
462
463
464 function ip_dispssc(A)
465 % simplified routine to display 8-bit gray scale images
466 % scales image to full range of display
467 % Syntax: ip_dispssc(A)
468 % where A is an image matrix, typically uint8
469 % This is similar to using imagesc
470 %
471 % Copyright 2004-2008 Cameron H. G. Wright
472
473
474 L=256;
475 L1=L-1;
476 A=double(A); % just in case
477 minA=min(min(A));
478 A=A-minA; % shift
479 maxA=max(max(A));

```

```
482 if maxA~=0
483     A=A*L1/maxA; % compress or expand
484 end
485 [X Y]=size(A);
486 % switch X and Y for image coordinates
487 image(0:Y-1,0:X-1,A)
488 axis ij
489 axis equal
490 axis tight
491 colormap(gray(L))
492 return
```


References

- [1] M. Pagnutti, R. E. Ryan, G. Cazenavette, M. Gold, R. Harlan, E. Leggett, and J. Pagnutti, “Laying the foundation to use Raspberry Pi 3 V2 camera module imagery for scientific and engineering purposes,” *SPIE J. Elect. Imag.*, vol. 26, pp. 013014:1–13, Feb. 2017.
- [2] M. F. Land and R. D. Fernald, “The evolution of eyes,” *Annu. Rev. Neurosci.*, vol. 15, pp. 1–29, 1992.
- [3] M. F. Land and D. Nilsson, *Animal Eyes*. New York: Oxford University Press, 2002 (corrected reprint 2006).
- [4] C. H. G. Wright and S. F. Barrett, “Biomimetic vision sensors,” in *Engineered Biomimicry: Bioinspiration, Biomimetics, and Bioreplication* (A. Lakhtakia and R. Martín-Palma, eds.), ch. 1, pp. 1–36, Oxford, UK: Elsevier, 2013.
- [5] G. P. Luke, C. H. G. Wright, and S. F. Barrett, “A multi-aperture bio-inspired sensor with hyperacuity,” *IEEE Sensors J.*, vol. 12, pp. 308–314, Feb. 2012.
- [6] R. S. Prabhakara, C. H. G. Wright, and S. F. Barrett, “Motion detection: a biomimetic vision sensor versus a CCD camera sensor,” *IEEE Sensors J.*, vol. 12, pp. 298–307, Feb. 2012.
- [7] S. Martinez-Conde, S. L. Macknik, and D. H. Hubel, “The role of fixational eye movements in visual perception,” *Nature Reviews*, vol. 5, pp. 229–240, Mar. 2004.
- [8] R. W. Ditchburn, *Eye Movements and Visual Perception*. Oxford, UK: Clarendon Press, 1973.
- [9] R. Sekuler and R. Blake, *Perception*. New York: McGraw-Hill, 3rd ed., 1994.
- [10] G. Saxby, *The Science of Imaging: An Introduction*. Boca Raton, FL (USA): CRC Press, 2nd ed., 2011.
- [11] F. W. Newell, *Ophthalmology: Principles and Concepts*. St. Louis, MO (USA): The C. V. Mosby Company, 6th ed., 1986.
- [12] D. G. Vaughan, T. Asbury, and P. Riordan-Eva, *General Ophthalmology*. Norwalk, CT (USA): Appleton & Lange, 13th ed., 1992.
- [13] W. F. Ganong, *Review of Medical Physiology*. Norwalk, CT (USA): Appleton & Lange, 16th ed., 1993.
- [14] Y. LeGrand and S. G. El Hage, *Physiological Optics*. New York: Springer-Verlag, 1980.
- [15] H. A. Quigley, A. E. Brown, J. D. Morrison, and S. M. Drance, “The size and shape of the optic disk in normal human eyes,” *Arch. Ophthalmol.*, vol. 108, pp. 51–57, Jan. 1990.
- [16] A. M. Mansour, “Measuring fundus landmarks,” *Invest. Ophthalmol. Vis. Sci.*, vol. 31, pp. 41–42, Jan. 1990.

- [17] N. Drasdo and C. W. Fowler, "Non-linear projection of the retinal image in a wide-angle schematic eye," *Brit. J. Ophthalmol.*, vol. 58, pp. 709–714, 1974.
- [18] E. Hecht, *Optics*. San Francisco, CA (USA): Addison-Wesley, 4th ed., 2002.
- [19] C. E. Shannon, "A mathematical theory of communication," *Bell Syst. Tech. J.*, vol. 27, pp. 623–656, Oct. 1948. Second of two parts.
- [20] V. Ronchi, *Optics: The Science of Vision*. New York: Dover, 1991. Republication of 1957 New York University Press edition.
- [21] W. J. Smith, *Modern Optical Engineering*. New York: McGraw-Hill, 4th ed., 2007.
- [22] C. L. Wyatt, *Electro-Optical System Design*. New York: McGraw-Hill, 1991.
- [23] M. Bass, ed., *Handbook of Optics*, vol. I. New York: McGraw-Hill, 2nd ed., 1995.
- [24] B. E. A. Saleh and M. C. Teich, *Fundamentals of Photonics*. New York: John Wiley & Sons, 1991.
- [25] P. P. Banerjee and T. C. Poon, *Principles of Applied Optics*. Boston, MA (USA): Irwin, 1991.
- [26] G. D. Boreman, *Basic Electro-Optics for Electrical Engineers*, vol. TT31 of *Tutorial Texts in Optical Engineering*. Bellingham, WA (USA): SPIE Press, 1998.
- [27] R. D. Guenther, *Modern Optics*. New York: John Wiley & Sons, 1990.
- [28] M. V. Klein and T. E. Furtak, *Optics*. New York: John Wiley & Sons, 2nd ed., 1986.
- [29] F. L. Pedrotti and L. S. Pedrotti, *Introduction to Optics*. Upper Saddle River, NJ (USA): Prentice Hall, 2nd ed., 1993.
- [30] L. J. Pinson, *Electro-Optics*. New York: John Wiley & Sons, 1985.
- [31] Leonrw, "16 Minolta 50mm." Licensed under Creative Commons Attribution 3.0 via Wikimedia Commons, 2009. http://commons.wikimedia.org/wiki/File:16_minolta_50mm.jpg.
- [32] Multimat, "Sony Alpha 55 with Minolta 500 F8 Reflex." Licensed under Creative Commons Attribution-Share Alike 3.0-2.5-2.0-1.0 via Wikimedia Commons, 2011. http://commons.wikimedia.org/wiki/File:Sony_Alpha_55_with_Minolta_500_F8_Reflex.jpg.
- [33] Bobarino, "Pentaprism." Licensed under Creative Commons Attribution-Share Alike 3.0 via Wikimedia Commons, 2006. <http://commons.wikimedia.org/wiki/File:Pentaprism.svg>.
- [34] B. Mellish, "Roof-pentaprism." Licensed under Creative Commons Attribution-Share Alike 3.0 via Wikimedia Commons, 2007. <http://en.wikipedia.org/wiki/File:Roof-pentaprism.svg>.
- [35] G. C. Holst and T. S. Lomheim, *CMOS/CCD Sensors and Camera Systems*. Bellingham, WA (USA): SPIE Press, 2nd ed., 2011.
- [36] C. A. DiMarzio, *Optics for Engineers*. Boca Raton, FL (USA): CRC Press, 2012.
- [37] P. K. Sinha, *Image acquisition and preprocessing for machine vision systems*. Bellingham, WA (USA): SPIE Press, 2012.
- [38] G. C. Holst, "Imaging system performance based upon $F\lambda/d$," *Opt. Eng.*, vol. 46, pp. 103204:1–8, Oct. 2007.

- [39] G. C. Holst, "Imaging system fundamentals," *Opt. Eng.*, vol. 50, pp. 052601:1–10, May 2011.
- [40] J. Nakamura, ed., *Image Sensors and Signal Processing for Digital Still Cameras*. Boca Raton, FL (USA): CRC Press, 2006.
- [41] R. H. Vollmerhausen, D. A. Reago, Jr., and R. G. Driggers, *Analysis and Evaluation of Sampled Imaging Systems*. Bellingham, WA (USA): SPIE Press, 2010.
- [42] G. C. Holst, *Electro-Optical Imaging System Performance*. Bellingham, WA (USA): SPIE Press, 3rd ed., 2003.
- [43] S. Inoué and K. R. Spring, *Video Microscopy: The Fundamentals*. New York: Plenum Press, 2nd ed., 1997.
- [44] R. C. Gonzalez and R. E. Woods, *Digital Image Processing*. Upper Saddle River, NJ (USA): Prentice Hall, 3rd ed., 2008.
- [45] R. N. Bracewell, *The Fourier Transform and Its Applications*. New York: McGraw-Hill, 3rd ed., 2000.
- [46] N. van Hulst, "Many photons get more out of diffraction," *OSA Optics and Photonics Focus*, vol. 4, Jan. 2009. Story 1. Online: <http://www.opfocus.org/index.php?topic=volume&v=4>.
- [47] BenFrantzDale, "Depth of field illustration." Licensed under Creative Commons Attribution-Share Alike 3.0 via Wikimedia Commons, 2010. http://commons.wikimedia.org/wiki/File:Depth_of_field_illustration.svg.
- [48] JWCreations, "Bokeh example." Licensed under Creative Commons Attribution-Share Alike 3.0 via Wikimedia Commons, 2008. http://commons.wikimedia.org/wiki/File:Bokeh_Example.jpg.
- [49] HHahn, "Spherical aberration 3." Licensed under Creative Commons Attribution-Share Alike 3.0 via Wikimedia Commons, 2011. http://commons.wikimedia.org/wiki/File:Spherical_aberration_3.svg.
- [50] ArtMechanic, "Pfeilhöhe." Licensed under Creative Commons Attribution-Share Alike 3.0 via Wikimedia Commons, 2012. <http://commons.wikimedia.org/wiki/File:Pfeilh%C3%B6he.svg>.
- [51] anonymous, "Lens-coma." Licensed under Creative Commons Attribution-Share Alike 3.0 via Wikimedia Commons, 2006. <http://commons.wikimedia.org/wiki/File:Lens-coma.svg>.
- [52] S. Kosch, "Astigmatism." Licensed under Creative Commons Attribution-Share Alike 3.0 via Wikimedia Commons, 2007. <http://commons.wikimedia.org/wiki/File:Astigmatism.svg>.
- [53] BenFrantzDale, "Field curvature." Licensed under Creative Commons Attribution-Share Alike 3.0 via Wikimedia Commons, 2010. http://commons.wikimedia.org/wiki/File:Field_curvature.svg.
- [54] B. Mellish, "Chromatic aberration lens diagram." Licensed under Creative Commons Attribution-Share Alike 3.0 via Wikimedia Commons, 2006. http://en.wikipedia.org/wiki/File:Chromatic_aberration_lens_diagram.svg.
- [55] DrBob, "Lens6b-en." Licensed under Creative Commons Attribution-Share Alike 3.0 via Wikimedia Commons, 2010. <http://commons.wikimedia.org/wiki/File:Lens6b-en.svg>.

- [56] Egmaskin, “Apochromat.” Licensed under Creative Commons Attribution-Share Alike 3.0 via Wikimedia Commons, 2010. <http://commons.wikimedia.org/wiki/File:Apochromat.svg>.
- [57] M. Zghal, H.-E. Bouali, Z. B. Lakhdar, and H. Hamam, “The first steps for learning optics: Ibn Sahl’s, Al-Haytham’s and Young’s works on refraction as typical examples,” in *Proceedings of the 10th SPIE Conference on Education and Training in Optics and Photonics*, June 2007. Online: <http://spie.org/etop/etop2007.html>.
- [58] J. W. Goodman, *Introduction to Fourier Optics*. New York: McGraw-Hill, 2nd ed., 1996.
- [59] R. G. Wilson, *Fourier Series and Optical Transform Techniques in Contemporary Optics*. New York: John Wiley & Sons, 1995.
- [60] G. D. Boreman, *Modulation Transfer Function in Optical and Electro-Optical Systems*, vol. TT52 of *Tutorial Texts in Optical Engineering*. Bellingham, WA (USA): SPIE Press, 2001.
- [61] R. D. Fiete, *Modeling the Imaging Chain of Digital Cameras*, vol. TT92 of *SPIE Tutorial Texts in Optical Engineering*. Bellingham, WA (USA): SPIE Press, 2010.
- [62] R. D. Fiete, *Formation of a Digital Image: The Imaging Chain Simplified*, vol. PM218 of *SPIE Press Monograph Series*. Bellingham, WA (USA): SPIE Press, 2012.
- [63] J. W. Coltman, “The specification of imaging properties by response to a sine wave target,” *J. Opt. Soc. Am.*, vol. 44, pp. 468–471, June 1954.
- [64] A. D. Ducharme and S. P. Temple, “Improved aperture for modulation transfer function measurement of detector arrays beyond the Nyquist frequency,” *Opt. Eng.*, vol. 47, pp. 093601:1–6, Sept. 2008.
- [65] T. B. Welch, C. H. G. Wright, and M. G. Morrow, *Real-Time Digital Signal Processing: From MATLAB to C with C6x DSPs*. Boca Raton, FL (USA): CRC Press, 2nd ed., 2012.
- [66] G. C. Holst, *Sampling, Aliasing, and Data Fidelity for Electronic Imaging Systems, Communications, and Data Acquisition*. Bellingham, WA (USA): SPIE Press, 1998.
- [67] G. C. Holst, *CCD Arrays, Cameras, and Displays*. Bellingham, WA (USA): SPIE Press, 1996.
- [68] T. S. Lomheim, “Modulation transfer function (MTF) of CCD imagers,” in *Proceedings of the IEEE Charge-Coupled Devices Workshop*, (University of Waterloo, Ontario, Canada), 1991.
- [69] E. L. Dereniak and D. G. Crowe, *Optical Radiation Detectors*. New York: John Wiley & Sons, 1984.
- [70] W. S. Boyle and G. E. Smith, “Charge coupled semiconductor devices,” *Bell Syst. Tech. J.*, vol. 49, pp. 587–593, 1970.
- [71] S. K. Park, R. Schowengerdt, and M.-A. Kaczynski, “Modulation-transfer-function analysis for sampled image systems,” *OSA Applied Optics*, vol. 23, pp. 2572–2582, Aug. 1984.
- [72] D. H. Sieb, “Carrier diffusion degradation of modulation transfer function in charge coupled imagers,” *IEEE Trans. Electron Devices*, vol. ED-21, pp. 210–217, Mar. 1974.
- [73] M. Unser, “Sampling—50 years after Shannon,” *Proc. IEEE*, vol. 88, pp. 569–587, Apr. 2000.

- [74] J. B. Benson, G. P. Luke, C. H. G. Wright, and S. F. Barrett, "Pre-blurred spatial sampling can lead to hyperacuity," in *Proceedings of the 13th IEEE Digital Signal Processing Workshop*, pp. 570–575, Jan. 2009.
- [75] J. E. Greivenkamp, "Color dependent optical prefilter for the suppression of aliasing artifacts," *Appl. Opt.*, vol. 29, pp. 676–684, Feb. 1990.
- [76] B. E. Bayer, "Color imaging array," July 1976. U.S. Patent 3,971,065.
- [77] D. T. Riley, W. M. Harmann, S. F. Barrett, and C. H. G. Wright, "Musca domestica inspired machine vision sensor with hyperacuity," *IOP Bioinsp. Biomim.*, vol. 3, no. 2, pp. 026003(+13), 2008.
- [78] G. P. Luke, C. H. G. Wright, and S. F. Barrett, "Multi-aperture visual sensor with hyperacuity," October 2013. U.S. Patent 8,569,680.
- [79] N. Dilmen, "Windflower-05237-nevit." Licensed under Creative Commons Attribution-Share Alike 3.0 via Wikimedia Commons, 2003. <http://commons.wikimedia.org/wiki/File:Windflower-05237-nevit.jpg>.
- [80] A. Dulyan, "Shutter speed in Greenwich." Licensed under Creative Commons Attribution 2.0 via Wikimedia Commons, 2005. http://commons.wikimedia.org/wiki/File:Shutter_speed_in_Greenwich.jpg.
- [81] M. Szklanny, "HDR image + 3 source pictures (Cerro Tronador, Argentina)." Licensed under Creative Commons Attribution-Share Alike 3.0 via Wikimedia Commons, 2009. http://commons.wikimedia.org/wiki/File:HDR_image_%2B_3_source_pictures_%28Cerro_Tronador,_Argentina%29.jpg.
- [82] S. Xiao, W. Tao, and H. Zhao, "Flexible and accurate camera calibration using imperfect planar target," *Proc. SPIE*, vol. 10250, pp. 102501C-1–102501C-6, 2017.
- [83] S. K. Mitra, *Digital Signal Processing: A Computer-Based Approach*. New York: McGraw-Hill, 4th ed., 2010.
- [84] A. V. Oppenheim and R. W. Schafer, *Discrete-Time Signal Processing*. Upper Saddle River, NJ (USA): Prentice Hall, 3rd ed., 2009.
- [85] S. W. Smith, *The Scientist and Engineer's Guide to Digital Signal Processing*. Poway, CA (USA): California Technical Publishing, 2011. Full text is available online at: <http://www.dspguide.com/>.
- [86] Canon Inc., Tokyo, Japan, *Canon EOS Rebel XS/450D Instruction Manual*, 2008.
- [87] B. Long, *The Canon EOS Digital Rebel XS/450D Companion*. Sebastopol, CA (USA): O'Reilly Media, 2008.